MIT-EL 76-004
ASRL TR 182-1

FINITE ELEMENT NONLINEAR TRANSIENT RESPONSE ANALYSIS OF SIMPLE 2-D STRUCTURES SUBJECTED TO IMPULSE OR IMPACT LOADS

by

José J.A. Rodal and Emmett A. Witmer

June 1976

FOREWORD

This research was carried out by the Aeroelastic and Structures Research Laboratory, Department of Aeronautics and Astronautics, Massachusetts Institute of Technology, Cambridge, Massachusetts under sponsorship by the New England Electrical System and the Northeast Utilities Service Company under the MIT Energy Laboratory Electric Power Program. Mr. William Hinkle of the MIT Energy Laboratory served as program coordinator.

The authors wish to acknowledge appreciatively the advice and assistance of their colleagues in the MIT Aeroelastic and Structures Research Laboratory: Fred Merlis, Earle Wassmouth, Thomas Stagliano, and Robert L. Spilker.

ABSTRACT

This study was intended to contribute to the development of more rational practical methods for predicting the transient responses of structures which are subjected to transient and impact loads. Attention is restricted to the global structural response; local (or stress-wave-induced) response is not included. The use of higher-order assumed-displacement finite elements (FE) is investigated to seek more efficient and accurate strain predictions; these studies were carried out for 2-d structural deformations typical of beams and curved rings to minimize cost and labor. These studies were done in conjunction with the use of various approximations to the nonlinear strain-displacement relations since large deflections and rotations need to be taken into account.

Transient large-deflection elastic-plastic structural response predictions are made for these various FE models for impulsively-loaded beams and a free initially-circular ring, for which high quality experimental measurements of strains and deflections are available. From comparisons of (a) predictions with each other for the various FE models investigated and (b) predictions vs. experimental data, it appears to be more efficient for the same number of degree-of-freedom (DOF) unknowns to use the simple 4 DOF/node elements rather than fewer of the more sophisticated 8 DOF/node elements although the latter provide a physically superior and more realistic distribution of strain along the structural span at any given time instant compared with the use of the 4 DOF/N elements. Comparisons of measured with predicted transient strain and final deformation of a thin aluminum beam with both ends clamped and impacted at midspan by a 1-inch diameter steel sphere show very good agreement.

Extensions to the present analysis to accommodate more general types of fragments and fragment-impacted structures are discussed briefly.

CONTENTS

Section		Page
1	INTRODUCTION	1
	1.1 Background	1
	1.1.1 Safety/Threat Problem	1
	1.1.2 Internally-Generated Missiles	2
	1.1.3 Externally-Generated Missiles	4
	1.2 Structural Response Considerations	5
	1.3 Synopsis of the Present Study	7
2	REVIEW OF FINITE ELEMENT FORMULATION AND SOLUTION PROCESS	9
	2.1 Introduction	9
	2.2 Unconventional Formulation	15
	2.3 Conventional Formulation	17
	2.4 Timewise Solution of the Governing Equations	19
	2.4.1 Solution Process	21
	2.4.2 Evaluation of Stresses and Plastic Strains	27
3	FORMULATIONS FOR SEVERAL CURVED-BEAM ELEMENTS	36
	3.1 Objectives	36
	3.2 Nonlinear Strain-Displacement Relations	38
	3.2.1 Brief Historical Background	38
	3.2.2 Formulation of the Strain-Displacement Relations	43
	3.2.2.1 Thin Shells	43
	3.2.2.2 Curved Beams	51
	3.2.2.3 Initially-Flat Beams	55
	3.2.2.4 Comments	56
	3.3 Assumed Displacement Field Considerations	62
	3.3.1 Description of Curved-Beam-Element Geometry	62
	3.3.2 Rigid-Body Modes and Displacement Field "Requirements"	67
	3.3.3 Displacement Interpolation Fields	73

Section			Page
	3.4	Finite Element Property Matrices	86
		3.4.1 Strain-Displacement Expressions and Strain Increments	87
		3.4.2 Mass Matrix	93
		3.4.3 Generalized Nodal-Force Matrices for the Unconventional Formulation	96
		3.4.4 Comments on the Conventional Formulation	99
4	EVALUATION AND DISCUSSION		103
	4.1	Objectives and Scope	103
	4.2	Experimental Beam Responses to Impulse Loading and Impact	104
	4.3	Effects of Nonlinear Strain-Displacement Terms	106
		4.3.1 General Considerations	106
		4.3.2 Impulsively-Loaded Beam Model	107
		4.3.3 Impulsively-Loaded Free Circular Ring	110
		4.3.4 Summary Comments	113
	4.4	Effects of the Number of Gaussian Stations	113
	4.5	Comparisons of Various Higher Order Elements	120
		4.5.1 Impulsively-Loaded Beam Models	120
		4.5.2 Impulsively-Loaded Free Circular Ring	127
		4.5.3 Comments	128
	4.6	Structural Response to Impact	129
5	SUMMARY, CONCLUSIONS, AND COMMENTS		133
	5.1	Summary	133
	5.2	Conclusions	135
	5.3	Comments	137
REFERENCES			138
TABLES			148
FIGURES			152

Appendix		Page
A	Description of the Mechanical-Sublayer Model for Strain Hardening, Strain-Rate-Sensitive Material Behavior	245
B	Definition of Finite Element Matrices Indicated Symbolically in the Text	251

LIST OF ILLUSTRATIONS

Figure		Page
1	Nomenclature for a Possible Finite-Element Representation of a General Two-Dimensional Structure	152
2	Flow Chart for Solution Process of Structural Large Deflection Elastic-Plastic Transient Responses	153
3	Nomenclature for Shell Geometry and Displacements	155
4	Nomenclature for Geometry, Coordinates, and Displacements of a Curved-Beam Finite Element	158
5	Nominal Dimensions for the 6061-T651 Aluminum Clamped-Beam Models	159
6	Clamped Beam Model Coordinates and Nomenclature	160
7	Schematic of Impulsive-Loading Tests on 6061-T651 Beams with Clamped Ends	161
8	Uncorrected Transient Strain Records for Impulsively-Loaded 6061-T651 Beam Model CB-1 with Clamped Ends	162
9	Uncorrected Transient Strain Records for Impulsively-Loaded 6061-T651 Beam Model CB-4 with Clamped Ends	164
10	Test Schematic for Steel-Sphere-Impacted 6061-T651 Aluminum Beams with Clamped Ends	166
11	Post-Test Views of Steel-Sphere-Impacted Beam Specimens CB-12 and CB-13 (Nominal Impact Velocity: 2500 IN/SEC)	167
12	Uncorrected Transient Strain Records for Steel-Sphere Impacted 6061-T651 Aluminum Beam Model CB-13	169
13	Uncorrected Transient Strain Records for Steel-Sphere Impacted 6061-T651 Aluminum Beam Model CB-18	171
14	Influence of Strain-Displacement Relations on Predicted Transient Strain on Impulsively-Loaded Beam CB-1	173

LIST OF ILLUSTRATIONS (Continued)

Figure		Page
15	Influence of Strain-Displacement Relations on Predicted Transient Midspan Deflection of Impulsively-Loaded Beam CB-1	178
16	Influence of Strain-Displacement Relations on Predicted Transient Outer- and Inner-Surface Circumferential Strain for the Impulsively-Loaded Free Circular Ring	179
17	Influence of Strain-Displacement Relations and Finite-Element Type on the Predicted Circumferential Distribution of Outer-Surface Strain at 1500 Microseconds for the Impulsively-Loaded Free Circular Ring	183
18	Influence of Strain-Displacement Relations on the Predicted Transient Centerline Midplane Separation for the Impulsively-Loaded Free Circular Ring	184
19	Influence of the Number of Spanwise Gaussian Stations on the Predicted Transient Response of Impulsively-Loaded Beam CB-1 (4 DOF/N, 10 ELEM/HALF)	185
20	Influence of the Number of Spanwise Gaussian Stations on the Predicted Transient Response of Impulsively-Loaded Beam CB-1 (5 DOF/N, 10 ELEM/HALF)	190
21	Influence of the Number of Spanwise Gaussian Stations on the Predicted Transient Response of Impulsively-Loaded Beam CB-1 (8 DOF/N, 4 ELEM/HALF)	195
22	Strain Distribution on Non-Loaded Surface of Beam CB-1 at 300 Microseconds for 4 DOF/N Element Vs. 5 DOF/N Element Predictions	200
23	Strain Distribution on Non-Loaded Surface of Beam CB-1 at 300 Microseconds for 5 DOF/N Element Vs. 6 DOF/N Element Predictions	201

LIST OF ILLUSTRATIONS (Continued)

Figure		Page
24	Strain Distribution on Non-Loaded Surface of Beam CB-1 at 300 Microseconds for 6 DOF/N Element Vs. 8 DOF/N Element Predictions	202
25	Spanwise Distribution of Strain on Lower and Upper Surfaces at 300 Microseconds for 4 DOF/N Element and 8 DOF/N Element Predictions	203
26	Predicted Strain Histories on the Upper Surface of Impulsively-Loaded Beam Model CB-1 at Station x=0 In	207
27	Predicted and Measured Strain Histories on the Upper Surface of Impulsively-Loaded Beam Model CB-1 at Station x=1.40 In	208
28	Predicted and Measured Strain Histories on the Upper Surface of Impulsively-Loaded Beam Model CB-1 at Station x=2.20 In	209
29	Predicted and Measured Strain Histories on the Lower Surface of Impulsively-Loaded Beam Model CB-1 at Station x=2.20 In	210
30	Predicted and Measured Strain Histories on the Upper Surface of Impulsively-Loaded Beam Model CB-1 at Station x=3.00 In	211
31	Predicted and Measured Strain Histories on the Upper Surface of Impulsively-Loaded Beam Model CB-1 at Station x=3.80 In	212
32	Predicted and Measured Strain Histories on the Lower Surface of Impulsively-Loaded Beam Model CB-1 at Station x=3.80 In	213
33	Predicted Transient Midspan Displacement w for Impulsively-Loaded Beam Model CB-1	214

LIST OF ILLUSTRATIONS (Continued)

Figure		Page
34	EL-SH-SR Predicted Transient Midspan Displacement w for Impulsively-Loaded Beam Model CB-1	215
35	Spanwise Distribution of Measured and Predicted Permanent Deflection for Impulsively-Loaded Beam CB-1	216
36	Predicted Strain Histories on the Lower and the Upper Surface of Impulsively-Loaded Beam CB-4 at Station x=0 In	217
37	Predicted and Measured Strain Histories on the Lower and Upper Surface of Impulsively-Loaded Beam Model CB-4 at Station x=1.40 In	218
38	Predicted and Measured Strain Histories on the Upper Surface of Impulsively-Loaded Beam Model CB-4 at Station x=2.20 In	219
39	Predicted and Measured Strain Histories on the Upper Surface of Impulsively-Loaded Beam Model CB-4 at Station x=3.00 In	220
40	Predicted and Measured Strain Histories on the Lower and the Upper Surface of Impulsively-Loaded Beam CB-4 at Station x=3.80 In	221
41	Predicted Transient Midspan Displacement w for Impulsively-Loaded Beam Model CB-4	222
42	Spanwise Distribution of Upper-Surface Strain and Lateral Deflection at Given Times for Impulsively-Loaded Beam CB-4 (4 DOF/N Vs. 8 DOF/N Elems)	223
43	Comparisons of Experimental and Predicted Strains on the Inner and the Outer Surface of the Impulsively-Loaded Free Circular Ring	225
44	Comparison of Centerline Midplane Separation Predicted by Using 4 DOF/N and 8 DOF/N Elements for the Impulsively-Loaded Free Circular Ring	228

LIST OF ILLUSTRATIONS (Concluded)

Figure		Page
45	Transient Strain at Various Spanwise Stations and Support Reactions of Steel-Sphere-Impacted 6061-T651 Aluminum Beam Model CB-18	229
46	Predicted Transient and Observed Permanent Lateral Deflection w at Spanwise Station x=1.0 In for Steel-Sphere Impacted 6061-T651 Aluminum Beam Specimen CB-18	239
47	Transient Strain at Various Spanwise Stations of Steel-Sphere Impacted 6061-T651 Aluminum Beam Model CB-18 (43 Elem., 4 DOF/N, Type B vs. Type C)	240

LIST OF TABLES

Table		Page
1	Pre-Test Dimensions of the 6061-T651 Beam Specimens	148
2	Strain Gage Locations and Permanent Strain Data for the 6061-T651 Aluminum Beams with Clamped Ends	149
3	Number of Spanwise Gaussian Integration Stations Needed for Evaluating the Mass Matrix, the Stiffness Matrix, and the Nonlinear-Deflection Contribution to the Generalized Loads Vector for Various Straight and Curved-Beam Elements	150
4	Influence of the Number of Spanwise Gaussian Stations on the Maximum Natural Frequency and Required Nodal Velocities to Produce a Given Initial Kinetic Energy for Beam Model CB-1 when Modeled by 4 DOF/N, 5 DOF/N, and 8 DOF/N Elements	151

SECTION 1

INTRODUCTION

1.1 Background

1.1.1 Safety/Threat Problem

Among the many factors that influence nuclear reactor safety, none is more important than structural safety and integrity. During its design lifetime, each of the many critical structural components is subjected to a history of mechanical, thermal, and other loads, some deliberate and others accidental. In the present discussion, however, attention shall be restricted to a small but vital portion of the total environmental conditions under which structural/operational safety of nuclear powerplants must continue to be assured -- that is, attack from missiles of various types and sources [1].*

Various types of missiles may be generated within one or more of the parts of nuclear powerplants; included in this category, for example, may be valves, valve stems, valve bonnets, control rods, drive mechanisms, pipes, turbine blades, turbine rotor disk fragments, etc. Careful detail design of many of these items may reduce their probability of occurrence to ignorably low levels. However, studies by licensing agencies and others may show that certain of these missiles threats must be assumed to occur during the useful life of the system. Accordingly, one must provide guaranteed protection against such missile attack.

Similarly, missiles originating external to a nuclear powerplant may threaten its safety. Missiles in this category include those produced by a tornado -- planks, pipes, utility poles, automobiles, and other objects -- each with various possible sizes, masses, and velocities. Also one must consider the possibility of impact by an aircraft; here again various sizes, masses, and impact velocities may be involved. In addition, impact of automobiles, trucks, or other vehicles against the nuclear reactor containment structure should be either prevented or the containment structure itself should be designed to provide adequate protection.

---

* Numbers in square brackets [ ] denote references listed at the end of the text.

Some of these missiles are nearly rigid, others are shatterable/splinterable, and others are comparatively crushable. Their geometries, mass-to-frontal-area ratios, and velocities are very different from military artillery-type missles for which extensive impact, penetration, and response data [2-5] have been obtained on a variety of target structures and materials (metals, reinforced concrete, etc.). Attempted extrapolation of "military" data to the above types of missile attack involves substantial uncertainties [3-5]. Therefore, to generate empirical threshold penetration and design data, an excellently conceived and executed experimental program of impact of tornado-type missiles (pipes, planks, automobiles, etc.) against reinforced concrete panels has commenced [6-7]; detailed transient response data for evaluating theoretical prediction methods will be sought in a later phase of that program.

Persuasive arguments can be made that missiles such as valve stems, valve bonnets, etc. can be eliminated as missile threats by proper design and/or by proper geometric layouts of valves, lines, etc. with respect to endangered critical items. Similar persuasive arguments are lacking concerning turbine blades, turbine rotor fragments, tornado-generated missiles, aircraft, and other external vehicles. Hence, protection against this latter class of missiles should be provided.

1.1.2 Internally-Generated Missiles

With respect to "internally-generated" missiles such as turbine blades, turbine rotor disks, etc., it is understood that studies by GE, Westinghouse, and the American Nuclear Society indicate that one must design against this type of missile attack. The specific threat which must be assumed in terms of geometry, mass, kinetic energy, etc., is currently under discussion and study -- draft recommendations are being examined.

On a smaller scale, similar missile attacks occur in aircraft jet engines. Because of fatigue, faulty seals and/or bearings, foreign object damage, and other causes, aircraft jet engines exhibit failures of fan blades, compressor blades and/or disks, turbine blades, and turbine disks. The lighter less energetic fragments such as a single compressor blade or a single turbine blade are usually (about 80% of the cases) contained within the engine casing. However, the much heavier and more energetic rotor rims and rotor disks always penetrate the casing of present engines. In order to develop

structural/mechanical concepts and methods of analysis to provide either containment of such fragments or to divert them away from critical regions of structure, fuel lines, etc., and to allow "fragment escape" into harmless regions, NASA has been sponsoring a program of both experimental research and theoretical analysis [8].

Under NASA sponsorship, a large spin chamber facility has been constructed at the Naval Air Development Center, Phila., Pa. This facility permits engine rotors of various sizes from very tiny to about a 10-foot diameter to be rotated at high rpm and to be failed. High speed photographic equipment is used to view the resulting fragment attack upon and interaction with various types of candidate containment or deflector structures [9-13]. Transient and permanent strain measurements of the fragment-attacked structure are also being made currently. These experimental studies have been of (1) parametric effects and materials screening type and (2) a more detailed and systematic study of structural response and fragment/structure impact and interaction in order to provide data for checking prediction methods.

Since mid-1968, the MIT Aeroelastic and Structures Research Laboratory has been developing for NASA methods for analyzing structural response to engine rotor fragment attack. The results of those continuing studies are reported in Refs. 14-22. Both finite-difference and finite-element methods for predicting the large-deflection, elastic-plastic, transient structural responses of two-dimensional, variable-thickness containment and/or deflector rings have been developed and verified to provide accurate predictions when these structures are subjected to known transient loads. During fragment attack, the transiently-applied loads or impact-imparted increments of velocity must be estimated in some rational way -- in this research two different schemes have been used: (a) the collision force method which makes use of the load-deflection behavior of the attacking fragment (this scheme is called the collision force method CFM; Ref. 19) and (2) the collision-imparted velocity method* (CIVM; Refs. 17,21,22). Both of these methods have been used to predict the structural response of a containment ring to impact from a single blade of a T58 turbine rotor as observed in NAPTC tests.

*Only a preliminary version of this method was used; a more comprehensive version is currently being explored and evaluated at the MIT-ASRL for problems of sphere impact on 2-d structures.

The CIVM scheme has also been employed to predict the response of a containment ring to attack from a T58 turbine rotor which was caused to fail into 3 equal-size 120-degree sectors. In these calculations, the changing kinetic energy of each attacking fragment is followed, as is the kinetic, elastic, and plastic energy in the containment ring.

It is apparent that analyses of this type could be used to make a rational estimate of the reduction of kinetic energy of powerplant turbine fragments as they rupture their metal casings and subsequently impact other containment structure such as reinforced concrete walls and panels. It should be noted that all of the cited MIT-ASRL calculations and comparisons have involved metal containment/deflector structures; fragment attack upon reinforced concrete has not been studied in that effort.

Recently the MIT-ASRL group has succeeded in developing the finite element method for predicting the large-deflection, elastic-plastic transient responses [23,24] of geometrically-stiffened (ring and/or longitudinal stiffeners) cylindrical and flat panels; this involves general three-dimensional shell deformations. Definitive transient response experiments conducted at MIT provided excellent data for checking the accuracy and reliability of the prediction method. Excellent theoretical-experimental agreement was achieved; ring-stiffened impulsively-loaded 6061-T6 aluminum cylindrical panels were employed. This structural response prediction capability could, if needed, be coupled with the fragment-impact CIVM analysis to provide a means for predicting the response of a fragment-impacted structure; as noted earlier, however, the adequacy of the CIVM model remains to be verified.

1.1.3 Externally-Generated Missiles

As noted earlier, Stevenson [3] has summarized some of the most recent thinking concerning the assortment of tornado-generated missiles which must be designed against. Concisely, these are typically:

Object	Dimensions	Weight	Velocity	Kinetic Energy (ft-lb)
Wood Plank	4"x12"x12'	200 lb.	250 fps	194,200
Steel Pipe	3"dx10',Sch.40	78 lb.	200 fps	48,500
Steel Rod	1"dx3'	8 lb.	170 fps	3,590
Steel Pipe	6"dx15',Sch.40	285 lb.	160 fps	---
Steel Pipe	12"dx15',Sch.40	743 lb.	150 fps	260,000
Utility Pole	13.5"dx35'	1490 lb.	180 fps	750,000
Automobile	20 sq.ft. frontal	4000 lb.	75 fps	350,000

These impact velocities and ratios of missile weight per unit front missile area (end-on-impact) contrast sharply* with experimental data used to obtain empirical estimates [4,5,25,26] of target penetration, perforation, and spalling of reinforced concrete walls. Current work such as [6,7] should aid greatly in remedying this deficiency.

1.2 Structural Response Considerations

Recent papers by Lindermann et al [4], Williamson et al [5], Chelapati et al [25], Doyle et al [26], Riera [27], Yang et al [28], Gwaltney [29], and Ferguson [30], summarize current methods for sizing reinforced concrete panels to resist missile attack. Three modes of behavior are considered: (1) perforation, (2) collapse (plastic limit), and (3) cracking. Although most of the approaches advocated are fairly rational, there are many aspects which involve very substantial uncertainties. The experimental data base cited is of very dubious applicability, scope, and resolution. Various analysis assumptions appear to warrant a more thorough examination and evaluation against high quality pertinent experimental data before assurance of their adequacy can be given. Recognizing this deficient state of knowledge, Stephenson [6,7] and his colleagues under ERDA and EPRI sponsorship are undertaking an extensive program of missile impact tests against reinforced concrete structures.

It should be emphasized that the present investigation is concerned with structural response, not material or stress-wave response; impact-induced stress-wave response can be addressed by computer codes such as HEMP[31], HELP[32], STRIDE[33], and PISCES[34]. Thus, the structural response behavior and analysis methods of concern apply to impact and structural response situations in which the structural response mode of deformation rather than penetration and/or spalling (scabbing) are present. Also, if one postulates that penetration and/or spalling are to be prevented, it follows that the structural response mode of deformation will be of dominant interest. First, however, for a given missile attack, one must design the structure with thickness and appropriate material sufficient to prevent penetration and spalling;

*This is the case on either a dimensional or dimensionless basis; dense projectiles with impact velocities substantially larger than those cited in the above tabulation provide the data employed.

designing additionally to avoid excessive structural response should provide the desired structural integrity.

With respect to the various types of attacking fragments, some are essentially "non-deformable" (steel rod, rotor disk segment) while others are "marginally deformable" (thick-wall steel pipes), some are perhaps shatterable/splinterable (planks and utility poles), and others such as automobiles and aircraft are (comparatively) readily crushable. Some tentative means for accounting for missile deformability are included in the cited method summaries. Rational bounds and uncertainties on the adequacy and accuracy of these estimates appear to be lacking. Hence, a rather substantial uncertainty exists concerning whether the resulting structural design is adequate, inadequate, or grossly overdesigned.

The general purpose of the present research effort is to develop more rational and accurate methods for predicting the structural responses of various kinds of powerplant structures which are subjected to impact by (the previously-cited): (1) internally-generated missiles and (2) externally-generated missiles. However, since structural responses to internally-generated missiles are being studied in other efforts [for example, 8-22, 35-38], attention is restricted herein to externally-generated missiles. Chosen for its versatility and convenience, the finite-element method will be used to analyze the response of the impacted structure; the present first-stage in this study is concentrated, therefore, upon developing and verifying the adequacy of the finite element analyses to provide accurate predictions of the large-deflection transient response of the structure -- particularly the transient strains. Further, to eliminate undesirable and burdensome complexities at this stage, attention will be restricted to isotropic structural material; after method verification has been achieved, it will be timely to include more complex material behavior.

For cases in which the attacking missile is essentially "rigid" compared with the attacked structure, it is planned to use an updated version of the collision-imparted velocity method [21,22] to predict the missile/structure impact-interaction response. In the case of deformable missiles, it is expected that both the attacked structure and the missile will be represented by suitable finite-element models.

1.3 Synopsis of the Present Study

This being the initial phase of the projected study, attention is restricted to developing the finite element analysis to predict transient strains reliably for large-deflection elastic-plastic structural response, while minimizing computing costs and related complexities. Accordingly, only two-dimensional straight and curved beamlike structures have been analyzed; the deformations of these structures occur essentially in one plane. In particular, the present work represents a logical extension of work in [17] to include now (a) a more comprehensive strain-displacement relation, (b) an improved rigid-body-mode representation, and (c) additional generalized degrees of freedom in order to obtain a better and/or more efficient strain description in each finite element. Some illustrative calculations with some earlier formulations revealed some anomalous behavior and deficiencies which steps (a), (b), and (c) seek to remedy.

Further, since attention is centered upon the finite-element analysis adequacy for the deforming structure, predictions are compared with each other and with experimentally observed transient structural response of an impulsively-loaded beam (not subjected to impact). This experiment involved a clamped-ended beam of well-known material and geometric properties subjected to well-defined uniform impulsive loading applied over a spanwise portion centered at the midspan of the beam.

Having utilized these studies to select the most promising and efficient of the finite-element versions studied, an example calculation was carried out to illustrate the predicted vs. experimental transient response of a clamped-ended 6061-T651 aluminum beam (nominal: span = 8 in, width = 1.5 in, thickness = 0.100 in) subjected to "midspan impact" of a steel sphere traveling at about 2900 in/sec. No further predictions of structural response to missile impact are included in this report; the ongoing effort will take into account other types of missiles and targets, and these results will be given in a future report.

Section 2 contains a review of the finite-element (FE) assumed-displacement formulation and solution process for transiently-loaded structures; this includes the conventional FE formulation, an unconventional FE formulation, and a description of the timewise solution process accounting for large deflections and elastic-plastic behavior. Section 3 contains a discussion

of the formulation of various types of assumed-displacement finite elements for straight- and cuved-beam type structures. An evaluation of the prediction capabilities and limitations of these elements via comparisons with each other and with pertinent experimental data is given in Section 4. Also included in Section 4 is an illustrative preliminary prediction of the response of a clamped-ended beam subjected to impact by a steel sphere. Section 5 contains a concise summary of the present study.

SECTION 2

REVIEW OF FINITE ELEMENT FORMULATION AND SOLUTION PROCESS

2.1 Introduction

The governing equations of motion for the finite element analysis of a structural continuum which undergoes transient large-deflection elastic-plastic behavior are developed most conveniently and systematically on the basis of a variational formulation. In particular, for the assumed-displacement version of the finite element method, the use of the Principle of Virtual Work together with D'Alembert's Principle provides an effective and appropriate framework [17,24,39-42]. References 17, 24, and 39-42 may be consulted for detailed derivations of various finite-element formulation versions; hence, only a brief description of the main aspects following [17,24] are repeated here.

For present purposes, let the deforming continuum be described in the Lagrangian sense -- all pertinent quantities are defined consistently with reference to the initial undeformed state. Further, the method of initial strain [17,43,44] rather than the tangent modulus method [45,46] is employed to accommodate material elastic-plastic behavior, because of its superior convenience for transient response problems.

In the following the equations which govern the large-deflection transient responses of a solid continuum are reviewed concisely following the presentations in [17,24]. For generality and clarity, the equations are presented in general three-dimensional tensor form. Indicial notation and the summation convention associated with vector and tensor analysis are used; index quantities using Latin miniscules range over the values 1, 2, and 3. Later these equations are specialized to treat both straight-beam and curved-beam structures.

The terminology "large deflection" as used here indicates that the lateral deflections of the structure (beam, panel, etc.) are large compared with the thickness dimension of the structure; the change of geometry is significant. Through the strain-displacement relations and the equilibrium equations, the geometric nonlinearities are introduced into the theory. One should note, however, that in the present analysis the strains are assumed to be small compared with unity.

Following [17,24], consider a deformed continuum in equilibrium under the action of body forces, externally-applied surface tractions, and with arbitrary deformation conditions consistent with the prescribed geometric boundary conditions. Let this equilibrium configuration be subjected to an arbitrary and independent set of infinitesimal virtual displacements without violating the prescribed geometric boundary conditions. The Principle of Virtual Work states that the virtual work, δW, done by the external forces (body forces and surface tractions), is equal to the virtual work, δU, of the internal stresses, i.e.,

$$\delta U - \delta W = 0 \tag{2.1}$$

where

$$\delta U = \int_V S^{ij}\, \delta \gamma_{ij}\, dV \tag{2.1a}$$

$$\delta W = \int_V \rho B^i \delta u_i\, dV + \int_{A_\sigma} \underset{\sim}{T}^i \delta u_i\, dA \tag{2.1b}$$

In this equation, S^{ij} is the Kirchhoff stress tensor (based on a unit area of the undeformed state), B^i is the body force (inertia, gravitational, magnetic, etc.) per unit mass, $\underset{\sim}{T}^i$ is the externally-applied surface tractions (measured per unit area of the undeformed state), γ_{ij} is the Lagrangian strain tensor, the u_i are the displacement components, ρ is the mass density in the original undeformed state, and only displacement variations (δ) are permitted. All pertinent quantities are described consistently with respect to a curvilinear coordinate system (termed Lagrangian coordinates) ξ^j. Also, the integrations extend over the entire undeformed volume, V, of the continuum which is bounded by the undeformed surface (area) A. The boundary surface A may be divided into a prescribed-surface-traction boundary, A_σ, and a prescribed-displacement boundary A_u (Fig. 1).

By employing the concept of D'Alembert's Principle, the body forces ρB^i may be regarded as consisting of D'Alembert inertia forces ($-\rho \ddot{u}^i$) and other body forces ρf^i (gravitational, magnetic, etc.). Thus one may write

$$\rho B^i = -\rho \ddot{u}^i + \rho f^i \tag{2.2}$$

where $(\dot{})$ denotes partial differentiation with respect to time t.

The nonlinear relation between the Lagrangian strain tensor and the displacement components may be expressed as

$$\gamma_{ij} = \frac{1}{2}\left(u_{i,j} + u_{j,i} + u_{a,i}\, u^a_{,j}\right) \tag{2.3}$$

where $(\,)_{,i}$ denotes covariant differentiation with respect to ξ^j using the metric tensor of the undeformed state. Then, the variation in the strain tensor associated with the displacement variation about the deformed equilibrium configuration may be expressed as

$$\delta\gamma_{ij} = \frac{1}{2}\left[\left(\delta^a_i + u^a_{,i}\right)\delta u_{a,j} + \left(\delta^a_j + u^a_{,j}\right)\delta u_{a,i}\right] \tag{2.4}$$

where δ^a_i is the Kronecker delta.

It should be recalled that this basic variational formulation, the Principle of Virtual Work, holds independently of the material stress-strain relations and the possible existence of potential functions of the external forces. Also, it embodies the equation of equilibrium of the continuum (overall and/or at any generic point):

$$\left[S^{ja}\left(\delta^i_a + u^i_{,a}\right)\right]_{,j} + \rho f^i = \rho \ddot{u}^i \tag{2.5}$$

and the prescribed surface traction boundary condition on A_σ:

$$S^{ja}\left(\delta^i_a + u^i_{,a}\right) n_j = \underset{\sim}{T}^i \tag{2.6}$$

where n_j is the component of the unit outward normal vector to the undeformed boundary surface.

In the finite-element-analysis method, the entire domain of the continuum is subdivided into a finite number of regions called "finite elements" or "discrete elements", each having a finite number of "nodes" as control points

(see Fig. 1). These nodes are usually located at the boundary of each element but may also be in the interior region of the element. The behavior of the actual continuum which has an infinite number of degrees of freedom is thereby described approximately in terms of a finite number of degrees of freedom at each of the finite number of nodes since the generalized displacements within each finite element are expressed in terms of (a) such variables called "generalized degrees of freedom" (q) which are defined at the node points in conjunction with (b) suitably-selected interpolation functions to describe the distribution of each quantity throughout the interior of each finite element. Applying this approach within the framework of the Principle of Virtual Work and D'Alembert's Principle results in a finite-sized system of second-order ordinary differential equations. The unknowns in these equations are the generalized degrees of freedom at each node of the complete assembled discretized structure (or continuum).

Although many different kinds of finite-element models exist (that is, displacement, equilibrium, hybrid, mixed, etc., -- see Ref. 47 for example), the assumed-displacement type of finite-element formulation or model has been chosen for development to analyze the present class of nonlinear transient response problems. A parallel study, of course, could be carried out by using perhaps each of the other types of finite-element models -- and the relative merits of each could be assessed; such an undertaking, however, is beyond the intended scope of this study.

In the assumed-displacement-type of finite-element analysis, the generalized displacements constitute the primary variables. Hence, one selects appropriate interpolation functions "anchored to" control-point values which are the nodal generalized displacements. In choosing appropriate interpolation functions for each finite element to be used in the assembled finite-element array, one should take into account certain "sufficiency conditions" which will insure that the finite-element solution will converge to the exact solution as the continuum is more and more finely subdivided; this matter is discussed in Subsection 3.3.

Let it be assumed that the continuum or structure being analyzed has been subdivided conceptually into n finite elements. Then, one may write Eq. 2.1 as the sum of the contributions from each of the finite elements as follows:

$$\sum_{n=1}^{n} (\delta U)_n = \sum_{n=1}^{n} (\delta W)_n \tag{2.7}$$

where for any element n:

$$(\delta \bar{U}) = \int_{V_m} S^{ij} \delta \gamma_{ij} \, dV \tag{2.7a}$$

$$(\delta \bar{W})_n = \int_{V_m} \rho (-\ddot{u}^i + f^i) \delta u_i \, dV + \int_{A_n} \underset{\sim}{T}^i \delta u_i \, dA \tag{2.7b}$$

In Eqs. 2.7a and 2.7b, V_n is the volume of the nth discrete element, and A_n is the portion of the surface area of element n, over which the surface traction $\underset{\sim}{T}^i$ is prescribed. Both V_n and A_n pertain to the <u>initial undeformed configuration</u>. The summation, Σ, extends over the n elements of the continuum.

If one chooses for each element an assumed displacement field of the form:

$$u_i(\xi^j, t) = \lfloor N_i(\xi^j) \rfloor \{\alpha(t)\} \tag{2.8}$$

where $N_i(\xi^j)$ is an appropriately assumed interpolation function expressed in the coordinates ξ^j of a generic point within the element, and $\{\alpha(t)\}$ represents a set of undetermined independent parameters which are function of time only, it follows that the nodal generalized degrees of freedom which are the nodal generalized displacements, $\{q\}$ are defined in terms of the local coordinate system of each element and can be obtained by substituting the coordinates of the nodal points into Eq. 2.8. Accordingly, one may write

$$\{q\} = [G] \{\alpha\} \tag{2.9}$$

If one takes the same number of displacement parameters as the nodal generalized displacements, the transformation matrix [G] is a square matrix. By inverting Eq. 2.9 for $\{\alpha\}$ and then substituting into Eq. 2.8, one has

$$u_i(\xi^j, t) = \lfloor N_i(\xi^j) \rfloor [G]^{-1} \{q(t)\} = \lfloor U_i(\xi^j) \rfloor \{q\} \quad (2.10)$$

where

$$\lfloor U_i(\xi^j) \rfloor = \lfloor N_i(\xi^j) \rfloor [G]^{-1} \quad (2.10a)$$

Because $N_i(\xi^j)$ and [G] are a priori chosen functions expressed in the ξ^j coordinate only, they are not subjected to variation; hence,

$$\delta u_i = \lfloor U_i \rfloor \{\delta q\} \quad (2.11)$$

Also, the time derivatives of Eq. 2.10 becomes

$$\ddot{u}_i = \lfloor U_i \rfloor \{\ddot{q}\} \quad (2.12)$$

By using Eqs. 2.3 and 2.10, one may obtain the corresponding strain γ_{ij} at any point in the element as a function of position and the nodal generalized displacements as follows:

$$\gamma_{ij} = \lfloor D_{ij} \rfloor \{q\} + \frac{1}{2} \lfloor q \rfloor \{D_{ai}\} \lfloor D_j^a \rfloor \{q\} \quad (2.13)$$

It follows that

$$\delta \gamma_{ij} = \lfloor D_{ij} \rfloor \{\delta q\} + \lfloor q \rfloor \{D_{ai}\} \lfloor D_j^a \rfloor \{\delta q\} \quad (2.14)$$

where D_{ij}, D_{ai}, and D_j^a are the appropriate associated differential operators which include both small and large deflection effects and which may be expressed symbolically in the form*

$$\lfloor D_{ij} \rfloor = \frac{1}{2} \lfloor U_{i,j} + U_{j,i} \rfloor$$

$$\lfloor D_{ai} \rfloor = \lfloor U_{a,i} \rfloor \qquad \lfloor D_j^a \rfloor = \lfloor U_{,j}^a \rfloor \quad (2.15)$$

*Explicit examples are given in Section 3.

Employing Eqs. 2.10 through 2.15, Eqs. 2.7 becomes

$$\sum_{n=1}^{n} \lfloor \delta q \rfloor \left(\int_{V_m} \{D_{ij}\} S^{ij} \, dV + \int_{V_m} \{D_{ai}\} \lfloor D_j^a \rfloor S^{ij} \, dV \{q\} \right.$$

$$\left. - \int_{V_n} \rho \{U_i\} f^i \, dV - \int_{A_n} \{U_i\}_b \underset{\sim}{T}^i \, dA + \int_{V_m} \{U_i\} \rho \lfloor U^i \rfloor dV \{\ddot{q}\} \right) = 0 \qquad (2.16)$$

where subscript "b" is used to signify that the $\{U_i\}$ are evaluated along the element boundaries.

Equation 2.16 is a convenient finite-element form of the Principle of Virtual Work and D'Alembert's Principle, from which one can write (a) an unconventional form or (b) a conventional form of the equation of motion; these forms are presented separately in Subsections 2.2 and 2.3, respectively.

2.2 Unconventional Formulation

Equation 2.16 may be written more compactly as follows representing a so-called "unconventional formulation":

$$\sum_{n=1}^{n} \lfloor \delta q \rfloor \left([m] \{\ddot{q}\} + \{p\} + [h] \{q\} - \{f\} \right) = 0 \qquad (2.17)$$

where the following are evaluated for each finite element:

$$[m] = \int_{V_m} \{U_i\} \rho \lfloor U^i \rfloor dV \qquad (2.17a)$$

$$\{p\} = \int_{V_m} \{D_{ij}\} S^{ij} \, dV \qquad (2.17b)$$

$$[h] = \int_{V_m} \{D_{ai}\} \lfloor D_j^a \rfloor S^{ij} \, dV \qquad (2.17c)$$

$$\{f\} = \int_{V_m} \rho \{U_i\} f^i \, dV + \int_{A_n} \{U_i\}_b \underset{\sim}{T}^i \, dA \qquad (2.17d)$$

Note that {p} and [h] involve stress information throughout the undeformed volume of each finite element.

Since the element nodal generalized displacements {q} for different elements are not completely independent, a transformation is required to relate the element nodal displacements to independent global (or common) nodal generalized displacements {q*} for the discrete-element assemblage by

$$\{q\} = [J]\{q^*\} \tag{2.18}$$

The quantity [J] includes the effect of transferring from local coordinates for each individual element to global reference coordinates for the system as a whole.

Applying Eq. 2.18 to Eq. 2.17 to describe the system in terms of the independent global generalized displacements {q*}, one obtains:

$$\sum_{n=1}^{n} \{\delta q^*\}^T \left([m^*]\{\ddot{q}^*\} + \{p^*\} + [h^*]\{q^*\} - \{f^*\} \right) = 0 \tag{2.19}$$

where

$$[m^*] = [J]^T [m] [J] \tag{2.19a}$$

$$\{p^*\} = [J]^T \{p\} \tag{2.19b}$$

$$[h^*] = [J]^T [h] [J] \tag{2.19c}$$

$$\{f^*\} = [J]^T \{f\} \tag{2.19d}$$

Performing the summation in Eq. 2.19 and because the {δq*} are independent and arbitrary, the following unconventional equations of motion are obtained for the complete assembled discretized structure (or continuum):

$$[M]\{\ddot{q}^*\} + \{P\} + [H]\{q^*\} = \{F\} \tag{2.20}$$

where [M] is the global mass matrix, [H] {q*} represents "forces" associated with large deflections (nonlinear terms in the strain-displacement relations) and plastic effects[+], {P} represents internal elastic forces, plastic forces, and some plasticity effects associated with the linear terms of the strain-displacement relations[+], and {F} represents the generalized nodal load vector accounting for externally-applied distributed or concentrated loads (see Eq. 2.17a). In terms of element information, [M], {P}, [H], and {F}, may be expressed as:

$$[M] = \begin{bmatrix} \underset{\sim}{m}_1^* & & & \\ & \underset{\sim}{m}_2^* & & \\ & & \ddots & \\ & & & \underset{\sim}{m}_n^* \end{bmatrix} \tag{2.20a}$$

$$\{P\} = \{ \underset{\sim}{P}_1^* \ \underset{\sim}{P}_2^* \ \cdots\cdots \ \underset{\sim}{P}_n^* \} \tag{2.20b}$$

$$[H] = \begin{bmatrix} \underset{\sim}{h}_1^* & & & \\ & \underset{\sim}{h}_2^* & & \\ & & \ddots & \\ & & & \underset{\sim}{h}_m^* \end{bmatrix} \tag{2.20c}$$

$$\{F\} = \{ \underset{\sim}{f}_1^* \ \underset{\sim}{f}_2^* \ \cdots\cdots \ \underset{\sim}{f}_n^* \} \tag{2.20d}$$

2.3 Conventional Formulation

The conventional form of the equations of motion corresponding to Eq. 2.20 may be obtained by applying Eq. 2.18 to Eq. 2.16 and by replacing the stress tensor S^{ij} in Eq. 2.16 by the following expression in terms of the strains $\gamma_{k\ell}$ (via the stress-strain relations and the strain-displacement relations):

[+]See Ref. 17, page 50.

$$S^{ij} = E^{ijkl}\left(\gamma_{kl} - \gamma_{kl}^{P}\right) =$$

$$= E^{ijkl}\left(\left[D_{kl}\right]\{q\} + \frac{1}{2}\left[q\right]\left\{D_{ck}\right\}\left[D_{l}^{c}\right]\{q\} - \gamma_{kl}^{P}\right) \tag{2.21}$$

where E^{ijkl} consists of elastic constants and γ_{kl}^{p} represents the components of the total plastic strain (or other given initial strain such as thermal strain, etc.). Applying Eqs. 2.18 and 2.21 to Eq. 2.16 one obtains:

$$\sum_{n=1}^{n}\left[\delta q^{*}\right]\left([m]\{\ddot{q}^{*}\} + [K]\{q^{*}\} - \{f\} - \{f_{q}^{NL}\} - \{f_{P}^{L}\} - \{f_{P}^{NL}\}\right) = 0 \tag{2.22}$$

where

$$[m] = [J]^{T}\int_{V_m}\{\bar{U}_i\}\,\rho\left[\bar{U}^{i}\right]dV\,[J]$$

$$[K] = [J]^{T}\int_{V_m}\{D_{ij}\}\,E^{ijkl}\left[D_{kl}\right]dV\,[J]$$

$$\{f\} = [J]^{T}\left(\int_{V_m}\rho\{U_i\}f^{i}dV + \int_{A_n}\{U_i\}_{b}\,\underset{\sim}{T}^{i}dA\right)$$

$$\{f_{q}^{NL}\} = [J]^{T}\left(-\int_{V_m}\{D_{ij}\}E^{ijkl}\left[\left[q\right]\{D_{ck}\}\left[D_{l}^{c}\right]\{q\}\frac{1}{2}\right]dV\right.$$

$$\left. -\int_{V_m}\{D_{ai}\}\left[D_{j}^{a}\right]E^{ijkl}\left[\left[D_{kl}\right]\{q\} + \left[q\right]\{D_{ck}\}\left[D_{l}^{c}\right]\{q\}\frac{1}{2}\right]dV\{q\}\right)$$

$$\{f_{P}^{L}\} = [J]^{T}\int_{V_m}\{D_{ij}\}\,E^{ijkl}\,\gamma_{kl}^{P}\,dV$$

$$\{f_{P}^{NL}\} = [J]^{T}\int_{V_m}\{D_{ai}\}\left[D_{j}^{a}\right]E^{ijkl}\,\gamma_{kl}^{P}\,dV\{q\} \tag{2.22a}$$

Performing the summation and because the variation $\{\delta q^*\}$ can be independent and arbitrary, the following conventional equilibrium equation is obtained:

$$[M]\{\ddot{q}^*\} + [K]\{q^*\} = \{F\} + \{F_q^{NL}\} + \{F_p^{L}\} + \{F_p^{NL}\} \quad (2.23)$$

where [M] is the global mass matrix, [K] is the usual global stiffness matrix (for linear-elastic small deflection behavior), {F} is the generalized nodal load vector representing externally applied distributed or concentrated loads, $\{F_q^{NL}\}$ represents a "generalized loads" vector arising from large deflections and is a function of quadratic and cubic displacement terms, $\{F_p^{L}\}$ and $\{F_p^{NL}\}$ are the generalized load vectors due to the presence of plastic strains and are associated, respectively, with the linear and nonlinear terms of the strain-displacement relations.

Equation 2.23 represents the so-called "conventional" formulation of the equation of motion for nonlinear responses, where the large deflection and plastic effects are taken into account through the use of generalized (or pseudo) loads which are functions of plastic strains and displacement.

2.4 Timewise Solution of the Governing Equations

Given a set of initial conditions $\{q^*\}_o$ and $\{\dot{q}^*\}_o$ at time t=0 and the proper boundary conditions, one may solve the system of second order differential equations represented by:

(a) Eq. 2.20: Unconventional Form

or

(b) Eq. 2.23: Conventional Form

in a step-by-step timewise fashion by using an appropriate finite-difference time operator.

Various timewise integration operators have been devised and can be divided conveniently into two types; one is of the explicit type (the central difference operator, for example) and the other is of the implicit type (for example, the Newmark operator, the Houbolt operator, etc.). If an implicit operator were used, an iterative solution of the nonlinear dynamic equations would be necessary, in principle, at each time step. This may require an excessive amount of computing time and cause the method to become impractical. However, the use of (a) an extrapolation method, (b) an explicit operator, or

(c) an implicit operator in conjunction with an explicit operator (predictor-corrector method) can be used readily. Some of these operators introduce artificial (false) damping, whereas others do not exhibit this undesirable feature. Also, almost all of these operators produce a phase-shift error in the predicted responses and the magnitude of this error depends upon the size of the time increment, Δt.

The selection of a suitable time increment size in the direct integration scheme is governed by (a) the stability criterion -- the condition under which the exponential error growth will be bounded, and (b) the convergence requirement -- the closeness of the temporal discretization solution to the exact differential solution as the timewise discretization mesh decreases. Although the criteria for stability of each of the commonly used time integration operators have been established definitively when applied to a linear dynamic system, no similar assessment is known to have been made for these methods when applied to nonlinear structural response problems involving large deflection and inelastic material behavior. Various of these methods, however, have been applied to such problems -- with Δt values guided by the stability and convergence behavior of a corresponding linear dynamic system as an initial selection; numerical experimentation then subsequently can provide the suitably small Δt to insure stability and convergence. Numerical experiments involving nonlinear large deflection transient responses of structures such that increased stiffening from geometric large deflection effects occurs, have shown that the "critical Δt" of a conditionally stable operator is smaller than for the linear case; further, all of the operators (thus far studied) which are unconditionally stable for the linear system become either conditionally stable or at least provide degraded (grossly inaccurate) solutions for the nonlinear problems if the time step Δt is too large [17,24].

Studies reported in Ref. 17 using both the unconventional and the conventional formulation for large-deflection elastic-plastic transient response problems indicate excellent agreement between predictions from these two formulations; in those comparisons the conditionally-stable explicit 3-point central-difference time operator was employed. However, it was noted that the unconventional formulation is much simplified compared with the conventional

formulation, and also requires less computer storage and fewer manipulations. In view of these advantages, it was decided for the purposes of this present study to employ only the unconventional formulation in conjunction with the central-difference time operator. Accordingly, the associated timewise solution process is described in the following.

2.4.1 Solution Process

Equation 2.20 is to be solved at a sequence of instants in time Δt apart by employing the following explicit, conditionally-stable, central difference, finite-difference time operator approximation for the acceleration $\ddot{q}_m$ at time t_m:

$$\ddot{q}_m = \frac{q_{m+1} - 2q_m + q_{m-1}}{(\Delta t)^2} + O(\Delta t)^2 \qquad (2.24a)$$

where $O(\Delta t)^2$ means that this finite-difference approximation has a truncation error of order $(\Delta t)^2$. Also, one may approximate the velocity $\dot{q}_m$ at time t_m by:

$$\dot{q}_m = \frac{q_{m+1} - q_{m-1}}{2(\Delta t)} + O(\Delta t)^2 \qquad (2.24b)$$

At time instant t_m the equations of motion (Eq. 20) become:

$$[M]\{\ddot{q}^*_m\} + \{P\}_m + [H]_m\{q^*\}_m = \{F\}_m \qquad (2.25)$$

In Eq. 2.25, all quantities, in general, except [M] change with time. If the solution of Eq. 2.25 has been obtained for earlier times, one can compute $\{\ddot{q}^*\}_m$ from Eq. 2.25 and then obtain $\{q^*\}_{m+1}$ from Eq. 2.24a.

Assuming that at t=0 the structure is in a known condition $\{q^*\}_o=0$ and $\{\dot{q}^*\}_o=\{a\}$, for example, one can readily obtain $\{q^*\}_1$ at $t=m\Delta t$ for m=1 from the following Taylor series expansion:

$$\{q^*\}_1 = \{q^*\}_o + \{\dot{q}^*\}_o \Delta t + \frac{1}{2}\{\ddot{q}^*\}_o (\Delta t)^2 + O(\Delta t)^3 \qquad (2.26)$$

since $\{F\}_o$ is prescribed and all other quantities are known.

In the timewise step-by-step solution process involving large-deflection elastic-plastic transient responses, $\{P\}_m$ and $[H]_m$ change with time and hence must be reevaluated, in general, at each instant in time. These quantities in turn are composed by assembling the contributions $\{p^*\}_m$ and $[h^*]_m$ from each finite element; see Eqs. 2.17b, 2.17c, 2.19b, and 2.19c. It is seen that these quantities involve <u>volume</u> integrals of information involving the stress state S^{ij}. In practice, these evaluations are carried out by appropriate numerical integration -- usually Gaussian quadrature.

At any instant in time t_m (m=0,1,2,...), one needs to solve Eq. 2.25 for $\{\ddot{q}^*\}_m$, which is of the form:

$$[M]\{x(t)\}_m = \{b(t)\}_m \qquad \text{for} \quad m = 0,1,2\ldots \tag{2.27}$$

where

[M]	is a <u>known</u> banded positive definite symmetric matrix (the mass matrix for the restrained or unrestrained structure, whichever case is being treated)
$\{x(t)\}_m$	is a vector of unknowns which must be determined by solving Eq. 2.27
$\{b(t)\}_m$ is	is a known vector (representing all terms except $[M]\{\ddot{q}^*\}_m$ in Eq. 2.25)

In principle, one can always form the inverse matrix $[M]^{-1}$ and pre-multiply Eq. 2.27 by $[M]^{-1}$ to obtain

$$[M]^{-1}[M]\{x(t)\}_m = [M]^{-1}\{b(t)\}$$

which results in the solution:

$$\{x(t)\}_m = [M]^{-1}\{b(t)\} \tag{2.28}$$

since $[M]^{-1}[M] = [I]$ where [I] is the unit diagonal matrix. However, it has been found that independent of the number of time instants at which one wishes to solve Eq. 2.27 such a procedure is not as efficient as is the Choleski method [48].

Briefly, the Choleski method involves factoring the matrix [M] to form a lower triangular matrix [L] and an upper triangular matrix (which is the transpose of the former) such that $[M] = [L]\,[L]^T$ where $[L]^T$ is the transpose of [L]. Thus, Eq. 2.27 may be rewritten as

$$[L][L]^T \{x(t)\}_m = \{b(t)\}_m \tag{2.29}$$

Next, form an intermediate matrix $\{y\}_m$ which is defined as

$$\{y\}_m = [L]^T \{x(t)\}_m \tag{2.30}$$

From Eqs. 2.29 and 2.30, it follows that

$$[L]\{y\}_m = \{b(t)\} \tag{2.31}$$

At each time instant, one solves Eq. 2.31 for $\{y\}_m$ very readily because [L] is a lower triangular matrix. One then solves Eq. 2.30 for $\{x\}_m$ very rapidly also by algebraic back-substitution.

The following gives a concise step-by-step description of the typical problem formulation and solution process.

Starting from a set of given initial conditions at time $t = t_o = 0$ on the generalized displacements ($\{q^*\} = \{0\}$, for example) and the generalized velocities $\{\dot{q}\}_o$, one can solve Eq. 2.25 for $\{\ddot{q}^*\}_o$ at time t_o and then employ Eq. 2.26 to compute $\{q^*\}_1$. A slightly different but similar procedure is then used to advance the solution in successive time increments Δt. The process involved in using the finite-element method and the present timewise solution procedure follows (see the information flow chart of Fig. 2):

Step 1: Construct the mass matrix [m] for each finite element and then assemble these contributions according to Eq. 2.20a to form the mass matrix [M] for the complete assembled discretized structure. This [M] represents the "final" mass matrix if the stucture has none of of its generalized displacements constrained (that is, held equal to zero, for example); however, if such constraints exist, one forms a reduced or constrained mass matrix (and, in fact, a reduced set

of the equations of motion) by deleting the rows and columns of [M] associated with those generalized displacements which are prescribed to be zero.

Next, this constrained mass matrix is factorized to consist of a lower triangular matrix [L] and an upper triangular matrix $[L]^T$ according to the Choleski scheme:

$$[M] = [L][L]^T \tag{2.32}$$

Since [M] does not change in value with time as the transient structural response proceeds, one needs to determine [L] and $[L]^T$ only once -- these quantities need not be re-evaluated at each time step of the calculation.

Step 2: The prescribed externally-applied transient forces can be employed to calculate the generalized applied forces $\{f^*\}$ acting on each discrete element at each time instant t_m of interest. These, in turn, can be assembled according to Eq. 2.20d to form the assembled applied-loads vector $\{F^*\}$ for the complete assembled discretized structure.

Step 3: Assuming that at zero time (t = 0), the generalized displacements $\{q^*\}_o = 0$, the generalized velocities are nonzero $\{\dot{q}^*\}_o = \{a\}$, and that nonzero external forces $\{F^*\}_o$ are present. In this case, Eq. 2.25 becomes

$$[M]\{\ddot{q}^*\}_o = \{F^*\}_o \tag{2.33}$$

or

$$[L][L]^T\{\ddot{q}^*\}_o = \{F^*\}_o \tag{2.33a}$$

from which one can calculate $\{\ddot{q}^*\}_o$ by using the earlier-described Choleski scheme. Then from Eq. 2.26 one obtains

$$\left\{\Delta q^*\right\}_1 = \frac{1}{2}(\Delta t)^2\left\{\ddot{q}^*\right\}_0 + \Delta t\left\{\dot{q}^*\right\}_0 \tag{2.34}$$

where

$$\left\{\Delta q^*\right\}_1 \equiv \left\{q^*\right\}_1 - \left\{q^*\right\}_0 \tag{2.35}$$

$\left\{\dot{q}^*\right\}_0 = \{a\}$ = prescribed initial generalized velocities (2.35a)

Also,

$$\left\{q^*\right\}_1 = \left\{q^*\right\}_0 + \left\{\Delta q^*\right\}_1 \tag{2.36}$$

For this case, however, it has been assumed that $\{q^*\}_0 = \{0\}$. Thus the displacement configuration $\{q^*\}_1$ at time $t_1 = t_o + \Delta t$ is known.

Step 4: Knowing the generalized nodal displacement increments $\{\Delta q^*\}_1 \equiv \{q^*\}_1 - \{q^*\}_o$ and the generalized nodal displacements $\{q^*\}_1$ at time t_1, one knows also the unstarred individual element quantities $\{\Delta q\}_1$ and $\{q\}_1$ via Eq. 2.18. Hence, one can calculate the strain increment $(\Delta\gamma_{ij})_1$ developed from time t_o to t_1 at every Gaussian station (or point) required over and depthwise through each finite element from Eq. 2.13:

$$\left(\Delta\gamma_{ij}\right)_1 \equiv \left(\gamma_{ij}\right)_1 - \left(\gamma_{ij}\right)_0$$

$$= \left[D_{ij}\right]\left\{\Delta q\right\}_1 + \left[q\right]_1\left\{D_{ai}\right\}\left[D_j^a\right]\left\{\Delta q\right\}_1 - \frac{1}{2}\left[\Delta q\right]_1\left\{D_{ai}\right\}\left[D_j^a\right]\left\{\Delta q\right\} \tag{2.37}$$

With a knowledge of (a) the stresses at $t_o = t_1 - \Delta t$, and (b) the strain increment $(\Delta\gamma_{ij})_1$, one can determine the stress increments $(\Delta S^{ij})_1$ and the stresses $(S^{ij})_1$ at time t_1 at each Gaussian station by using the pertinent elastic-plastic stress-

strain relations, including the yield condition and flow rule (this matter is discussed in detail in Subsection 2.4.2).

Step 5: Next, one can calculate $\{p\}_1$ and $[h]_1$ for each individual finite element by using Eqs. 2.17b and 2.17c, respectively. Assembly of this information according to Eqs. 2.20b and 2.20c, respectively, provides $\{P\}_1$ and $[H]_1$. Since the prescribed generalized force vector $\{F\}_1$ is available from known $\{f\}_1$ information, the equation of motion, Eq. 2.25, at time instant t_1 becomes:

$$[M]\{\ddot{q}^*\}_1 = \{F^*\}_1 - \{P\}_1 - [H]_1\{q^*\}_1 \tag{2.38}$$

In the interest of minimizing computer storage and the number of manipulations, one first forms for each individual element $\{b_n\}_1 \equiv (\{f\} - \{p\} - [h]\{q\})_1$. Then one forms the right-hand side vector of Eq. 2.38 by

$$[J]^T \{\underset{\sim}{b}_1\ \underset{\sim}{b}_2 \cdots\cdots \underset{\sim}{b}_N\}_1 \tag{2.39}$$

For clarity of discussion, however, the form of the equation represented by Eq. 2.38 is used here.

Step 6: Since the right-hand side of Eq. 2.38 is now known, one can use the Choleski scheme to solve the following equation for the acceleration $\{\ddot{q}^*\}_1$:

$$[L][L]^T\{\ddot{q}^*\}_1 = \left(\{F\} - \{P\} - [H]\{q^*\}\right)_1 \tag{2.39a}$$

Step 7: With $\{\ddot{q}^*\}$ now known, one can calculate the generalized displacement increment $\{\Delta q^*\}_2$ from Eq. 2.24a as

$$\{\Delta q^*\}_2 = \{\Delta q^*\}_1 + (\Delta t)^2\{\ddot{q}^*\}_1 \tag{2.39b}$$

where

$$\{\Delta q^*\}_2 = \{q^*\}_2 - \{q^*\}_1 \tag{2.40a}$$

$$\{\Delta q^*\}_1 = \{q^*\}_1 - \{q^*\}_0 \tag{2.40b}$$

Thus, from Eq. 2.40a one has

$$\{q^*\}_2 = \{q^*\}_1 + \{\Delta q^*\}_2 \tag{2.41}$$

The process then proceeds cyclically from Step 4 onwards for as many time steps as desired.

For the central-difference time operator applied to a system of equations such as Eq. 2.20 or Eq. 2.23, it has been shown [49,50] that Δt must be less than or equal to $2/\omega_{max}$ to avoid exponential growth of error (round-off, truncation, gross) where ω_{max} is the largest frequency embedded in the mathematical model of the system. The criterion $\Delta t < 2/\omega_{max}$ must be satisfied for a linear dynamic system such as that involving small-displacement linear-elastic behavior. However, for nonlinear large-displacement elastic or elastic-plastic behavior, numerical experimentation [17, for example] has confirmed that a smaller Δt is usually required to avoid this instability. As a rough guide one may try $\Delta t \lesssim 0.8(2/\omega_{max})$ as an initial selection; if this value is not small enough, the calculation will blow up (overflow) before many time steps have elapsed -- this behavior will be readily apparent. In such a case one must choose a smaller time increment Δt.

2.4.2 Evaluation of Stresses and Plastic Strains

There are two types of common plasticity theories, termed "flow" and "deformation" [43,51]. The deformation theory of plasticity assumes that, as in elasticity, there exists a one-to-one correspondence between stress and strain. The flow theory of plasticity states that there is a functional relation between the incremental stress and the incremental strain. Only for proportional loading where the stress ratio remains constant, and for a certain restricted range of loading paths other than

proportional loading [52] (through the assumption of the possibility of singularity in the yield surface) does the deformation theory agree with the flow theory. In order to include the capability to analyze general loading paths including loading, unloading, and cyclic loading, the "flow-type" theory will be incorporated into the present analysis.

The behavior of a general elastic-plastic material can be characterized by the following two ingredients. First, assume the existence of a boundary (yielding surface) in stress space which defines the elastic domain. Within the boundary the continuum deforms elastically. Only at the boundary, the onset of plastic flow (irreversible deformation in a thermodynamic sense) is possible and no meaning is associated with the region that is beyond the boundary. Second, one employs a flow rule which describes the behavior of the material after yielding has started; it gives the relation of plastic flow (strain increments) to the stress (or stress increment) and the loading history.

Another basic assumption in the theory of an elastic-plastic continuum is the introduction of a plastic strain tensor. The plastic strain tensor, γ_{ij}^{p}, is assumed to have the same invariance properties as does the Lagrangian strain tensor, γ_{ij}. The quantity γ_{ij}^{p} is related to γ_{ij} by an elastic strain tensor γ_{ij}^{e}, in the form [53]:

$$\gamma_{ij} = \gamma_{ij}^{e} + \gamma_{ij}^{p} \tag{2.42}$$

No kinematic meaning is given to γ_{ij}^{e} and γ_{ij}^{p}, but only their sum, γ_{ij} is related to displacements by Eq. 2.3.

Various yield criteria and flow rules have been suggested for the predictions of the onset of plastic flow and the relation among plastic flow, stress, and stress history [43,51]. Among them is the Mises-Hencky yield criterion and its associated flow rule which usually show close agreement with experimental observations and yet is mathematically simple. The Mises-Hencky rules will be adopted in the present analysis.

The Mises-Hencky yield criterion may be interpreted physically as "yielding begins whenever the distortion energy equals the distortion energy at yield in simple tension". Thus, hydrostatic pressure, for an isotropic material, (tension or compression) does not affect the yielding, plastic flow,

and resultant hardening. Stated otherwise, no plastic work is done by the hydrostatic component of the applied stress. This implies that there is no plastic (or irreversible) change in volume. Thus,

$$\left(\dot{\gamma}_{ii}\right)^{P}=0 \qquad \text{or} \qquad \left(\dot{\gamma}_{ij}\right)^{Sp}=0 \tag{2.43}$$

where $(\dot{\gamma}_{ij})^{Sp}$ is the spherical plastic strain-rate tensor. For an initially isotropic material, the Mises-Hencky yield function can be written in the form

$$\Phi = I_2^D - \frac{1}{3}\sigma_o^2 = 0 \tag{2.44}$$

where

$$I_2^D = \frac{1}{2}\left(S_j^i\right)^D\left(S_i^j\right)^D = \frac{1}{2}\left[S_j^i S_i^j - \frac{1}{3}\left(S_a^a\right)^2\right] \tag{2.44a}$$

$(S_j^i)^D$ is the deviatoric stress tensor of S_j^i in mixed component form.

σ_o is the yield stress in simple tension.

The associated flow rule can be expressed as

$$\left(\dot{\gamma}_j^i\right)^{Dp} = \dot{\lambda}\left(\frac{\partial \Phi}{\partial S_i^j}\right) = \dot{\lambda}\left(S_j^i\right)^D \tag{2.45}$$

where $(\dot{\gamma}_j^i)^{Dp}$ is the deviatoric plastic strain-rate tensor and $\dot{\lambda}$ is a real non-negative scalar quantity.

For certain materials, the yield surface will change in case of continued straining beyond the initial yield. The change of the yield surface (called subsequent yield function) that characterizes the strain hardening (or work hardening) behavior of the material depends on the loading history. In the present analysis, the strain-hardening behavior of the material will be accounted for by using the well-known "mechanical sublayer model" [54,55, 56]. A useful feature of this model is the inclusion of kinematic hardening and the Bauschinger effect. In this model, the material at any point is conceived of as consisting of "sublayers"; each sublayer behaves as an elastic,

perfectly-plastic medium, having a common strain and a common elastic modulus but appropriately different yield stresses. For the sake of the present report's being self-contained and for the reader's convenience, this model will be described in detail in Appendix A.

For some engineering materials, the uniaxial stress-strain curve of dynamic loading tests will usually be different from those of static tests. The yield stress frequently increases with the increase of strain rate. However, this strain-rate effect arises in a less understood fashion.

One of the simple methods for approximating the strain-rate effect and which is in good agreement with experiments on certain types of common metals and alloys is to assume that the uniaxial stress-strain curve is affected by strain-rate only by a quasi-steady increase in the yield stress above the "static" test yield stress and that the elastic deformation is independent of strain rate. The increase in the yield stress under strain rate may be expressed in the following simple form [57]:

$$\sigma_y = \sigma_o \left(1 + \left| \frac{\dot{\varepsilon}}{D} \right|^{\frac{1}{p}} \right) \tag{2.46}$$

where

σ_o is the static yield stress

$\dot{\varepsilon}$ is the uniaxial strain rate

D and p are empirically-determined constants for the material

σ_y is the yield stress under $\dot{\varepsilon}$

A convenient way to compute the stress increment and/or plastic strain increment at any station (such as Gaussian, for example) in each element at time t_{m+1}, as discussed in Ref. 58 will be presented. Also, because the "mechanical sublayer material model" is adopted, the only constitutive relation utilized is that for a homogeneous, initially isotropic, elastic, perfectly-plastic, strain-rate dependent solid; strain hardening is automatically accommodated by this model which includes kinematic hardening and the Bauschinger effect.

It is assumed that all stresses and strains are known at time t_{m_i} and that all displacements are known at time t_{m+1}. To find the stresses $(S_j^i)_{m+1}$

at time t_{m+1}, one begins by assuming that the strain increment $(\Delta\gamma^i_j)_{m+1}$ from time t_m to time t_{m+1} as calculated by Eq. 2.41, is entirely elastic, and a trial (superscript T) value of stress increment is calculated from the following relation:

$$\left(\Delta S^i_j\right)^T_{m+1} = \frac{E}{1+\nu}\left[\left(\Delta\gamma^i_j\right)_{m+1} + \frac{\nu}{1-2\nu}\left(\Delta\gamma^k_k\right)_{m+1}\delta^i_j\right] \tag{2.47}$$

where E is Young's modulus, ν is Poisson's ratio and δ^i_j is the Kronecker delta. Hence, the trial stresses at time t_{m+1} are given by

$$\left(S^i_j\right)^T_{m+1} = \left(S^i_j\right)_m + \left(\Delta S^i_j\right)^T_{m+1} \tag{2.48}$$

Then a check is performed by substituting this trial value of the stress into the Mises-Hencky yield function, Φ of Eq. 2.44, to determine whether or not the trial stress state lies inside of the yield surface. Thus one may write

$$\underline{\Phi}^T_{m+1} = \left\{\left(S^i_j\right)^T_{m+1}\left(S^j_i\right)^T_{m+1} - \frac{1}{3}\left[\left(S^k_k\right)^T_{m+1}\right]^2\right\} - \frac{2}{3}\sigma_y^2 \tag{2.49}$$

where σ_y is the appropriately known uniaxial yield stress of a given mechanical sublayer of the material-behavioral model.

If $\Phi^T_{m+1} \leq 0$, the trial stress state lies within the elastic domain bounded by the yield surface or lies exactly on the yield surface. Therefore, for this time step there has been no plastic flow and the actual stress increments did, in fact, arise from wholly-elastic behavior as initially assumed in the trial examination. Hence, the actual stress $(S^i_j)_{m+1}$ is equal to the trial stress; thus,

$$\left(S^i_j\right)_{m+1} = \left(S^i_j\right)^T_{m+1} \tag{2.50}$$

and the plastic strain state has not changed from the previous time instant:

$$\left(\gamma^i_j\right)^P_{m+1} = \left(\gamma^i_j\right)^P_m \tag{2.51}$$

However, if $\Phi^{T}_{m+1} > 0$, the trial stress state lies outside of the yield surface (i.e., in the undefined region). Therefore, the trial assumption that the entire strain increment is an elastic-strain increment is not valid. Plastic flow has occurred within this time step and the actual stress state must lie on the yield surface according to the theory of perfect plasticity; then the calculation proceeds as follows. The total strain increment may be decomposed into elastic and plastic components

$$\left(\Delta \gamma^{i}_{j}\right)_{m+1} = \left(\Delta \gamma^{i}_{j}\right)^{e}_{m+1} + \left(\Delta \gamma^{i}_{j}\right)^{P}_{m+1} \qquad (2.52)$$

Since the material is assumed to be incompressible with regard to plasticity and by the flow rule Eq. 2.45, one has the following relation in finite-increment form:

$$\left(\Delta \gamma^{i}_{j}\right)^{P}_{m+1} = \left(\Delta \gamma^{i}_{j}\right)^{Dp}_{m+1} = \left(\tilde{S}^{i}_{j}\right)^{D} \Delta \lambda \qquad (2.53)$$

where $(\Delta\gamma^{i}_{j})^{Dp}$ is the deviatoric component of the plastic strain increment, $\Delta\lambda$ is a real non-negative scalar quantity of proportionality and $(\tilde{S}^{i}_{j})^{D}$ represents the deviatoric stress component of an appropriate stress state between time t_m and time t_{m+1}. One may approximate $(\tilde{S}^{i}_{j})^{D}$ by using the deviatoric stress component of either the stress state at t_m, $(S^{i}_{j})^{D}_{m}$, or the yet to-be-determined stress state at t_{m+1}, $(S^{i}_{j})^{D}_{m+1}$, or any intermediate state between the two such as the trial stress state, $(S^{i}_{j})^{DT}_{m+1}$ adopted in Refs. 58 and 59. For infinitesimal incremental changes between two states, these approximation would not lead to any significant differences of the predictions among one another. However, for finite (or large) incremental changes, the use of $(S^{i}_{j})^{D}_{m}$ has been found in Ref. 60 to be more accurate than using $(S^{i}_{j})^{DT}_{m+1}$ for states of two-dimensional stress. Therefore, the present analysis will employ the relation

$$\left(\Delta \gamma^{i}_{j}\right)^{P}_{m+1} = \left(S^{i}_{j}\right)^{D}_{m} \Delta \lambda \qquad (2.53a)$$

Consequently, the stress increment from time t_m to t_{m+1} is

$$\left(\Delta S_j^i\right)_{m+1} = \frac{E}{1+\nu}\left[\left(\Delta\gamma_j^i\right)_{m+1} + \frac{\nu}{1-2\nu}\left(\Delta\gamma_k^k\right)\delta_j^i - \left(S_j^i\right)_m^D \Delta\lambda\right] \quad (2.54)$$

and the actual stress at time t_{m+1} is

$$\left(S_j^i\right)_{m+1} = \left(S_j^i\right)_m + \left(\Delta S_j^i\right)_{m+1} = \left(S_j^i\right)_{m+1}^T - \left(S_j^i\right)_m^D \Delta\lambda^* \quad (2.55)$$

The plastic strain at time t_{m+1} is

$$\left(\gamma_j^i\right)_{m+1}^P = \left(\gamma_j^i\right)_m^P + \left(S_j^i\right)_m^D \Delta\lambda \quad (2.56)$$

The quantity $\Delta\lambda$ and $\Delta\lambda^*(\equiv \Delta\lambda E/1+\nu)$ in Eqs. 2.55 and 2.56 can be determined from the fact that $(S_j^i)_{m+1}$ must satisfy the yield condition:

$$\Phi_{m+1} = \left[\left(S_j^i\right)_{m+1}\left(S_i^j\right)_{m+1} - \frac{1}{3}\left(S_k^k\right)_{m+1}^2\right] - \frac{2}{3}\sigma_y^2 = 0 \quad (2.57)$$

Substituting Eq. 2.55 into Eq. 2.57 and solving for $\Delta\lambda^*$ one obtains the physically valid value

$$\Delta\lambda^* = \frac{C}{B + \sqrt{B^2 - AC}} \quad (2.58)$$

where

$$A = \left(S_j^i\right)_m^D \left(S_i^j\right)_m^D - \frac{1}{3}\left[\left(S_k^k\right)_m^D\right]^2$$

$$B = \left(S_j^i\right)_{m+1}^T \left(S_i^j\right)_m^D - \frac{1}{3}\left(S_k^k\right)_{m+1}^T \left(S_k^k\right)_m^D$$

$$C = \Phi_{m+1}^T = \left(S_j^i\right)_{m+1}^T \left(S_i^j\right)_{m+1}^T - \frac{1}{3}\left[\left(S_k^k\right)_{m+1}^T\right]^2 - \frac{2}{3}\sigma_y^2 \quad (2.58a)$$

and the following requirements must be satisfied:

$$B^2 - AC \geq 0$$

$$B + \sqrt{B^2 - AC} > 0 \qquad (2.58b)$$

The preceding discussion has pertained to the use of elastic, perfectly-plastic rate-independent material whose uniaxial yield stress is $\sigma_y \equiv \sigma_o$, the static value. If the yield stress is rate dependent, the same procedure applies except that the yield stress σ_y in Eqs. 2.49 and 2.57 is the strain-rate dependent yield stress. It perhaps should be noted that the strain-rate dependence relation as expressed by Eq. 2.46 is valid, strictly speaking, only for the uniaxial behavior. To generalize this rate dependence equation to three-dimensional behavior, various expressions for $\dot{\varepsilon}$ have been proposed [58, for example]. One such suggestion is to replace $\dot{\varepsilon}$ by the second invariant of the deviatoric strain-rate tensor; thus

$$\dot{\mathcal{E}} = \sqrt{\frac{3}{2}\left[\dot{\gamma}^i_j \dot{\gamma}^j_i - \frac{1}{3}\left(\dot{\gamma}^k_k\right)^2\right]} \qquad (2.59)$$

where the strain-rate components $\dot{\gamma}^i_j$ are given by $\dot{\gamma}^i_j = (\Delta\gamma^i_j/\Delta t)$.

During the operation of the solution process for intense loading problems, instances of larger strain increments can occur which sometimes may lead to an imaginary (or negative) value of $\Delta\lambda$; that is, the conditions of Eq. 2.58b are violated. Since the time-step size for that particular instance cannot be economically reduced, a subincrement procedure to circumvent this difficulty as discussed in Ref. 61 can be and is used. Although the flow rule is strictly valid only for incremental changes of differential size, if it is employed during a finite-time increment, then it may also be used to relate changes which occur over a fraction of that time increment. Hence, the basic finite-time increment, Δt, is divided into a number, say L, of equal subincrements; the size of the subincrements is chosen to be sufficiently small so that a positive real value of $\Delta\lambda$ for each subincrement can be derived successively. The value of the finite-

strain increments $(\Delta\gamma_j^i)_{m+1}$ as calculated by an equation similar to Eq. 2.37 during the time interval t_m to t_{m+1} are also divided into L equal parts, $(\Delta\gamma_j^i)_{m+1}/L$. It is assumed that during each subincrement of length $\Delta t/L$ this change in strain is approximately correct. Then, by employing the previously mentioned procedure, a valid value for $\Delta\lambda$ along with stress increments and plastic strain increments are calculated for each subinterval, and in the meanwhile, the stresses and plastic strains are kept updated. The process is continued until either (a) the information needed at time t_{m+1} is calculated or (b) a complex (or negative) $\Delta\lambda$ is encountered. In the latter case, the process is repeated from time t_m using a larger value of L. If the stresses at time t_{m+1} can be derived successfully, the solution procedure continues with L henceforth set to unity until an imaginary $\Delta\lambda$ is again encountered.

It perhaps should be noted that the discussion spanning Eq. 2.47 to Eq. 2.59 applies to any given mechanical sublayer of the material model at any spanwise or depthwise Gaussian (or checking) station in the structure. Such a procedure is applied to every mechanical sublayer of the material model at that Gaussian station.

During the course of the research reported in Ref. 17, it has been found that by assuming the material to be strain-rate sensitive and by using Eqs. 2.46 and 2.59, very good agreement of the transient responses between predictions and the experiment is observed for beam and ring (planar) problems. However, a significantly stiffer response compared with experiment has been predicted for plate and cylindrical panel problems when strain-rate effects have been included; similar results have been reported in the finite-difference calculations of Ref. 58. Therefore, the validity of the approximate expression, Eq. 2.59 for $\dot{\varepsilon}$, and the appropriate values of the parameters D and p used in Eq. 2.46 remain to be determined for the general two-dimensional and three-dimensional problem.

SECTION 3

FORMULATIONS FOR SEVERAL CURVED-BEAM ELEMENTS

3.1 Objectives

The present investigation is concerned with developing finite elements which are capable of efficiently representing large generalized displacement behavior: large in-plane and lateral displacements as well as large rotations. Although for computational convenience attention is devoted principally to structures whose deformations lie essentially in one plane (2-d deformation), it is more effective and instructive to develop the governing equations for more general structural configurations and behavior. Then, these relations can be specialized in an orderly sequence of approximations to describe several categories of deformation behavior for 2-d type structures. Further, for generality and convenience, this analysis is developed in general tensor form and, hence, is valid for any coordinate system or configuration. Later, certain relations are recast into the more-familiar physical notation.

In structural analysis it is often useful to introduce simplifying but restrictive assumptions in order to simplify the governing equations. Accordingly, the Bernoulli-Euler assumptions for beams (that plane cross sections remain plane and normal to the deflected axis), the Kirchhoff assumptions for thin plates, and the Love assumptions for thin shells are very often invoked: (a) normals to the reference surface before deformation remain normal after deformation, and (b) each material point along the normal does not change its distance from the reference surface during deformation. The approximate character of the Bernoulli-Euler assumptions for beams has been pointed out, for example, by Love [62, p. 365], Southwell [63, p. 46], and Rivello [64, p. 141].

That the Kirchhoff assumptions are not generally satisfied has been indicated, for instance, by Love [62, pp. 482 and 484] and Fung [65, p. 458]. For small deflections and infinitesimal strain, these assumptions are reasonably good and self consistent. However, when large displacements and rotations and small strain occur, the approximate and mutually contradictory character of these assumptions becomes more evident.

Koiter [66,67,68] replaced the contradictory Love-Kirchhoff assumptions by the single assumption that: an approximate state of plane stress ($\tau_{33} \tilde{\sim} \tau_{31} \tilde{\sim} \tau_{32} \tilde{\sim} 0$) exists in the midsurface of the shell.* This assumption turns out to be consistent (as proven with mathematical rigor by John [69]) in the linear theory of shells; such a rigorous proof is lacking in the nonlinear theory. Koiter's assumption is in its consequences [66, p. 15] equivalent to the usual Love-Kirchhoff assumption.

Since the inclusion of large strains and completely general deformation behavior would represent a much more extensive and ambitious effort than presently planned, the present effort is restricted to extending the studies of Refs. 17 and 24 to include more general nonlinear deformation behavior while retaining the assumption of (1) small to moderate strain and (2) the simplifying assumptions of the Bernoulli/Euler/Kirchhoff/Love theories. It is planned to test "the limits of applicability" of the simplifying assumptions by comparing a sequence of predictions with each other and with well-defined experimental data involving very large deflections, and strains ranging from small to moderately large.

Accordingly, Subsection 3.2 deals with the strain-displacement relations; a sequence of such relations including a progressively greater number of nonlinear terms is defined. Subsection 3.3 is devoted to discussing various finite-element formulations which utilize these strain-displacement relations. Finite element property matrices based upon one of the selected strain-displacement relations and the unconventional finite-element formulation (see Subsections 2.1 and 2.2) are discussed illustratively in Subsection 3.4.

---

*In contradiction to the original Love-Kirchhoff displacement field (by which $\gamma_{33}=0$), the normals to the middle surface in a Koiter displacement field undergo an extension given by the expression $\gamma_{33}(z) = -\frac{\nu}{1-\nu}\gamma_{\alpha}^{\alpha}(z)$ where $\gamma_{33}(z)$ is the transverse strain, ν is Poisson's ratio, and $\gamma_{\alpha}^{\alpha}(z)$ is the first invariant of the strains parallel to the middle surface. This condition ensures a zero value of the transverse normal stress.

3.2 Nonlinear Strain-Displacement Relations

3.2.1 Brief Historical Background

One of the main topics under investigation in the present study is the influence (on finite-element predictions of large elastic-plastic deflections of structures) of nonlinear terms in the bending part of the strain-displacement relations. With this purpose in mind, the literature concerning the nonlinear theory of shells (with special emphasis on general formulations) was surveyed.

The subject of shell theory (to provide a two-dimensional representation of an intrinsically three-dimensional phenomenon) is still far from being exactly solved. Still today it constitutes an active part of theoretical and applied investigations. As mentioned on page 4 of [70], the productivity of papers relating to shells and their design, analysis, and failure has followed an exponential curve since 1886.

Excellent reviews exist about the history and foundations of shell theory. Among these are: E.E. Sechler [70], Naghdi [71,72], Naghdi and Nordgren [73], Koiter [74], Sanders [75] and Hildebrand, Reissner, and Thomas [76], etc.

Quoting Sechler [70, p. 24]: "No longer can one take a material off the shelf, look up its properties in a handbook, use the latest shell analysis methods, and emerge with the best shell structure for the job. Everything is now coupled, and it will be a distinct challenge to find the simplest engineering solutions to this coupled problem."

To give an idea of what is the state of the art in the general theory of shells, some quotes from two leading authors in the field may be useful. In 1962, P.M. Naghdi [71] writes: "In the seventy-four years which have elapsed since the appearance of Love's work, so far as the foundations of the theory are concerned, despite extensions, generalizations, re-examinations, and re-derivation of the equations of the linear theory, there are still unsettled questions." In 1970, W.T. Koiter (Ref. 68, page 193) writes "Several attempts have already been made to establish a more refined shell theory in such cases, but we concur in Naghdi's view [71, p.77] that an adequate solution to this problem has not yet been attained." In the

same article (Ref. 68, page 194) referring to a justification of the non-linear theory of shells: "This problem seems to represent a virtually open issue for future research."

Naghdi, in his extensive work on the fundamental, mathematical theory of thin shells of 1972, (Ref. 72, p. 587) writes: "In nearly all of the approximate theories, the underlying kinematic assumptions are such that the strains are small while the rotation may be large or moderately large and linear constitutive equations are assumed to be valid. In general, however, a systematic development of such approximate theories is not available; and even those few contributions which have been striven toward a more satisfactory derivation either employ assumptions which are too special or else still contain a number of ad hoc approximations."

W.T. Koiter and J.G. Simmonds [77] expressed in 1972: "For example in nonlinear problems virtually nothing is known concerning bounds on the errors of shell solutions. The best results to date, obtained by John, consist of effective error estimates for the two-dimensional differential equations in the interior domain in the absence of surface loads, but they say nothing about the equally important question of boundary conditions."

A major advance in the foundations of the linear theory of thin elastic shells was achieved in 1965 by F. John [69]. Exploiting modern developments on the behavior of the solutions of elliptic systems of partial differential equations, he published a rigorous proof, with concrete estimates of the errors involved, that the state of stress in the interior domain of a shell (i.e. at a sufficient distance from the edge of a shell) and in the absence of surface loads is approximately plane with an approximately linear distribution through the thickness of the stress parallel to the middle surface. Koiter in 1959 [66] employed the single physical assumption of an approximately-plane state of stress in order to justify Love's additive property of extensional and flexural strain energies. In 1970 Koiter [68] rigorously established the validity of a consistent version of classical linear shell theory with his modified Kirchhoff field as an approximation

to three-dimensional elasticity theory. Unfortunately, the method employed does not enable one to obtain a similar justification of the nonlinear theory of thin elastic shells.

The early contributions to nonlinear theory of thin shells were of a restrictive geometrical nature. Among these: Donell's [78] nonlinear theory for cylinders published in 1934, Marguerre's [79] nonlinear theory for shallow shells published in 1938, Mushtari's [80] nonlinear theory for "quasi-shallow shells" published in English in 1961, and E. Reissner's [81] nonlinear theory for axisymmetrical shells of revolution under the Kirchhoff hypothesis published in 1950.

Another approach is the asymptotic approach followed for example, by Johnson and Reissner [82] in 1959, Reiss [83] in 1960, and Green [84] in 1962. Here, an incomplete set of equations is obtained by an asymptotic procedure, extended to membrane approximation, inextensional approximation, boundary layer, etc. As Naghdi points out [72, p. 587]: "The derivations

> by asymptotic expansion techniques, at first sight, may appear to be free from ad hoc assumptions; but, in fact, this is not the case. The scaling of stresses and displacements is tantamount to a priori special assumptions regarding the transverse components u_3^* and τ^{i3}, although subsequent developments are carried out systematically+."

Probably the first work of a general nature was that by Synge and Chien [85] in 1941, where the intrinsic approach is used. That is to say, direct reference to displacements is avoided. This theory of shells is deduced from the three-dimensional theory by means of a series of expansions in powers of a small thickness parameter.

Galimov [80] published a nonlinear theory for small midsurface strains where midsurface shear strains are neglected. Green and Adkins [86] published

---

+The asterisk added to the symbol u_3 is used to represent a field defined over a 3-D body (to distinguish it clearly from fields defined over two-dimensional manifold); u_3^* = transverse component of displacement and τ^{i3} = transverse component of stress.

in 1960 a general derivation of a nonlinear membrane theory with nonlinear constitutive equations, with no approximation for tangential components.

Most of the work done in nonlinear theories of shells invoke small strain and the Love-Kirchhoff hypothesis or a similar set of assumptions. For example, see the treatise on nonlinear elasticity by Novozhilov [87] published in Russian in 1947. The expressions given in this book are for small strain and Kirchhoff behavior; their approximate character is manifested, for example, in the fact that some of the expressions do not provide zero values as they should for purely rigid-body motion.

C. Truesdell [88] made a careful review of [87] from which it is quoted: "Although the author founds all his analysis in the fully general theory, his main interest is in the case next in order of generality past the fully linear one, when the extensions are small, but the displacements and rotations may be large. The cause of this restriction, on which he lays considerable emphasis, is his desire to furnish structural engineers with the basic theories needed for rational solution of their nonlinear elastic problems. Since typical structural material, such as steel, fail to retain their elastic reversibility when subjected to extensions as great as 1%, there are essentially only two such nonlinear problems: (1) elastic stability, which the author interprets as determining the smallest load at which Kirchhoff's uniqueness theorem breaks down, and (2) bending of "flexible" bodies, such as thin rods, plates and shells."

Also under the assumptions of small strain and Kirchhoff behavior is the article of Sanders [75] of 1963. Here, a nonlinear strain-displacement relation for large displacements is derived, and then specialized to the case of small midsurface strain and "moderately small rotations." Its potential use for stability investigations is suggested. Equations of equilibrium for large deflections are discussed. A similar discussion for compatibility equations is omitted. The author remarks that: "Despite the potential usefulness of a general nonlinear theory, the literature on the

subject is sparse." Later on, Budiansky [89] in 1968 published an article where this theory is applied to nonlinear membrane shell theory, and tensor equations (consistent with Koiter's) of applicability to instability analysis are translated into classical notation.

Naghdi and Nordgren [73] published in 1963 an article on the nonlinear theory of elastic shells under the Kirchhoff hypothesis. The tensor expressions given are "exact" under the Kirchhoff hypothesis. A reduction to the linear theory and a discussion of the use of fully nonlinear constitutive equations are presented.

Also in 1963, Wainwright [90] published a nonlinear theory of elastic shells under the assumption of small strain and the Love-Kirchhoff hypothesis, but where the material response is assumed to be nonlinear. This is then specialized to membrane theory. Displacements and their gradients considered, are "small". Power series are used in the strain energy function.

Due to the contradictory character of the Kirchhoff assumption, Koiter [66] replaced them by the single assumption of an approximate state of plane stress in the midsurface of the shell. This assumption turns out to be consistent, and in its consequences is equivalent to the usual Kirchhoff assumption.

The transverse strain instead of being considered zero, as in the usual Kirchhoff assumption of no elongation of points along normals, is assumed to be $\gamma_{33} = -\frac{\nu}{1-\nu} g^{\alpha\beta}\gamma_{\alpha\beta}$ where ν is Poisson's ratio , $g^{\alpha\beta}$ is the contravariant metric tensor in shell space and $\gamma_{\alpha\beta}$ is the strain tensor on the middle surface. Koiter [67] in 1965 presents an extensive article on the nonlinear theory of thin elastic shells where the basic assumptions are: (1) his modified Kirchhoff displacement field and (2) the strains are small everywhere in the shell. This is simplified to a general theory of "quasi-shallow shells" which includes the more restricted theory of shallow shells as a special case. The case of "small finite deflections" is discussed and some remarks are made on "moderate deflections". His choice for the tensor of changes of curvature reduces to Sanders' choice for lines-of-curvature coordinates. The nonlinear strain-displacement relations for large deflections, in tensor form, are recognized as "extremely complicated".

Biricikoglu and Kalnins [91] developed in 1971 a theory for large elastic deformations of shells with the inclusion of transverse normal strain. They did so, because "A theory of shells which is subjected

> to the kinematic constraint that the thickness of the shell before and after deformation remains the same is not realistic when large strains are admitted in the deformation process. To enforce such a constraint, the density of the material would have to change in a special way during deformation, and since most materials which are capable of undergoing large strains, are nearly incompressible, such density change cannot be admitted."

This theory is restricted to cases where membrane strains are much larger than bending strains.

A fundamentally different approach from the previously-mentioned one is that in which it is postulated that the shell is a two-dimensional continuum, subject to certain physical principles analogous to those of three-dimensional mechanics. This notion was originated by the Cosserat brothers [92]. This description is elegant and has logical consistency. Ericksen and Truesdell [93] published in 1958 an "exact theory of stress and strain in rods and shells" where they adopted this method of description. They are able to account for transverse shear and strain, and the rotations associated with stress couples. Constitutive equations were not considered.

Naghdi [72] published in 1972 an exhaustive exposition of shell theory under this method of description. The lack of comparison, or even a connection, with three-dimensional theory, of the method of description originated by the Cosserats, was considered a "virtue" by Sanders [75] in 1963, and a "serious weakness" by Koiter and Simmonds [77] in 1972.

3.2.2 Formulation of the Strain-Displacement Relations

3.2.2.1 Thin Shells

The nonlinear strain-displacement relations for a curved beam will be derived from the general nonlinear theory of thin shells, specializing it to, successively, small strain, two-dimensional behavior, Kirchhoff assumptions, and finally, different assumptions on the magnitude of the displacements that will lead to a set of strain-displacement relations.

One cannot avoid the use of tensor calculus when treating the general theory of thin shells; accordingly, the notation* used here follows closely that of most books on the subject. The interested reader should refer, for example, to: McConnell [94], Sokolnikoff [95], Truesdell and Toupin [96], Ericksen [97], Synge and Schild [98], Green and Zerna [99], Eisenhart [100], or Willmore [101]. In order to keep the following description reasonably compact, the reader is assumed to have some familiarity with elementary differential geometry and tensor calculus.

Only shells with lines-of-curvature coordinates ξ^1, ξ^2, and ξ^3 ($\equiv \zeta$) will be considered. The coordinates ξ^1 and ξ^2 define the <u>midsurface</u> of a thin shell and ζ measures the distance along an outwardly-directed normal. Any point p on the undeformed shell is located by the position vector $\bar{r}^o$ to the middle surface and the unit vector normal $\bar{n}$ to the middle surface in the form (Fig. 3):

$$\bar{r}(\xi^1, \xi^2, \zeta) = \bar{r}^o(\xi^1, \xi^2) + \zeta \bar{n} \tag{3.1}$$

The base vectors associated with the undeformed and deformed shell space are denoted, respectively, by:*

$$\bar{g}_1 = \frac{\partial \bar{r}}{\partial \xi^1} \qquad \bar{g}_2 = \frac{\partial \bar{r}}{\partial \xi^2} \qquad \bar{g}_3 = \frac{\partial \bar{r}}{\partial \xi^3} \equiv \frac{\partial \bar{r}}{\partial \zeta} \tag{3.2a}$$

$$\bar{G}_1 = \frac{\partial \bar{R}}{\partial \xi^1} \qquad \bar{G}_2 = \frac{\partial \bar{R}}{\partial \xi^2} \qquad \bar{G}_3 = \frac{\partial \bar{R}}{\partial \xi^3} \equiv \frac{\partial \bar{R}}{\partial \zeta} \tag{3.2b}$$

where point p in the undeformed shell is identified as point P in the deformed state; P is located by the position vector $\bar{R}$. The base vectors associated with the undeformed and deformed shell <u>midsurface</u> are denoted by:

---

*Greek indices have values of 1 or 2 while Latin indices have values 1,2,3. Lower case letters refer to the <u>undeformed</u> configuration, while upper case letters refer to the <u>deformed</u> configuration. Superscript "o" refers to the midsurface.

$$\bar{a}_\alpha = \frac{\partial \bar{r}^0}{\partial \xi^\alpha} \qquad \bar{a}_1 = \frac{\partial \bar{r}^0}{\partial \xi^1} \qquad \bar{a}_2 = \frac{\partial \bar{r}^0}{\partial \xi^2} \tag{3.3a}$$

$$\bar{A}_\alpha = \frac{\partial \bar{R}^0}{\partial \xi^\alpha} \qquad \bar{A}_1 = \frac{\partial \bar{R}^0}{\partial \xi^1} \qquad \bar{A}_2 = \frac{\partial \bar{R}^0}{\partial \xi^2} \tag{3.3b}$$

The fundamental metric tensors of the undeformed and deformed shell midsurface are:

$$a_{\alpha\beta} = \bar{a}_\alpha \cdot \bar{a}_\beta = \begin{pmatrix} a_{11} & 0 \\ 0 & a_{22} \end{pmatrix} \tag{3.4a}$$

$$A_{\alpha\beta} = \bar{A}_\alpha \cdot \bar{A}_\beta = \begin{pmatrix} A_{11} & 0 \\ 0 & A_{22} \end{pmatrix} \tag{3.4b}$$

The determinants of these arrays are denoted by the symbols a and A:

$$a = a_{11} a_{22} \tag{3.5a}$$

$$A = A_{11} A_{22} \tag{3.5b}$$

The contravariant metric quantities are

$$a^{11} = \frac{1}{a_{11}} \qquad a^{22} = \frac{1}{a_{22}} \qquad a^{12} = a^{21} = 0 \tag{3.6a}$$

$$A^{11} = \frac{1}{A_{11}} \qquad A^{22} = \frac{1}{A_{22}} \qquad A^{12} = A^{21} = 0 \tag{3.6b}$$

The unit normals to the midsurface are given by

$$\bar{n} = \frac{\bar{a}_1 \times \bar{a}_2}{\sqrt{a}} \qquad (3.7a) \qquad \bar{N} = \frac{\bar{A}_1 \times \bar{A}_2}{\sqrt{A}} \qquad (3.7b)$$

The Christoffel symbols are defined as:

$$\left\{ \begin{matrix} \delta \\ \alpha \quad \beta \end{matrix} \right\} \equiv \bar{a}^{\delta} \cdot \frac{\partial \bar{a}_\alpha}{\partial \xi^\beta} \qquad (3.8)$$

The second fundamental tensors of the surface are:

$$b_{\alpha\beta} \equiv \bar{n} \cdot \frac{\partial \bar{a}_\alpha}{\partial \xi^\beta} \qquad (3.9a) \qquad B_{\alpha\beta} \equiv \bar{N} \cdot \frac{\partial \bar{A}_\alpha}{\partial \xi^\beta} \qquad (3.9b)$$

and are symmetric.

In terms of these quantities, one can write the Gauss-Weingarten relations:

$$\frac{\partial \bar{a}_\alpha}{\partial \xi^\beta} = \left\{ \begin{matrix} \delta \\ \alpha \quad \beta \end{matrix} \right\} \bar{a}_\delta + b_{\alpha\beta} \bar{n} \qquad (3.10)$$

$$\frac{\partial \bar{n}}{\partial \xi^\beta} = - b_\beta^\sigma \bar{a}_\sigma \qquad (3.11)$$

where

$$b_\beta^\alpha = a^{\alpha\sigma} b_{\sigma\beta} \qquad (3.12)$$

Since lines-of-curvature coordinates are defined as those for which:

$$a_{12} = 0 \quad b_{12} = 0$$

$$b_1^1 = a^{11} b_{11} = \frac{b_{11}}{a_{11}} = \frac{1}{R_1} \qquad b_2^2 = \frac{b_{22}}{a_{22}} = \frac{1}{R_2}$$

where the R_α are the radii of curvature, one can express the base vectors for shell space in terms of the base vectors in the middle surface as

$$\bar{g}_1 = \frac{\partial \bar{r}}{\partial \xi^1} = \frac{\partial \bar{r}^o}{\partial \xi^1} + \zeta \frac{\partial \bar{n}}{\partial \xi^1} = \bar{a}_1 - \zeta b_1^\gamma \bar{a}_\gamma = \bar{a}_1 \left(1 - \frac{\zeta}{R_1}\right)$$

$$\bar{g}_2 = \frac{\partial \bar{r}}{\partial \xi^2} = \bar{a}_2 - \zeta b_2^\gamma \bar{a}_\gamma = \bar{a}_2 \left(1 - \frac{\zeta}{R_2}\right)$$

$$\bar{g}_3 = \frac{\partial \bar{r}}{\partial \zeta} = \bar{n} \tag{3.13}$$

$$\bar{G}_\alpha = \frac{\partial \bar{R}}{\partial \xi^\alpha} = \bar{A}_\alpha - \zeta B_\alpha^\beta \bar{A}_\beta \qquad \bar{G}_3 = \bar{N} \tag{3.14}$$

The midsurface base vectors and the shell normal to the deformed midsurface will be described in terms of the midsurface displacements. The midsurface displacement field in terms of its components $v^{o\alpha}$ along the coordinate axes and its component w along the undeformed normal is

$$\bar{v}^o = v^{o\alpha} \bar{a}_\alpha + w \bar{n} \tag{3.15}$$

Hence,

$$\bar{A}_\alpha = \frac{\partial \bar{R}^o}{\partial \xi^\alpha} = \bar{a}_\alpha + \frac{\partial}{\partial \xi^\alpha}\left(v^{o\gamma}\bar{a}_\gamma + w\bar{n}\right) \tag{3.16}$$

Introducing the Gauss-Weingarten relations, (Eqs. 3.10 and 3.11) this becomes

$$\bar{A}_\alpha = \bar{a}_\alpha + \left[v^{o\sigma}_{,\alpha} - w b^\sigma_\alpha\right]\bar{a}_\sigma + \left[\frac{\partial w}{\partial \xi^\alpha} + v^{o\gamma} b_{\gamma\alpha}\right]\bar{n} \tag{3.16a}$$

Or, defining

$$\theta^\sigma_\alpha \equiv v^{o\sigma}_{,\alpha} - w b^\sigma_\alpha$$
$$\theta^3_\alpha \equiv \frac{\partial w}{\partial \xi^\alpha} + v^{o\gamma} b_{\gamma\alpha} \tag{3.17}$$

one obtains:

$$\bar{A}_\alpha = \bar{a}_\alpha + \theta^\sigma_\alpha \bar{a}_\sigma + \theta^3_\alpha \bar{n} \tag{3.18}$$

Also from Eq. 3.7b, namely $\bar{N} = (\bar{A}_1 x \bar{A}_2)/(A)^{1/2}$, one obtains:

$$\bar{N} = \sqrt{\frac{a}{A}}\left[\left(1+\theta^1_1+\theta^2_2+\theta^1_1\theta^2_2-\theta^2_1\theta^1_1\right)\bar{n}+\left(-\theta^3_1-\theta^3_1\theta^2_2+\theta^3_2\theta^2_1\right)\bar{a}^1 + \left(-\theta^3_2-\theta^3_2\theta^1_1+\theta^3_1\theta^1_1\right)\bar{a}^2\right] \tag{3.18}$$

For small strain of a differential element of area, one can set $(a/A)^{1/2} \sim 1$, and then obtain the following expression for $\bar{N} - \bar{n}$:

$$\bar{N}-\bar{n} \approx \left(\theta_1^1+\theta_2^2+\theta_1^1\theta_2^2-\theta_1^2\theta_1^1\right)\bar{n}+\left(-\theta_1^3-\theta_1^3\theta_2^2+\theta_2^3\theta_1^2\right)\bar{a}^1+$$
$$\left(-\theta_2^3-\theta_2^3\theta_1^1+\theta_1^3\theta_1^1\right)\bar{a}^2 \qquad (3.19)$$

For a curved beam, only coordinates ξ^2 and ζ appear; hence,

$$\theta_2^2 = \frac{\partial v^{02}}{\partial \xi^2} - \frac{w}{R_2} + \frac{1}{\sqrt{a_{22}}}\frac{\partial \sqrt{a_{22}}}{\partial \xi^2} \qquad (3.20)$$

$$\theta_2^3 = \frac{\partial w}{\partial \xi^2} + \frac{a_{22}}{R_2} v^{02}$$

Thus,

$$\bar{N}-\bar{n} = \theta_2^2 \bar{n} - \theta_2^3 \bar{a}^2 \qquad (3.21)$$

where the term $\theta_2^2 \bar{n}$ is retained (this term is dropped in the Sanders approximation for "moderately small rotations" [75]).

Now let the (mutually contradictory) Kirchhoff assumptions be invoked:

(a) Points normal to the undeformed midsurface remain normal after deformation.

(b) These points do not change their distance from middle surface.

As a consequence of this, γ_{33} and $\gamma_{23}=\gamma_{32}$ should be zero. These assumptions are usually termed in the literature: for beams "Bernoulli-Euler", for plates "Kirchhoff", and for shells "Love" assumptions (although Love introduced more than one set of assumptions with respect to shells).

The displacement field at any point ξ^1,ξ^2,ζ in a shell may be written as follows for a Kirchhoff-type displacement field:

$$\bar{V}(\xi_1,\xi_2,\zeta) = \bar{V}^0(\xi_1,\xi_2) + \zeta(\bar{N}-\bar{n}) \tag{3.22}$$

where, for a curved beam:

$$\bar{V}^0 = v^{02}\,\bar{a}_2 + w\bar{n}$$

$$\bar{N}-\bar{n} = \theta_2^2\,\bar{n} - \theta_2^3\,\bar{a}^2 \tag{3.22a}$$

Observe that this is equivalent to:

$$\tilde{w} = w + \zeta\,\theta_2^2 \tag{3.22b}$$

$$\tilde{v} = v^{02} - \zeta\,\theta_2^3$$

where $\tilde{w}$ is the displacement component of $\bar{v}(\xi^1,\xi^2,\zeta)$ in the $\bar{n}$ direction and $\tilde{v}$ is the component in the $\bar{a}_2$ direction. Expression 3.22b contradicts assumption (b) of the Kirchhoff hypothesis, since in the case of pure membrane extension, $\theta_2^3=0$, $\theta_2^2\neq 0$, and $\tilde{w}$ is seen to depend on ζ.

The Green or Lagrangian strain tensor* γ_{mn} compares the square of the lengths of differential line elements in the deformed (dS) and undeformed (ds) configurations with respect to the undeformed configuration and is defined to be

$$\gamma_{mn} = \frac{1}{2}\,\frac{(dS)^2-(ds)^2}{(ds)^2} = \frac{1}{2}\left(G_{mn}-g_{mn}\right) \tag{3.23}$$

*For a definition of the concept of the strain tensor, consult, for example, Truesdell and Toupin [96, p. 255] or Fung [65, p. 91].

Expressing the strain tensor in terms of the undeformed base vectors in a Lagrangian description:

$$G_{mn} = \left(\bar{g}_m + \frac{\partial \bar{v}}{\partial \xi^m}\right) \cdot \left(\bar{g}_n + \frac{\partial \bar{v}}{\partial \xi^n}\right) \qquad (3.24)$$

$$g_{mn} = \bar{g}_m \cdot \bar{g}_n$$

$$\gamma_{mn} = \frac{1}{2}\left[\frac{\partial \bar{v}}{\partial \xi^m} \cdot \bar{g}_n + \frac{\partial \bar{v}}{\partial \xi^n} \cdot \bar{g}_m + \frac{\partial \bar{v}}{\partial \xi^m} \cdot \frac{\partial \bar{v}}{\partial \xi^n}\right] \qquad (3.25)$$

3.2.2.2 Curved Beams

Now the previous results are specialized to the case of the curved beam whose geometry leads to*;

$$\eta \equiv \xi^2 \qquad \zeta \equiv \xi^3 \qquad R \equiv -R_2$$

$$\bar{a}_2 = \frac{\partial \bar{r}^0}{\partial \eta}$$ (unit tangent vector to the centroidal axis)

$$a_{22} = a^{22} = 1$$

$$g_{22} = \left(1 + \frac{\zeta}{R}\right)^2 \qquad g^{22} = \frac{1}{\left(1 + \frac{\zeta}{R}\right)^2}$$

$$\theta_2^2 = \frac{\partial v^{02}}{\partial \eta} + \frac{w}{R}; \quad \theta_2^3 = \frac{\partial w}{\partial \eta} - \frac{v^{02}}{R}; \quad \begin{Bmatrix} 2 \\ 2\ 2 \end{Bmatrix} = 0 \qquad (3.26)$$

*Notice that this choice for the radius of curvature R is opposite in sign to that usually found in tensor books and which was used previously.

After some tedious algebra one obtains:

$$\gamma_{22} = \left(1+2\frac{\zeta}{R}\right)\gamma_{22\varepsilon_o} + \zeta\gamma_{22\kappa} + \frac{1}{2}\zeta^2\gamma_{22\mathcal{H}} \tag{3.27}$$

where

$$\gamma_{22_{\varepsilon_o}} = \theta_2^2\left(1+\frac{1}{2}\theta_2^2\right) + \frac{1}{2}\left(\theta_2^3\right)^2 \tag{3.27a}$$

$$\gamma_{22_{\kappa}} = \left(-\theta_{2,\eta}^3\right)\left(1+\theta_2^2\right) + \theta_2^3\theta_{2,\eta}^2 \tag{3.27b}$$

$$\gamma_{22_{\mathcal{H}}} = \left(\theta_{2,\eta}^3\right)^2 + \left(\theta_{2,\eta}^2\right)^2 \tag{3.27c}$$

and where all terms with the common factor ζ^2/R have been neglected; also, $(\quad)_{,\eta}$ denotes partial differentation with respect to η, since $\{^2_{22}\} = 0$.

The physical components ε_{mn} of these tensor quantities do not transform according to the tensor transformation law and are not components of tensors; however, they are useful in later parts of the present analysis. Defining the physical components of strain as:

$$\epsilon_{mn} \equiv \frac{\gamma_{mn}}{\sqrt{g_{mm}}\sqrt{g_{nn}}} \tag{3.28}$$

one obtains in this case

$$\epsilon \equiv \epsilon_{22} = \frac{\gamma_{22}}{\left(1+\frac{\zeta}{R}\right)^2} \tag{3.28a}$$

Expressing the midsurface quantities v^{o2}, w, θ_2^2, and θ_2^3 in terms of the physical components v, w, χ, and ψ:

$$v = \sqrt{a_{22}}\, v^{02} = v^{02} \qquad w = w$$

$$\chi = \sqrt{a_{22}}\, \theta_2^2 = \frac{\partial v}{\partial \eta} + \frac{w}{R} \qquad \text{(extension)} \qquad (3.29a)$$

$$\psi = \theta_2^3 = \frac{\partial w}{\partial \eta} - \frac{v}{R} \qquad \text{(rotation)} \qquad (3.29b)$$

Finally (dropping terms multiplied by $\frac{\zeta^2}{R}$), one has

$$\epsilon(\eta, \zeta) = \epsilon_o(\eta) + \zeta \mathcal{K}(\eta) + \frac{1}{2}\zeta^2 \mathcal{H}_b(\eta) \qquad (3.30)$$

where

$$\epsilon_o(\eta) = \chi\left(1 + \frac{1}{2}\chi\right) + \frac{1}{2}\psi^2 \qquad (3.30a)$$

$$\mathcal{K}(\eta) = \left(-\frac{\partial \psi}{\partial \eta}\right)(1+\chi) + \psi \frac{\partial \chi}{\partial \eta} \qquad (3.30b)$$

$$\mathcal{H}_b(\eta) = \left(\frac{\partial \psi}{\partial \eta}\right)^2 + \left(\frac{\partial \chi}{\partial \eta}\right)^2 \qquad (3.30c)$$

As one can see, even in the context of a curved beam, under the assumptions of small strain and Kirchhoff behavior that the strain-displacement relations become very complicated, and the influence of higher order

terms (as Koiter [66] said) is of doubtful validity and significance when compared with the errors involved in adopting the Kirchhoff assumptions made to obtain those terms.

Equation 3.30 represents the most comprehensive nonlinear strain-displacement relation taken into account in the present study. Note that the terms $\varepsilon_o(\eta)$ represent the complete nonlinear membrane behavior (see, for example, Ref. 65). For less severe deflections than contemplated in this study, the term H is usually omitted and κ consists of fewer terms.

In the usual version of the linear theory, Eq. 3.30 reduces to

$$\epsilon(\eta,\zeta) = \chi - \zeta \frac{\partial \psi}{\partial \eta} \tag{3.31}$$

In nonlinear theories, additional terms are included. For example, the strain-displacement relations of Ref. 17 as well as those of Sanders [75] for "moderately small rotations" and Koiter [67] for "small finite deflections" in the case of a beam with the geometry of Eq. 3.26 are represented by the following subcase of Eq. 3.30 -- identified for convenient reference herein as (strain-displacement relation) Type A:

$$\epsilon(\eta,\zeta) = \left[\chi + \frac{1}{2}\psi^2\right] + \zeta\left(-\frac{\partial \psi}{\partial \eta}\right) \tag{3.32}$$

Note that only 2 of the 3 membrane terms, 1 of the 3 κ terms, and none of the H terms are retained in this approximation.

In a second version only the missing membrane term is added to Eq. 3.32 -- to define Type B:

$$\epsilon(\eta,\zeta) = \left[\chi + \frac{1}{2}\psi^2 + \frac{1}{2}\chi^2\right] + \zeta\left(-\frac{\partial \psi}{\partial \eta}\right) \tag{3.33}$$

Equation 3.30 with all terms retained is identified as Type C and is repeated here for convenient reference:

$$\epsilon(\eta,\zeta) = \left[\chi + \frac{1}{2}\psi^2 + \frac{1}{2}\chi^2\right] + \zeta\left[-\frac{\partial\psi}{\partial\eta} - \chi\frac{\partial\psi}{\partial\eta} + \psi\frac{\partial\chi}{\partial\eta}\right] + \frac{1}{2}\zeta^2\left[\left(\frac{\partial\psi}{\partial\eta}\right)^2 + \left(\frac{\partial\chi}{\partial\eta}\right)^2\right] \tag{3.34}$$

Next in order to study the importance of certain terms in κ retained in Type C compared with the simpler Type B expression, it is useful to define and employ two intermediate expressions (Types D and E). Type D is formed by adding the term $(-\chi\frac{\partial\psi}{\partial\eta})$ in κ of Eq. 3.33 to obtain:

$$\epsilon(\eta,\zeta) = \left[\chi + \frac{1}{2}\psi^2 + \frac{1}{2}\chi^2\right] + \zeta\left[-\frac{\partial\psi}{\partial\eta} - \chi\frac{\partial\psi}{\partial\eta}\right] \tag{3.35}$$

Type E is formed by adding the term $\psi\frac{\partial\chi}{\partial\eta}$ to the κ term of Eq. 3.35 to obtain:

$$\epsilon(\eta,\zeta) = \left[\chi + \frac{1}{2}\psi^2 + \frac{1}{2}\chi^2\right] + \zeta\left[-\frac{\partial\psi}{\partial\eta} - \chi\frac{\partial\psi}{\partial\eta} + \psi\frac{\partial\chi}{\partial\eta}\right] \tag{3.36}$$

With reference to the more comprehensive Type C expression, Eq. 3.34, it may be of interest to note that shell theories not restricted to the Kirchhoff assumption often include terms in ζ^2; such theories include those of Hildebrand, Reissner, and Thomas [76], Love's "second approximation" [62, 76], and that of Biricikoglu and Kalnins [91].

3.2.2.3 Initially-Flat Beams

For initially-flat beams, strain-displacement relations Types A through E apply directly since 1/R = 0, and χ and ψ take on the following definitions:

$$\chi = \frac{\partial v}{\partial \eta} \qquad (3.37a) \qquad\qquad \psi = \frac{\partial w}{\partial \eta} \qquad (3.37b)$$

Strain-displacement relation Type C is "exact" for arbitrarily large rotations and displacements of initially-flat beams under the Love-Kirchhoff hypothesis, since the only neglected terms in Type C were terms with the common factor $\frac{\zeta^2}{R}$.

In Section 4, the application of strain-displacement relations Types A through E to an initially-flat clamped-ended beam subjected to severe impulsive loading such that large elastic-plastic deformations are produced is discussed. The relative importance of the sequence of added nonlinear terms is illustrated.

3.2.2.4 Comments

In this subsection some pertinent comments will be made concerning the scope and/or validity of the nonlinear strain-displacement relations treated in Subsection 3.2.2.2.

Although most of what has been accomplished in the nonlinear theory of shells is based upon the Love-Kirchhoff assumptions (as was indicated in Subsection 3.1), many authors dislike these ad hoc assumptions because of the fact that they are mutually contradictory.

To indicate this contradiction, the derivation of the strain tensor tensor γ_{mn} for a flat beam (so that $\frac{1}{R}$ terms do not complicate the picture) is shown in what follows using Eqs. 3.26 and 3.22 to form the following quantities:

$$\left(\frac{\partial \bar{v}}{\partial \xi^2}\right) \cdot \left(\frac{\partial \bar{v}}{\partial \xi^2}\right) = \left(\theta_2^2\right)^2 + \left(\theta_2^3\right)^2 + 2\zeta\left(\theta_2^3 \theta_{2,2}^2 - \theta_{2,2}^3 \theta_2^2\right) + \zeta^2\left[\left(\theta_{2,2}^2\right)^2 + \left(\theta_{2,2}^3\right)^2\right] \qquad (3.38a)$$

$$\left(\frac{\partial \bar{v}}{\partial \zeta}\right)\cdot\left(\frac{\partial \bar{v}}{\partial \zeta}\right) = \left(\theta_2^2\right)^2 + \left(\theta_2^3\right)^2$$

$$\left(\frac{\partial \bar{v}}{\partial \zeta}\right)\cdot\left(\frac{\partial \bar{v}}{\partial \xi^2}\right) = \zeta\left[\theta_2^2\,\theta_{2,2}^2 + \theta_2^3\,\theta_{2,2}^3\right] \tag{3.38b}$$

Thus employing these quantities and using Eqs. 3.24, 3.25, 3.38a, and 3.38b, the strains become

$$\gamma_{22} = \frac{1}{2}\left(G_{22} - g_{22}\right) = \theta_2^2 - \zeta\,\theta_{2,2}^3 + \frac{1}{2}\left(\theta_2^2\right)^2 + \frac{1}{2}\left(\theta_2^3\right)^2 + \zeta\left[\theta_2^3\,\theta_{2,2}^2 - \theta_{2,2}^3\,\theta_2^2\right] + \frac{1}{2}\zeta^2\left[\left(\theta_{2,2}^3\right)^2 + \left(\theta_{2,2}^2\right)^2\right]$$

$$\gamma_{32} = \gamma_{23} = \frac{1}{2}\left(G_{32} - g_{32}\right) = \frac{1}{2}\zeta\left[\left(1+\theta_2^2\right)\theta_{2,2}^2 + \theta_2^3\,\theta_{2,2}^3\right] \tag{3.39}$$

$$\gamma_{33} = \frac{1}{2}\left(G_{33} - g_{33}\right) = \theta_2^2 + \frac{1}{2}\left(\theta_2^2\right)^2 + \frac{1}{2}\left(\theta_2^3\right)^2$$

These last two formulas (for γ_{32} and γ_{33}) express a contradiction: according to the Love-Kirchhoff hypothesis invoked in deriving these expressions, the transverse normal strain γ_{33} and transverse shear strain $\gamma_{32}=\gamma_{23}$ should be zero; but, because of the introduction of the nonlinear terms in the expression, they are not. As a matter of fact, the magnitude of γ_{33} as computed from the Kirchhoff-type of formulation with nonlinear bending terms is the same as the membrane part of γ_{22}. This unfortunate contradiction does not take place in the linear theory of shells; in the case of Sanders' [75] expression for "moderately small rotations", the contradiction is small (in that case $\gamma_{33} = \frac{1}{2}(\theta_2^3)^2$ for a flat beam). As can be seen, the contradiction comes from the inclusion of the term $\theta_2^2 \bar{n}$ in the expression for the difference between the normals to the deformed and undeformed surfaces $\bar{N} - \bar{n}$. Still today, authors disagree on what the "best" expression for the curvature terms should look like.

W.T. Koiter [74] expressed: "Since the theory we have to deal with is approximate in character, we feel that extreme rigor in its development is hardly desirable. Extreme rigor in the analysis of physical problems, we are inclined to believe, may easily lead to rigor mortis. Likewise, too much insistence on a systematic approach seems inadvisable to us. Flexible bodies like thin shells require a flexible approach."

Novozhilov [87, page 197], in his incomplete treatment of nonlinear elasticity published in Russian in 1947, made strong remarks about the validity of the Kirchhoff assumption:

"(a) Kirchhoff's hypothesis in the theory of plates and shells rests on simplifications which result when elongations and shears are neglected in comparison with rotations in determining the direction of fibers of the strained body. Since thin plates and shells are flexible bodies whose angles of rotation under a deformation ordinarily are large in comparison with the elongations and shears, the adoption of this hypothesis usually introduces only a negligible error into the calculations. Hence, it is clear that the simplification

in the theory of plates proposed by Kirchhoff and subsequently extended by Love to shells, can hardly be called a hypothesis as is ordinarily done. For, in essence we are dealing with purely geometric approximations whose error can always be estimated.

(b) Kirchhoff's "hypothesis" does not include any assumptions about the properties of the materials of which the plates and shells are made. Thus, a theory based on this "hypothesis" can be used with equal effectiveness both for bodies which obey Hooke's law and for bodies which do not. It is only important that the basic condition be satisfied, namely, that the strains be small in comparison with the angles of rotation."

C. Truesdell [88], in his extensive review of Novozhilov's book [87] replies: "There is some question about the author's distinction between "geometrical" and "physical" nonlinearity (#34, and again on p. 197). For example, whether or not the rotations are large cannot be determined by "geometric considerations" a priori; the rotations result from loading, and (unless one is using an inverse method) one cannot know in advance whether for given loading of a material defined by a given strain energy function the nonlinear terms in the strain components will need to be retained or not. True, after the problem is solved the question becomes purely geometric, but if we have the exact solution then it is no longer very important whether we can neglect certain terms or not. The question of whether certain approximations are valid in advance is avoided by the author; its treatment would require a new type of approximation theorem for partial differential equations."

Another point in question is the validity and meaningfulness of adding nonlinear terms in the bending strain under the Kirchhoff assumption. About this, Koiter [66] wrote in 1959:

"Many writers (e.g., 6) retain in their energy expressions, derived on the basis of the LOVE-KIRCHHOFF assumptions (or equivalent assumptions) additional terms of the type of some or all of the terms (2.18) to (2.23) neglected in Love's expression. Such a supposedly higher approximation is also implied in the analysis of other writers (e.g., 1,4,9,21), who develop the theory without direct reference to the strain energy. On the other hand, it has been pointed out repeatedly by several writers (e.g., 5,10,12) that such a refinement is doubtful if the basic Love-Kirchhoff assumptions (which are of course only approximately valid) are retained.

In fact, the transverse shear stresses, obtained from equilibrium conditions, are in general of order h/L times the bending stresses, and neglection of the corresponding strain energy therefore already implies a relative error of order h^2/L^2. Moreover, the transverse normal stress, in general, of order h^2/L^2 or h/R times the bending or direct stresses, and its neglection in the strain energy density involves relative errors of the same orders. Hence a refinement of Love's approximation is indeed meaningless, in general, unless the effects of transverse shear and normal stresses are taken into account at the same time."

Now, some comments about strain-displacement relations (3-32) through (3-36) are given. All of these equations were derived under the assumptions:

(a) the problem is two-dimensional.

(b) the beam is thin; the parameter in question is $\frac{h}{R}$ or $\frac{h}{L}$, whichever is larger. *

(c) the Love-Kirchhoff hypothesis.

(d) the strains are small everywhere.

Observe that one can write Eq. 3.30 in a form that shows the relative order of the terms in a more readily perceived fashion as:

* h is the half-thickness of the beam, R is the radius of curvature, and L is the minimum wavelength of the deformation pattern.

$$\epsilon(\eta,\zeta)=\chi\left(1+\frac{1}{2}\chi\right)+\frac{1}{2}\psi^2+\zeta\left[-\frac{\partial\psi}{\partial\eta}\left(1+\chi-\frac{1}{2}\zeta\frac{\partial\psi}{\partial\eta}\right)+\frac{\partial\chi}{\partial\eta}\left(\psi+\frac{1}{2}\zeta\frac{\partial\chi}{\partial\eta}\right)\right] \tag{3.40}$$

where one may identify:

Membrane terms:

$$\chi\left(1+\frac{1}{2}\chi\right)+\frac{1}{2}\psi^2 \tag{3.40a}$$

Bending terms:

$$\zeta\left[-\frac{\partial\psi}{\partial\eta}\left(1+\chi-\frac{1}{2}\zeta\frac{\partial\psi}{\partial\eta}\right)+\frac{\partial\chi}{\partial\eta}\left(\psi+\frac{1}{2}\zeta\frac{\partial\chi}{\partial\eta}\right)\right] \tag{3.40b}$$

The expressions of Sanders [75] for "moderately small rotations" and Koiter [67] for "small finite deflections" reduce to Eq. 3.32 in the case of a beam with the specified geometry given by Eq. 3.26. About the range of validity of his approximation, Sanders [75] wrote:

> "Equilibrium equations are derived by making certain simplifying assumptions. In particular the middle surface strains are assumed small and the rotations are assumed moderately small. The resulting equations are suitable as a basis for stability investigations or other problems in which the effects of deformation on equilibrium cannot be ignored, but in which the rotations are not too large."

Koiter [67] wrote:

> "Small finite deflections (are) characterized by small displacement gradients and by rotations whose squares do not exceed the middle surface strains in order of magnitude."

In the version of Eq. 3.33 "Type B", all membrane strain terms are retained. Usually when all nonlinear terms are retained in the membrane strain

expression, the bending strain terms are neglected. Observe that for problems where the membrane and bending strain are of the same order, it would be inconsistent to use the "Type B" expression since it implies a neglection of χ in the bending strain term $\zeta(-\frac{\partial\psi}{\partial\eta})\ (1+\chi)$, and not neglecting χ in the membrane strain term $\chi(1+\frac{1}{2}\chi)$.

Type B is kept here as an alternative, because of those problems in which there is mainly membrane action but bending is not negligible, and to be able to treat nonlinear membrane problems (under small strain) in a general-purpose program. Once again, W.T. Koiter [102, page 194] can be quoted (now about elastic stability for thin shells): "If we restrict ourselves

> to fundamental states I in which the bending stresses do not exceed the membrane stresses in order of magnitude, we may therefore presumably neglect the nonlinear terms in the changes of curvature. The restriction implied by this simplification is not at all serious. We are not aware of any significant shell buckling problem in which the fundamental state involves membrane stresses which are small in comparison with the bending stresses. Moreover, if we restrict our attention to "small finite deflections" in the sense of [67], the changes of curvature may always be represented by their linear approximation without any loss in accuracy within the framework of shell theory."

The nonlinear terms in ζ and ζ^2 are kept in Type C (Eq. 3.34) because of cases in which bending is important. In those cases it is consistent to include the term χ in the bending expression $\zeta(-\frac{\partial\psi}{\partial\eta})\ (1+\chi)$ since one includes χ in the membrane part as $\chi(1+\frac{1}{2}\chi)$. And since one knows from the linear theory that $\zeta\frac{\partial\psi}{\partial\eta}$ is comparable to χ, one should probably also include $\frac{1}{2}\zeta^2(\frac{\partial\psi}{\partial\eta})^2$ in the expression as $\zeta(-\frac{\partial\psi}{\partial\eta})\ (1+\chi-\frac{1}{2}\zeta\frac{\partial\psi}{\partial\eta})$. The term $\frac{1}{2}\zeta^2(\frac{\partial\chi}{\partial\eta})^2$ is probably smaller but was kept here because it did not represent any major calculating effort.

3.3 Assumed Displacement Field Considerations

3.3.1 Description of Curved-Beam-Element Geometry

In order to represent the initial geometry of an arbitrarily-curved variable-thickness beam, it is convenient to employ the approximate

description utilized in Ref. 17 for a curved beam element, as depicted in Fig. 4. The centroidal axis may be located by a position vector $\bar{r}^o$ described by

$$\bar{r}^o(\eta) = Y(\eta)\bar{j} + Z(\eta)\bar{K} \tag{3.41}$$

where η is the length coordinate along the centroidal axis measured from node i where $\eta=0$ to node i+1 where $\eta=\eta_i$, and Y,Z represent Cartesian global coordinates of the plane in which the curved beam lies. The unit tangent vector, $\bar{a}_2$, to the centroidal axis, and the unit normal vector, $\bar{n}$, are defined as

$$\bar{a}_2 = \frac{d\bar{r}^o}{d\eta} \tag{3.42}$$

$$\bar{n} = -\frac{1}{\mu}\frac{d\bar{a}_2}{d\eta} = -\frac{1}{\mu}\frac{d^2\bar{r}^o}{d\eta^2} \tag{3.43}$$

where μ is the magnitude of the curvature vector $\frac{d\bar{a}_2}{d\eta}$, and the reciprocal of μ is known as the radius of curvature, R, taken here as in Ref. 17, positive when the center of curvature lies in the negative direction of $\bar{n}$ (which is identical to the convention followed by Sanders, but opposite in sign to that usually given in books on tensors).

It is assumed that the slope, ϕ, of the centroidal axis, which is the angle between the unit tangent vector and the y-axis of the local reference Cartesian coordinate system (y,z) may be approximated with sufficient accuracy by a quadratic polynomial in η as follows:

$$\phi(\eta) = b_0 + b_1\eta + b_2\eta^2 \tag{3.44}$$

The constants b_0, b_1, and b_2 can be determined from the known initial geometry of the curved-beam element by requiring (1) the slopes of the idealized approximated beam element and the actual beam element to have the same slopes at nodes i and i+1 and (2) the ends to be on the y-axis (i.e., z=0 at both ends):

$$\phi(\eta=0)=\phi_i \tag{3.45a}$$

$$\phi(\eta=\eta_i)=\phi_{i+1} \tag{3.45b}$$

$$\int_{\phi_i}^{\phi_{i+1}} (\sin\phi)R\,d\phi = -\int_0^{\eta_i} \sin\phi\,d\eta = 0 \approx \int_0^{\eta_i} \phi\,d\eta \tag{3.45c}$$

since one defines $R = -\left(\frac{d\phi}{d\eta}\right)^{-1}$. It is assumed that the change in element slope between nodes i and i+1 is small so that

$$\cos\left(\phi_{i+1}-\phi_i\right) \approx 1 \tag{3.46a}$$

$$\sin\left(\phi_{i+1}-\phi_i\right) \approx \phi_{i+1}-\phi_i \tag{3.46b}$$

This restricts the slope change within an element to $\lesssim$ 15 degrees. The arc length, η_i, of the element is approximated to be the same as the length of a circular arc passing through the nodal points at the slope ϕ_i and ϕ_{i+1}; η_i is given by

$$\eta_i = \frac{L_i\left(\phi_{i+1}-\phi_i\right)}{2\sin\left(\frac{\phi_{i+1}-\phi_i}{2}\right)} \tag{3.47}$$

where L_i is the length of the chord joining nodes i and i+1 and is given by

$$L_i = \left[\left(Z_{i+1}-Z_i\right)^2 + \left(Y_{i+1}-Y_i\right)^2\right]^{1/2} \tag{3.48}$$

One can obtain an idea of the error that the Eq. 3.45c approximation

entails by considering the case of constant radius of curvature R. In that case

$$\int_0^{\eta_i} \sin\phi \, d\eta = -\int_{\phi_i}^{\phi_{i+1}} \sin\phi \, R \, d\phi = 0$$

and so

$$\int_{\phi_i}^{\phi_{i+1}} \sin\phi \, d\phi = 0 \tag{3.49}$$

or approximating sin ϕ by its power series:

$$\int_{\phi_i}^{\phi_{i+1}} \left(\phi - \frac{\phi^3}{3!} + \cdots\right) d\phi = 0 \tag{3.50}$$

Hence, the error term is

$$\int_{\phi_i}^{\phi_{i+1}} \frac{\phi^3}{3!} \, d\phi = \left.\frac{\phi^4}{24}\right|_{\phi_i}^{\phi_{i+1}} \tag{3.50a}$$

This error is very small for small ϕ. In order to have an error (in the approximation represented by Eq. 3.45c) of the same magnitude as the restriction $(\phi_{i+1}-\phi_i) \lesssim 15^\circ$ in Eq. 3.46b, the limit on ϕ would be $\phi \lesssim 37^\circ$. Thus, the error in the determination of the constants is smaller than that made by approximating an arbitrary slope by a quadratic polynomial in η.

The constants in the quadratic polynomial for ϕ are found to be

$$b_0 = \phi_i \tag{3.51a}$$

$$b_1 = -2\,\frac{(\phi_{i+1} + 2\phi_i)}{\eta_i} \tag{3.51b}$$

$$b_2 = \frac{3(\phi_{i+1} + \phi_i)}{(\eta_i)^2} \tag{3.51c}$$

with the radius of curvature of the centroidal axis expressed as

$$R = -\left(\frac{d\phi}{d\eta}\right)^{-1} = -\left(b_1 + 2b_2\eta\right)^{-1} \tag{3.52}$$

The coordinates Y(η) and Z(η) are given by

$$Y(\eta) = Y_i + \int_0^{\eta} \cos\left[\phi(\eta) + \alpha\right] d\eta \tag{3.53a}$$

$$Z(\eta) = Z_i + \int_0^{\eta} \sin\left[\phi(\eta) + \alpha\right] d\eta \tag{3.53b}$$

where

$$\alpha = \tan^{-1}\left(\frac{Z_{i+1} - Z_i}{Y_{i+1} - Y_i}\right) \tag{3.53c}$$

The thickness h of the beam is approximated as being linear in η between nodes; thus

$$h(\eta) = h_i\left(1 - \frac{\eta}{\eta_i}\right) + h_{i+1}\frac{\eta}{\eta_i} \tag{3.54}$$

where h_i and h_{i+1} represents the beam thickness at nodes i and i+1, respectively.

3.3.2 Rigid-Body Modes and Displacement Field "Requirements"

By using successively finer meshes of elements, this sequence may be expected to provide results which converge to the correct result if the assumed displacement fields (in each element) satisfy certain criteria. These criteria have been summarized by Cook [103, page 87-90]:

"The mandatory criteria are as follows:

1. The displacement field within an element must be continuous. This requirement is so easily satisfied that we need not mention it again.
2. When nodal d.o.f. are given values corresponding to a state of constant strain, the displacement field must produce the constant strain state throughout the element (2,3). In the case of a thin plate element we might speak of "constant curvature" instead of "constant strain."

Two more requirements that elements should satisfy are as follows. As the mesh of elements is refined, but not necessarily in larger elements:

3. Rigid body modes must be represented. That is, when nodal d.o.f. are given values corresponding to a state of rigid body motion, the element must exhibit zero strain and therefore zero nodal forces (1).
4. Compatibility must exist between elements; elements must not overlap or separate. In the case of beam, plate, and shell elements it is also required that there be no sudden changes in slope across interelement boundaries (1,2,12).

If Requirement 3 is violated, extraneous nodal forces appear, and thus the equations of nodal equilibrium are altered. Some successful shell elements satisfy this requirement only if elements are made vanishingly small. The elements have been widely used because the error remains small for the size of element used in practice. Nevertheless, other things being equal, better results are obtained when rigid body modes are included (7).

Requirement 4 is violated by many successful elements (2,5); however, such elements do satisfy interelement compatibility in the limit of mesh refinement as each element approaches a state of constant

strain. Another requirement that an element should satisfy is:

5. The element should have no preferred directions. That is, under any set of loads having a fixed orientation with respect to the element, the element response should be independent of how it and its loads are oriented in global xy coordinates. "Response" means element strain energy or element strains in a coordinate system that moves with the element. Elements that satisfy this requirement will be called invariant. There is some opinion (3,7) that invariance is mandatory if convergence to correct results is to be obtained. In any case it is a quite desirable attribute, and there is no necessity to violate it."

That the requirement of exact representation of rigid-body motion need be obtained only in the limit, has been observed, for example, by Oden [104, p. 116]:

"In their finite-element analysis of plate bending, Bazeley, Cheung, Irons, and Zienkiewicz [1966] proposed as completeness ("convergence") criteria that the displacement function be such that "self-straining due to a rigid body motion of the element" not be permitted and that the displacement function within each element be such that constant "strain" and curvature conditions be possible over the element. Similar requirements were noted earlier by Irons and Draper [1965]. Since the functional involved in their analysis was of class C^1, their criteria amount to requiring that constant values of the displacement function and its first and second partial derivatives be possible over each element. A proof for polynomial approximations was later furnished by Arantes e Oliveira [1968]. Theorem 10.7 shows that such constant values need only be obtained in the limit as [element size] $\delta \to 0$. Unfortunately, many subsequent writers interpreted criteria proposed by Bazeley et al. for plates too literally and used the "rigid motion" and "constant strain" requirements as fundamental conditions for completeness for all finite-element approximations of displacement fields. It is easily shown, however, that a finite-element approximation of the

displacement field in an elastic body can be constructed that satisfies the completeness requirements of Theorem 10.7, and yet does not lead to either a rigid motion or a constant strain when δ_e is finite. This can be seen by regarding the x^i in Theorem 10.6 as curvilinear coordinates (e.g. cylindrical; then u_r = constant does not produce rigid motion nor does it necessarily lead to constant strain, while $u_r = a + br$ may be admissible for a C^0 problem). Such rigid motions and constant strains need be obtained only in the limit as $\delta \to 0$. On the other hand, Murray [1970] has shown by means of numerical examples that the inclusion of rigid-body motion in elements of finite dimension may significantly improve rates of convergence."

Since the rigid-body displacements for curved beam elements are seen to depend on trigometric functions, it is impossible to represent these exactly by means of polynomial interpolation. However, they can be approximated by the polynomial functions and for some degree of mesh refinement they can be considered as implicitely included. This was noticed numerically, for example, by Coco [105] in 1969, Petyt and Fleischer [106] in 1971, and Mebane and Stricklin [107] in 1971. They noticed that the cubic-cubic (in v and w, respectively) formulation without exact representation of rigid-body body modes exhibits a marked improvement over the linear in v, cubic in w, formulation, because of among other factors, the ability of the former to satisfy rigid-body equilibrium better.

Cantin and Clough [108] in 1968 and Murray [109] in 1970 showed that linear in v and cubic in w elements with exact representation of rigid-body motions show a significant improvement in convergence over linear-cubic elements without exact rigid-body representation when analyzing a cylindrical shell.

Furthermore, Petyt and Fleischer [106] noted that the cubic-cubic formulation without exact representation of rigid body modes represented them with sufficient accuracy (produced zero frequency modes for the examples executed) for small displacements, and its overall performance was superior to the linear in v and cubic in w formulation with exact representation of rigid-body motion.

Fonder and Clough [110] showed in 1973 that:

"1) When curvilinear coordinates are used and rigid-body modes not included in the element interpolation functions, polynomials of equal degree should be used for u, v, w to insure a consistent approximation of the rigid modes even though all of these displacements may not be of equal importance in the deformation process.

2) If rigid-body modes can be added without introducing any incompatibility (as in the case of curved beams) they are more efficient than degrees of freedom which increase the order of the interpolation polynomials.

3) The general technique proposed by Cantin[20] to add rigid-body modes to a curved element generally renders the element incompatible. In circular plates, the favorable effect of rigid modes and the adverse effect of incompatibility are both negligible; in cylindrical shells, the favorable effects of the rigid modes overshadow the incompatibility effects; unfortunately the opposite holds true in shells with nonzero Gaussian curvature. Although no direct experience was gained with a three-dimensional element, it can be conjectured that a lack of compatibility over the warped interelement surface of such an element would be even more detrimental than the incompatibility over the curved boundary of a thin shell element."

Reference 17 uses as the displacement field a cubic-cubic polynomial in v and w, with exact (for small displacements) representation of all possible rigid-body modes. Since it is rather complicated to follow the procedure (used for example by Cantin [111]) of solving the partial differential equation obtained by equating to zero the expression for the strain ε_{11} to find the displacements v and w due to rigid body modes in curved beam elements in the case of linear strain-displacement relations, and it is extremely complicated if not impossible in the case of nonlinear strain-displacement relations, the kinematic approach seems preferable. Also, the former approach may lead to erroneous expressions for the strain-free modes in the case of shell theories which give non-zero strains under rigid-body motions.

Following the kinematic approach [112], the rigid-body translations in the y, z coordinates of the element can be represented by:

$$\begin{Bmatrix} V \\ W \end{Bmatrix}_{\text{TRANSLATION}} = \begin{bmatrix} \cos\phi & \sin\phi \\ -\sin\phi & \cos\phi \end{bmatrix} \begin{Bmatrix} V_y \\ V_z \end{Bmatrix} \tag{3.55}$$

where ϕ is the angle between the tangent at the point in question and the semichord, V_y is the translation in y, and V_z the translation in z. The rotation Ω_x about the x axis (out of the plane), can be described by the translations A (in y) and B (in z) as

$$\begin{aligned} A &= y \cos \Omega_x - z \sin \Omega_x - y = -y\,(1-\cos \Omega_x) - z \sin \Omega_x \\ B &= y \sin \Omega + z \cos \Omega_x - z = -y \sin \Omega_x - z\,(1-\cos \Omega_x) \end{aligned} \tag{3.56}$$

or

$$\begin{Bmatrix} A \\ B \end{Bmatrix} = \begin{bmatrix} -z & -y \\ +y & -z \end{bmatrix} \begin{Bmatrix} \sin \Omega_x \\ 1-\cos \Omega_x \end{Bmatrix} \tag{3.57}$$

Then the rigid-body rotation Ω_x about x can be expressed as

$$\begin{Bmatrix} V \\ W \end{Bmatrix}_{\substack{\text{RIGID BODY} \\ \text{ROTATION } \Omega_x}} = \begin{bmatrix} \cos\phi & \sin\phi \\ -\sin\phi & \cos\phi \end{bmatrix} \begin{Bmatrix} A \\ B \end{Bmatrix}$$

$$= \begin{bmatrix} \cos\phi & \sin\phi \\ -\sin\phi & \cos\phi \end{bmatrix} \begin{bmatrix} -z & -y \\ y & -z \end{bmatrix} \begin{Bmatrix} \sin \Omega_x \\ 1-\cos \Omega_x \end{Bmatrix} =$$

$$= \begin{bmatrix} (-z\cos\phi + y\sin\phi) & -(y\cos\phi + z\sin\phi) \\ (z\sin\phi + y\cos\phi) & (-z\cos\phi + y\sin\phi) \end{bmatrix} \begin{Bmatrix} \sin \Omega_x \\ 1-\cos \Omega_x \end{Bmatrix}$$

(3.58)

Adding up the rigid-body translations and rotations, one obtains the following expression for large rigid-body motions:

$$\begin{Bmatrix} V \\ W \end{Bmatrix}_{\substack{\text{LARGE} \\ \text{RIGID BODY} \\ \text{MOTIONS}}} = \begin{bmatrix} \cos\phi & \sin\phi & (-z\cos\phi + y\sin\phi) & -(z\sin\phi + y\cos\phi) \\ -\sin\phi & \cos\phi & (z\sin\phi + y\cos\phi) & (-z\cos\phi + y\sin\phi) \end{bmatrix} \begin{Bmatrix} V_y \\ V_z \\ \sin\Omega_x \\ 1-\cos\Omega_x \end{Bmatrix} \tag{3.59}$$

When the rigid-body rotation Ω_x is small enough, one can set:

$$\sin\Omega_x \approx \Omega_x \qquad 1-\cos\Omega_x \approx 0 \tag{3.60}$$

Hence, Eq. 3.59 becomes

$$\begin{Bmatrix} V \\ W \end{Bmatrix}_{\substack{\text{SMALL} \\ \text{RIGID BODY} \\ \text{ROTATIONS}}} = \begin{bmatrix} \cos\phi & \sin\phi & (-z\cos\phi + y\sin\phi) \\ -\sin\phi & \cos\phi & (z\sin\phi + y\cos\phi) \end{bmatrix} \begin{Bmatrix} V_y \\ V_z \\ \Omega_x \end{Bmatrix} \tag{3.61}$$

Observe that for flat elements:

$$\cos\phi = 1 \qquad \sin\phi = 0$$

$$-z\cos\phi + y\sin\phi = 0 \qquad z\sin\phi + y\cos\phi = y = \eta \tag{3.62}$$

and the rigid body modes for an initially-flat beam become:

$$\begin{Bmatrix} V \\ W \end{Bmatrix}_{\substack{\text{LARGE} \\ \text{RIGID} \\ \text{BODY MOTIONS} \\ \text{(FLAT BEAM)}}} = \begin{bmatrix} 1 & 0 & 0 & -\eta \\ 0 & 1 & \eta & 0 \end{bmatrix} \begin{Bmatrix} V_y \\ V_z \\ \sin\Omega_x \\ 1-\cos\Omega_x \end{Bmatrix} \tag{3.63}$$

In order to have an invertable A matrix* in the case of initially-flat beams, one cannot include both the trigonometric functions that represent the rigid-body modes and the constant and linear terms in the polynomial expansion (since they are the same for $\phi=0$).

Since for initially-straight structures the large rigid-body motions are automatically included exactly, the difference between the formulation for small rigid-body motions and that for large rigid-body motions increases with increasing initial curvature of the element (or deepness of the curved beam element) but should be expected to be small for elements with small (shallow) curvatures (one should have in mind that deep curved beams can be represented by many elements, each of them with small -shallow- curvatures).

3.3.3 Displacement Interpolation Fields

Polynomial interpolation functions are chosen to represent displacements throughout each element in Ref. 17. It was concluded in Ref. 17 that the use of a cubic polynomial to express both the axial displacement v and the normal displacement w was superior to choosing a linear polynomial in v and cubic polynomial in w. For that reason the choice (termed CC -- cubic cubic -- in Ref. 17) was used as one of the FE categories investigated in the present study. With the inclusion of rigid-body modes represented "explicitly", this cubic-cubic expansion takes the form:

$$\left\{\underset{\sim}{u}\right\} \equiv \left\{\begin{matrix} v \\ w \end{matrix}\right\} = \begin{bmatrix} \cos\phi & \sin\phi & B_1 & \eta & 0 & 0 & \eta^2 & \eta^3 \\ -\sin\phi & \cos\phi & B_2 & 0 & \eta^2 & \eta^3 & 0 & 0 \end{bmatrix} \left\{\begin{matrix} \beta_1 \\ \vdots \\ \beta_8 \end{matrix}\right\}$$

where

$$B_1 = -(Z-Z_i)\cos(\phi+\alpha) + (Y-Y_i)\sin(\phi+\alpha)$$

$$B_2 = (Z-Z_i)\sin(\phi+\alpha) + (Y-Y_i)\cos(\phi+\alpha) \qquad (3.64)$$

*$\left\{\begin{matrix} v \\ w \end{matrix}\right\} = [U(\eta)]\ [A]^{-1}\ \{q\}$, where $[U(\eta)]$ is the interpolation displacement field and $\{q\}$ the generalized degrees of freedom at the nodes.

and where β_1, β_2, .. β_8 are parameters which will shortly be expressed in terms of the eight selected generalized displacements {q} of the element. In matrix form, Eq. 3.64 becomes*:

$$\underset{2\times 1}{\left\{\underset{\sim}{u}\right\}} = \underset{2\times 8}{\left[U_4(\eta)\right]} \underset{8\times 1}{\left\{\beta\right\}} \tag{3.65}$$

The generalized displacements, termed {q}, are chosen to characterize the deformation state of the element, and are selected such that there are four degrees of freedom at each node (i and i+1) of the element (formulation is identified for convenience as 4 DOF*/node):

$$\left\{q\right\} = \left\lfloor v_i \;\; w_i \;\; \psi_i \;\; \chi_i \;\; v_{i+1} \;\; w_{i+1} \;\; \psi_{i+1} \;\; \chi_{i+1} \right\rfloor^T \tag{3.66}$$

where $\psi = \frac{\partial w}{\partial \eta} - \frac{v}{R}$ and $\chi = \frac{\partial v}{\partial \eta} + \frac{w}{R}$, and the displacement field $\tilde{v},\tilde{w}$ of the beam under the Kirchhoff hypothesis may be written as

$$\tilde{v}(\eta,\zeta) = v(\eta) - \zeta\psi(\eta) \tag{3.67}$$

$$\tilde{w}(\eta,\zeta) = w(\eta)$$

Observe that under the mutually-contradicting Kirchhoff hypothesis, as derived from** Eq. 3.22:

$$\begin{aligned} \tilde{v}(\eta,\zeta) &= v(\eta) - \zeta\psi(\eta) \\ \tilde{w}(\eta,\zeta) &= w(\eta) + \zeta\chi(\eta) \end{aligned} \tag{3.68}$$

Corresponding to this assumed displacement field, one finds

---

*The subscript "4" in $U_4(\eta)$ denotes that this quantity is associated with the 4 DOF/node element.

**In the case of pure extension with no rotation of the normal, $\psi=0$, $\chi\neq 0$, $\tilde{v}=v(\eta)$, but $\tilde{w}=w+\zeta\chi$, and this last expression contradicts the assumption of no elongation of the normal; this is because of the small strain assumption $(a/A)^{1/2} \approx 1$.

$$\psi = \frac{\partial w}{\partial \eta} - \frac{v}{R} = \left[\, 0 \;\; 0 \;\; 1 \;\; -\frac{\eta}{R} \;\; 2\eta \;\; 3\eta^2 \;\; -\frac{\eta^2}{R} \;\; -\frac{\eta^3}{R} \,\right] \{\beta\}$$

$$\equiv \left[\, 0 \;\; 0 \;\; 1 \;\; \eta\frac{\partial \phi}{\partial \eta} \;\; 2\eta \;\; 3\eta^2 \;\; \eta^2\frac{\partial \phi}{\partial \eta} \;\; \eta^3\frac{\partial \phi}{\partial \eta} \,\right] \{\beta\}$$

$$\equiv \left[G_{\psi_4} \right] \{\beta\} \qquad (3.69)$$

$$\chi = \frac{\partial v}{\partial \eta} + \frac{w}{R} = \left[\, 0 \;\; 0 \;\; 0 \;\; 1 \;\; \frac{\eta^2}{R} \;\; \frac{\eta^3}{R} \;\; 2\eta \;\; 3\eta^2 \,\right] \{\beta\}$$

$$\equiv \left[\, 0 \;\; 0 \;\; 0 \;\; 1 \;\; -\eta^2\frac{\partial \phi}{\partial \eta} \;\; -\eta^3\frac{\partial \phi}{\partial \eta} \;\; 2\eta \;\; 3\eta^2 \,\right] \{\beta\}$$

$$\equiv \left[G_{\chi_4} \right] \{\beta\} \qquad (3.70)$$

The generalized nodal displacements, {q}, and the parameters, {β}, of the assumed displacement field are related by a transformation matrix [A] which may be obtained by substituting the coordinates of nodes i and i+1 into Equations 3.64, 3.69, and 3.70. Thus,

$$\underset{8\times 1}{\{q\}} = \underset{8\times 8}{[A_4]} \; \underset{8\times 1}{\{\beta\}} \qquad (3.71)$$

With a correct choice of the polynomial displacement interpolation field, A is a square nonsingular matrix; then one may write:

$$\underset{8\times 1}{\{\beta\}} = \underset{8\times 8}{[A_4]^{-1}} \; \underset{8\times 1}{\{q\}} \qquad (3.72)$$

Substituting Eq. 3.72 into Eq. 3.64 one obtains:

$$\underset{2\times 1}{\{\underset{\sim}{u}\}} = \underset{2\times 8}{[U_4(\eta)]} \; \underset{8\times 8}{[A_4]^{-1}} \; \underset{8\times 1}{\{q\}} \qquad (3.73)$$

As one can see from strain-displacement relations Types A through E (Eqs. 3.32-3.36) using the 4 generalized displacements (namely v, w, ψ and χ) at each node of the CC formulation, provides continuity of the membrane strain only, but the bending part of the strain is discontinuous since $\frac{\partial\psi}{\partial\eta}$ and $\frac{\partial\chi}{\partial\eta}$ are not employed as generalized displacements at the nodes.

In order to investigate what effects would be encountered if complete strain continuity were utilized, a formulation with 5 generalized displacements at each node was also studied in conjunction with strain-displacement relations, Type A through E. In this formulation, 5 generalized displacements: v, w, ψ, χ and $\frac{\partial\psi}{\partial\eta}$ were employed and provide strain continuity for relations Types A, B, and D but not for Types C and E. Furthermore, the discontinuity in strain arising from the use of strain-displacement relations Types C and E are expected to be small, since the term $\frac{\partial\chi}{\partial\eta}$ appears only in nonlinear terms (namely as $\zeta\,\psi\,\frac{\partial\chi}{\partial\eta}$ and $\frac{1}{2}\zeta^2\,(\frac{\partial\chi}{\partial\eta})^2$).

This 5 DOF/node formulation, in order to have a nonsingular [A] matrix, takes the form (cubic in v and quintic in w)*:

$$\underset{2\times1}{\begin{Bmatrix} v \\ w \end{Bmatrix}} = \underset{2\times10}{\begin{bmatrix} \cos\phi & \sin\phi & B_1 & \eta & 0 & 0 & \eta^2 & \eta^3 & 0 & 0 \\ -\sin\phi & \cos\phi & B_2 & 0 & \eta^2 & \eta^3 & 0 & 0 & \eta^4 & \eta^5 \end{bmatrix}} \underset{10\times1}{\begin{Bmatrix} \beta \end{Bmatrix}} \tag{3.74}$$

or concisely,

$$\underset{2\times1}{\begin{Bmatrix} v \\ w \end{Bmatrix}} \equiv \underset{2\times1}{\{\underset{\sim}{u}\}} = \underset{2\times10}{[U_5(\eta)]} \underset{10\times1}{\{\beta\}} \tag{3.75}$$

The generalized displacements are:

$$\underset{10\times1}{\{q\}} = \left[v_i \;\; w_i \;\; \psi_i \;\; \chi_i \;\; \left(-\frac{\partial\psi}{\partial\eta}\right)_i \;\; v_{i+1} \;\; w_{i+1} \;\; \psi_{i+1} \;\; \chi_{i+1} \;\; \left(-\frac{\partial\psi}{\partial\eta}\right)_{i+1} \right]^T \tag{3.76}$$

---

*Pertinent quantities associated with the 5 DOF/node element are denoted by subscript "5"; such quantities shown symbolically in this section are given in full in Appendix B.

Further one may write symbolically for this case:

$$\underset{1\times 1}{\psi} = \underset{1\times 10}{[G_{\psi_5}]}\ \underset{10\times 1}{\{\beta\}} \tag{3.77}$$

$$\underset{1\times 1}{\chi} = \underset{1\times 10}{[G_{\chi_5}]}\ \underset{10\times 1}{\{\beta\}} \tag{3.78}$$

$$\underset{1\times 1}{\left(-\frac{\partial\psi}{\partial\eta}\right)} = \underset{1\times 10}{[G_{(-\psi,\eta)_5}]}\ \underset{10\times 1}{\{\beta\}} \tag{3.79}$$

Also,

$$\underset{10\times 1}{\{q\}} = \underset{10\times 10}{[A_5]}\ \underset{10\times 1}{\{\beta\}} \tag{3.80}$$

$$\underset{10\times 1}{\{\beta\}} = \underset{10\times 10}{[A_5]^{-1}}\ \underset{10\times 1}{\{q\}} \tag{3.81}$$

$$\underset{2\times 1}{\{\underset{\sim}{u}\}} = \underset{2\times 10}{[U_5(\eta)]}\ \underset{10\times 10}{[A_5]^{-1}}\ \underset{10\times 1}{\{q\}} \tag{3.82}$$

One of the purposes of this study is to see how useful this element really is. It has the advantage of providing strain continuity when one uses strain displacement relations Types A, B, and E, and also provides a better description of the strain inducing modes, since now the polynomial displacement interpolation function consists of a cubic polynomial in v and a quintic polynomial in w giving a better representation of the rotation term ψ and the bending term $(-\frac{\partial\psi}{\partial\eta})$. Also, the fact of having more degrees of freedom per element should result in permitting the use of a coarser mesh of finite

elements for a given prediction accuracy. One can also anticipate some disadvantages: (1) the higher order polynomial may cause the element to be "too flexible" and (2) [A] matrix, now will become more ill-conditioned for inversion since the determinant of A will be significantly smaller than the terms in [A], especially, in the case of straight beams, with $\frac{1}{R} = 0$, and this may cause numerical troubles in computing the stiffness matrix.

Going one step further, one may consider the use of 6 DOF/node, where continuity of $\frac{\partial \chi}{\partial \eta}$ is also guaranteed thereby insuring complete strain continuity also in strain-displacement relations Types C and E. For this case, one can assume displacement polynomials quintic in both v and w as follows:

$$\underset{2\times 1}{\begin{Bmatrix} v \\ w \end{Bmatrix}} = \underset{2\times 12}{\begin{bmatrix} \cos\phi & \sin\phi & B_1 & \eta & 0 & 0 & \eta^2 & \eta^3 & 0 & 0 & \eta^4 & \eta^5 \\ -\sin\phi & \cos\phi & B_2 & 0 & \eta^2 & \eta^3 & 0 & 0 & \eta^4 & \eta^5 & 0 & 0 \end{bmatrix}} \underset{12\times 1}{\begin{Bmatrix} \beta \end{Bmatrix}} \quad (3.83)$$

or more concisely

$$\underset{2\times 1}{\begin{Bmatrix} \underset{\sim}{u} \end{Bmatrix}} = \underset{2\times 12}{\left[U_6(\eta) \right]} \underset{12\times 1}{\begin{Bmatrix} \beta \end{Bmatrix}} \quad (3.83a)$$

The appropriate generalized displacements are:

$$\underset{2\times 1}{\begin{Bmatrix} q \end{Bmatrix}} = \left\lfloor v_i \quad w_i \quad \psi_i \quad \chi_i \quad \left(-\frac{\partial \psi}{\partial \eta}\right)_i \quad \left(\frac{\partial \chi}{\partial \eta}\right)_i \right.$$

$$\left. v_{i+1} \quad w_{i+1} \quad \psi_{i+1} \quad \chi_{i+1} \quad \left(-\frac{\partial \psi}{\partial \eta}\right)_{i+1} \quad \left(\frac{\partial \chi}{\partial \eta}\right)_{i+1} \right\rfloor^T \quad (3.84)$$

Similarly for the 6 DOF/node, one may write

$$\underset{1\times 1}{\psi} = \underset{1\times 12}{\left\lfloor G\psi_6 \right\rfloor} \underset{12\times 1}{\begin{Bmatrix} \beta \end{Bmatrix}} \quad (3.85)$$

$$\underset{1\times 12}{\chi} = \underset{1\times 12}{\left[G_{\chi_6} \right]} \underset{12\times 1}{\{\beta\}} \tag{3.86}$$

$$\underset{1\times 12}{\left(-\frac{\partial \psi}{\partial \eta}\right)} = \underset{1\times 12}{\left[G_{(-\psi,\eta)_6} \right]} \underset{12\times 1}{\{\beta\}} \tag{3.87}$$

$$\underset{1\times 12}{\frac{\partial \chi}{\partial \eta}} = \underset{1\times 12}{\left[G_{(\chi,\eta)_6} \right]} \underset{12\times 1}{\{\beta\}} \tag{3.88}$$

Also,

$$\underset{12\times 1}{\{q\}} = \underset{12\times 12}{[A_6]} \underset{12\times 1}{\{\beta\}} \tag{3.89a}$$

$$\underset{12\times 1}{\{\beta\}} = \underset{12\times 12}{[A_6]^{-1}} \underset{12\times 1}{\{q\}} \tag{3.89b}$$

$$\underset{2\times 1}{\{\underset{\sim}{\mu}\}} = \underset{2\times 12}{[U_6(\eta)]} \underset{12\times 12}{[A_6]^{-1}} \underset{12\times 1}{\{q\}} \tag{3.89c}$$

This formulation has the advantages of providing continuity of strain no matter which of the nonlinear strain-displacement relations is used. It also provides continuity of the first derivative of the membrane strain $\varepsilon_o = \chi(1+\frac{1}{2}\chi)+\frac{1}{2}\psi^2$. Also it is generally known that a polynomial description of the same order for both v and w provide a better description than one for which the polynomial for v is of lower order than that for w*; accordingly, the displacement interpolation formulation employed is quintic-quintic. Another advantage of the 6 DOF/node formulation is that one can use the same number of Gaussian

*See Subsection 3.3.2.

integration points to evaluate {p} and [h] exactly for both the cubic-quintic and the quintic-quintic cases since the highest polynomial degree appearing in {p} and [h] is the same in both cases. Among the disadvantages are: (a) the matrix [A] becomes even more ill-conditioned for inversion, (b) the elements may tend to become "too flexible" under a 5th order interpolation polynomial in both v and w, (c) the computation becomes somewhat more complicated with such a high number of degrees of freedom per node. Part of the advantages associated with simple descriptions for each finite element are lost.

Some additional observations concerning the use of higher order finite elements may be noted: to quote Cook [103, page 174]

> "Such "higher order" elements are usually quite accurate, but have two significant disadvantages. First, where adjacent elements have different thicknesses or different elastic properties, or where stiffeners are attached, curvatures and twist change abruptly across interelement boundaries. Therefore, continuity of these higher order nodal d.o.f. must not be enforced; instead, the extra freedoms should be viewed as internal d.o.f. and should be removed by condensation before assembly of elements. Second, boundary conditions involving the higher order d.o.f. may not be obvious and are often cumbersome as, for example, along curved boundaries, in shell problems where in-plane displacements and their derivatives may also be used as nodal freedoms, and if adjacent elements are not coplanar. In summary, we may conclude that higher order d.o.f. make the finite element method awkward in application to problems for which it is usually best suited -- for problems involving thickness changes, stiffness, mixtures of different element types, and members meeting at angles. Abel and Desai (2) have compared several plate elements on the basis of accuracy versus computational expense. It is worth noting that when judged in this way, the higher order elements mentioned above may be surpassed by simpler elements."

It should be noted, however, that all of these appraisals are made in the

context of linear-elastic, small-displacement behavior whereas nonlinear large-displacement behavior is of principal interest in the present study; hence, the observations in Ref. 103 may need to be modified for the present class of problems.

Also, it should be noted that after the formulations in this subsection were carried out and explored Refs. 113, 114, and 115 by Dawe were discovered. Dawe [113,114] investigated various arch (curved beam) finite elements to analyze the following small displacement, elastic problems:

1. A deep clamped arch carrying a central point load ($\frac{h}{R} = \frac{1}{17}$ and $\frac{h}{R} = \frac{1}{272}$ were considered).
2. The same deep clamped arch but with the central point load replaced by a uniform normal pressure; here extensive results were obtained only for the case $\frac{h}{R} = \frac{1}{272}$.
3. A pinched ring problem.
4. A shallow clamped arch carrying a point load, and subtending an angle of 30^{o} ($\frac{h}{R} \simeq \frac{1}{66}$ and $\frac{h}{R} \simeq \frac{1}{1051}$ were considered).

Some of the assumed-displacement finite elements considered were:

(a) a cubic in u and cubic in w element, with degrees of freedom u, w, $\frac{du}{ds}$ and $\frac{dw}{ds}$. (Called CC element).

(b) a cubic in u and quintic in w element, with degrees of freedom

$$u,\ w,\ \frac{du}{ds},\ \frac{dw}{ds} \text{ and } \frac{d^2w}{ds^2}$$ (Dawe calls it a QC element).

(c) a quintic in u and cubic in w element, with degrees of freedom

$$u,\ w,\ \frac{du}{ds},\ \frac{dw}{ds} \text{ and } \frac{d^2u}{ds^2}$$ (Dawe calls it a CQ element).

(d) a quintic in u and quintic in w element, with degrees of freedom

$$u,\ w,\ \frac{du}{ds},\ \frac{dw}{ds},\ \frac{d^2u}{ds^2} \text{ and } \frac{d^2w}{ds^2}.$$

Among Dawe's findings are:

(1) Calculations based on cubic (u), quintic (w) elements and cubic

(u), cubic (w) elements show that the force distributions for these models exhibit some waviness in all considered applications and this becomes very pronounced in some deep thin arch problems where the waviness is many times greater than the true magnitude of the force.

(2) No significant improvement in accuracy is achieved by increasing the order of the normal deflection component (w) from cubic to quintic if the tangential component (u) is not similarly increased. It seems even more efficient to increase the order of the tangential component (u) rather than the normal one (w) when treating thin sections.

(3) The finite element model which successfully deals with both thick and thin deep arches is the quintic-quintic model. The bending moment distributions obtained by using the quintic-quintic model are much more accurate than those based on the other models. It also exhibits very rapid convergence.

(4) There is still some waviness in the force distribution obtained using the quintic-quintic model in deep, thin, nearly inextensional applications, but such waviness is small.

As will be seen later, these findings for small-displacement linear-elastic conditions are consistent with the present study in which highly nonlinear large-displacement elastic-plastic transient response conditions are of principal interest.

Going one step further, one may consider the use of more DOF/node. The next step could be a 7 DOF/node element, where continuity of the rate of change of the change of curvature $(\frac{\partial^2 \psi}{\partial \eta^2})$ is also guaranteed, thereby insuring complete strain continuity in all the nonlinear strain displacement relations considered (A thru E), as with the 6 DOF/node element, plus continuity of the first rate of change of the strain, in strain displacement relations A, B and D.

For this case, one assumes displacement polynomials quintic in v and 7th degree in w:

$$\underset{2\times 1}{\begin{Bmatrix} v \\ w \end{Bmatrix}} = \underset{2\times 14}{\begin{bmatrix} \cos\phi & \sin\phi & B_1 & \eta & 0 & 0 & \eta^2 & \eta^3 & 0 & 0 & \eta^4 & \eta^5 & 0 & 0 \\ -\sin\phi & \cos\phi & B_2 & 0 & \eta^2 & \eta^3 & 0 & 0 & \eta^4 & \eta^5 & 0 & 0 & \eta^6 & \eta^7 \end{bmatrix}} \underset{14\times 1}{\{\beta\}} \quad (3.90a)$$

or more concisely

$$\underset{2\times1}{\{\underset{\sim}{u}\}} = \underset{2\times14}{[U_7(\eta)]} \underset{14\times1}{\{\beta(t)\}} \tag{3.90b}$$

The appropriate generalized displacements are

$$\underset{14\times1}{\{q\}} = \lfloor v_i \; w_i \; \psi_i \; \chi_i \; \left(-\frac{\partial\psi}{\partial\eta}\right)_i \; \left(\frac{\partial\chi}{\partial\eta}\right)_i \; \left(-\frac{\partial^2\psi}{\partial\eta^2}\right)_i \; v_{i+1} \; w_{i+1} \; \psi_{i+1} \; \chi_{i+1} \; \left(-\frac{\partial\psi}{\partial\eta}\right)_{i+1} \left(\frac{\partial\chi}{\partial\eta}\right)_{i+1} \left(-\frac{\partial^2\psi}{\partial\eta^2}\right)_{i+1} \rfloor^T \tag{3.90c}$$

Similarly for the 7 DOF/node, one may write

$$\psi = \underset{1\times14}{\lfloor G_{\psi_7} \rfloor} \underset{14\times1}{\{\beta\}} \tag{3.90d}$$

$$\chi = \underset{1\times14}{\lfloor G_{\chi_7} \rfloor} \underset{14\times1}{\{\beta\}} \tag{3.90e}$$

$$\left(-\frac{\partial\psi}{\partial\eta}\right) = \underset{1\times14}{\lfloor G_{(-\psi,\eta)_7} \rfloor} \underset{14\times1}{\{\beta\}} \tag{3.90f}$$

$$\frac{\partial\chi}{\partial\eta} = \underset{1\times14}{\lfloor G_{(\chi,\eta)_7} \rfloor} \underset{14\times1}{\{\beta\}} \tag{3.90g}$$

$$\left(-\frac{\partial^2\psi}{\partial\eta^2}\right) = \underset{1\times14}{\lfloor G_{(-\psi,\eta\eta)_7} \rfloor} \underset{14\times1}{\{\beta\}} \tag{3.90h}$$

Also,

$$\underset{14\times1}{\{q\}} = \underset{14\times14}{[A_7]} \underset{14\times1}{\{\beta\}} \tag{3.90i}$$

$$\underset{14\times1}{\{\beta\}} = \underset{14\times14}{[A_7]^{-1}} \underset{14\times1}{\{q\}} \tag{3.90j}$$

$$\underset{2\times1}{\{\underset{\sim}{u}\}} = \underset{2\times14}{[U_7(\eta)]} \underset{14\times14}{[A_7]^{-1}} \underset{14\times1}{\{q\}} \tag{3.90k}$$

Since it was previously shown that a polynomial description of the same order for both v and w provide a better description than one for which that is not so; it was considered appropriate to investigate an 8 DOF/node element right after the 6 DOF/node. This 8 DOF/node element has the added feature of continuity of the second rate of change of extension $(\frac{\partial^2 \chi}{\partial \eta^2})$, thereby insuring complete continuity of strain and its first rate of change in all the nonlinear strain displacement relations considered (A thru E), plus continuity of the second rate of change of the membrane strain $\varepsilon_o(\eta)=\chi+\frac{1}{2}\psi^2+\frac{1}{2}\chi^2$.

One assumes displacement polynomials of the 7th degree both in v and w:

$$\underset{2\times1}{\begin{Bmatrix} v \\ w \end{Bmatrix}} = \underset{2\times16}{\begin{bmatrix} \cos\phi & \sin\phi & B_1\eta & 0 & 0 & \eta^2 & \eta^3 & 0 & 0 & \eta^4 & \eta^5 & 0 & 0 & \eta^6 & \eta^7 \\ -\sin\phi & \cos\phi & B_2 & 0 & \eta^2 & \eta^3 & 0 & 0 & \eta^4 & \eta^5 & 0 & 0 & \eta^6 & \eta^7 & 0 & 0 \end{bmatrix}} \underset{16\times1}{\{\beta\}} \tag{3.91a}$$

or more concisely:

$$\underset{2\times1}{\{\underset{\sim}{u}\}} = \underset{2\times16}{[U_8(\eta)]}\ \underset{16\times1}{\{\beta\}} \tag{3.91b}$$

The appropriate generalized displacements are:

$$\{q\} = \left\lfloor v_i\ w_i\ \psi_i\ \chi_i\ \left(-\frac{\partial\psi}{\partial\eta}\right)_i\ \left(\frac{\partial\chi}{\partial\eta}\right)_i\ \left(-\frac{\partial^2\psi}{\partial\eta^2}\right)_i\ \left(\frac{\partial^2\chi}{\partial\eta^2}\right)_i \right.$$

$$\left. v_{i+1}\ w_{i+1}\ \psi_{i+1}\ \chi_{i+1}\ \left(-\frac{\partial\psi}{\partial\eta}\right)_{i+1}\ \left(\frac{\partial\chi}{\partial\eta}\right)_{i+1}\ \left(-\frac{\partial^2\psi}{\partial\eta^2}\right)_{i+1}\ \left(\frac{\partial^2\chi}{\partial\eta^2}\right)_{i+1} \right\rfloor^T \tag{3.91c}$$

where

$$\psi = \underset{1\times16}{\lfloor G\ \psi_8 \rfloor}\ \underset{16\times1}{\{\beta\}} \tag{3.91d}$$

$$\chi = \underset{1\times16}{\lfloor G\ \chi_8 \rfloor}\ \underset{16\times1}{\{\beta\}} \tag{3.91e}$$

$$\left(-\frac{\partial\psi}{\partial\eta}\right) = \underset{1\times16}{\lfloor G_{(-\psi,\eta)_8} \rfloor}\ \underset{16\times1}{\{\beta\}} \tag{3.91f}$$

$$\frac{\partial \chi}{\partial \eta} = \underset{1\times 16}{\left[G_{(\chi,\eta)\,8} \right]} \underset{16\times 1}{\{\beta\}} \tag{3.91g}$$

$$\left(-\frac{\partial^2 \psi}{\partial \eta^2}\right) = \underset{1\times 16}{\left[G_{(-\psi,\eta\eta)\,8} \right]} \underset{16\times 1}{\{\beta\}} \tag{3.91h}$$

$$\frac{\partial^2 \chi}{\partial \eta^2} = \underset{1\times 16}{\left[G_{(\chi,\eta\eta)\,8} \right]} \underset{16\times 1}{\{\beta\}} \tag{3.91i}$$

Also,

$$\underset{16\times 1}{\{q\}} = \underset{16\times 16}{\left[A_8 \right]} \underset{16\times 1}{\{\beta\}} \tag{3.91k}$$

$$\underset{16\times 1}{\{\beta\}} = \underset{16\times 16}{\left[A_8 \right]^{-1}} \underset{16\times 1}{\{q\}} \tag{3.91l}$$

$$\underset{2\times 1}{\{\underset{\sim}{u}\}} = \underset{2\times 16}{\left[U_8(\eta) \right]} \underset{16\times 16}{\left[A_8 \right]^{-1}} \underset{16\times 1}{\{q\}} \tag{3.91m}$$

Finally, it may be worth summarizing the physical significance of the different degrees of freedom chosen at the element nodes:

DOF	related to*
v	in-plane displacement
w	out-of-plane displacement
$\psi = \frac{\partial w}{\partial \eta} - \frac{v}{R}$	rotation (If the beam rotates an angle θ, $\psi = \sin\theta$ in absence of strain)
$\chi = \frac{\partial v}{\partial \eta} + \frac{w}{R}$	extension (If the beam rotates an angle θ, $\chi = \cos\theta - 1$ in absence of strain) If the strain is nonzero χ is the membrane strain in the linear theory, and hence χ is related to the <u>axial force</u> for small displacements ($P \tilde{\sim} EA\chi$).

DOF	related to*
$(-\frac{\partial\psi}{\partial\eta}) = -\frac{\partial^2 w}{\partial\eta^2} + \frac{\partial}{\partial\eta}(\frac{v}{R})$	change of curvature Related to the moment, for small displacements, $(M \simeq EI \frac{\partial\psi}{\partial\eta})$.
$\frac{\partial\chi}{\partial\eta} = \frac{\partial^2 v}{\partial\eta^2} + \frac{\partial}{\partial\eta}(\frac{w}{R})$	rate of change of extension For small displacements this is related to the axial pressure $(p_\eta \simeq \frac{\partial}{\partial\eta}(EA\chi))$.
$(-\frac{\partial^2\psi}{\partial\eta^2}) = -\frac{\partial^3 w}{\partial\eta^3} + \frac{\partial^2}{\partial\eta^2}(\frac{v}{R})$	rate of change of the change of curvature Related, for small displacements, to the shear force $(Q \simeq \frac{\partial}{\partial\eta}(EI \frac{\partial\psi}{\partial\eta}))$.
$\frac{\partial^2\chi}{\partial\eta^2} = \frac{\partial^3 v}{\partial\eta^3} + \frac{\partial^2}{\partial\eta^2}(\frac{w}{R})$	second rate of change of extension

3.4 Finite Element Property Matrices

In this subsection curved-beam finite element property matrices based upon the unconventional assumed-displacement variational formulation of Subsections 2.1 and 2.2 are illustrated for only one of the strain-displacement relations defined in Subsection 3.2.2, for generality, conciseness, and avoiding unnecessary repetition; chosen for use is Eq. 3.34 (Type C) which includes the other discussed relations as special cases. The finite element property matrices [m], {p}, [h], and {f} defined by Eqs. 2.17a-2.17d are displayed here in symbolic form without regard to any specific one of the three assumed displacement fields defined in Subsection 3.3.3; all finite

*Observe that $\psi \neq \sin\theta$ and $\chi \neq \cos\theta - 1$ for nonzero strain, and that for large displacements and rotations $EI \frac{\partial\psi}{\partial\eta}$ is not completely and uniquely related to the moment, that $\frac{\partial}{\partial\eta}(EI \frac{\partial\psi}{\partial\eta})$ is not completely and uniquely related to the shear force, and that χ and its derivatives are not completely and uniquely related to the membrane strain and its derivatives.

element matrices including the three types of selected assumed-displacement fields are given in full in Appendix B.

3.4.1 Strain-Displacement Expressions and Strain Increments

For convenient reference the Type C strain-displacement relation is repeated here:

$$\epsilon(\eta,\zeta)=\epsilon_o(\eta)+\zeta\,\mathcal{K}(\eta)+\tfrac{1}{2}\zeta^2\,\mathcal{H}_b(\eta) \tag{3.92}$$

where

$$\epsilon_o(\eta)=\chi\left(1+\tfrac{1}{2}\chi\right)+\tfrac{1}{2}\psi^2 \tag{3.93}$$

$$\mathcal{K}(\eta)=-\frac{\partial\psi}{\partial\eta}(1+\chi)+\psi\frac{\partial\chi}{\partial\eta} \tag{3.94}$$

$$\mathcal{H}_b(\eta)=\left(\frac{\partial\psi}{\partial\eta}\right)^2+\left(\frac{\partial\chi}{\partial\eta}\right)^2 \tag{3.95}$$

$$\chi=\frac{\partial v}{\partial\eta}+\frac{w}{R} \tag{3.96}$$

$$\psi=\frac{\partial w}{\partial\eta}-\frac{v}{R} \tag{3.97}$$

As in Section 2, let the midsurface displacement field v,w within the element be denoted by $\underset{\sim}{u}$ and expressed in terms of suitable interpolation functions $U(\eta)$ as:

$$\{\underset{\sim}{u}\}=[U(\eta)]\{\beta(t)\} \tag{3.98}$$

Hence, the generalized nodal displacements {q} and the parameters {β(t)} are related by substituting the nodal coordinates for nodes i and i+1 into Eq. 3.98 to obtain

$$\{q\} = [A]\{\beta(t)\} \tag{3.99}$$

Hence,

$$\{\beta\} = [A]^{-1}\{q\} \tag{3.100}$$

Accordingly, Eqs. 3.98 and 3.100 yield

$$\{\underset{\sim}{u}\} = [U(\eta)][A]^{-1}\{q\} \tag{3.101}$$

One can then express the strain quantities $\varepsilon_o(\eta)$, $\kappa(\eta)$, and $H(\eta)$ of Eq. 3.92 in terms of the {q} and the assumed displacement field to obtain

$$\epsilon_o = \left(1 + \frac{1}{2}\lfloor \underset{\sim}{u} \rfloor \{B_1\}\right)\lfloor B_1 \rfloor \{\underset{\sim}{u}\} + \frac{1}{2}\lfloor \underset{\sim}{u} \rfloor \{B_2\}\lfloor B_2 \rfloor \{\underset{\sim}{u}\} \tag{3.102}$$

$$\mathcal{K} = \left(1 + \lfloor \underset{\sim}{u} \rfloor \{B_1\}\right)\lfloor B_3 \rfloor \{\underset{\sim}{u}\} + \lfloor \underset{\sim}{u} \rfloor \{B_2\}\lfloor B_4 \rfloor \{\underset{\sim}{u}\} \tag{3.103}$$

$$\mathcal{H}_o = \lfloor \underset{\sim}{u} \rfloor \{B_3\}\lfloor B_3 \rfloor \{\underset{\sim}{u}\} + \lfloor \underset{\sim}{u} \rfloor \{B_4\}\lfloor B_4 \rfloor \{\underset{\sim}{u}\} \tag{3.104}$$

where

$$\{\underset{\sim}{u}\} = \lfloor \underset{\sim}{u} \rfloor^T = \begin{Bmatrix} v \\ w \end{Bmatrix} \tag{3.105}$$

$$\lfloor B_1 \rfloor = \lfloor \frac{\partial}{\partial \eta} \quad \frac{1}{R} \rfloor \qquad (3.106a)$$

$$\lfloor B_2 \rfloor = \lfloor -\frac{1}{R} \quad \frac{\partial}{\partial \eta} \rfloor \qquad (3.106b)$$

$$\lfloor B_3 \rfloor = -\frac{\partial}{\partial \eta} \lfloor B_2 \rfloor \qquad (3.106c)$$

$$\lfloor B_4 \rfloor = \frac{\partial}{\partial \eta} \lfloor B_1 \rfloor \qquad (3.106d)$$

$$\lfloor B_1 \rfloor \{ \underset{\sim}{u} \} = \chi \qquad (3.106e)$$

$$\lfloor B_2 \rfloor \{ \underset{\sim}{u} \} = \psi \qquad (3.106f)$$

$$\lfloor B_3 \rfloor \{ \underset{\sim}{u} \} = -\frac{\partial \psi}{\partial \eta} \qquad (3.106g)$$

$$\lfloor B_4 \rfloor \{ \underset{\sim}{u} \} = \frac{\partial \chi}{\partial \eta} \qquad (3.106h)$$

and, since

$$\{ \underset{\sim}{u} \} = [U(\eta)] [A]^{-1} \{ q \} \qquad (3.107a)$$

$$\lfloor B_i \rfloor \{ \underset{\sim}{u} \} = \lfloor B_i \rfloor [U(\eta)] [A^{-1}] \{ q \} \qquad (3.107b)$$

It is useful to express ε_o, κ, and H in terms of the generalized displacements {q} by using Eq. 3.93 thru 3.95 and defining convenient matrices D_i as follows:

$$\lfloor D_i \rfloor \equiv \lfloor B_i \rfloor [U(\eta)] [A]^{-1} \qquad (3.108)$$

Thus, one may write*

$$\lfloor D_1 \rfloor = \lfloor G_\chi \rfloor [A]^{-1} \quad (3.109a) \qquad \lfloor D_1 \rfloor \{q\} = \chi \quad (3.109e)$$

$$\lfloor D_2 \rfloor = \lfloor G_\psi \rfloor [A]^{-1} \quad (3.109b) \qquad \lfloor D_2 \rfloor \{q\} = \psi \quad (3.109f)$$

$$\lfloor D_3 \rfloor = \lfloor G_{(-\psi,\eta)} \rfloor [A]^{-1} \quad (3.109c) \qquad \lfloor D_3 \rfloor \{q\} = -\frac{\partial \psi}{\partial \eta} \quad (3.109g)$$

$$\lfloor D_4 \rfloor = \lfloor G_{\chi,\eta} \rfloor [A]^{-1} \quad (3.109d) \qquad \lfloor D_4 \rfloor \{q\} = \frac{\partial \chi}{\partial \eta} \quad (3.109h)$$

Accordingly, one obtains

$$\epsilon_o = \left(1 + \frac{1}{2} \lfloor q \rfloor \{D_1\}\right) \lfloor D_1 \rfloor \{q\} + \frac{1}{2} \lfloor q \rfloor \{D_2\} \lfloor D_2 \rfloor \{q\} \quad (3.110)$$

$$\mathcal{K} = \left(1 + \lfloor q \rfloor \{D_1\}\right) \lfloor D_3 \rfloor \{q\} + \lfloor q \rfloor \{D_2\} \lfloor D_4 \rfloor \{q\} \quad (3.111)$$

$$\mathcal{H}_o = \lfloor q \rfloor \{D_3\} \lfloor D_3 \rfloor \{q\} + \lfloor q \rfloor \{D_4\} \lfloor D_4 \rfloor \{q\} \quad (3.112)$$

*Matrices $\lfloor G \rfloor$ were defined in Subsection 3.3.3.

In the process of transient-response solution, it is necessary to evaluate the strain increment, $\Delta\varepsilon_{m+1}$ from time instant t_m to time t_{m+1}. This strain increment is related to both the displacement and the displacement increment by

$$\Delta\epsilon_{m+1} = \Delta\epsilon_{o\,m+1} + \zeta\,\Delta\mathcal{K}_{m+1} + \frac{1}{2}\zeta^2\,\Delta\mathcal{H}_{m+1} \tag{3.113}$$

where the associated incremental quantities are

$$\Delta\chi_{m+1} = \chi_{m+1} - \chi_m \tag{3.114a}$$

$$\Delta\psi_{m+1} = \psi_{m+1} - \psi_m \tag{3.114b}$$

$$\Delta\left(-\frac{\partial\psi}{\partial\eta}\right)_{m+1} = \left(-\frac{\partial\psi}{\partial\eta}\right)_{m+1} - \left(-\frac{\partial\psi}{\partial\eta}\right)_m \tag{3.114c}$$

$$\Delta\left(\frac{\partial\chi}{\partial\eta}\right)_{m+1} = \left(\frac{\partial\chi}{\partial\eta}\right)_{m+1} - \left(\frac{\partial\chi}{\partial\eta}\right)_m \tag{3.114d}$$

$$\Delta\epsilon_{o\,m+1} = \epsilon_{o\,m+1} - \epsilon_{o\,m} \tag{3.114e}$$

$$\Delta\mathcal{K}_{m+1} = \mathcal{K}_{m+1} - \mathcal{K}_m \tag{3.114f}$$

$$\Delta\mathcal{H}_{m+1} = \mathcal{H}_{m+1} - \mathcal{H}_m \tag{3.114g}$$

Hence, the "incremental strain" quantities in Eq. 3.113 become

$$\Delta\epsilon_{o_{m+1}} = \left(1+\chi_{m+1}-\frac{1}{2}\Delta\chi_{m+1}\right)\Delta\chi_{m+1} + \left(\psi_{m+1}-\frac{1}{2}\Delta\psi_{m+1}\right)\Delta\psi_{m+1} \tag{3.115}$$

$$\Delta\kappa_{m+1} = \left(1+\chi_{m+1}-\Delta\chi_{m+1}\right)\Delta\left(-\frac{\partial\psi}{\partial\eta}\right)_{m+1} + \left[\left(\frac{\partial\chi}{\partial\eta}\right)_{m+1} - \Delta\left(\frac{\partial\chi}{\partial\eta}\right)_{m+1}\right]\Delta\psi_{m+1}$$

$$+\left(-\frac{\partial\psi}{\partial\eta}\right)_{m+1}\Delta\chi_{m+1} + \psi_{m+1}\,\Delta\left(\frac{\partial\chi}{\partial\eta}\right)_{m+1} \tag{3.116}$$

$$\Delta\mathcal{H}_{m+1} = \left[\left(-\frac{\partial\psi}{\partial\eta}\right)_{m+1} - \frac{1}{2}\Delta\left(-\frac{\partial\psi}{\partial\eta}\right)_{m+1}\right]\Delta\left(-\frac{\partial\psi}{\partial\eta}\right)_{m+1}$$

$$+\left[\left(\frac{\partial\chi}{\partial\eta}\right)_{m+1} - \frac{1}{2}\Delta\left(\frac{\partial\chi}{\partial\eta}\right)_{m+1}\right]\Delta\left(\frac{\partial\chi}{\partial\eta}\right)_{m+1} \tag{3.117}$$

Expressed in matrix form in terms of the generalized displacements and their increments, these strain increment quantities become

$$\Delta\epsilon_{o\,m+1} = \left(1 + \left[q_{m+1}\right]\{D_1\} - \frac{1}{2}\left[\Delta q_{m+1}\right]\{D_1\}\right)\left[D_1\right]\{\Delta q_{m+1}\}$$

$$+\left(\left[q_{m+1}\right]\{D_2\} - \frac{1}{2}\left[\Delta q_{m+1}\right]\{D_2\}\right)\left[D_2\right]\{\Delta q_{m+1}\} \tag{3.118}$$

$$\Delta K_{m+1} = \left(1 + \lfloor q_{m+1} \rfloor \{D_1\} - \lfloor \Delta q_{m+1} \rfloor \{D_1\}\right) \lfloor D_3 \rfloor \{\Delta q_{m+1}\}$$
$$+ \left(\lfloor q_{m+1} \rfloor \{D_4\} - \lfloor \Delta q_{m+1} \rfloor \{D_4\}\right) \lfloor D_2 \rfloor \{\Delta q_{m+1}\}$$
$$+ \lfloor q_{m+1} \rfloor \{D_3\} \lfloor D_1 \rfloor \{\Delta q_{m+1}\} + \lfloor q_{m+1} \rfloor \{D_2\} \lfloor D_4 \rfloor \{\Delta q_{m+1}\} \quad (3.119)$$

$$\Delta H_{m+1} = \left(\lfloor q_{m+1} \rfloor \{D_3\} - \frac{1}{2} \lfloor \Delta q_{m+1} \rfloor \{D_3\}\right) \lfloor D_3 \rfloor \{\Delta q_{m+1}\}$$
$$+ \left(\lfloor q_{m+1} \rfloor \{D_4\} - \frac{1}{2} \lfloor \Delta q_{m+1} \rfloor \{D_4\}\right) \lfloor D_4 \rfloor \{\Delta q_{m+1}\} \quad (3.120)$$

The terms of higher order of the form $\lfloor \Delta q_{m+1} \rfloor \{D_j\} \lfloor D_k \rfloor \{\Delta q_{m+1}\}$ could be dropped for a sufficiently small time increment step (or sufficiently small Δq), but are retained for subsequent study.

3.4.2 Mass Matrix

To be consistent with the assumption of Kirchhoff behavior*, the consistent mass matrix of the finite element including both rotary ($\dot{\psi}$) and translational effects ($\dot{v}, \dot{w}$) may be obtained from the expression for the kinetic energy K_E, as follows:

$$K_E = \frac{1}{2} \iiint_{V_n} \rho_o \left(\dot{\tilde{v}}^2 + \dot{\tilde{w}}^2\right) dV = \quad (3.121)$$
$$= \frac{1}{2} \int_0^{\eta_i} \int_{-\frac{b}{2}(\zeta,\eta)}^{\frac{b}{2}(\zeta,\eta)} \int_{-\frac{h}{2}(\eta)}^{\frac{h}{2}(\eta)} \rho_o \left[(\dot{v} - \zeta\dot{\psi})^2 + \dot{w}^2\right] \left(1 + \frac{\zeta}{R}\right) d\zeta \, d\xi \, d\eta$$

*Kirchhoff displacement field: $\tilde{v} = v - \zeta\psi$, $\tilde{w} = w$; see comment on Eq. 3.68 in Subsection 3.3.3.

where $(1+\frac{\zeta}{R})d\eta^*$ is the line element, $h(\eta)$ is the thickness of the beam, $b(\zeta,\eta)$ is the width and ρ_o is the mass per unit volume of the undeformed body, and the integrations are performed over the undeformed volume. For a beam (ring) of uniform width b, one may write,

$$K_E = \frac{1}{2}\int_0^{\eta_i} \begin{bmatrix}\dot{v} & \dot{w} & \dot{\psi}\end{bmatrix} [B(\eta)] \begin{Bmatrix}\dot{v}\\ \dot{w}\\ \dot{\psi}\end{Bmatrix} d\eta \tag{3.122}$$

where

$$B(\eta) = \rho_o b h(\eta) \begin{bmatrix} 1 & 0 & -\frac{h^2(\eta)}{12R(\eta)} \\ 0 & 1 & 0 \\ -\frac{h^2(\eta)}{12R(\eta)} & 0 & \frac{h^2(\eta)}{12} \end{bmatrix} \tag{3.123}$$

Depending on the ratio of the thickness h to the radius of curvature R of the beam, and the assumed strain displacement relations, one may or may not keep the off-diagonal terms involving $\frac{h^2}{R}$.

One may express $\dot{v}, \dot{w}$, and $\dot{\psi}$ in terms of the $\{\dot{q}\}$:

$$\begin{Bmatrix}\dot{v}\\ \dot{w}\\ \dot{\psi}\end{Bmatrix} = \begin{bmatrix} U(\eta) \\ G_\psi(\eta) \end{bmatrix} \{\dot{\beta}\} \equiv [N(\eta)] \{\dot{q}\} \tag{3.124}$$

where

$$[N(\eta)] = \begin{bmatrix} U(\eta) \\ G_\psi(\eta) \end{bmatrix} [A]^{-1} \tag{3.125}$$

*See for example Krauss [116, p.29] or Sokolnikoff [95].

Applying Eq. 3.124 to Eq. 3.122, one obtains:

$$K_E = \frac{1}{2} \{\dot{q}\}^T [m] \{\dot{q}\} \tag{3.126}$$

where

$$[m] = \int_0^{\eta_i} [N(\eta)]^T [B(\eta)] [N(\eta)] \, d\eta \tag{3.127}$$

where the consistent mass matrix [m] of the element is symmetric and positive definite.

Mass matrices may be formed in various ways, with two widely used categories: consistent and lumped. Widespread experience with these categories may be summarized by quoting Cook [103, page 239 and 240]:

> "When shape functions [N] are identical to those used in formulating the element stiffness matrix, [m] is called the consistent mass matrix. It is always positive definite. Alternatively, simpler forms of [N] may be used in computing [m]. The simplest mass matrix is that obtained by placing point masses m_i at the displacement d.o.f. The latter form of [m] is called a lumped mass matrix.
>
> .
> .
> .
>
> The lumped mass matrix is a diagonal matrix. The consistent mass matrix is fully populated and more time consuming to generate. There are computational advantages if mass matrices are diagonal instead of full, as we will see below. However, if the lumped mass approximation is crude, many elements may be needed to obtain sufficiently accurate results. Thus, we have the question: can we say which type of mass matrix is generally to be preferred? The answer appears to be "no". Use of lumped masses usually tends to lower natural frequencies, while the excess stiffness present in a mesh of compatible elements tend to raise them. Thus, the two opposite tendencies

tend to cancel, and for a given mesh size lumped masses may give more accurate results than a consistent formulation."

3.4.3 Generalized Nodal-Force Matrices for the Unconventional Formulation

The equivalent generalized nodal forces which correspond to or represent the externally-applied loading can be obtained by placing the assumed displacement field into the expression for the variation of the work of the externally-applied loading:

$$\delta \bar{W} = \int_0^{\eta_i} \left(F_v(t)\,\delta v + F_w(t)\,\delta w + \underset{\sim}{M}(t)\,\delta \psi \right) \left[1 + \frac{\zeta}{R} \right] d\eta \qquad (3.128)$$

where $\bar{F}(t) = F_v(t)\,\bar{a}_2 + F_w(t)\,\bar{n}$ is the applied time varying force per unit length (3.129a)

$\bar{M}(t) = \underset{\sim}{M}(t)\,\bar{a}_1$ is the applied-time varying moment per unit length (3.129b)

Substituting the assumed displacement function into Eq. 3.128 in terms of $\{q\}$ one obtains:

$$\delta \bar{W} = \lfloor \delta q \rfloor \{ f \} \qquad (3.130)$$

where the generalized nodal force matrix $\{f\}$ for the element is given by

$$\{ f \} = \int_0^{\eta_i} [N(\eta)]^T \begin{Bmatrix} F_v \\ F_w \\ \underset{\sim}{M} \end{Bmatrix} \left(1 + \frac{\zeta}{R} \right) d\eta \qquad (3.131)$$

The equivalent nodal forces associated with the internal axial stress σ are represented by the terms $\{p\}$ and $[h]\{q\}$ in the unconventional assumed-displacement variational formulation (see Eqs. 2.16 and 2.17), and may be identified by writing the following expression for the variation δU of the internal strain energy in the element:

$$\delta U = \iiint_{V_n} \sigma \, \delta\epsilon \, dV = \iiint_{V_n} \sigma \left[\delta\epsilon_o + \zeta \delta K + \tfrac{1}{2}\zeta^2 \delta H\right] dV \tag{3.132}$$

First performing the integration on $d\xi d\zeta$ over the cross section of the curved beam at any η station, the following convenient stress-related quantities L, M, and I may be identified:

$$L = \iint_{A_{C\text{-}S}} \sigma \, d\xi \, d\zeta \qquad M = \iint_{A_{C\text{-}S}} \sigma \, \zeta \, d\xi \, d\zeta \tag{3.133}$$

$$I = \iint_{A_{C\text{-}S}} \sigma \, \zeta^2 \, d\xi \, d\zeta$$

Introducing these quantities into Eq. 3.132, one obtains

$$\delta U = \int_0^{\eta_i} \left[\left(L + \frac{M}{R}\right)\delta\epsilon_o + M \delta K + \frac{1}{2} I \, \delta H\right] d\eta \tag{3.134}$$

Since ϵ_o, K, and H are given by Eqs. 3.110, 3.111, and 3.112, respectively, in terms of the generalized displacements, the variations $\delta\epsilon_o$, δK, and δH become:

$$\delta\epsilon_o = [\delta q]\{D_1\}\left(1 + [D_1]\{q\}\right) + [\delta q]\{D_2\}[D_2]\{q\} \tag{3.135}$$

$$\delta K = [\delta q]\{D_3\}(1 + [D_1]\{q\}) + [\delta q]\{D_1\}[D_3]\{q\} +$$

$$[\delta q]\{D_4\}[D_2]\{q\} + [\delta q]\{D_2\}[D_4]\{q\} \tag{3.136}$$

$$\frac{1}{2}\delta \mathcal{H}_0 = [\delta q]\{D_3\}[D_3]\{q\} + [\delta q]\{D_4\}[D_4]\{q\} \tag{3.137}$$

where only generalized-displacement variations are permitted. Applying Eqs. 3.135-3.137 to Eq. 3.134, one finds:

$$\delta U = [\delta q](\{P\} + [h]\{q\}) \tag{3.138}$$

where

$$\{P\} = \int_0^{\eta_i} \left[\{D_1\}\left(L + \frac{M}{R}\right) + \{D_3\}M\right] d\eta \tag{3.139}$$

$$[h] = \int_0^{\eta_i} \Big[\left(\{D_1\}[D_1] + \{D_2\}[D_2]\right)\left(L + \frac{M}{R}\right)$$

$$+ \left(\{D_1\}[D_3] + \{D_3\}[D_1] + \{D_2\}[D_4] + \{D_4\}[D_2]\right)M$$

$$+ \left(\{D_4\}[D_4] + \{D_3\}[D_3]\right)I\Big] d\eta \tag{3.140}$$

In practice, the integrations along η and those over the cross section for L, M, and I are evaluated numerically by Gaussian quadrature. These evaluations are discussed further in Section 4.

3.4.4 Comments on the Conventional Formulation

As noted in Subsection 2.3, one can derive the conventional formulation from the unconventional formulation explained in Subsections 2.2 and 3.4.3 by replacing via the stress-strain and strain-displacement relations. Accordingly, only the terms {p} and [h] {q} of the unconventional formulation are affected -- the element matrices [m] and {f} are unchanged. Hence, although the unconventional formulation is used almost exclusively in the studies discussed in Section 4, it is useful to see the much greater complexity that would result if one were to use the conventional formulation.

Accordingly, the stress-strain relation given by Eq. 2.21 becomes for the present "uniaxial strain and stress conditions":

$$\sigma = E\left(\epsilon - \epsilon^P\right) \tag{3.141}$$

where σ and ϵ are, respectively, the uniaxial stress and the total strain, and ϵ^P is the plastic part of the strain. One can perhaps visualize sufficiently the large number of terms resulting from forming {p} and [h] {q} by substituting the following expressions for L, M, and I in Eq. 3.139 for {p} and in Eq. 3.140 for [h]:

$$L = \iint_A \sigma \, d\xi \, d\zeta = \iint_A E\left(\epsilon - \epsilon^P\right) d\xi \, d\zeta =$$

$$= \iint_A \left[E\epsilon_0 + E\zeta\cancel{\mathcal{K}} + \frac{1}{2}E\zeta^2\mathcal{H} - E\epsilon^P\right] d\xi \, d\zeta \tag{3.142}$$

$$M = \iint_A \sigma\zeta \, d\xi \, d\zeta = \iint_A E\zeta\left(\epsilon - \epsilon^P\right) d\xi \, d\zeta =$$

$$= \iint_A \left[\cancel{E\zeta\epsilon_0} + E\zeta^2\mathcal{K} + \frac{1}{2}E\zeta^3\mathcal{H} - E\zeta\epsilon^P\right] d\xi \, d\zeta \tag{3.143}$$

$$I = \iint_A \sigma \zeta^2 \, d\xi \, d\zeta = \iint_A E \zeta^2 [\epsilon - \epsilon^P] \, d\xi \, d\zeta =$$

$$= \iint_A [E \zeta^2 \epsilon_o + \underset{\approx}{E \zeta^3 \mathcal{K}} + \tfrac{1}{2} E \zeta^4 \mathcal{H} - E \zeta^2 \epsilon^P] \, d\xi \, d\zeta \quad (3.144)$$

Terms crossed out (X) vanish since the reference axis of the curved beam is assumed to be the centroidal axis of bending. Underlined terms ($\approx$) vanish if a ring of uniform width b is used, but not otherwise. Next, noting the expressions for ε_o, κ, and H in terms of the {q} from Eqs. 3.110, 3.111, 3.112, and using these to carry out the multiplications indicated in Eq. 3.139 and 3.140, one can readily appreciate the great number of terms which result from forming {p} and [h] {q} to provide the conventional-formulation terms. Thus, it is apparent that the unconventional formulation will often be more convenient and efficient for the analyst.

For present purposes it suffices to note that (see Ref. 17, page 50) for the conventional formulation:

$$\delta U = \lfloor \delta q \rfloor \left([k] \{q\} - \{f_P^L\} - \{f_P^{NL}\} - \{f_q^{NL}\} \right) \quad (3.145)$$

Also, for the unconventional formulation

$$\delta U = \lfloor \delta q \rfloor \left(\{p\} + [h] \{q\} \right) \quad (3.146)$$

where it can be shown that

$$\{p\} = [k]\{q\} - \{{}^{I}f_q^{NL}\} - \{f_p^{L}\} \tag{3.147}$$

$$[h]\{q\} = -\{{}^{II}f_q^{NL}\} - \{f_p^{NL}\} \tag{3.148}$$

In turn, $\{f_q^{NL}\} = \{{}^{'}f_q^{NL}\} + \{{}^{''}f_q^{NL}\}$ and consists of large deflection (NL: nonlinear) equivalent force contributions from both {p} and [h] {q}. In the above expressions:

[k] = usual element stiffness matrix

$\{f_q^{NL}\}$ = generalized force arising from internal forces associated with the nonlinear terms of the strain-displacement relations

$\{f_p^{L}\}$ = generalized plastic force terms associated with the plastic strains and the linear terms of the strain-displacement relation

$\{f_p^{NL}\}$ = generalized plastic force terms associated with the plastic strains and the nonlinear terms of the strain-displacement relation

Finally, one can readily show that the element stiffness matrix for the curved beam element may be evaluated by, assuming that $(1+\zeta/R) \approx 1$:

$$[k] = \iiint_{V_M} \left(E\{D_1\}\lfloor D_1 \rfloor + E\zeta^2\{D_3\}\lfloor D_3 \rfloor \right) d\xi\, d\zeta\, d\eta \tag{3.149}$$

For a curved beam of uniform width b, this becomes

$$[k] = \int_0^{\eta_i} \left(E b h \{D_1\}\lfloor D_1 \rfloor + \frac{1}{12} E b h^3 \{D_3\}\lfloor D_3 \rfloor \right) d\eta \tag{3.150}$$

where $h = h(\eta)$. This stiffness matrix will be of interest later in connection with determining the highest natural frequency embedded in the finite-element model of a given structure; this frequency is of interest since it is related to the largest time increment size Δt allowed in the transient solution process when the central-difference time operator is employed.

SECTION 4

EVALUATION AND DISCUSSION

4.1 Objectives and Scope

In this section the finite element formulations presented in Sections 2 and 3 are employed to examine their features and consequences by comparing predictions with each other for example impulsively-loaded structures undergoing large-deflection, elastic-plastic transient structural response. Highly nonlinear geometric and material behavior are involved. The main example problem chosen for illustration and evaluation purposes is an impulsively-loaded aluminum beam with both ends clamped; high quality experimental data are also available for this case and are used for theoretical-experimental comparisons. Also, a free initially-circular impulsively-loaded thin ring is analyzed. The principal matter under scrutiny concerns the performance of the finite-element models for highly nonlinear geometric and material behavior.

Since comparisons of predictions with pertinent high-quality experimental data provide the "final" evaluation of any prediction method, appropriate experimental data are employed herein and are described briefly in Subsection 4.2 for convenient reference.

Various analysis features are discussed in Subsections 4.3 through 4.5. The effects of including nonlinear bending terms (as well as nonlinear membrane terms) in the strain-displacement relations are discussed in Subsection 4.3. The effects upon the accuracy of evaluating various volume integrals numerically by employing various numbers of Gaussian stations in each element are described in Subsection 4.4. In Subsection 4.5, the effects upon the predicted spatial distributions and time histories of strains and displacements for the example beam problem are examined; comparisons are made also with experimental results for impulsively loaded beams. Subsection 4.5 also includes predictions versus experimental results for the free ring cited earlier.

To illustrate structural response to fragment impact, example calculations involving one finite element model are shown in Subsection 4.6

for an aluminum beam with clamped ends subjected to impact at its midspan by a one-inch diameter steel sphere.

Finally, a summarized assessment of these comparisons is given in Subsection 4.7.

4.2 Experimental Beam Responses to Impulse Loading and Impact

A definitive evaluation of transient structural response prediction methods requires finally that predictions be compared with well-defined experimental transient response data. Well-defined experimental data of this type are reported in Ref. 117 for impulsively-loaded and for steel-sphere-impacted 6061-T651 aluminum beams with both ends integrally clamped; specimens CB-1 through CB-4 were loaded impulsively while specimens CB-8 through CB-18 were subjected to steel sphere impact. Some of these data are repeated here for convenient reference since theoretical-experimental comparisons will be shown in later subsections of Section 4, and will pertain principally to specimen CB-1 with some attention also to specimens CB-4 and CB-18.

The nominal dimensions of the beam specimens (see Fig. 5) are: span 8.00 inch, width 1.50 inch, and thickness 0.100 inch; the actual dimensions are given in Table 1. Figure 6 indicates clamped beam model nomenclature and descriptive coordinates. Spanwise oriented strain gages were installed at the midwidth station (y=0) at various spanwise locations on the lower (L or loaded) surface and on the upper (U or non-loaded) surface; these locations and the resulting permanent strains indicated by all surviving strain gages on specimens CB-1, CB-4, CB-13, and CB-18 are given in Table 2.

The test schematic for the impulsively-loaded beams is shown in Fig. 7. Sheet explosive (HE) of known dimensions and weight, centered at midspan, and covering the entire width of the beam was employed. The sheet HE was separated from the aluminum beam specimen by a suitable layer of polyurethane foam buffer to prevent stress-wave-induced spalling of the beam specimen. The result is that the beam experiences essentially a uniform initial velocity in the HE-covered region. For specimens CB-1 and CB-4 the pertinent data are:

Specimen	HE-Covered Spanwise Length x(in)	Imparted Velocity (in/sec)	Imparted Kinetic Energy (in-lb)
CB-1	1.80	6657	1542
CB-4	1.80	10,589	3930

Transient strains were recorded via oscilloscopes and oscilloscope cameras; the recorded transient strains for specimens CB-1 and CB-4 are shown in Figs. 8 and 9, respectively. The "strain value" shown is actually the "uncorrected" relative elongation E_x in the spanwise (x) direction. For sufficiently large values, the following nonlinear correction must be applied to obtain correct values E_{xc} (tension is +; compression is -):

$$E_{xc} = \frac{GF\ E_x}{GF + E_x} \tag{4.1}$$

where

GF = gage factor of the strain gage (2.06 $\pm$ 1%)

E_x = reading in the oscilloscope picture; units of in/in.

Figure 10 shows a test schematic for the impact tests. Examples of post-test impacted specimens are given in Fig. 11 for specimens CB-12 and CB-13. Transient strains recorded for specimens CB-13 and CB-18 are given in Figs. 12 and 13, respectively; the measured permanent strains are given in Table 2. For these two typical specimens, the weight of the 1-inch diameter impacting sphere and its initial impact velocity are:

Specimen	Weight of Steel Sphere (grams)	Initial Impact Velocity (in/sec)
CB-13	66.738	2490
CB-18	66.810	2794

Model CB-13 experienced a moderate amount of permanent deformation while specimen CB-18 exhibited large permanent deformation. Permanent deformation data reported in Ref. 117 are indicated later where needed in this report.

Of principal interest for comparison with predictions are the transient and permanent strain data. Secondary comparisons will be made with the observed permanent deflection results.

4.3 Effects of Nonlinear Strain-Displacement Terms

4.3.1 General Considerations

To be discussed in this subsection are the effects upon transient response predictions of including certain nonlinear membrane and bending terms in (a) calculations of strain, (b) incremental strain computations, and (c) the evaluation of generalized forces arising from nonlinear geometric (and material property) effects when applied to 2-d beam and ring structures which undergo transient large displacements and rotations. In assessing the effects of these nonlinear terms, particular attention is given to the predicted strains because strains are both a more sensitive and a more important indicator of the worth and necessity of including such terms than are the displacements themselves.

As discussed in Subsection 3.2.2.2, several strain-displacement relations identified as Types A, B, and C were investigated; also, two nonlinear versions intermediate between Types B and C were studied and are identified as Types D and E. for convenient reference, these relations are shown concisely in the following for large-displacement, small-strain conditions:

Membrane (Linear, Nonlinear) Bending (Linear, Nonlinear)

$$\epsilon = \underbrace{\chi + \tfrac{1}{2}\psi^2}_{\text{Type A}} + \tfrac{1}{2}\chi^2 + \zeta\left[\underbrace{\left(-\frac{\partial\psi}{\partial\eta}\right)}_{\text{Type B}} + \underbrace{\left(-\frac{\partial\psi}{\partial\eta}\right)\chi + \frac{\partial\chi}{\partial\eta}\psi}_{\text{Type D}}\right] + \frac{\zeta^2}{2}\underbrace{\left[\left(\frac{\partial\psi}{\partial\eta}\right)^2 + \left(\frac{\partial\chi}{\partial\eta}\right)^2\right]}_{\text{Type E}} \qquad \text{Type C} \qquad (4.2)$$

where $\chi = \frac{\partial v}{\partial \eta} + \frac{w}{R}$ is the "extension" and $\psi = \frac{\partial w}{\partial \eta} - \frac{v}{R}$ is the "rotation"; note that if a beam has zero midsurface strain* (ε_o=0) and rotates by an angle θ, $\psi = \sin\theta$, and $\chi = -1 + \cos\theta$ since $\chi = \sqrt{1+2\varepsilon_o}\cos\theta - 1$ and $\psi = \sqrt{1+2\varepsilon_o}\sin\theta$.

The effects of these various types of strain-displacement relations clearly must depend upon the severity and type of structural deformations present. Two types of illustrative situations were employed in assessing these effects and, hence, that assessment validity is restricted accordingly. These two problem types studied include (1) impulsively-loaded beams CB-1 and CB-4 with clamped ends -- see Subsection 4.2 -- and (2) a free thin circular ring subjected to severe impulse loading on a 120-degree sector of its exterior [118,119]. The beam structures undergo significant membrane straining and some bending but the rotations and spanwise strain gradients are not large over most of the structure. On the other hand, the impulsively-loaded free ring experiences severe rotations and bending in certain regions but the membrane strains are small over most of the ring except in the peripheral region spanned by the impulsive loading for a short time following the impulsively-applied loading. Each of these two categories of problems is discussed separately in the following.

4.3.2 Impulsively-Loaded Beam Model

Transient response calculations were carried out for beam model CB-1 by using various of the cited types of strain displacement relations. However, for the more-severely loaded CB-4 specimen, only the "complete nonlinear" Type C strain-displacement relation was used. Hence, the following discussion and comparisons will pertain to the CB-1 case.

Beam specimen CB-1 was modeled by 10 finite elements per beam half span, with 5 DOF/N CQ elements. At midspan (x=0) symmetry was imposed, while at the clamped end (x=4.00 in.) ideally-clamped conditions were applied. To represent the mechanical behavior of the 6061-T651 aluminum material, its unaxial stress-strain curve was approximated by piecewise-linear segments via the mechanical sublayer model with the following stress-strain (σ,ε) pairs; 41,000 psi, .0041 in/in; 45,000 psi, .012 in/in; and 53,000 psi, .10 in/in. For present purposes the material was assumed to be strain-rate insensitive; hence, the material was represented as behaving in an elastic, strain hardening

*See Eq. 3.30a for ε_o.

(EL-SH) fashion. Impulsively-applied uniform upward loading over a 1.80-in region centered at midspan was assumed to produce a uniform initial velocity of 6657 in/sec. Predicted transient extensional strains on the lower (L) or loaded surface and/or on the upper (U) or nonloaded surface are shown in various figures for the various spanwise stations (x) indicated in the following:

Station, x (in)	Surface U or L	Dominant Strain Type B or M	Figure
0	U and L	B and M	14a
1.40	U and L	B and M	14b
2.20	U and L	M	14c
3.00	U and L	M	14d
3.80	U and L	B and M	14e

Indicated here is the dominant type of strain behavior: bending (B) or membrane (M). That membrane behavior is dominant at stations x=2.20 and 3.00 in may be seen readily from Figs. 14c and 14d. Similarly, the important presence of both bending (B) and membrane (M) behavior at x=3.80 in may be appreciated by inspecting Fig. 14e; the mean between these two curves represents the membrane part of the strain and the extent to which each trace deviates from this mean curve represents the severity of the bending contribution to the strain.

An inspection of the strain predictions in Figs. 14c and 14d which include dominantly membrane behavior shows that the effects of using strain-displacement relation Types A, B, or C is very small; however, the least comprehensive relation (Type A) shows poorer agreement with the "best" relation (Type C) than does B with C.

At spanwise locations where both membrane and bending behavior are significant (x=0, 1.40 and 3.80 in -- see Figs. 14a, 14b, and 14e), these two types of behavior relative to each other change as time progresses. At station x=3.80 in, for example, which is near the clamped edge, membrane behavior dominates for about the first 150 microseconds; from t=150 to

about 350 microseconds, the strain is significantly of the bending type although the membrane strain has also increased importantly; and thereafter, both bending and membrane behavior are very significant. Note that beyond about 300 microseconds (as the rotations become larger and the membrane strain remains large), the Type A and Type B predictions differ markedly indicating that the parameter χ is playing an important role; however, the nonlinear bending terms in Type C contribute in a "compensatory fashion" such that the more reliable Type C predictions turn out to compare favorably with the "relatively crude" Type A predictions.

In the clamped beam example, the membrane effects dominate only after considerable changes of curvature have already taken place, and significant amounts of both bending and stretching effects are present in the beam. Where membrane effects are predominant, the nonlinear membrane term $\frac{1}{2}\chi^2$ prevails over the nonlinear change of curvature terms (since $\zeta \frac{\partial \psi}{\partial \eta}$ and $\zeta \frac{\partial \chi}{\partial \eta}$ are small there). The portions of the clamped beam where stretching behavior is most important is the region extending from some distance from the loaded region to some distance from the clamp. The nonlinear change of curvature terms are important at places that experience considerable bending; that is, near the clamps, in the impulsively-loaded region, and just beyond the edges of the impulsively-loaded region.

A considerable degree of mutual cancelling effect is observed between the nonlinear terms. Although in some instances the results obtained from strain-displacement relations Types A and C look very similar, this is sometimes the result of this mutual cancelling, as was observed from comparisons between the predictions obtained by using relations A, B, D, E, and C; for brevity and conciseness reasons, however, these "D and E results" are not shown here. As expected, the effect of the nonlinear terms (appearing in relations B, D, E and C) becomes significant after considerable displacements have occurred; for the clamped beam CB-1 example, this time is about 300 μsec. The central deflection and maximum rotation at that time (about 7.25 times the beam thickness and 17°, respectively) are close to the maximum

deflection and rotation experienced by the beam (about 7.5 times the beam thickness and 21^{o}, respectively).

At the center of the beam (where the peak deflection takes place) the membrane term $\frac{1}{2}\chi^2$ becomes significant at an earlier time than do the nonlinear bending terms, and although the effects of these nonlinear curvature terms eventually become as important, the peak strain takes place at an early time in the structural response (70 μsec.) when there is practically no difference between strain-displacement relations Types B, C, D, and E.

Finally, shown in Fig. 15 are comparisons between predictions of the midspan vertical deflection versus time for the Type A, B, and C strain-displacement relations for beam model CB-1. It is seen that this displacement information appears to be relatively insensitive to the type of strain-displacement relation used, whereas strain comparisons exhibit more pronounced differences.

From these (of many) example comparisons, it is clear that for general applications involving a time-varying mixture of membrane (both extensional and rotational action) and bending behavior, the more comprehensive Type C strain-displacement relation should be employed.

4.3.3 Impulsively-Loaded Free Circular Ring

A free initially-circular 6061-T6 aluminum ring of 2.937-in midsurface radius, 0.124-in thickness, and 1.195-in width was loaded impulsively uniformly over a 120-degree sector (centered at $\theta=0^{o}$) of its exterior, resulting in an initial inward velocity of 6853 in/sec for that loaded region. The static uniaxial stress-strain behavior of this material was approximated in a piecewise linear fashion with the following stress-strain pairs employed in the mechanical-sublayer model: (σ,ε) = 42,800 psi, .004076 in/in and 58,219 psi, 0.20 in/in; the material was assumed to be strain-rate sensitive, with strain-rate constants D and p taken to be D=6500 sec^{-1} and p=4. The mass per unit volume was taken to be .0002526 $(lb\text{-}sec^2)/in^4$.

For economy and convenience reasons, advantage was taken of symmetry; hence, the half ring was modeled by 18 uniform-length CC 4 DOF/N elements. Strain-displacement relations A and C each were used. In the timewise solution process, a time increment of 0.6 microseconds was employed.

For the initial conditions of this problem, it is evident that bending behavior will be dominant throughout the time history of the transient response in all portions of the ring except for the impulsively-loaded sector. In that sector, the ring will experience mainly compressive membrane strain for a short period of time following the impulsive loading, thereafter, the strain changes that occur will be mainly induced by bending. In a region just beyond the edge of the impulsive-loading zone (and near $\theta=180^{o}$), the ring will undergo very severe changes of curvature and bending strains, and rotations. Elsewhere, the strains produced will be principally of bending/rotation character. It is expected, therefore, that the very restricted Type A strain-displacement relation (with linear bending terms and including only the more important one of the two nonlinear membrane terms) may result in reasonable predictions in portions of the ring experiencing relatively small changes of curvature, but to provide less reliable predictions elsewhere. On the other hand, the Type C strain-displacement relation should provide superior predictions in all portions of the ring.

To illustrate the cited types of behavior, the circumferential strains predicted as a function of time are shown at both the inner surface and the outer surface at the following representative locations:

Location θ (deg.)	Dominant Strain Type B or M	Figure
15	M	16a
85	B	16b
155	B	16c
175	B	16d

As seen from Fig. 16a for location $\theta=15^{o}$ (in the impulsively-loaded region), at very early times the strains are of the membrane compression type; later, appreciable bending contributions are evident. At this location, the Type A and the Type C predictions are in reasonably close agreement throughout the transient response.

Representative of severe bending regions are the strain time histories for $\theta=85^{o}$ as shown in Fig. 16b. The Type A and Type C predictions agree well only for about the first 200 microseconds, and then exhibit increasing differences until about 1200 microseconds which is near the peak-response time. Thereafter, a near-constant but significant disparity remains. This agrees with the previously-indicated expected behavior.

Location $\theta=155^{o}$ involves an insignificant amount of membrane straining but does experience some bending action although the rotations are small. Hence, one would expect to see only minor differences between the Type A and Type C predictions at this location. This is confirmed by the plots given in Fig. 16c, where it is seen that these strains do not exceed 1 per cent.

Figure 16d for location $\theta=175^{o}$ indicates similar predominant bending behavior; here the inner surface experiences tension while the outer surface is in compression since "inward" deflection occurs in that region; only at the inner surface beyond about 1200 microseconds do the Type A and Type C predictions differ significantly.

To supplement the above information, it is instructive to examine the circumferential distribution of outer-surface and inner-surface strain at a fixed instant of time -- here selected as 1500 microseconds to display the near-maximum strain condition -- as shown in Fig. 17. Note that for the 4 DOF/N calculations the Type A and Type C predictions are in fairly close agreement except for the circumferential region $70^{o} \lesssim \theta \lesssim 90^{o}$ which lies just beyond the edge of the impulsively-loaded zone where very severe bending and rotations occur. Shown also for convenient comparison are strain predictions obtained by using 8 of the 8 DOF/N elements and the Type C strain-displacement relation; element node locations used were $\theta=0$, 30, 50, 70, 90, 110, 135, 160 and 180 degrees.

Finally, shown in Fig. 18 are time histories of the midsurface separation between locations $\theta=0$ and $\theta=180$ degrees as a function of time for the Type A and the Type C calculation when 18 4 DOF/N CC elements are used to model the half ring. These predictions are seen to be in good agreement with each other until nearly peak deformation (minimum separation) has occurred. Thereafter, the disparity increases as the influence of the nonlinear terms neglected in Type A manifest themselves in the Type C result through their contribution to the nonlinear equivalent load terms associated with large deflections and plastic behavior.

Here again, the general advisability of using the more comprehensive Type C strain-displacement relation is evident.

4.3.4 Summary Comments

For the clamped-beam type of problem examined, it was observed that the nonlinear term of principal importance in the strain-displacement relation is $\frac{1}{2}\psi^2$. Accordingly, the use of the Type A relation results in good displacement and strain predictions over all regions of the beam except near the clamped end where significant rotations occur at "late" times. To accommodate the behavior in this latter region, use of the Type C relation is recommended.

In the second illustrative example (the impulsively-loaded free ring) of numerous types of applicable structural/loading behavior accommodated, it was found that significantly different transient strains are predicted in certain severe-bending regions of the ring when the "complete" Type C rather than the Type A strain-displacement relation was used.

Hence, for general use it is recommended that the Type C strain-displacement relation be used in conjunction with any of the finite elements noted in this study: 4, 5, 6 or 8 DOF/N. Later discussions will center upon the comparative performances of these elements.

4.4 Effects of the Number of Gaussian Stations

The evaluation of finite-element property matrices for the present class of beam and ring (2-d) problems is carried out in practice by the numerical evaluation of volume integrals, except for the contributions to the loading vector $\{f\}$ arising from prescribed loading applied to the external surfaces of the element. In the present study of the behavior of higher-order elements, the unconventional finite element formulation is employed. It should be recalled, however, that the conventional formulation differs only from the former in terms of how one expresses the variation δU of the work of the internal forces; all other finite-element-property matrices are identical between these two formulations (see Eq. 2.17 and 2.22 for the unconventional and the conventional formulation, respectively; note that the individual element properties are cited, respectively, in Eqs. 2.17a-2.17d and in Eq. 2.22a).

For convenient reference, the expressions for δU for these two formulations are repeated here:

Unconventional Formulation

$$\delta U = \lfloor \delta q \rfloor \left(\{p\} + [h]\{q\} \right) \tag{4.3}$$

Conventional Formulation

$$\delta U = \lfloor \delta q \rfloor \left([k]\{q\} - \{f_q^{NL}\} - \{f_p^{L}\} - \{f_p^{NL}\} \right) \tag{4.4}$$

where [k] represents the usual stiffness matrix for small-deflection, linear-elastic behavior. It has been shown [17] that

$$\{p\} = [k]\{q\} - \{'f_q^{NL}\} - \{f_p^{L}\} \tag{4.5}$$

$$[h]\{q\} = -\{''f_q^{NL}\} - \{f_p^{NL}\} \tag{4.6}$$

where

$$\{f_q^{NL}\} = \{'f_q^{NL}\} + \{''f_q^{NL}\} \tag{4.7}$$

Thus, the correspondence between these two formulations is evident. The only two additional finite element matrices needed are the mass matrix [m] given by Eq. 2.17a and the prescribed applied-loads vector {f} given by Eq. 2.17d.

In evaluating the element property matrices for the present class of 2-d structures, one performs volume integrations to evaluate all of these matrices except for {f} which involves (usually) integrations only over a surface area. For the unconventional formulation, it is seen from Eq. 2.17b and 2.17c for {p} and [h], respectively, that one must integrate the product of the stress S^{ij} times quantities that vary with the spanwise location along the element. Hence, since S^{ij} varies with both the spanwise and the depthwise location within the element, one must select a suitably large number of numerical integration stations (a) through the depth and (b) along the span of an element in order to achieve an accurate evaluation. Because the stress S^{ij}

varies with both space and time during a typical transient response problem, it is somewhat more convenient for present illustrative/discussion purposes to examine the numerical-integration accuracy question by considering only a few of the element-property matrices as expressed in conventional form; that is, [m], [k], and $\{f_q^{NL}\}$ as given for the present Bernoulli-Euler beam behavior by:

$$[m] = \iiint \{U_i\} \rho [U^i] \, dV \tag{2.17a}$$

$$= \int_0^{\eta} [N(\eta)]^T [B(\eta)] [N(\eta)] \, d\eta \tag{3.127}$$

and for $(1+\zeta/R) \approx 1$:

$$[k] = \iiint \{D_{ij}\} E^{ijkl} [D_{kl}] \, dV \qquad \text{(from 2.22a)}$$

$$= \iiint_{\eta} \left(E\{D_1\}[D_1] + E\zeta^2 \{D_3\}[D_3] \right) d\xi \, d\zeta \, d\eta \tag{3.149}$$

$$= \int_0 E b h(\eta) \{D_1\}[D_1] + \frac{E b h^3(\eta)}{12} \{D_3\}[D_3] \, d\eta \tag{3.150}$$

Note that Eqs. 3.127 and 3.150 pertain to a beam or ring of uniform width b. Also,

$$\{f_q^{NL}\} = -\iiint \{D_{ij}\} E^{ijkl} \left[\frac{1}{2} [L_q]\{D_{ck}\}[D_l^c]\{q\} \right] dV$$

$$-\iiint \{D_{ai}\}[D_j^a] E^{ijkl} \left[[D_{kl}]\{q\} + \frac{1}{2}[L_q]\{D_{ck}\}[D_l^c]\{q\} \right] dV \{q\} \tag{4.8}$$

where Eq. 4.8 is obtained for Eq. 2.22a. For the present Bernoulli-Euler beam/ring type of finite-element analysis, Eqs. 3.127, 3.150, and 4.8 involve

integrand quantities which depend only upon the spanwise location η. Hence, since the displacement field within the element is herein expressed in terms of polynomials "anchored to" the nodal generalized displacements, it is seen that each integrand, in turn, is representable in terms of polynomials in η, the degrees of these polynomials depending upon the degree of the polynomial selected (and appearing in $N(\eta)$ -- see Eqs. 3.66-3.73, 3.107a-3.112, and 3.150, for example). Since n-station Gaussian integration (quadrature) is exact for polynomials of degree 2n-1 or less, one can assess each of the quantities [m], [k], and $\{f_q^{NL}\}$ to determine the number of spanwise Gaussian stations required to produce exact evaluations of each of these quantities for each of the higher-order elements considered in this study; 4, 5, 6, 7, and 8 DOF/node; that assessment is given in Table 3 for both straight-beam and curved-beam elements of constant width b and thickness h when the Type C strain-displacement relation is used, ignoring any trigonometric terms in the assumed displacement field.

To illustrate the "accuracy" sensitivity of [m] and [k] to the number of Gaussian quadrature stations employed, beam CB-1 was modeled with (a) ten 4 DOF/N elements, (b) ten 5 DOF/N elements, and (c) four 8 DOF/N elements, all per half span. The resulting maximum natural frequency ω_{max} of each mathematical model was determined for each of these cases when each of several numbers of Gaussian stations was used. Shown in Table 4 for each of the modelings (a), (b), and (c) are the number of spanwise Gaussian stations: (1) actually used, (2) needed for an exact [m], (3) needed for an exact [k], and the resulting value for $2/\omega_{max}$. In each case $2/\omega_{max}$ reaches a value that does not change as the number of spanwise Gaussian stations used is increased; that experimentally-determined value for each is: 4 for 4 DOF/N, 4 for 5 DOF/N and 8 for 8 DOF/N modeling; this ω_{max} type result depends essentially upon the polynomial degree used for v. This assessment involves a combination of both [m] and [k] accuracies.

Shown also in Table 4 are the imparted nodal velocities required to represent a given total kinetic energy of 770.8 in-lb. This computation shows that once [m] has been evaluated exactly, no change in the cited imparted velocities occurs as the number of spanwise Gaussian stations is increased; this indication of the number of Gaussian stations needed is essentially: (a) 4 for 4 DOF/N, (b) 5 for 5 DOF/N and (c) 6 for 8 DOF/N modeling.

The above assessment applies to small-deflection linear-elastic behavior. However, when large deflections are present, the $\{f_q^{NL}\}$ force terms can contribute. The importance of their contribution to the transient structural response depends nonlinearly upon both the prescribed force $\{f\}$ and the magnitude of the deflections. Although, in principle, the large number of Gaussian stations cited in Table 3 as being needed for an exact evaluation of $\{f_q^{NL}\}$ would be required, fewer spanwise Gaussian stations are needed typically in practice for a satisfactory evaluation of $\{f_q^{NL}\}$. For example, studies in Ref. 17 involving the use of 4 DOF/N elements and the Type A strain-displacement relation revealed that 3 spanwise Gaussian stations suffice to produce "converged" large transient displacements of impulsively-loaded beams and rings. A more elaborate evaluation of the needed number of spanwise Gaussian stations would be required in the (unlikely) event that the following combination of conditions is encountered: (a) that the element size be large enough so that the highest-order polynomial terms become of major importance and (b) that the largest order nonlinear strain terms (i.e., quartic in strain) become of dominant importance in the full expression for the equations of motion:

$$\sum_{n=1}^{N} \{\delta q\}^T \left([m]\{\ddot{q}\} + [k]\{q\} - \{f\} - \{f_q^{NL}\} - \{f_p^{L}\} - \{f_p^{NL}\} \right) = 0 \qquad (4.9)$$

In addition to evaluating $\{f_q^{NL}\}$, one must evaluate $\{f_p^{L}\}$ and $\{f_p^{NL}\}$ which are generalized loads arising from plastic straining throughout the volume of the element and associated with, respectively, the linear and nonlinear terms of the strain-displacement relations. These plastic strains vary both depth-wise and spanwise throughout the element and change, in general, as the transient response proceeds. Therefore, in practice, numerical experimentation is the most satisfactory means of determining the number of Gaussian stations needed to provide a converged prediction of large-deflection, elastic-plastic transient deformations of transiently- or impulsively-loaded structures.

Studies reported in Refs. 58 and 118 on finite-difference analyses of this type of transient structural response show that the number of depthwise Gaussian stations needed to produce accurate evaluations of stress resultants

is 4; numbers of stations used in those studies included 2, 3, 4, 5, 6, 8 and 10. No significant differences were noted when more than 4 depthwise Gaussian stations were used. Similarly, finite-element studies reported in Fig. 25 of Ref. 17 for large-deflection, elastic-plastic transient responses of impulsively-loaded beams wherein the finite element properties were evaluated by Gaussian quadrature with 2, 3, 4, and 5 depthwise stations at each of 3 spanwise Gaussian stations also revealed that 4 depthwise Gaussian stations were adequate to produce converged results. Therefore, in the present studies, 4 depthwise Gaussian stations were employed for all calculations, but the number of spanwise Gaussian stations was varied to assess finite-element property evaluation convergence and accuracy for the 4, 5, and 8 DOF/N elements discussed herein.

To demonstrate the effect of the number of spanwise Gaussian stations employed, the following cases were studied for beam specimen CB-1 (4 depthwise Gaussian stations were used in all cases):

Element DOF/N	No. of Elems. per Half Span	Type of Strain-Displ. Relation	No. of Spanwise Gaussian Stations*
4	10	D	[3], 4, 5
4	20	C	[3], 4
5	10	D	3, 4, [5], 6, 7
8	4	C	5, 6, [7], 9

The following illustrations of the resulting transient upper-surface strains and midspan-deflection responses are shown here to demonstrate the sensitivities of the predictions to the number of spanwise Gaussian stations employed. For all of these calculations, the unconventional finite-element formulation and the central-difference timewise finite-difference operator were used.

*The number in the box ☐ indicates what is judged to be an adequate number for "converged behavior" in this CB-1 clamped beam example.

	Figure where Data Appear		
Case (DOF/N; No. Elems per Half)	4; 10	5; 10	8; 4
No. of Spanwise Gaussian Stations	3, 4, 5	3, 4, 5, 6, 7	5, 6, 7, 9
ε vs. t at the second node	19a	20a	21a
ε vs. t at x = 1.40 in	19b	20b	21b
ε vs. t at x = 3.80 in	19c	20c	21c
ε vs. span at t = 600 μsec	19d	20d	21d*
Midspan Defl. vs. t	19e	20e	21e

For the 4 DOF/N, 10 element per half span modeling, Figs. 19a-19e illustrate that 3 spanwise Gaussian stations (3G) suffice to produce converged strain and deflection predictions. It is seen that the 3G is closer to the 5G than is the 4G prediction for this case. Accordingly, one might elect to require 5 spanwise Gaussian stations to be conservative; however, 3 or more would probably be adequate for most practical purposes. Note in Fig. 19d where the spanwise distribution of upper-surface strain is shown at t=600 microseconds that the number of spanwise Gaussian stations employed has an especially pronounced effect upon the strain at nodal locations, but locations within the element remote from the nodal stations are less sensitively affected.

The effects of a wider range of spanwise Gaussian stations are shown in Figs. 20a-20e for the 5 DOF/N, 10 element per half span modeling of beam model CB-1. It is seen that the transient response predicted when too few (3, for example) Gaussian stations are used is in serious disagreement with the converged result. For this case the number of spanwise Gaussian stations judged required to produce converged predictions of strain and (midspan) displacement is 5 and 3, respectively. Here also, Fig. 20d demonstrates the sensitivity of nodal strains to the number of spanwise Gaussian stations employed.

For the 8 DOF/N, 4 element per half span modeling, Figs. 2la-2le provide similar demonstrations for this higher order element. Trends similar to those noted for the other two types of elements are evident. For this 8 DOF/N element/structure modeling, it is judged that the number of spanwise Gaussian stations needed to produce converged predictions of strain and (midspan) displacement is 7 and 5, respectively.

*At 450 microseconds.

In all of these cases, it is seen that deflection predictions are much less sensitive than are the strains to the number of spanwise Gaussian stations employed in each element.

It should be noted that it may be advantageous to use more spanwise Gaussian stations than the minimum amount necessary for satisfactory integration of the even-numbered DOF/N elements (namely 4, 6, and 8 DOF/N). The reason for this is that the maximum frequency of the structure ω_{max} decreases just before attaining the converged value. Since smaller ω_{max} permits the use of larger time increment sizes (Δt), the added computation time associated with more spanwise Gaussian stations (and therefore with more exact integation) may be balanced by the smaller computing time associated with a larger Δt. This interesting effect is not important in the odd-numbered DOF/N finite elements (5 DOF/N and 7 DOF/N), since only the in-plane displacement v affects the maximum natural frequency. Hence for these elements, ω_{max} (dependent on the lower order v polynomial) has already converged before the element property matrices (dependent on the higher order w polynomial) have converged.

4.5 Comparisons of Various Higher Order Elements

Having examined the effects of (a) using various strain-displacement relations and (b) employing various number of spanwise Gaussian integration stations for evaluating finite element property matrices, it is useful next to compare the performances of the various finite elements discussed here. For these comparisons the comprehensive Type C strain-displacement relation is used in all cases. Predictions from example calculations are included for clamped beam specimens CB-1 and CB-4 and for free-ring specimen F15; all are impulsively-loaded 2-d structures.

4.5.1 Impulsively-Loaded Beam Models

For beam specimen CB-1, prediction comparisons are shown for the following modelings, where EL-SH material behavior is assumed:

Elements		
DOF/N	No. Per Half Span	No. Spanwise Gaussian Stations
4	20	4
5	16	5
6	13	5
8	10	7

The combinations of the DOF/N and the number of elements per half span provide roughly a comparable number of generalized-displacement unknowns amongst these cases.

For convenient reference, the following reminder is given of the nodal generalized-displacement quantities employed for each of these elements:

$$v\ ,\ w\ ,\ \psi\ ,\ \chi\ ,\ \left(-\frac{\partial\psi}{\partial\eta}\right),\ \frac{\partial\chi}{\partial\eta}\ ,\left(-\frac{\partial^2\psi}{\partial\eta^2}\right),\ \frac{\partial^2\chi}{\partial\eta^2}$$

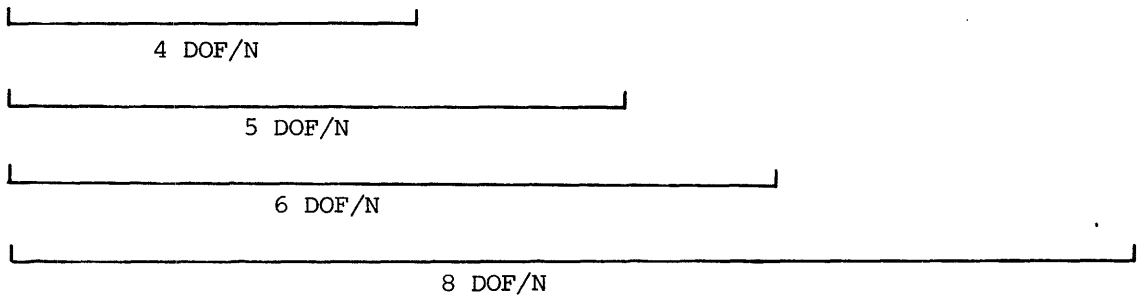

An examination of these "nodal control quantities" in conjunction with the Type C strain-displacement relation shown in Eq. 4.2 will serve one to recall that all of these elements exhibit continuity of membrane strain at the nodes but continuity of (a) the bending strain, (b) the spanwise derivative of the membrane strain, and (c) the spanwise derivative of the bending strain are accommodated differently as the following summarized tabulation indicates:

DOF per Node	Polynomial* in		Continuity in Membrane			Continuity in Bending	
				Derivative			
	v	w	Strain	First	Second	Strain	First Deriv.
3	L	C	No	No	No	No	No
4	C	C	Yes	No	No	No	No
5	C	Q	Yes	No	No	No	No
6	Q	Q	Yes	Yes	No	Yes	No
7	Q	7th	Yes	Yes	No	Yes	No
8	7th	7th	Yes	Yes	Yes	Yes	Yes

*L means linear, C: cubic, Q: quintic (or fifth degree).

The comparative character of the strains predicted by these various elements, perhaps, is demonstrated most conveniently by the spanwise distribution of the upper (non-loaded) surface spanwise strain at a "typical" instant in time -- here taken at 300 microseconds for beam model CB-1. These comparisons are shown in the following figures:

Figure	Comparison: DOF/N (No. of Elems/Half-Span)
22	4(20) vs. 5(16)
23	5(16) vs. 6(13)
24	6(13) vs. 8(10)
25	4(20) vs. 8(10)

From Fig. 22, nodal strain discontinuity evident for the 4 DOF/N element has been remedied by the 5 DOF/N element but the lack of strain gradient continuity in the latter is seen to result in "cuspiness" at many nodal stations. The 6 DOF/N element accommodates (over the 5 DOF/N element) continuity of membrane strain gradient and continuity of bending strain, and these consequences are evident in Fig. 23; however, some cuspiness remains in regions of severe bending strain. This latter cuspiness is removed by the use of the 8 DOF/N element which additionally provides continuity in the spanwise derivative of the bending strain as well as continuity of the spanwise second derivative of the membrane strain; this effect is evident in Fig. 24. Finally, Fig. 25 contrasts the strain distribution predicted by using the lowest-order 4 DOF/N elements with that for the highest-order 8 DOF/N elements included in this study. The latter provides the physically expected continuities in both strain and strain gradients.

Since in transient structural response problems the strain at any given location in the structure may vary appreciably with time, it is useful to examine the time history of strain for the present CB-1 beam example at various spanwise locations. To provide a convenient composite comparison, predictions obtained by using the DOF/N (No. Elem.) combinations 4(20) and 8(10) for beam material behavior EL-SH and EL-SH-SR (where $D=6500\ \text{sec.}^{-1}$ and p=4) are presented as follows:

Figure	Strain Location: Span, x (in)	Strain Location: Surface U or L	Experimental Data [117]
26	0	U	--
27	1.40	U	X
28	2.20	U	X
29	2.20	L	X
30	3.00	U	X
31	3.80	U	X
32	3.80	L	X

Note that the predictions for the 4 DOF/N modeling are in good agreement with those for the 8 DOF/N modeling at spanwise locations (x=2.20 and 3.00 in) where membrane behavior is dominant throughout the response; both of these predictions are in reasonable agreement with experimental measurements (of the relative elongation). Since the relative elongations are small (less than about 2 to 3 per cent), no distinction has been made here between the computed extensional strain (ε of Eq. 4.2) and the measured relative elongation. At x=1.40 in where both bending and membrane strains are significant, the predictions disagree by only a small amount at times when bending behavior is dominant. Note in Figs. 31 and 32 that these two strain predictions deviate from each other at station x=3.80 in, probably because of the presence of a significant amount of bending that occurs; although the measured strains are small here, neither prediction compares very well with the measurement.

Shown in Figs. 33 and 34 for, respectively, EL-SH and EL-SH-SR material behavior, are predictions of the midspan deflection w as a function of time for the four modelings: 4(20), 5(16), 6(13), and 8(10). Within each figure these three predictions differ little from each other; displacement time history information is a less sensitive indicator of the effects of using different types of finite elements than is strain. Comparing Fig. 33 with Fig. 34, it is seen that the inclusion of only this very small degree of strain-rate sensitivity results in a larger effect than does the use of these four types of elements for the CB-1 beam example. Incidentally, the computer runs for the results shown in Fig. 34 were carried out for

the "same amount" of computer time on the IBM 370/168 system at the MIT Information Processing Center; the cases, the Δt values, and the response duration computed are shown as follows to provide a rough idea of this comparison aspect:

Elem Type	No. of Elem/Half	Total DOF	DOF Unknowns	Δt Used (μsec)	Response Duration (μsec)	Job Run Time (min)
4 DOF/N	20	84	79	0.25	920	8.45
5 DOF/N	16	85	80	0.25	880	9.45
6 DOF/N	13	84	79	0.20	780	9.45
8 DOF/N	10	88	83	0.15	450	9.44

Finally, Fig. 35 shows permanent deflection as a function of spanwise location, comparing measurements and 4(20) predictions for EL-SH and EL-SH-SR behavior. Note that both predictions are in good qualitative agreement with experiment, with the EL-SH-SR result being in closest agreement with measurements.

For the more severely loaded beam specimen CB-4, EL-SH-SR calculations using strain-displacement relation Type C and two FE modelings (a) 4(20) and (b) 8(10) have been carried out. Comparisons of predicted strains with each other and with experimental measurements are included as follows:

	Strain Location		
Figure	Span, x (in)	Surface U or L	Experiment Gage No. [117]
36	0	U and L	--
37	1.40	U and L	G2
38	2.20	U	G7
39	3.00	U	G4
40	3.80	U and L	G5 and G13

Because the measured relative elongations E_x approach 6 per cent in some cases, they have been corrected to form E_{xc} according to Eq. 4.1; further these values have been converted to correspond to the extensional strain ε given by Eq. 4.2 by applying the relation:

$$\epsilon = E_{xc} + \frac{1}{2}(E_{xc})^2$$

Figures 36-40 represent ϵ vs. time. Except at station x=3.80 in, both predictions are in reasonably good agreement with each other and with experiment. Near the clamped edge, the simpler 4 DOF/N modeling provides a strain prediction which is closer to the experimental result than that given by the "more sophisticated" 8 DOF/N element. Some of the factors which may be responsible for this state of affairs may include the following. An examination of the quantities appearing in the strain-displacement relations reveals that the degree of the polynomials involved (for a straight beam) are:

Term:	χ	$\frac{1}{2}\psi^2$	$\frac{1}{2}\chi^2$	$\frac{\partial\psi}{\partial\eta}$	$\chi\frac{\partial\psi}{\partial\eta}$	$\psi\frac{\partial\chi}{\partial\eta}$	$(\frac{\partial\psi}{\partial\eta})^2$	$(\frac{\partial\chi}{\partial\eta})^2$
4 DOF/N CC	2nd	4th	4th	1st	3rd	3rd	2nd	2nd
8 DOF/N 7th 7th	6th	12th	12th	5th	11th	11th	10th	10th
	MEMBRANE			BENDING				

It is evident that the 4 DOF/N CC element involves polynomials of substantially lower order for the strain representation than does the 8 DOF/N 7th 7th element, particularly for bending. Thus, the use of two CC elements in a spanwise region represented by only one 7th 7th element could lead to different overall behavior. This is especially true when the region in question involves high levels of nonlinearity, such as near the clamped end for the CB-4 beam problem. Further, near the clamped end, an examination of specimen CB-4 reveals the important presence of transverse shear strain in a narrow spanwise zone extending entirely across the width of the beam; this behavior (1) is not taken into account in the FE models employed and (2) could act to "alleviate" the bending behavior which otherwise would exist adjacent to an ideally-clamped Bernoulli-Euler edge. These factors contribute to a plausible explanation of the noted discrepancies. Time and fund restrictions, however, have prevented a more thorough study of this matter; hence, it remains for future study to delineate the full set of reasons for this "discrepancy".

Shown in Fig. 41 are the 4(20) and 8(10) predictions for the transient midspan deflection of beam model CB-4; the Type C strain-displacement relation and EL-SH-SR conditions were assumed. These predictions agree very well with each other. For these same conditions: (1) the spanwise distributions of upper-surface strain are shown in Fig. 42a at t=300 microseconds and (b) the measured vs. the predicted (4 DOF/N, 20 ELEM/HALF) spanwise distribution of the permanent deflection are given in Fig. 42b, where excellent theoretical-experimental agreement is observed. Note in Fig. 42a that an appreciable difference exists between the 4(20) and 8(10) strain predictions over most of the span of the beam at the 300 microsecond time instant; also observe the usual nodal strain discontinuity for the 4(20) calculation, but the improved continuity behavior for the 8(10) prediction. Finally, at the midspan location (x=0) the exhibited 8(10) prediction is one for which the following symmetry conditions were imposed: $v = \psi = \frac{\partial \chi}{\partial \eta} = \frac{\partial^2 \psi}{\partial \eta^2} = 0$; these are believed to be the "proper" symmetry conditions. A calculation was carried out in which the entire beam was modeled by 8 DOF/N elements; the resulting transient strain distributions and time histories agreed exactly with the calculation just described, thereby confirming the validity of the symmetry conditions employed at x=0.

An examination of the predicted transient strains revealed the influence of constraining the higher order derivatives

$\frac{\partial \chi}{\partial \eta} = \frac{\partial^2 v}{\partial \eta^2} + \frac{\partial}{\partial \eta}\left(\frac{w}{R}\right) = 0$ and $\frac{\partial^2 \psi}{\partial \eta^2} = \frac{\partial^3 w}{\partial \eta^3} - \frac{\partial^2}{\partial \eta^2}\left(\frac{v}{R}\right) = 0$ to be confined within a distance of about 0.15 in from midspan, and are essentially negligible beyond this location. At midspan (where these symmetry conditions are imposed), the prediction for the 8(10) modeling with only $v = \psi = 0$ imposed, strongly resembles the 4(20) prediction. The higher-order derivative $\frac{\partial \chi}{\partial \eta}$ has a strong influence on the highest frequency of the structure. For example, for a mesh of 4 unequal 8 DOF/N elements per half beam (CB-1), one finds:

Symmetry Condition Imposed at Midspan (x=0)	Highest Frequency of Model (rad/sec.)
$v = \psi = 0$	0.63571×10^7
$v = \psi = \frac{\partial^2 \psi}{\partial \eta^2} = 0$	0.63571×10^7
$v = \psi = \frac{\partial^2 \psi}{\partial \eta^2} = \frac{\partial \chi}{\partial \eta} = 0$	0.4430×10^7
WHOLE BEAM (8 of 8 DOF/N)	0.4431×10^7

It is apparent that setting the higher order derivative $\frac{\partial \chi}{\partial \eta} = 0$ as a symmetry condition would enable one to use a larger Δt when the central-difference timewise operator is employed.

4.5.2 Impulsively-Loaded Free Circular Ring

The impulsively-loaded free initially-circular thin ring discussed in Subsection 4.3.3 was analyzed by using 18 uniform 4 DOF/N elements and 8 elements of the 8 DOF/N type with nodes at θ=0, 30, 50, 70, 90, 110, 135, 160, and 180 degrees for the half ring, taking advantage of symmetry; these FE modelings provide a comparable number of generalized displacement unknowns. The symmetry conditions used were (a) $v = \psi = 0$ for the 4(18) and (b) $v = \psi = \frac{\partial \chi}{\partial \eta} = \frac{\partial^2 \psi}{\partial \eta^2} = 0$ for the 8(8) FE modeling. The aluminum ring material was assumed to behave in an EL-SH-SR fashion, with the strain rate constants taken to be D=6500 sec^{-1} and p=4. In both of these calculations the Type C strain-displacement relation was used.

Shown in Fig. 43a are experimentally-measured and predicted inside-surface strain histories at $\theta = 87^\circ$ 20' and 92° 30' for this impulsively-loaded free ring. At each location both predictions are in reasonably good agreement with each other but exceed the measured values substantially. Much better theoretical-experimental agreement is observed for outer-surface circumferential strains at $\theta = 86^\circ$ 10' and 92° 30' as shown in Fig. 43b. On the outside surface at $\theta = 176^\circ$ where "reversed bending" leads to compression strain, Fig. 43c shows fairly good qualitative and quantitative agreement between predictions and experiment. Included in Fig. 43c are the 4(18) and 8(8) predictions for the inside-surface circumferential strain at this same

$\theta=176^{\circ}$ location; this figure illustrates the existence of essentially pure bending. Hence, the present predictions are seen to be in reasonable agreement with measurements at outer-surface location; however, predictions tend to overestimate the inner-surface strains.* Unfortunately time and fund limitations have prevented a more extensive set of modelings and calculations to illuminate further the various factors contributing to these discrepancies.

Figure 44 shows the predicted and photographically-measured time histories of the separation between the midplanes of θ-stations 0 and 180° of the free impulsively-loaded ring for both calculations; these predictions are in very good agreement with each other and with experiment. Here again one finds better theoretical-experimental agreement for deflection than for strains.

Finally, the following summarizes the computing time for these two cases (a Δt of 0.6 microsecond was used in each case):

Elem Type	No. of Elem/Half	Total DOF	DOF Unknowns	No. of Gauss. Depth.	Sta. Span.	Response Duration (μsec)	Job Run Time (min)
4 DOF/N	18	76	72	4	4	2700	9.41
8 DOF/N	8	72	64	4	7	2700	12.44

4.5.3 Comments

For the beam and ring examples studied, comparisons of the performances of the 4, 5, 6, and 8 DOF/N elements on the basis of roughly an equal number of unknown generalized displacements and essentially the Type C strain-displacement relation reveals no significant superiority amongst these elements for this type of nonlinear large-deflection, elastic-plastic transient response problem. The 8 DOF/N element exhibits much more plausible spanwise (or circumferential) distributions of strain at any time instant than those provided by these other elements. Hence, in general, more realistic strain predictions are expected when the 8 DOF/N element is employed. However, if one uses the (simplest) 4 DOF/N element and computes nodal-average strain, it appears that strain values and distributions of sufficient accuracy for most engineering purposes would be obtained.

---

*At those locations where measurements have been made successfully.

Near a clamped boundary 4 DOF/N modeling leads to plausible values and distributions of strain, and reasonably good agreement with experiment. On the other hand, the "more comprehensive" 8 DOF/N element results in seemingly excessive strain values in this region (see Figs. 25, 32, 40, and 42a, for example). Further study is required to explain this behavior and to carry out remedial measures.

Hence, for the standpoints of accuracy, cost, and efficiency, it appears advisable to employ the 4 DOF/N element as just described in conjunction with the Type C strain-displacement relation, in general, for analyzing the present types of large-deflection, elastic-plastic 2-d transient structural response problems.

4.6 Structural Response to Impact

As noted in Subsection 4.2, an assessment of the accuracy and adequacy of a method for predicting the transient structural response of a structure which is subjected to fragment impact is accomplished most effectively and reliably by comparing predictions with pertinent high-quality experimental transient strain and deflection response data. Accordingly, such use is made of the experimental data cited in Subsection 4.2 for clamped aluminum beam specimen CB-18 subjected to impact by a 1-inch diameter steel sphere having an initial impact velocity of 2794 in/sec.

A computer code CIVM-JET 4B developed at the MIT Aeroelastic and Structures Research Laboratory [120] combines (1) a finite-element structural analysis capability for 2-d structures experiencing large-deflection elastic-plastic transient structural response with (2) an approximate impact-interaction analysis utilizing momentum and energy conservation principles to predict structural response to impact by "rigid" missiles or fragments. A timewise step-by-step solution procedure in small increments of time is employed. If impact occurs at some point on the structure during the small time increment Δt, an appropriate region of the structure near that impact point is assumed to be affected by that "instantaneous impact process", thereby experiencing an impact-induced increment in its velocity components and, accordingly, the impacting fragment suffers a decrease in its velocity. The analysis provides for treating the local impact process as being (a) perfectly-elastic, (b) perfectly-inelastic, of (c) intermediate between

(a) and (b), as preselected by the analyst. The reader is invited to consult Ref. 120 for the various analysis features and computer code capabilities.

For present illustrative purposes, the results from two calculations for the CB-18 sphere-beam impact example are presented here. Both calculations involve the use of 43 equal-length 4 DOF/N elements to represent the entire span of the beam. In one case the Type B strain-displacement relation (used in the current version of CIVM-JET 4B) was employed; in the other calculation, the code was modified to use the Type C strain-displacement relation. In both cases the local impact was assumed to be perfectly elastic; the geometric properties, material uniaxial stress-strain (σ,ε) properties, and mass density of the beam used in these calculations were:

Span, L = 8.000 in

Width, w = 1.498 in

Thickness, h = 0.097 in

σ_1,ε_1: 41,000 psi, .0041 in/in

σ_2,ε_2: 45,000 psi, .012 in/in

σ_3,ε_3: 53,000 psi, .100 in/in

Mass per unit volume, $\rho = 0.25384 \times 10^{-3}$ (lb-sec^2)/in^4

Beam material mechanical behavior was assumed to be either (a) EL-SH or (b) EL-SH-SR with D=6500 sec^{-1} and p=4. In all cases, a time increment size Δt of 0.5 microsecond was used.

An examination of steel-sphere-impacted beam specimen CB-18 reveals that except near (beyond about 0.75 in from) the midspan lower-surface impact point (x=0), the beam underwent essentially two-dimensional deformation. Hence, since the CIVM-JET 4B analysis and code pertains strictly to 2-d structural behavior, meaningful theoretical experimental comparisons can be made only for the 2-d structural response region: $0.8 \lesssim x \lesssim 4.00$. Accordingly, predicted and measured strain time histories are shown as follows:

Figure	Location: Span, x (in)	Location: Surface U or L	Strain Gage No.	Strain-Displ Rel. Type	Mechanical Behavior: EL-SH	Mechanical Behavior: EL-SH-SR
45a	1.50	U and L	G5, G12	B	X	X
45b	1.20	U	G4	B	X	X
45c	0.6	U	G3*	B	X	X
45d	0	U	--	B	X	X

*Involves 3-d structural deformation behavior.

Spanwise strains for both the upper and the lower surface are shown in Fig. 45a for station x=1.50 in; the mean value represents the membrane contribution and the deviation from the mean identifies the bending contribution to the strain. At early times $0 \lesssim t \lesssim 170$ microseconds, bending dominates; during $170 \lesssim t \lesssim 350$ μsec, almost pure membrane strain exists; and after about 350 μsec, membrane behavior dominates but a significant amount of bending-induced strain is present. Note that the EL-SH and the EL-SH-SR predictions exhibit slightly different time histories, with the EL-SH case predicting somewhat larger peak strain values. Also, with respect to the peak strain values: (1) the EL-SH prediction is in better agreement with experiment than is the EL-SH-SR prediction for the lower-surface location, whereas (2) on the upper surface, the EL-SH-SR prediction agrees better with experiment than does the EL-SH prediction. Note that these theoretical strains are those given by Eq. 4.2; the experimentally-measured relative elongation data were corrected and converted to this same basis, as described in Subsection 4.5.1.

Predictions of upper-surface strains at stations x=1.20 and 0.6 in are compared with measurements in Figs. 45b and 45c, respectively. At station x=1.20 in where 2-d structural response occurs, the predictions are in fairly good agreement with experiment, with the EL-SH results being in better qualitative and quantitative agreement. At station x=0.6 in the structural behavior shows signs of 3-d rather than essentially 2-d deformation; hence, one observes a poorer theoretical-experimental correlation but, again, the EL-SH prediction provides the better correlation.

Finally, as a matter of curiosity, the predicted upper-surface strains are shown in Fig. 45d for midspan station x=0. The predictions, of course, apply strictly to 2-d structural response, whereas the actual response (not measured successfully) is strongly of 3-d character. Here the predicted peak strains reach about 16 per cent for the EL-SH calculation and about 13 per cent for the EL-SH-SR case.

Shown in Figs. 45e, 45f, and 45g for the EL-SH calculation are the time histories of the beam-support reactions: moment M_y, vertical force F_z, and horizontal force F_x at x = 4.00 in. These support reactions are shown with expanded time scales in Figs. 45h, 45i, and 45j. Note that F_x is nearly zero until about 18 μsec after initial impact and then becomes and remains

to the right (positive) thereafter. On the other hand both F_z and M_y remain essentially zero until about 30 μsec after initial impact. Thereafter F_z oscillates rapidly during about the next 100 μsec; relatively slow oscillations occur subsequently. The support reaction moment M_y exhibits an oscillatory behavior similar to that of F_z.

Shown in Fig. 46, are EL-SH and EL-SH-SR predictions of the lateral displacement w as a function of time at spanwise station x=1.0 in where 2-d structural response occurs. Also indicated is the measured permanent deflection at this station; both calculations agree rather well with the experimentally-determined value of .60 in. At later times, the predicted deflection oscillates slightly about mean values of .63±.02 in and .58±.03 in for the EL-SH and the EL-SH-SR case, respectively.

In the second category of these predictions, the Type C rather than the Type B strain-displacement relation formerly used was applied; only the EL-SH condition was used. Compared in Figs. 47a, 47b, 47c, and 47d are the "Type B" and "Type C" predictions of upper surface strain at, respectively, spanwise stations x=3.9, 1.5, 0.6, and 0 in. Only at stations x=3.9 in and x=0 in where severe bending occurs does one observe notable differences between these two predictions. Since sufficiently severe steel-sphere impact produces rupture of the beam at the midspan-impact location, one may choose to employ the Type C strain-displacement relation as affording "improved predictions" for the general case.

SECTION 5

SUMMARY, CONCLUSIONS, AND COMMENTS

5.1 Summary

The present study was intended to contribute to the development of more rational practical methods for predicting the responses of structures which are subjected to intense transient and impact loads. Accordingly, interest centered upon the use of the finite-element (FE) method in a quest to predict strains accurately since these quantities are of primary interest in many cases wherein incipient failure associated with structural response is of concern. In order to predict strains accurately, the use of higher-order assumed displacement elements was expected to be useful since such elements can approximate spatially-varying strains more accurately on an element-by-element basis than can lower-order elements. However, no information was found concerning the utility and efficiency of employing higher-order vs. lower-order elements when applied to large-deflection, elastic-plastic transient response problems. Hence, higher-order elements were explored for 2-d rather than 3-d structural response to minimize cost and labor. Further, for similar reasons only initially-isotropic materials were taken into account; more complex material mechanical behavior could be accommodated later when warranted.

In view of these considerations, the finite-element formulation (based upon the Principle of Virtual Work and D'Alembert's Principle) and the solution process was reviewed, noting the features of both the unconventional and the conventional formulation. When a higher nonlinear strain-displacement relation is used for problems of this type, the unconventional formulation is much more convenient and efficient than is the conventional formulation and, accordingly, was used. Further, since it was desired that the analysis apply to ductile as well as brittle materials, large deflections and rotations can occur and must be taken into account properly in the strain-displacement relations (which are highly nonlinear). Hence, appropriate strain-displacement relations were examined in Subsection 3.2 for various simple structural configurations. Next, appropriate geometric approximations

for simple shapes and assumed displacement fields for a succession of higher-order elements: 4, 5, 6, and 8 DOF/node were investigated, providing for both rigid-body and deformation displacements. The consequent finite element property matrices were determined.

For computational efficiency, storage, and convenience, the present calculations utilize the unconventional formulation and the timewise central-difference operator. Accordingly, the time increment size Δt required to prevent calculation instability is approximately 0.8 $(2/\omega_{max})$, where ω_{max} is the maximum natural vibration frequency of the mathematical model of the system. It appears that for a given FE modeling, typically the use of a Δt small enough to avoid calculation instability provides essentially a converged result in the sense that the use of a smaller Δt results in essentially the same predicted transient response. However, when Δt is too large, a self-evident calculation blow-up occurs. While larger Δt values may be used with various of the common "unconditionally stable" timewise finite-difference operators, one must resort to numerical experimentation to insure that the chosen Δt will provide a converged transient response solution.

For highly nonlinear transient structural response problems of the present type, one can assess the accuracy and adequacy of proposed prediction methods only by comparing predictions with reliable experimental transient strain data for appropriate well-defined experiments. Accordingly, experimental data for impulsively-loaded (a) initially-flat aluminum beams (CB-1 and CB-4) with clamped ends [117] and (b) free initially-circular ring [118,119] were employed to assess the various higher-order elements considered. For these cases, the effects of using various successively-more-comprehensive approximations for the strain-displacement relations were studied (Type A being the simplest and Type C the most comprehensive). Type A is adequate for "gentle" nonlinear response but Type C is needed when severe deflections and rotations occur; these studies are given in Subsection 4.3.

Since some of the finite element property matrices depend upon the stress state throughout the volume of the element and this state changes as the transient response proceeds, it is necessary to evaluate these properties by performing certain volume integrals at a succession of times

Δt apart during the transient-response solution process. This integration is done numerically by Gaussian quadrature. The accuracies of such evaluations (for the present 2-d type structures) depend upon the number of depthwise and spanwise Gaussian stations employed. Accordingly, this matter was investigated for each type of finite element studied (see Subsection 4.4).

Having established the necessary number of Gaussian integration stations for each type of element and the desirability of employing the Type C strain-displacement relation (Eq. 3.34 or Eq. 4.2), transient response calculations were carried out. These predictions were compared with each other and with experimental transient strain and permanent defleciton data for both the beam and the ring models.

To illustrate an application to impact-induced structural response, two calculations (one using the Type B and one using the Type C strain-displacement relation) were carried out by using the CIVM-JET 4B computer code of Ref. 120; in both calculations the 8-inch span beam was modeled by 43 uniform 4 DOF/N elements. The predictions were compared with measured transient strain and permanent deflection data [117].

5.2 Conclusions

Based upon currently available information, including the present study, the following conclusions concerning the use of assumed-displacement finite elements for predicting Bernoulli-Euler large-deflection elastic-plastic transient structural responses of 2-d structures may be stated:

1. For general application, the Type C strain-displacement (Eq. 4.2) should be used.

2. From the standpoints of accuracy, efficiency, and cost, it is preferable to use the 4 DOF/N element (in conjunction with nodal averaging of strain) rather than, for example, the 8 DOF/N element despite its superior strain-representing ability; implied is the use of many 4 DOF/N vs. fewer 8 DOF/N elements such that one has a comparable number of unknown generalized displacements to be determined during the transient response analysis. Although these comparisons and observations were made by using the timewise central difference operator, similar qualitative comparisons are

expected should one elect to use a less restrictive (regarding Δt size) timewise finite-difference operator such as, for example, that of Houbolt [17, for example] or Park [121]; however, direct calculations to explore this matter are recommended.

3. Large differences in strain distribution between the 4 DOF/N and the 8 DOF/N elements were found only at the boundaries and the loaded regions of the beam and ring specimens. At the clamp of impulsively-loaded beams CB-1 and CB-4, the 4 DOF/N element produces results that are closer to the experiment. At the impulsively-loaded regions of beams CB-1 and CB-4 and of the free circular ring, there is no experimental strain information available for comparison with the 4 DOF/N and 8 DOF/N element predictions.

4. The use of the 8 DOF/N element in conjunction with the Type C strain-displacement relation provides physically realistic and superior spatial distributions of strain at each time instant compared with those from the lower-order elements. This element prevents the physically unrealistic strain and strain-gradient discontinuities found with various of the lower order elements.

5. Considering only the simplest (4 DOF/N) and the most comprehensive (8 DOF/N) element examined in the present study, the following summarizes the recommended number of spanwise and/or depthwise Gaussian stations needed within an element for an accurate overall evaluation, based mainly upon a study of transient strain predictions:

No. of Gaussian Stations			
4 DOF/N		8 DOF/N	
Depth.	Spanwise	Depth.	Spanwise
4	3	4	7

6. The 5 DOF/N element (quintic in w and cubic in v) was shown to be less accurate with respect strain predictions than the 4 DOF/N, 6 DOF/N, and 8 DOF/N elements. This is due to: (a) the 5 DOF/N element enforces continuity of bending strain for strain-displacement relations Types A, B, and D, without enforcing continuity of the (membrane and bending) strain gradients; this results in cusps at the nodes, that produce very inaccurate strain distribution,

and (b) the normal component of displacement (w) is of higher order than the tangential component; for large displacements and rotations (and for an accurate representation of rigid body modes) both components of deflection should be represented by polynomials of the same order.

7. Application of the 4 DOF/N element via the CIVM-JET 4B analysis and code of Ref. 120 to analyze beam response to steel-sphere impact (beam model CB-18) provides fairly good agreement between predicted and measured transient strain at beam spanwise stations where 2-d structural response applies. In these calculations, the steel sphere was treated as being non-deformable; a modified impact-interaction analysis would be required if the attacking missile were comparatively deformable.

5.3 Comments

Appropriate methods for predicting the structural response of structures subjected to impact by fragments depends upon the mechanical behavior or type of material in both the structure and the attacking fragment. For either hard or crushable-rigid missiles striking ductile isotropic metallic targets, one must accommodate in the analysis large deflections and large strains if one seeks to predict the structural response up to and including rupture of the material. The present analysis includes arbitrarily large deflections but only small to moderate strains; also transverse shear deformation is neglected. It is advisable, therefore, to pursue the inclusion of these two aspects in future analysis developments.

If the target consists of complex anisotropic material such as reinforced concrete or structural composites, one need account generally for much smaller deflections than in the former case but the mechanical behavior properties and failure behavior are much more complex. Recent studies contributing to achieving a better understanding of the responses of reinforced concrete, metallic, and composite structural panels subjected to impact by various types of missiles are reported in Refs. 122-129. Work on measurement and characterization of the constitutive relations for reinforced concrete is described in Ref. 130, while Ref. 131 reports recent finite element structural analysis developments accommodating a complex but useful descriptive model of reinforced-concrete mechanical behavior. The continuation of the Refs. 123, 129, 130, 131 category of studies promises to produce valuable improvements in both understanding and in prediction capabilities in the near future.

REFERENCES

1. Anon. "Plant Design Against Missiles", ANSI NI77 (Draft), American Nuclear Society, February 1974.

2. Anon. "Effects of Impact and Explosion". Summary Technical Report of Division 2, Volume 1, National Defense Research Committee, Washington, D.C., 1946, AD 221586, ASTIA.

3. Stevenson, J.D., "Part II: Engineering and Management Guide to Tornado, Missile Jet Thrust and Pipe Whip Effects on Equipment and Structures". Nuclear Structural Systems Association, Inc. 1974.

4. Linderman, R.B. et al, "Design of Structures for Missile Impact", Topical Report BC-TOP-9-A, Revision 2, Bechtel Power Corporation, September 1974.

5. Williamson, R.A. and Alvy, R.R., "Impact Effect of Fragments Striking Structural Elements", Holmes and Narver, Inc., Revised Ed., Nov. 1973.

6. Stephenson, A.E., "Tornado Vulnerability Nuclear Production Facilities", Environmental Test Department, Sandia Laboratories, Albuquerque, New Mexico, April 1975.

7. Stephenson, A.E., "Addendum to Tornado Vulnerability, Nuclear Production Facilities", Environmental Test Department, Sandia Laboratories, Albuquerque, New Mexico, June 2, 1975.

8. Chiarito, P.T., "Status of Engine Rotor Burst Protection Program for Aircraft". NASA Aircraft Safety and Operating Problems Conference, Volume 1. Langley Research Center, NASA SP-270, May 4-6, 1971, pp. 75-88. Also see AIAA Journal of Aircraft, Vol. 9, No. 7, July 1972, pp. 449-450.

9. Martino, Albert A., "Turbine Disk Burst Protection Study. Phase I - Final Report on Problem Assignment NASA DPR R-105". NAEC-AEL-1973, U.S. Navy, Mar. 1965. (Available as NASA CR-80962.)

10. Martino, A.A., and Mangano, G.J., "Turbine Disk Burst Protection Study Phases II-III - Final Report on Problem Assignment NASA DPR R-105". NAEC-AEL-1848, U.S. Navy, Feb. 1967. (Available as NASA CR-84967.)

11. Martino, A.A., and Mangano, G.J., "Rotor Burst Protection Program Initial Test Results. Phase IV - Final Report (on Problem Assignment) NASA DPR R-105". NAPTC-AED-1869, U.S. Navy, Apr. 1968. (Available as NASA CR-95967.)

12. Martino, A.A., and Mangano, G.J., "Rotor Burst Protection Program. Phase V - Final Report [on] Problem Assignment NASA DPR R-105". NAPTC-AED-1901, U.S. Navy, May 1969. (Available as NASA CR-106801.)

13. Mangano, G.J., "Rotor Burst Protection Program. Phases VI & VII - Exploratory Experimentation to Provide Data for the Design of Rotor Burst Fragment Containment Rings". NAPTC-AED-1968, U.S. Navy, Mar. 1972. (Available as NASA CR-120962.)

14. McCallum, R., Leech, J.W., and Witmer, E.A., "Progress in the Analysis of Jet Engine Burst-Rotor Containment Devices", ASRL TR 154-1, Aeroelastic and Structures Research Laboratory, Massachusetts Institute of Technology, August 1969. (Available as NASA CR-107900.)

15. McCallum, R.B., Leech, J.W., and Witmer, E.A., "On the Interaction Forces and Responses of Structural Rings Subjected to Fragment Impact". ASRL TR 154-2, Aeroelastic and Structures Research Laboratory, Massachusetts Institute of Technology, Sept. 1970. (Available as NASA CR-72801.)

16. Leech, J.W., Witmer, E.A., and Yeghiayan, R.P., "Dimensional Analysis Consideration in the Engine Rotor Fragment Containment/Deflection Problem", ASRL TR 154-3, Aeroelastic and Structures Research Laboratory, Massachusetts Institute of Technology, Dec. 1971. (Available as NASA CR-120841).

17. Wu, R.W.-H. and Witmer, E.A., "Finite-Element Analysis of Large Transient Elastic-Plastic Deformations of Simple Structures, with Application to the Engine Rotor Fragment Containment/Deflection Problem", ASRL TR 154-4, Aeroelastic and Structures Research Laboratory, Massachusetts Institute of Technology, Jan. 1972. (Available as NASA CR-120886.)

18. Yeghiayan, R.P., Leech, J.W., and Witmer, E.A., "Experimental Data Analysis Techniques for Deducing Collision-Induced Forces from Photographic Histories of Engine Rotor Fragment Impact/Interaction with a Containment Ring", ASRL TR 154-5, Aeroelastic and Structures Research Laboratory, Massachusetts Institute of Technology, Oct. 1973, (Available as NASA CR-134548.)

19. Zirin, R.M. and Witmer, E.A., "Examination of the Collision Force Method for Analyzing the Responses of Simple Containment/Deflection Structures to Impact by One Engine Rotor Blade Fragment", ASRL TR 154-6, Aeroelastic and Structures Research Laboratory, Massachusetts Institute of Technology, May 1972. (Available as NASA CR-120952.)

20. Wu, R.W.-H and Witmer, E.A., "Computer Program - JET 3 - to Calculate the Large Elastic-Plastic Dynamically-Induced Deformations of Free and Restrained, Partial and/or Complete Structural Rings", ASRL TR 154-7, Aeroelastic and Structures Research laboratory, Massachusetts Institute of Technology, Aug. 1972. (Available as NASA CR-120993.)

21. Collins, T.P. and Witmer, E.A., "Application of the Collision-Imparted Velocity Method for Analyzing the Responses of Containment and Deflector Structure to Engine Rotor Fragment Impact", ASRL TR 154-8, Aeroelastic and Structures Research Laboratory, Massachusetts Institute of Technology, Aug. 1973. (Available as NASA CR-134494.)

22. Wu, Richard, W-H. and Witmer, E.A., "Approximate Analysis of Containment/ Deflection Ring Responses to Engine Rotor Fragment-Impact", AIAA Journal of Aircraft, Vol. 10, No. 1, January 1973.

23. Witmer, E.A., Wu, Richard W-H., and Merlis, F., "Experimental Transient and Permanent Deformation Studies of Impulsively-Loaded Rings and Cylindrical Panels, both Stiffened and Unstiffened", AMMRC CTR 74-29 (MIT ASRL TR 171-3), April 1974.

24. Wu, Richard W-H. and Witmer, E.A., "Finite Element Predictions of Transient Elastic-Plastic Large Deflections of Stiffened and/or Unstiffened Rings and Cylindrical Shells", AMMRC CTR 74-31 (MIT ASRL TR 171-4), April 1974.

25. Chelapati, C.V., Kennedy, R.P., and Wall, I.B., "Probabilistic Assessment of Aircraft Hazard for Nuclear Power Plants", Nuclear Engineering and Design 19 (1972) S. 333/364.

26. Doyle, J.M., Klein, M.J., and Shah, H., "Design of Missile Resistant Concrete Panels", Preprints of the Second International Conference on Structural Mechanics in Reactor Technology, Berlin, Germany, 10-14 Sept., 1973, Vol. 4 Part J, Paper J3/3.

27. Riera, J.D., "On the Stress Analysis of Structures Subjected to Aircraft Forces", Nuclear Engng. and Design 8 (1968) Nr. 3, S. 415/26.

28. Yang, H.T.Y. and Godfrey, D.A., "Structural Analysis of Aircraft Impact", Nuclear Engng. Design 11 (1969) Nr. 2, S. 295/307.

29. Gwaltney, R.C., "Missile Generation and Protection in Lightwater Cooled Power Reactor Plants", Oak Ridge National Laboratory Report ORNL-NSIC-22, Oak Ridge, Sept. 1968.

30. Ferguson, P.M., Reinforced Concrete Fundamentals, John Wiley and Sons, New York, Third Ed., 1973.

31. Wilkins, M.L., "Calculation of Elastic-Plastic Flor". Lawrence Radiation Laboratory, Livermore, UCRL-7322, Rev. I, Jan. 1969.

32. Hageman, L.J. and Walsh, J.M., "HELP: A Multimaterial Eulerian Program for Compressible Fluid and Elastic-Plastic Flows in Two Space Dimensions and Time". (Vol. I - Formulation; Vol. II - Fortran Listing of HELP), BRL CR No. 39, Systems, Science, and Software, La Jolla, Calif., May 1971.

33. Kreyenhagen, K.N., Read, H.E., Rosenblatt, M., and Moore, W.C., "Hardening Technology Studies - III, STRIDE Code Solutions and Extension to Multimaterial Systems". SAMSO-TR-69-16, Dec. 1968.

34. Hofman, R., "PISCES 2DL, Manual 2, Input Manual". Physics International, April 1972.

35. Hagg, A.C. and Sankey, G.O., "The Containment of Disk Burst Fragments by Cylindrical Shells". Journal of Engineering for Power, Trans. ASME, April 1974, pp. 114-123.

36. Clarke, R.B., "Rotor Disk Burst Characteristics Data Analysis". Boeing Commercial Airplane Co., Report No. S&A 73-1, Feb. 28, 1973.

37. Gerstle, J.H., "Analysis of Rotor Fragment Impact on Ballistic Fabric Engine Burst Containment Shells". Boeing Commercial Airplane Co., Paper presented at the Symposium on Propulsion System Structural Integrity and Engine Integrity, Naval Postgraduate School, Monterey, Calif., Sept. 3-6, 1974.

38. Goatham, J.I. and Stewart, R.M., "Missile Firing Tests at Stationary Targets in Support of Blade Containment Design", Paper 75-GT-47, American Society of Mechanical Engineers, Gas Turbine Conference, Houston, Texas, March 2-6, 1975.

39. Wu, R.W.-H., and Witmer, E.A., "Nonlinear Transient Responses of Structures by the Spatial Finite-Element Method", AIAA Journal, Vol. 11, No. 8, August 1973, pp. 1110-1117.

40. Hibbitt, H.D., Marcal, P.V., and Rice, J.R., "A Finite Element Formulation for Problems of Large Strain and Large Displacements." Division of Engineering, Brown University, Report N00014-0007/2, June 1969.

41. Stricklin, J.A., Haisler, W.E., Von Riesemann, W.A., Leick, R.D., Hunsaker, B., and Saczalski, K.E., "Large Deflection Elastic-Plastic Dynamic Response of Stiffened Shells of Revolution", TEES RPT-72-25 and SLA-73-0128, Dec. 1972, Aerospace Engineering Dept., Texas A & M Univ., College Station, Texas.

42. Bathe, K.J., Ramm, E., and Wilson, E.L., "Finite Element Formulations for Large Deformation Dynamic Analysis", International Journal for Numerical Methods in Engineering, Vol. 9, 1975, pp. 353-386.

43. Mendelson, A., Plasticity: Theory and Application, The Macmillan Company, New York, 1968.

44. Marcal, P.V., "A Comparative Study of Numerical Methods of Elastic-Plastic Analysis". AIAA Journal, Vol. 6, No. 1, January 1968, pp. 157-158.

45. Pope, G., "A Discrete Element Method for Analysis of Plane Elastic-Plastic Stress Problems". Royal Aeronautical Establishment, TR 65028, 1968.

46. Marcal, P.V., and King, I.P., "Elastic-Plastic Analysis of Two-Dimensional Stress Systems by the Finite-Element Method". Int. J. Mech., Vol. 9, No. 3, 1967, pp. 143-155.

47. Pian, T.H.H., and Tong, P., "Basis of Finite Element Methods for Solid Continua". International Journal for Numerical Methods in Engineering, Vol. 1, 1969, pp. 3-28.

48. Wilkinson, J.H., The Algebraic Eigenvalue Problem, Oxford University Press, New York, 1965.

49. Leech, J.W., "Stability of Finite-Difference Equations for the Transient Response of a Flat Plate". AIAA Journal, Vol. 3, No. 9, Sept. 1965, pp. 1772-1773.

50. Leech, J.W., Hsu, P.T., and Mack, E.W., "Stability of a Finite-Difference Method for Solving Matrix Equations". AIAA Journal, Vol. 3, No. 11, November 1965, pp. 2172-2173.

51. Hill, R., Mathematical Theory of Plasticity, Clarendon Press, Oxford, 1950.

52. Budiansky, B., "A Reassessment of Deformation Theories of Plasticity", J. Appl. Mech., Vol. 26, June 1959, pp. 259-264.

53. Green, A.E., and Naghdi, P.M., "A General Theory of an Elastic-Plastic Continuum". Arch. Rational Mech. Anal., Vol. 18, 1965, pp. 251-281.

54. Prager, W., and Hodge, P.G., Jr., Theory of Perfectly Plastic Solids, Dover, New York, 1951.

55. White, G.N., Jr., "Application of the Theory of Perfectly Plastic Solids to Stress Analysis of Strain Hardening Solid". Graduate Div. of Applied Math., Brown University, Tech. Report 51, August 1950.

56. Besseling, J.F., "A Theory of Plastic Flow for Anisotropic Hardening in Plastic Deformation of an Initially Isotropic Material". Rept. S410, National Aeronautical Research Institute, Amsterdam, The Netherlands, 1953.

57. Ting, T.C.T., "The Plastic Deformation of a Cantilever Beam with Strain Rate Sensitivity Under Impulsive Loading", Brown University, Providence, R.I., TR 70, ONR Contract 562(10), July 1961.

58. Morino, L., Leech, J.W., and Witmer, E.A., "PETROS 2: A New Finite-Difference Method and Program for the Calculation of Large Elastic-Plastic Dynamically-Induced Deformations of General Thin Shells", Massachusetts Institute of Technology, ASRL TR 152-1, (BRL CR 12) December 1969, Cambridge, Mass. (also Journal of Applied Mechanics, Vol. 38, No. 2, June 1971, pp. 423-436).

59. Pirotin, S.D., Berg, B.A., and Witmer, E.A., "PETROS 3.5: New Developments and Program Manual for the Finite-Difference Calculation of Large Elastic-Plastic Transient Deformations of Multilayer Variable-Thickness Shells", BRL CR 211 (also MIT-ASRL TR 152-4), February 1975.

60. Barr, G.W., and Loring, E.G., "MAT2D: A Plane-Stress Material Model for an Elastic-Plastic Anisotropic Strain-Hardening Material", Research Report SC-RR-69-656, Sandia Laboratories, Albuquerque, New Mexico, Jan. 1970.

61. Huffington, N.J., Jr., "Numerical Analysis of Elastoplastic Stress". U.S. Army Ballistic Research Laboratory, Aberdeen Proving Ground, Maryland, Memorandum Report No. 2006, Sept. 1969.

62. Love, A.E.H., A Treatise on the Mathematical Theory of Elasticity, Dover, New York, 1944. (Republication of 4th Edition, 1927.)

63. Southwell, R.V., An Introduction to the Theory of Elasticity, Dover, New York, 1969. (Republication of 2nd printing, 1941.)

64. Rivello, R.M., Theory and Analysis of Flight Structures, McGraw-Hill, New York, 1969.

65. Fung, Y.C., Foundations of Solid Mechanics, Prentice Hall, New Jersey, 1965.

66. Koiter, W.T., "A Consistent First Approximation in the General Theory of Thin Elastic Shells", Proc. IUTAM Symposium on the Theory of Thin Elastic Shells, Delft, 1959, pp. 12-33.

67. Koiter, W.T., "On the Nonlinear Theory of Thin Elastic Shells", Proceedings of the Koninklyke Nederlandse Akademie van Wetenschappen, B.69, 1966, pp. 1-54.

68. Koiter, W.T., "On the Foundations of the Linear Theory of Thin Elastic Shells", I and II, Proc. Koninklyke Nederlandse Akademie van Wetenschappen, Ser. B.73, 1970, pp. 169-195.

69. John, F., "Estimates for the Derivatives of the Stresses in a Thin Shell and Interior Shell Equations", Comm. Pure and Appl. Math. 18, 1965, pp. 235-267.

70. Fung, Y.C. and Sechler, E.E., Ed.: Thin-Shell Structures, Prentice-Hall, N.J., 1974.

71. Naghdi, P.M., "Foundations of Elastic Shell Theory", Tech. Rept. No. 15, Contract Nonr-222 (69), Univ. of California, Berkeley, Jan. 1962.

72. Naghdi, P.M., The Theory of Shells and Plates, Handbuck der Physik Herausgegeben von S. Flügge, B. VI a/2, Springer Verlag, 1972.

73. Naghdi, P.M. and Nordgren, R.P., "On the Nonlinear Theory of Elastic Shells Under the Kirchhoff Hypothesis", Quart. Appl. Math. 21, pp. 49-59, 1963.

74. Koiter, W.T., "Foundations and Basic Equations of Shell Theory -- A Survey of Recent Progress", Second Symposium on the Theory of Thin Shells, Copenhagen, Sept. 1967, F.I. Niordson, Editor, Springer Verlag, 1969.

75. Sanders, J.L., Jr., "Nonlinear Theories for Thin Shells", Quart. Appl. Math. 21, 1963, pp. 21-36.

76. Hildebrand, F.B., Reissner, E., and Thomas, G.B., "Notes on the Foundation of the Theory of Small Displacements of Orthotropic Shells", NACA TN 1833, 1949.

77. Koiter, W.T. and Simmonds, J.G., "Foundations of Shell Theory", In Proceedings of the 13th Int. Congress of Theor. and App. Mech., Moscow Univ. August 21-26, 1972, E. Becker and G.K. Mikhailov Editors.

78. Donnell, L.H., "Stability of Thin-Walled Tubes Under Torsion", N.A.C.A. TR-479, 1934.

79. Marguerre, K., "Zur Theorie der gekrümmten Platte grosser Formänderung", Proc. of Fifth International Congress of Appl. Mech., Wiley & Sons, 1938, pp. 93-101.

80. Mushtari Kh. M., and Galimov, K.Z., Non-linear Theory of Thin Elastic Shells, Israel Program for Sceintific Translations, 1961.

81. Reissner, E., "On Axisymmetrical Deformations of Thin Shells of Revolution", Proc. of Symposia in Appl. Math., Vol. 3, McGraw-Hill, 1950, pp. 27-52.

82. Johnson, M.W., and Reissner, E., "On the Foundations of the Theory of Thin Elastic Shells", J. Math. Phys. 37, 1959, pp. 371-392.

83. Reiss, E.L., "A Theory for Small Rotationally Symmetric Deformations of Cylindrical Shells, Comm. Pure Appl. Math. 13, 1960, pp. 531-550.

84. Green, A.E., "On the Linear Theory of Thin Elastic Shells", Proc. Roy. Soc. London, Ser. A. 266, 1962, pp. 143-160.

85. Synge, J.L. and Chien, W.Z., "The Intrinsic Theory of Elastic Shells and Plates", Th. von Kármán Anniversary Volume, Calif. Inst. of Tech., 1941, p. 103.

86. Green, A.W. and Adkins, J.E., Large Elastic Deformations, Clarendon Press, Oxford, Second Edition, 1970.

87. Novozhilov, V.V., Foundations of the Nonlinear Theory of Elasticity, [translated from the 1947 Russian edition] Rochester, N.Y., Graylock Press, 1953.

88. Truesdell, C., "Review of [87]", Bull. Am. Math Soc. 59, 1953, pp. 467-473.

89. Budiansky, B., "Notes on Nonlinear Shell Theory", J. Appl. Mech. 35, 1968, pp. 393-401.

90. Wainwright, W.L., "On a Nonlinear Theory of Elastic Shells", Int. J. Engng. Sci. 1, 1963, pp. 339-358.

91. Biricikoglu, V., and Kalnins, A., "Large Elastic Deformations of Shells with the Inclusion of Transverse Normal Strain", Int. J. Solids and Structures 7, 1971, pp. 431-444.

92. Cosserat, E., et F., "Théorie des Corps Déformables", Paris, vi +226 pp.=Appendix, pp. 953-1173, of Chwolson's Traité de Physique, 2nd ed. Paris, 1909.

93. Ericksen, J.L., and Truesdell, C., "Exact Theory of Stress and Strain in Rods and Shells", Arch. Rational Mech. 1, 1958, pp. 295-323.

94. McConnell, A.J., Applications of Tensor Analysis, Dover Publications, Inc., New York, 1957. (Republication of the original "Applications of the Absolute Differential Calculus" by Blackie Company in 1931.)

95. Sokolnikoff, I.S., Tensor Analysis: Theory and Applications to Geometry and Mechanics of Continua, John Wiley & Sons, New York, 2nd Edition, 1964.

96. Truesdell, C. and Toupin, R.A., "The Classical Field Theories" in Handbuch der Physik, Edited by S. Flügge, Volume III/1, Principles of Classical Mechanics and Field Theory, Springer Verlag, Berlin, 1960.

97. Ericksen, J.L., "Tensor Fields", Appendix to [96] in Handbuch der Physik, Ed. S. Flügge, Volume III/1, Principles of Classical Mechanics and Field Theory, Springer Verlag, Berlin, 1960.

98. Synge, J.L. and Schild, A., Tensor Calculus, Toronto, 1949.

99. Green, A.E. and Zerna, W., Theoretical Elasticity, Oxford, Second Edition, 1968.

100. Eisenhart, L.P., Introduction to Differential Geometry, Princeton, 1940.

101. Willmore, T.J., An Introduction to Differential Geometry, Oxford, Clarendon Press, 1959.

102. Koiter, W.T., "General Equations of Elastic Stability for Thin Shells", in Proceedings - Symposium on the Theory of Shells to honor L.H. Donnell, Ed. D. Muster, University of Houston, Texas, 1967.

103. Cook, R.D., Concepts and Applications of Finite Element Analysis, John Wiley, New York, 1974.

104. Oden, J.T., Finite Elements of Nonlinear Continua, McGraw-Hill, 1972.

105. Coco, R.H., "Stiffness Matrix for Curved-Tapered and Straight-Tapered Shell Stiffners", ASRL TR 146-6, (SAMSO TR 69-135), March 1969.

106. Petyt, M., and Fleischer, C.C., "Free Vibration of a Curved Beam", Journal of Sound and Vibration, 18 (1) 1971, pp. 17-30.

107. Mebane, P.M. and Stricklin, J.A., "Implicit Rigid Body Motion in Curved Finite Elements", AIAA Journal, Vol. 9, No. 2, Feb. 1971, pp. 344-345.

108. Cantin, G. and Clough, R.W., "A Curved, Cylindrical-Shell, Finite Element", AIAA Journal, Vol. 6, No. 6, June 1968, pp. 1057-1062.

109. Murray, K.M., "Comments on the Convergence of Finite Element Solutions", AIAA Journal, Vol. 8, No. 4, April 1970, pp. 815-816.

110. Fonder, G.A. and Clough, R.W., "Explicit Addition of Rigid-Body Motions in Curved Finite Elements", AIAA Journal, Vol. 11, No. 3, March 1973, pp. 305-312.

111. Cantin, G., "Strain Displacement Relationships for Cylindrical Shells", AIAA Journal, Vol. 6, No. 9, September 1968, pp. 1787-1788.

112. Wu, R. W-H, Private Communication, Feb. 4, 1975.

113. Dawe, D.J., "Curved Finite Elements for the Analysis of Shallow and Deep Arches", Computers & Structures, Pergamon Press, Vol. 4, 1974, pp. 559-580.

114. Dawe, D.J., "Numerical Studies Using Circular Arch Finite Elements", Computers & Structures, Pergamon Press, Vol. 4, 1974, pp. 729-740.

115. Dawe, D.J., "High-Order Triangular Finite Element for Shell Analysis", Int. J. Solids and Structures, Vol. 11, Oct. 1975, pp. 1097-1110.

116. Kraus, Harry, Thin Elastic Shells, John Wiley & Sons, N.Y., 1967.

117. Witmer, E.A., Merlis, F., and Spilker, R.L., "Experimental Transient and Permanent Deformation Studies of Steel-Sphere-Impacted or Impulsively-Loaded Aluminum Beams with Clamped Ends", MIT ASRL TR 154-11, October 1975 (Available as NASA CR-134922).

118. Balmer, H.A. and Witmer, E.A., "Theoretical-Experimental Correlation of Large Dynamic and Permanent Deformations of Impulsively-Loaded Simple Structures". Massachusetts Institute of Technology, AFFDL-TDR-64-108, July 1964.

119. Clark, E.N., Schmitt, F.H., and Nicolaides, S., "Plastic Deformation of Structures. II: Plastic Deformation of Rings". Picatinny Arsenal, FDL-TDR-64-64, Vol. II, March 1968.

120. Stagliano, T.R., Spilker, R.L., and Witmer, E.A., "User's Guide to Computer Program CIVM-JET 4B to Calculate the Transient Structural Response of Partial and/or Complete Structural Rings to Engine-Rotor-Fragment Impact", MIT ASRL TR 154-9, March 1976 (Available as NASA CR-134907).

121. Park, K.C., "An Improved Stiffly Stable Method for Direct Integration of Nonlinear Structural Dynamic Equations", Journal of Applied Mechanics, June 1975, pp. 464-470.

122 Stephenson, A.E., Sliter, G.E., and Burdette, E., Full-Scale Tornado-Missile Impact Tests Using a Rocket Launcher", ASCE Specialty Conference on the Structural Design of Nuclear Plant Facilities, New Orleans, La., Dec. 1975, Vol. 1-A, pp. 611-636.

123 Stephenson, A.E., "Full Scale Tornado-Missile Impact Tests", Sandia Laboratories, Interim Report, EPRI NP-148, April 1976.

124 Rotz, J.V., Results of Missile Impact Tests on Reinforced Concrete Panels", Bechtel Power Corp., ASCE Specialty Conference on the Structural Design of Nuclear Plant Facilities, New Orleans, La., Dec. 1975, Vol. 1-A, pp. 720-738.

125 Barber, R.B., "Steel-Rod/Concrete-Slab Impact Test (Experimental Simulation)", Bechtel Power Corp., Oct. 1973.

126 Vassalo, F.A., "Missile Impact Testing of Reinforced Concrete Panels", Calspan Corp., Buffalo, N.Y., (prepared for Bechtel Power Corp.), Jan. 1975.

127 Ting, R.M.L., "Non-Composite Steel Panels for Tornado Missile Barrier Walls", H.H. Robertson Co., Pgh, Pa. (tests by Calspan Corp.), ASCE Specialty Conference on the Structural Design of Nuclear Plant Facilities, New Orleans, La., Dec. 1975, Vol. 1-A, pp. 663-687.

128 Baker, W.E., Hokanson, J.C., and Cervantes, R.A., "Model Tests of Industrial Missiles", Southwest Research Institute, San Antonio, Texas, Final Report, SWRI Project No. 02-9153-001, May 1, 1976.

129 Gupta, Y.M. and Seaman, L., "Dynamic Behavior of Reinforced Concrete Under Missile Impact Loading", ASCE Specialty Conference on the Structural Design of Nuclear Plant Facilities, New Orleans, La., Dec. 1975, Vol. 1-A, pp. 637-653.

130 Gupta, Y.M. and Seaman, L., "Development of Dynamic Constitutive Relations for Reinforced Concrete", Stanford Research Institute, Quarterly Progress Report 2 to EPRI, SRI Project PYH-4078, Nov. 1975.

131 Sarne, Y., "Material Nonlinear Time Dependent Three-Dimensional Finite Element Analysis for Reinforced and Prestressed Concrete Structures", Ph.D. Thesis, Dept. of Civil Engineering, MIT, Dec. 1974.

TABLE 1

PRE-TEST DIMENSIONS OF THE 6061-T651 BEAM SPECIMENS

Spec. No.	Beam Region (in)			Support "Collar" (in)				
	h	w	L	h_1	h_2	w_1	w_2	L_c
CB-1	.102	1.493	8.006	1.501	1.501	3.500	.948	1.997
CB-2	.102	1.509	8.011	1.474	1.474	3.499	.946	1.994
CB-3	.102	1.501	8.006	1.475	1.475	3.499	.946	1.998
CB-4	.102	1.497	8.005	1.476	1.476	3.499	.948	1.998
CB-8	.100	1.508	8.004	1.501	.752	2.469	.435	2.491
CB-9	.101	1.482	8.001	1.501	.752	2.469	.434	2.494
CB-10	.101	1.488	8.000	1.502	.753	2.469	.434	2.491
CB-11	.099	1.506	8.000	1.501	1.005	2.469	.435	2.493
CB-12	.101	1.492	8.000	1.502	1.004	2.468	.434	2.490
CB-13	.100	1.501	8.002	1.502	1.004	2.468	.436	2.490
CB-14	.099	1.506	8.002	1.501	1.004	2.468	.434	2.490
CB-15	.098	1.506	8.017	1.501	1.501	2.522	.456	2.480
CB-16	.098	1.495	8.002	1.500	1.500	2.535	.467	2.490
CB-17	.097	1.497	8.005	1.502	1.502	2.537	.468	2.488
CB-18	.097	1.498	8.002	1.501	1.501	2.535	.466	2.490

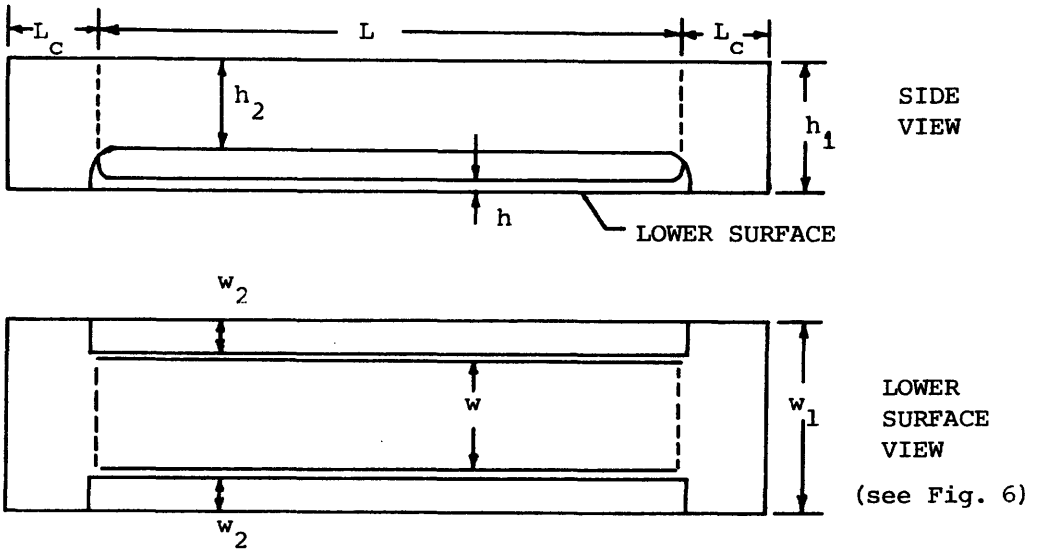

TABLE 2

STRAIN GAGE LOCATIONS AND PERMANENT STRAIN DATA FOR THE 6061-T651 ALUMINUM BEAMS WITH CLAMPED ENDS

Strain Gage Identif. Number	IMPULSIVELY LOADED BEAMS				STEEL-SPHERE-IMPACTED BEAMS			
	Location		Permanent Strain[a] (per cent)		Location		Permanent Strain[a] (per cent)	
	x(in)	Surface (U or L)	Model CB-1	Model CB-4	x(in)	Surface (U or L)	Model CB-13	Model CB-18
1	0	U	-*[b]	--	0	U	--*	--
2	+1.40	U	0.51*	--*	+.30	U	--*	--
3	+2.20	U	0.77*	--*	+.60	U	0.40*	2.24*
4	+3.00	U	1.35*	--*	+1.20	U	0.64	1.13*
5	+3.80	U	0.16*	1.78*	+1.50	U	0.73*	1.48*
6	-1.40	U	0.59	2.55	+3.00	U	0.66	1.34*
7	-2.20	U	0.75	--*	+3.70	U	0.35*	0.56*
8	-3.00	U	1.67*	--*	-.30	U	--*	4.02
9	-3.80	U	1.22	2.36	-.60	U	0.69*	2.36*
10	+1.40	L	1.30	--	-1.50	U	0.56	1.13*
11	+2.20	L	1.36*	--*	-3.70	U	0.48	0.68
12	+3.00	L	0.02	0.89	+1.50	L	0.60*	1.31*
13	+3.80	L	0.02*	1.27*	+3.00	L	0.49	1.23
14	-2.20	L	1.32	--	+3.70	L	0.26	1.07
15	-3.00	L	0.35	1.57	-1.50	L	0.74	1.27
16	-3.80	L	0.18	1.15	-3.70	L	0.20	0.47

a: This permanent strain is actually the relative elongation E_1 defined by $E_1 = \sqrt{1+2\gamma_{11}} - 1$ where γ_{11} is the extensional strain tensor component in the spanwise direction; tension is (+), compression is (-).

b: A dash (-) indicates that the strain gage was gound to be detached after the test.

*: Denotes that transient strain measurements were attempted.

TABLE 3

NUMBER OF SPANWISE GAUSSIAN INTEGRATION STATIONS NEEDED FOR EVALUATING THE MASS MATRIX, THE STIFFNESS MATRIX, AND THE NONLINEAR-DEFLECTION CONTRIBUTION OF THE GENERALIZED LOADS VECTOR FOR VARIOUS STRAIGHT AND CURVED-BEAM ELEMENTS

Element Matrix \ Type of Element	NUMBER OF SPANWISE GAUSSIAN STATIONS NEEDED FOR EXACT INTEGRATION*									
	4 DOF/N		5 DOF/N		6 DOF/N		7 DOF/N		8 DOF/N	
	C_v	C_w	C_v	Q_w	Q_v	Q_w	Q_v	7^{th}_w	7^{th}_v	7^{th}_w
	STRAIGHT	CURVED	STRAIGHT	CURVED	STRAIGHT	CURVED	STRAIGHT	CURVED	STRAIGHT	CURVED
Consistent Mass	4	4	6	6	6	6	8	8	8	8
Stiffness	3	4	4	6	5	6	6	8	7	8
$\{f_q^{NL}\}$	5	7	9	11	9	11	13	15	13	15

*Ignoring trigonometric terms in the assumed displacement field, and assuming constant thickness.

TABLE 4

INFLUENCE OF THE NUMBER OF SPANWISE GAUSSIAN STATIONS ON THE MAXIMUM NATURAL FREQUENCY AND REQUIRED NODAL VELOCITIES TO PRODUCE A GIVEN INITIAL KINETIC ENERGY FOR BEAM MODEL CB-1 WHEN MODELED BY 4 DOF/N, 5 DOF/N, and 8 DOF/N ELEMENTS

No. of Spanwise Gaussian Stations			Computed Results	
Used	Needed for Exact [m] Integration	Needed for Exact [k] Integration	ω^2_{max} (μsec)	Nodal Velocity to Produce $(KE)_o$ = 770.8 in-lb (in/sec)
10 Equal Elements per Half Span: 4 DOF/N, (C,C;v,w)				
5	4	3	0.622001	6294.13[a]
4	4	3	0.622001	6294.13[a]
3	4	3	0.520353	6299.23[a]
2	4	3	1.126926	--
10 Equal Elements per Half Span: 5 DOF/N, (C,Q;v,w)				
7	6	4	0.622001	6218.59[a]
6	6	4	0.622001	6218.59[a]
5	6	4	0.622001	6218.77[a]
4	6	4	0.622001	6215.84[a]
3	6	4	0.520353	6248.15[a]
4 Elements per Half Span*: 8 DOF/N, (7th,7th;v,w)				
9	8	7	0.458108	6921.52[b]
8	8	7	0.458108	6921.52[b]
7	8	7	0.451270	6921.53[b]
6	8	7	0.372488	6921.42[b]
5	8	7	0.226864	6922.58[b]

a: This is velocity at the last "loaded node" (node 3); at nodes 1 and 2 velocity is 6656.79 in/sec. Node 1 is at midspan (x=0).

b: Velocity applied to all loaded nodes (i.e. nodes 1 and 2).

* Element nodes located at x=0, 0.6, 1.2, 3.2, and 4.0 in; model CB-1.

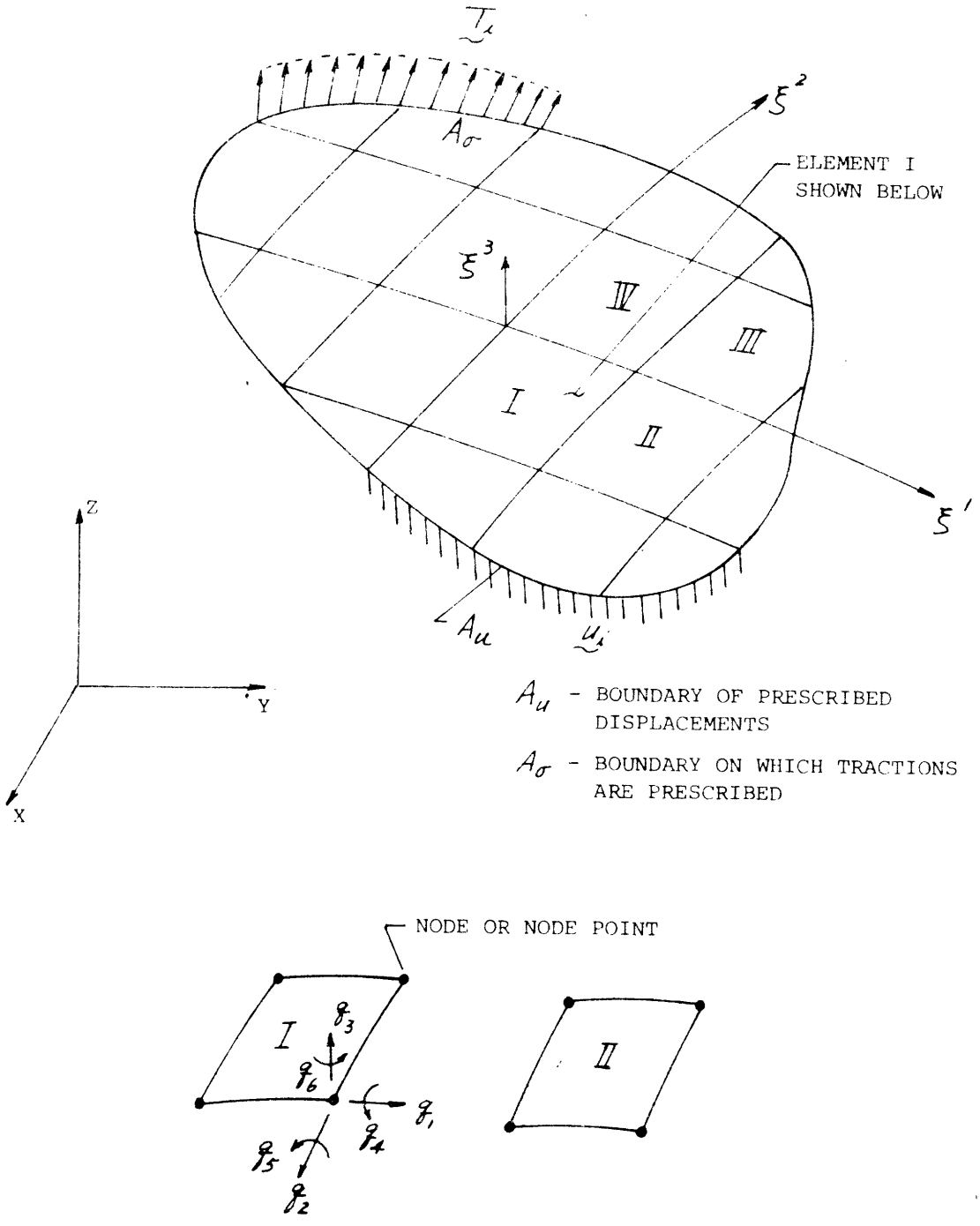

FIG. 1 NOMENCLATURE FOR A POSSIBLE FINITE-ELEMENT REPRESENTATION OF A GENERAL TWO-DIMENSIONAL STRUCTURE

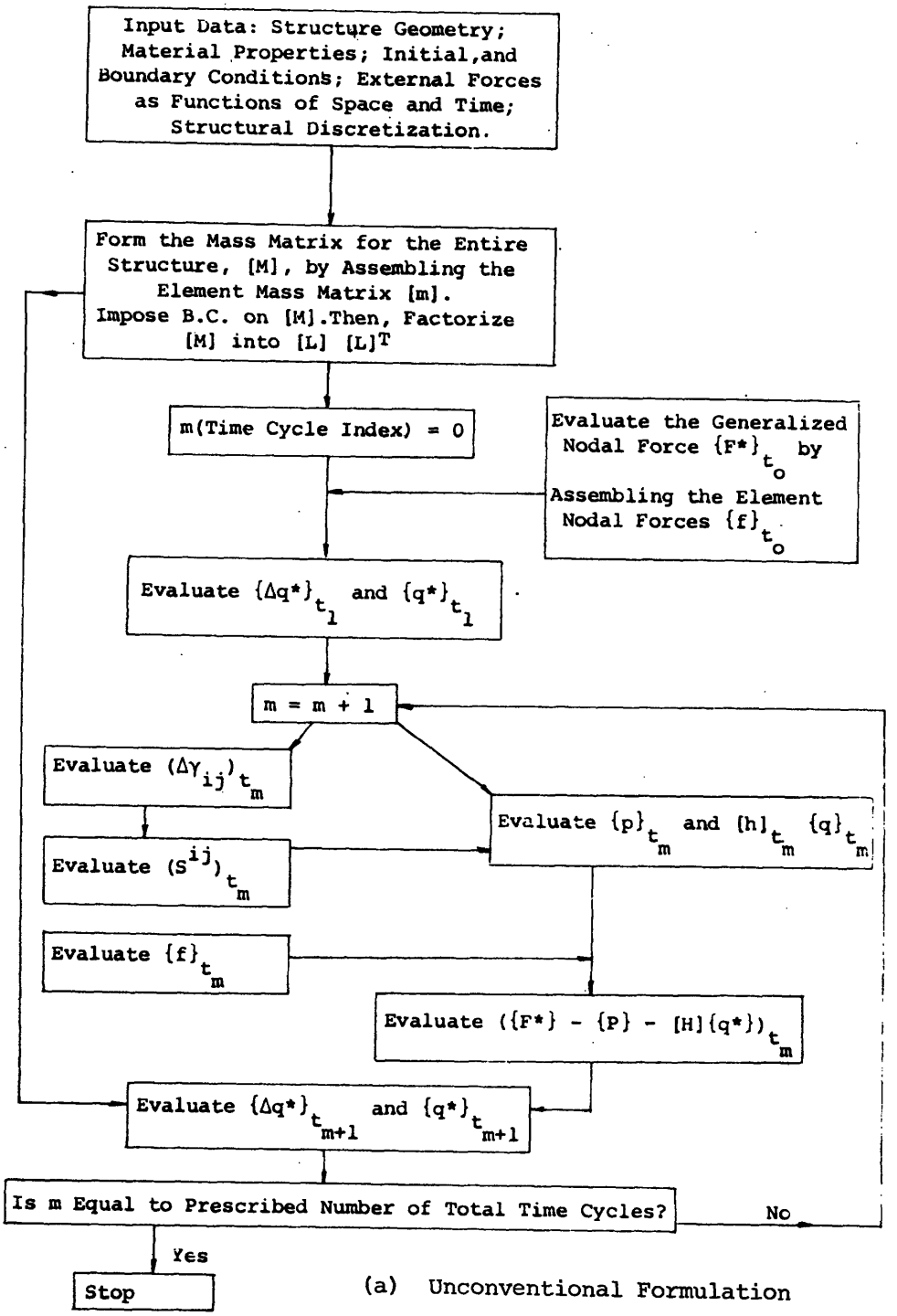

FIG. 2 FLOW CHART FOR SOLUTION PROCESS OF STRUCTURAL LARGE-DEFLECTION ELASTIC-PLASTIC TRANSIENT RESPONSES

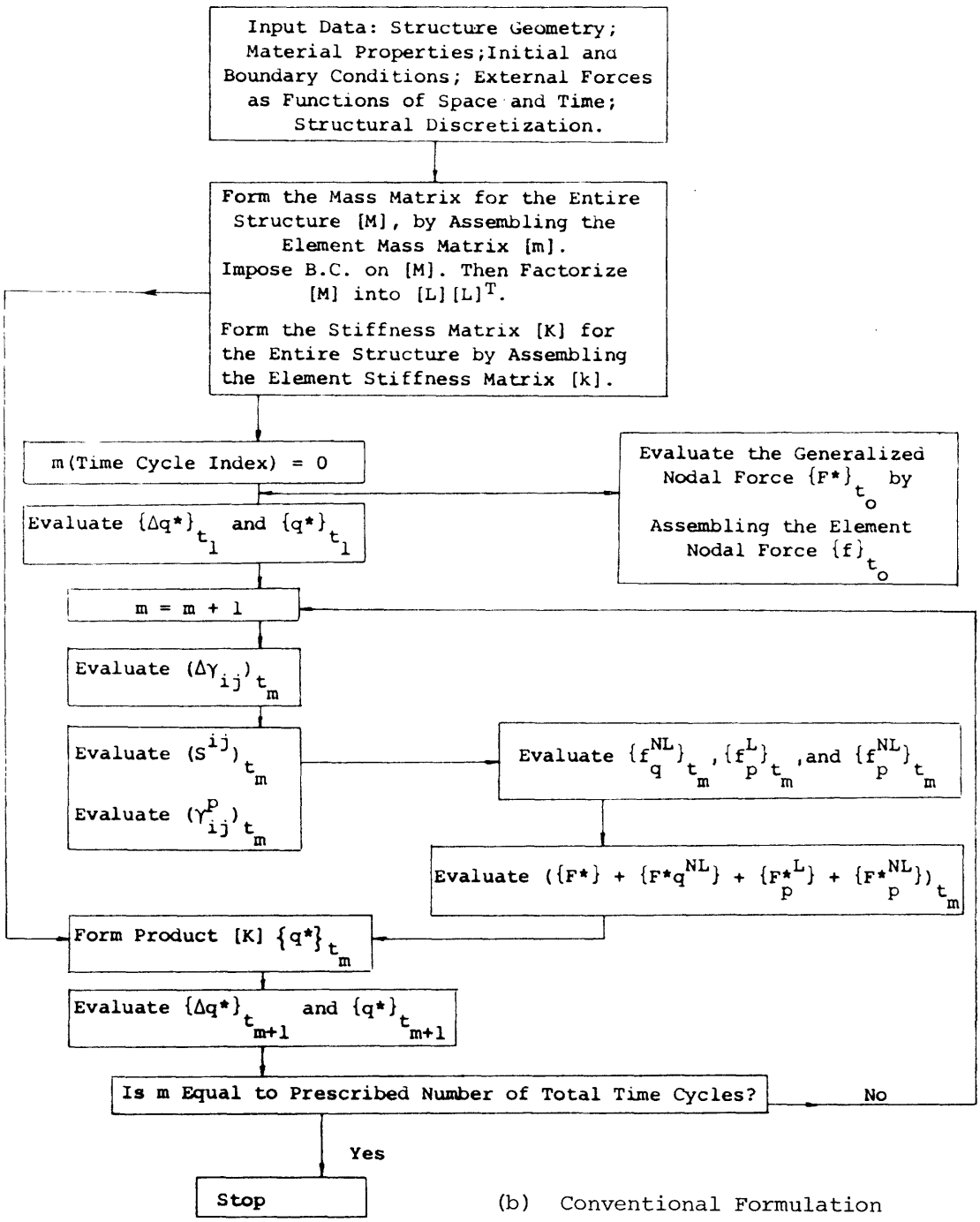

(b) Conventional Formulation

FIG. 2 CONCLUDED

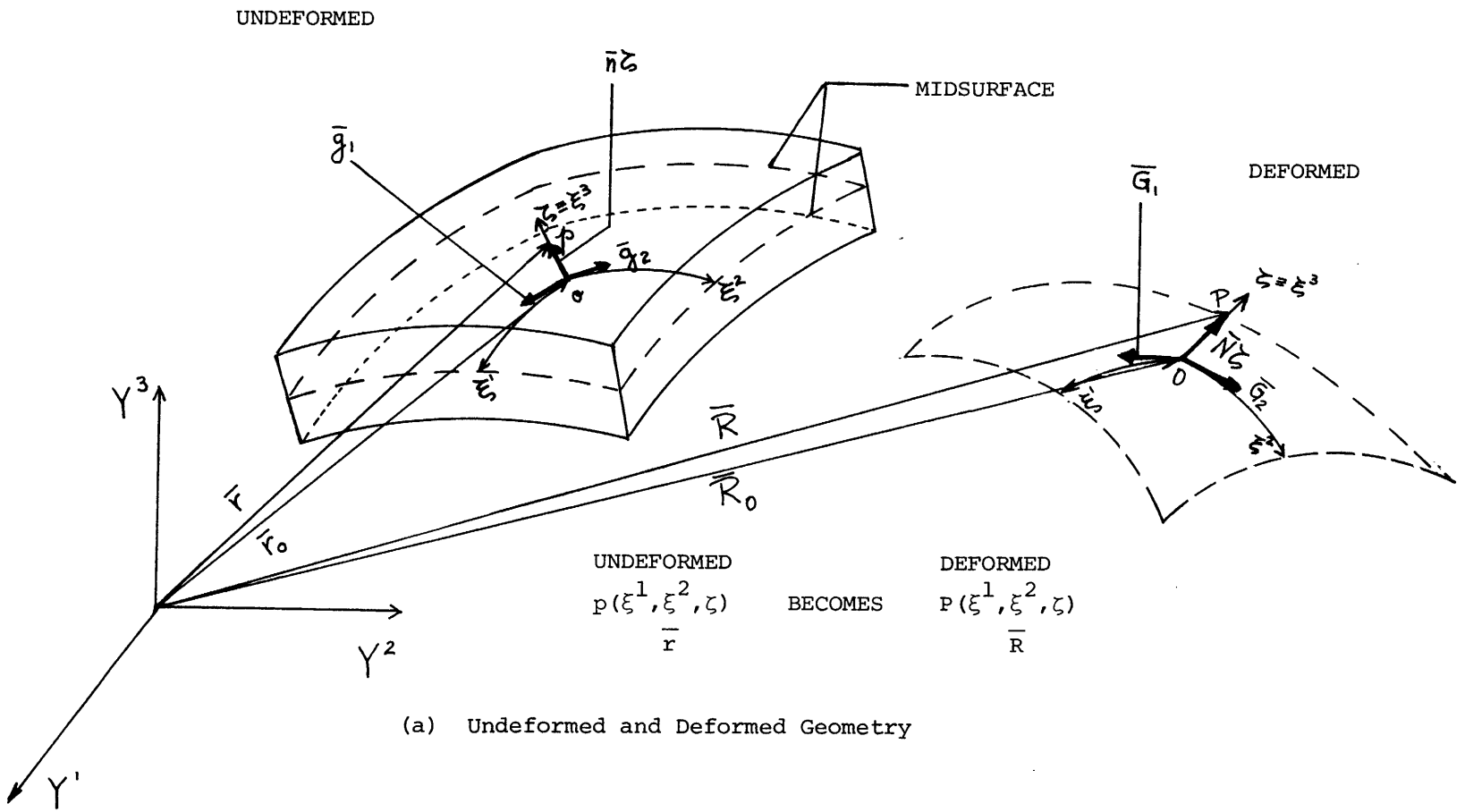

(a) Undeformed and Deformed Geometry

FIG. 3 NOMENCLATURE FOR SHELL GEOMETRY AND DISPLACEMENTS

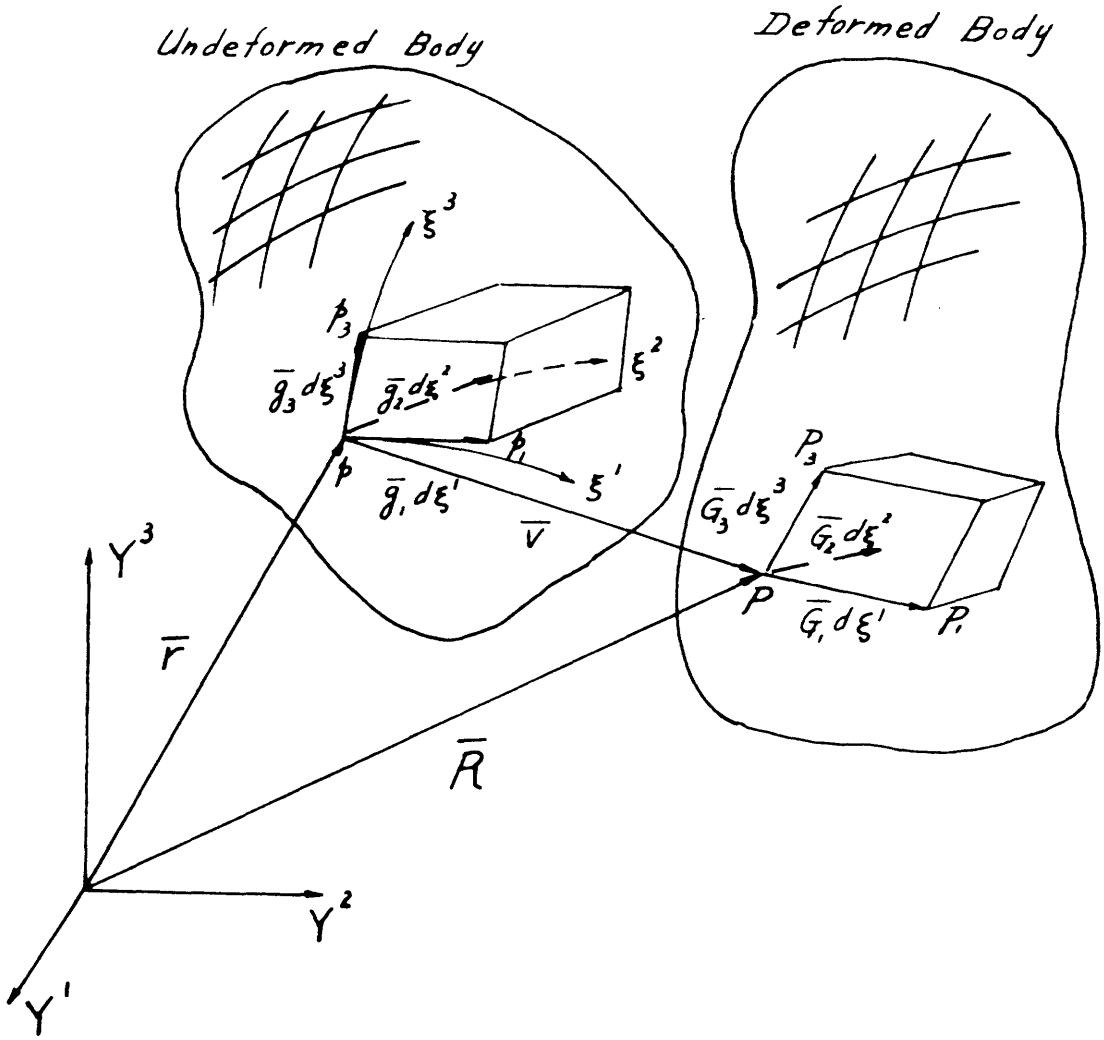

(b) Undeformed and Deformed Volume Element

FIG. 3 CONTINUED

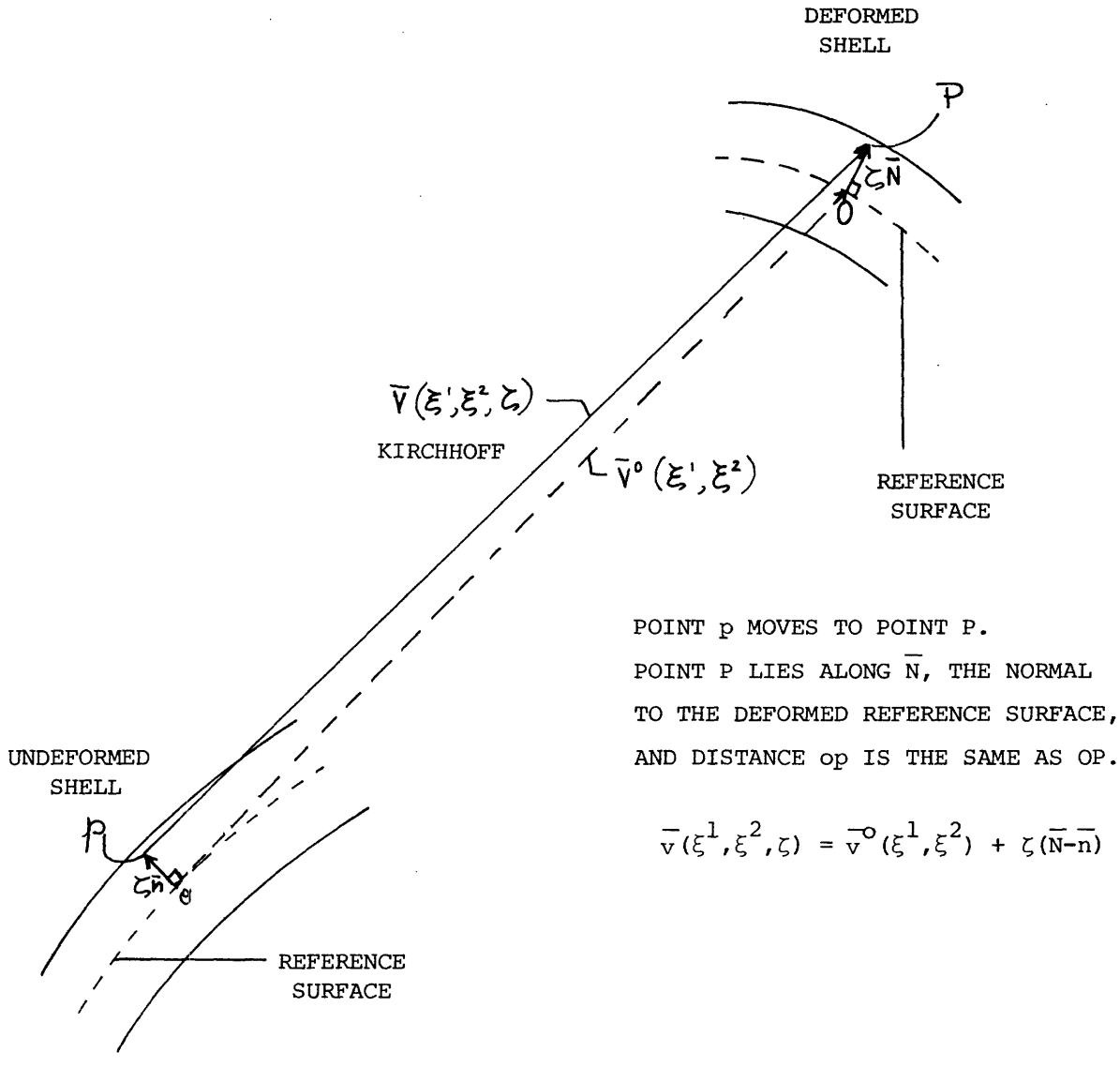

(c) Kirchhoff Displacement Field Diagram

FIG. 3 CONCLUDED

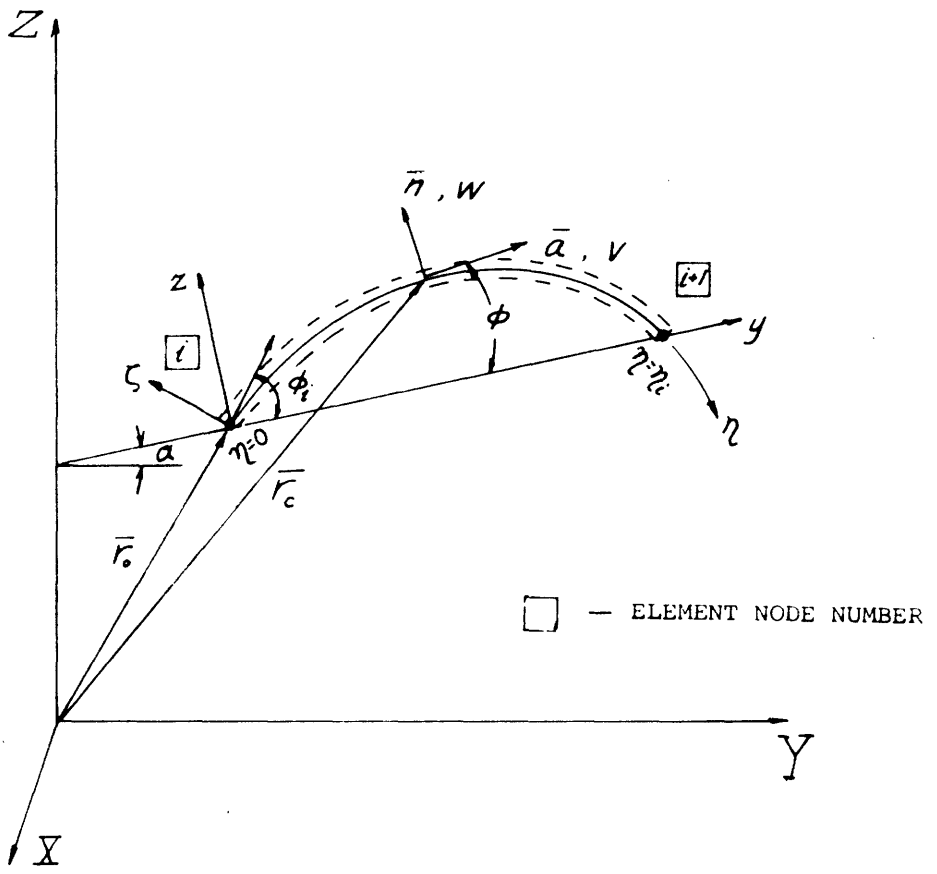

FIG. 4 NOMENCLATURE FOR GEOMETRY, COORDINATES, AND DISPLACEMENTS OF A CURVED-BEAM FINITE ELEMENT

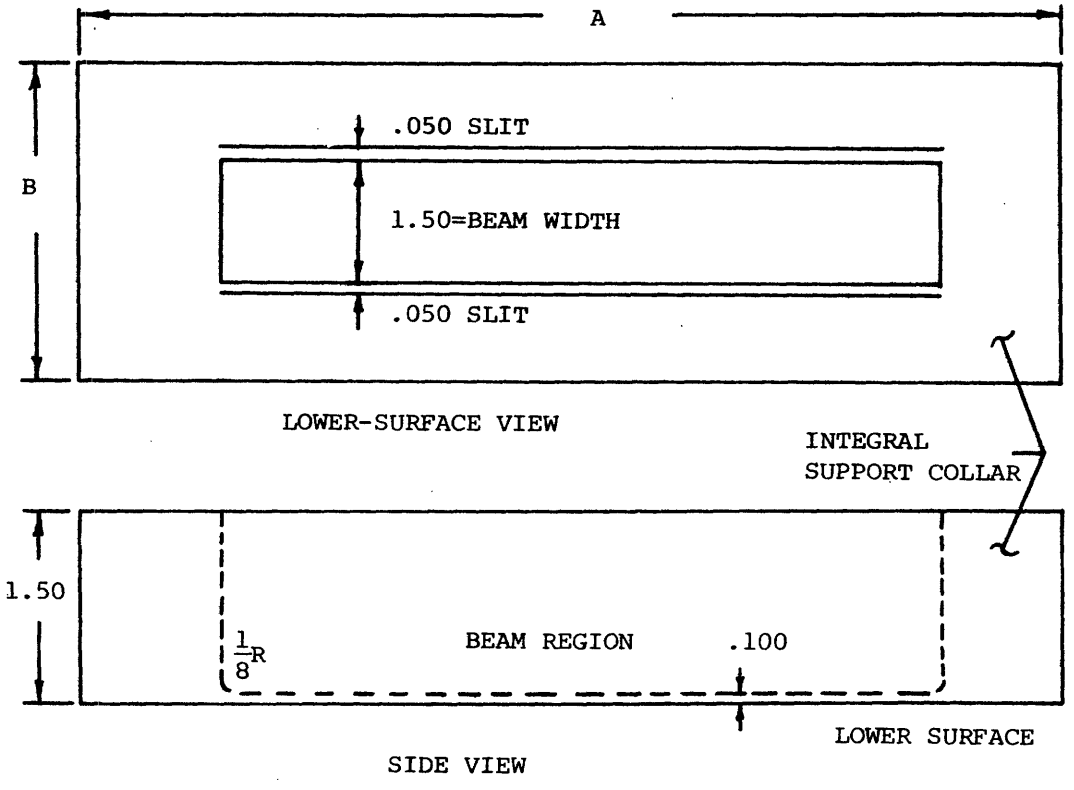

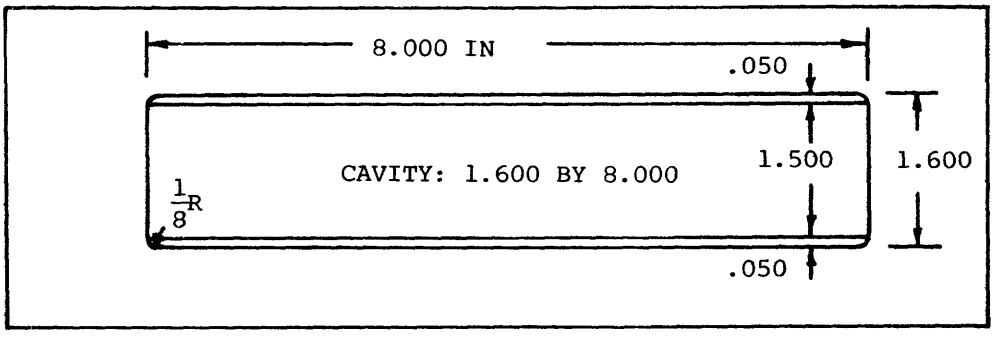

FOR MODELS CB-1,-2,-3,AND -4 A=12.00 IN
B=3.50 IN

FOR MODELS CB-8,-9,...,-18 A=13.00 IN
B=2.55 IN

FIG. 5 NOMINAL DIMENSIONS FOR THE 6061-T651 ALUMINUM CLAMPED-BEAM MODELS

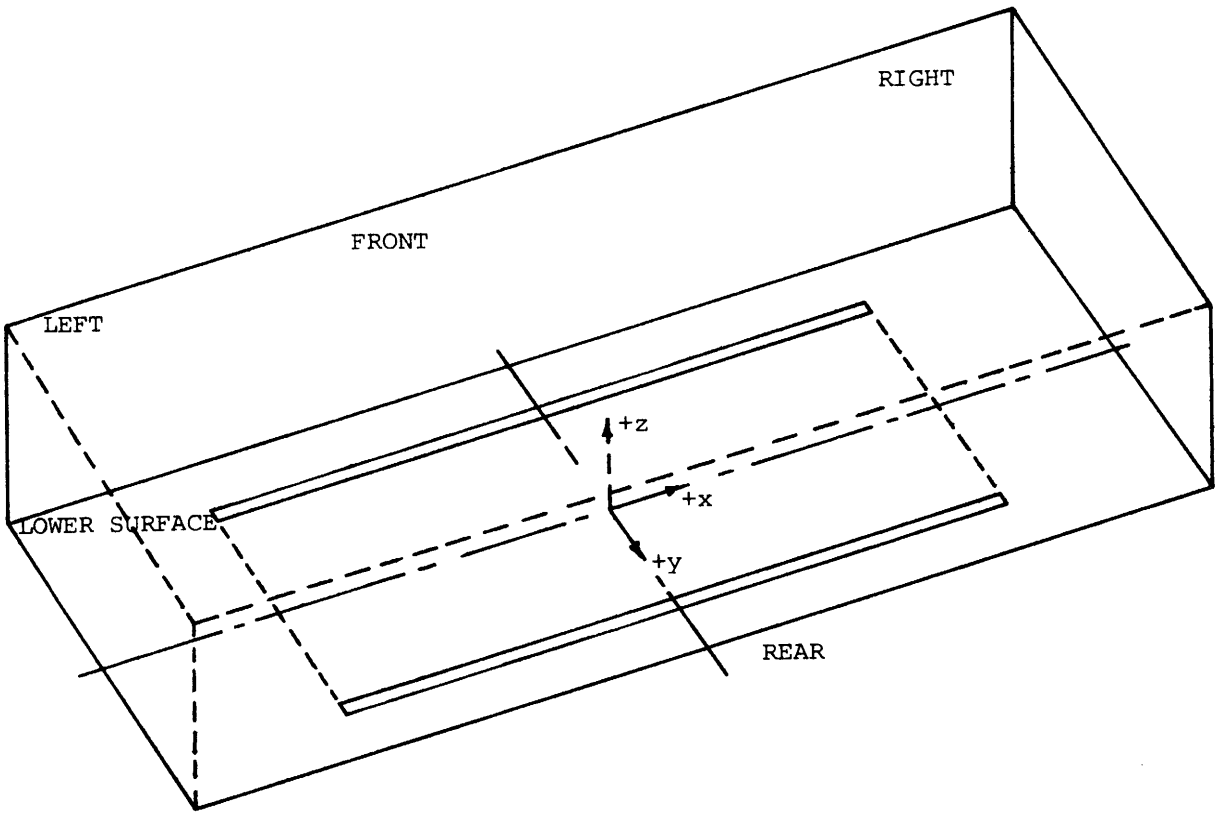

FIG. 6 CLAMPED BEAM MODEL COORDINATES AND NOMENCLATURE

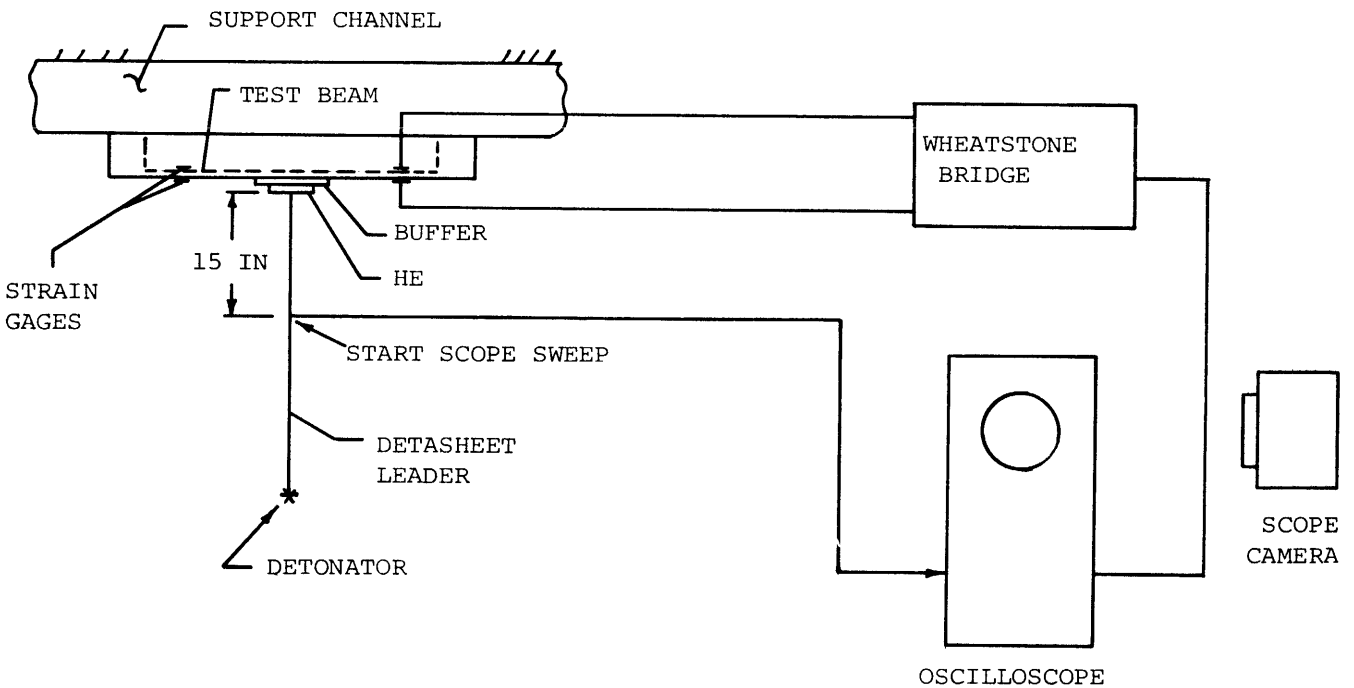

FIG. 7 SCHEMATIC OF IMPULSIVE-LOADING TESTS ON 6061-T651 BEAMS WITH CLAMPED ENDS

ABSCISSA: TIME, 50 μSEC/DIV
ORDINATE: UNCORRECTED RELATIVE ELONGATION E_x IN PER CENT
+ = TENSION (UP)
- = COMPRESSION (DOWN)
∇: TIME = 0

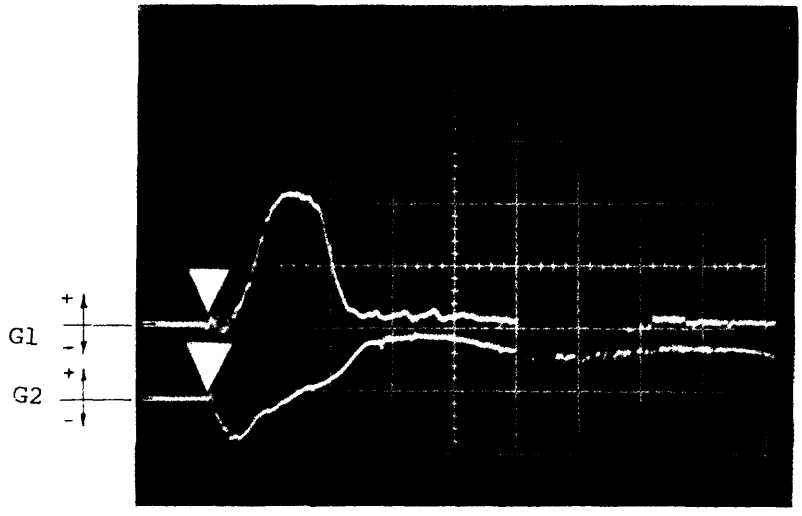

GAGE 1
E_x: 3%/DIV

GAGE 2
E_x: 2%/DIV

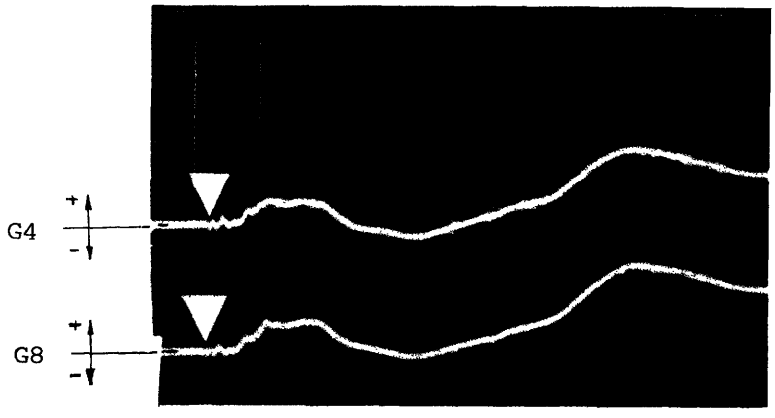

GAGE 4
E_x: 2%/DIV

GAGE 8
E_x: 2%/DIV

FIG. 8 UNCORRECTED TRANSIENT STRAIN RECORDS FOR IMPULSIVELY-LOADED 6061-T651 BEAM MODEL CB-1 WITH CLAMPED ENDS

ABSCISSA: TIME, 100 μSEC/DIV
ORDINATE: UNCORRECTED RELATIVE ELONGATION E_x IN PER CENT
+ = TENSION (U))
- = COMPRESSION (DOWN)
∇: TIME = 0

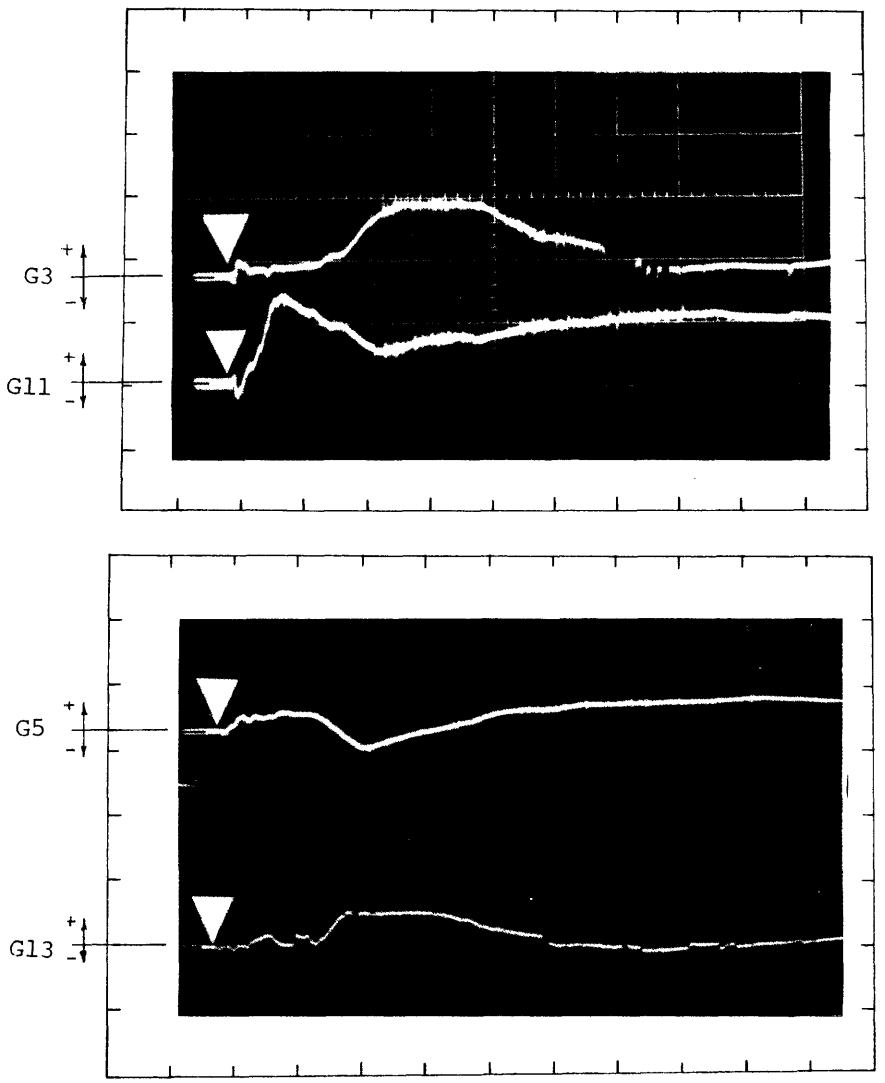

GAGE 3
E_x: 2%/DIV

GAGE 11
E_x: 2%/DIV

GAGE 5
E_x: 2%/DIV

GAGE 13
E_x: 3%/DIV

FIG. 8 CONCLUDED (CB-1)

ABSCISSA: TIME, 50 μSEC/DIV
ORDINATE: UNCORRECTED RELATIVE ELONGATION E_x IN PER CENT
+ = TENSION (UP)
- = COMPRESSION (DOWN)
∇: TIME = 0

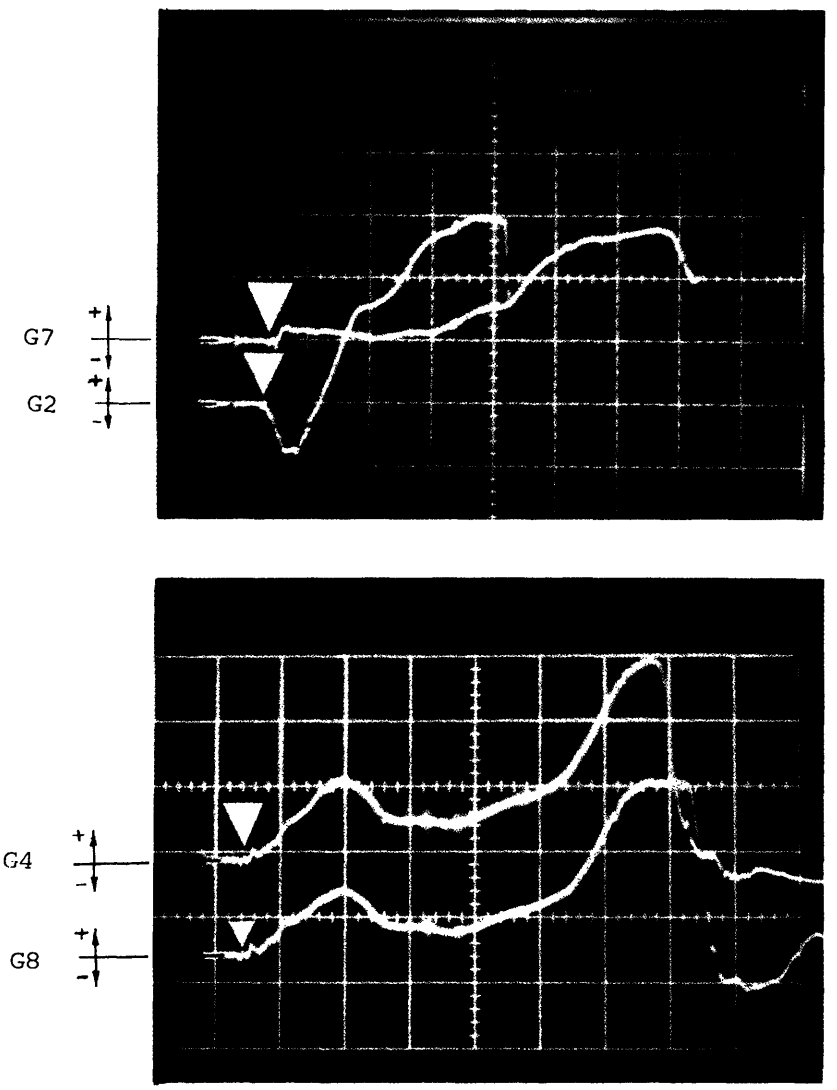

GAGE 2
E_x: 2%/DIV

GAGE 7
E_x: 2%/DIV

GAGE 4
E_x: 2%/DIV

GAGE 8
E_x: 2%/DIV

FIG. 9 UNCORRECTED TRANSIENT STRAIN RECORDS FOR IMPULSIVELY-LOADED 6061-T651 BEAM MODEL CB-4 WITH CLAMPED ENDS

ABSCISSA: TIME, 100 μSEC/DIV
ORDINATE: UNCORRECTED RELATIVE ELONGATION E_x IN PER CENT
+ = TENSION (UP)
- = COMPRESSION (DOWN)
∇: TIME = 0

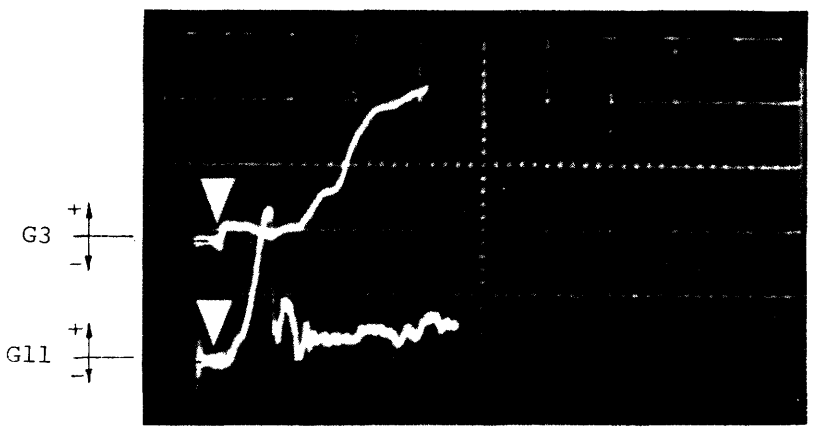

GAGE 3
E_x: 2%/DIV

GAGE 11
E_x: 2%/DIV

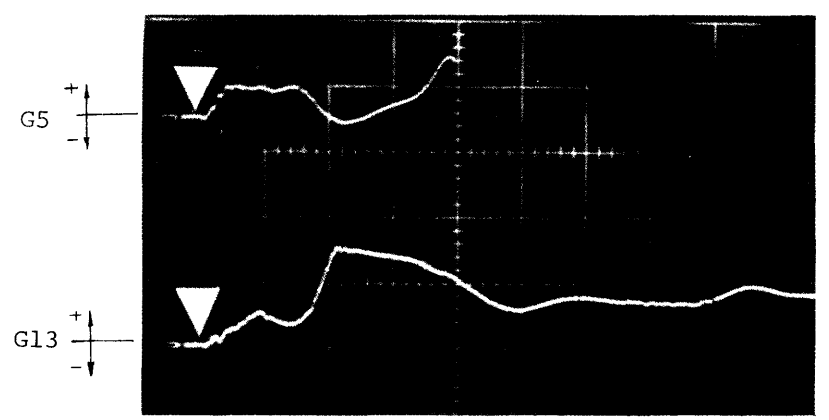

GAGE 5
E_x: 2%/DIV

GAGE 13
E_x: 2%/DIV

FIG. 9 CONCLUDED (CB-4)

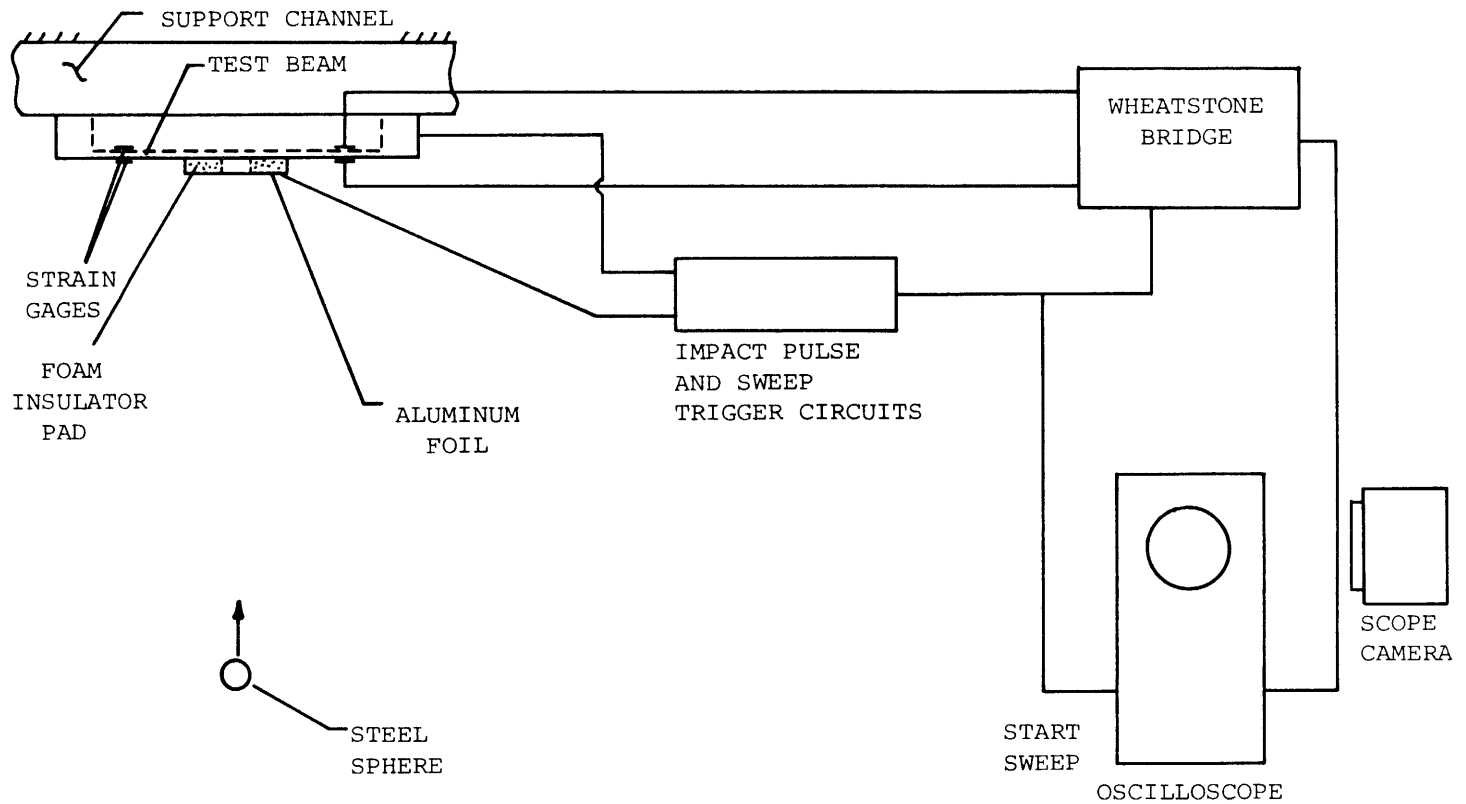

FIG. 10 TEST SCHEMATIC FOR STEEL-SPHERE-IMPACTED 6061-T651 ALUMINUM BEAMS WITH CLAMPED ENDS

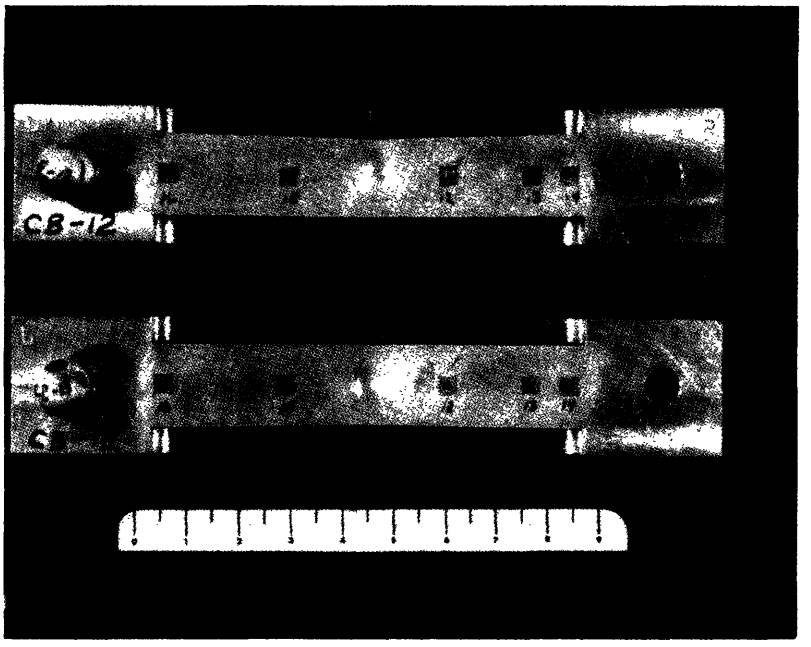

LOWER SURFACE VIEW

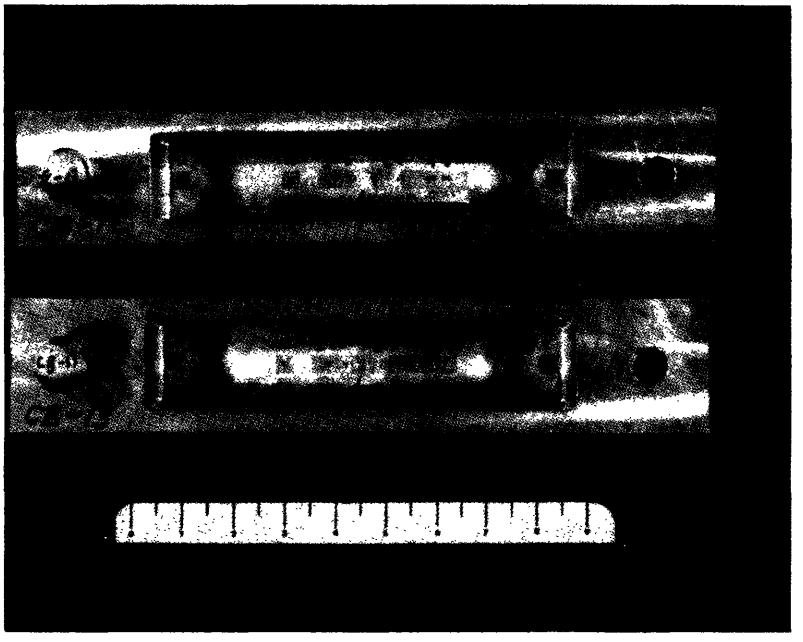

UPPER SURFACE VIEW (INTO CAVITY)

FIG. 11 POST-TEST VIEWS OF STEEL-SPHERE-IMPACTED BEAM SPECIMENS CB-12 AND CB-13 (NOMINAL IMPACT VELOCITY: 2500 IN/SEC)

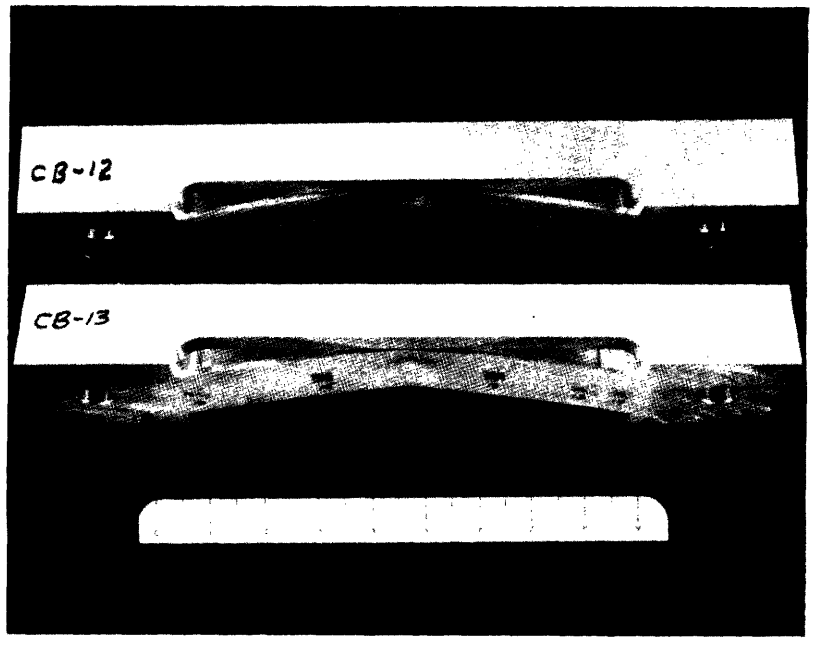

SIDE
VIEW

FIG. 11 CONCLUDED

ABSCISSA: TIME, 50 μSEC/DIV
ORDINATE: UNCORRECTED RELATIVE ELONGATION E_x IN PER CENT
+ = TENSION
- = COMPRESSION
∇: INSTANT OF IMPACT

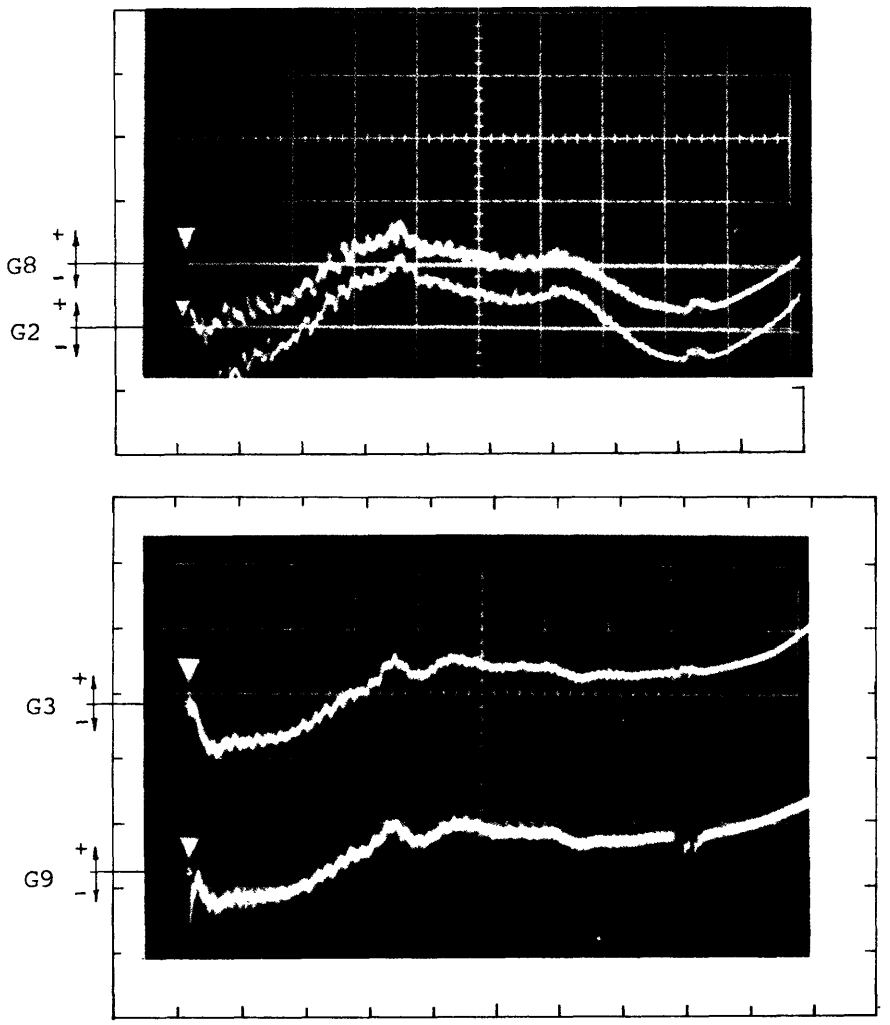

FIG. 12 UNCORRECTED TRANSIENT STRAIN RECORDS FOR STEEL-SPHERE IMPACTED 6061-T651 ALUMINUM BEAM MODEL CB-13

ABSCISSA: TIME
ORDINATE: UNCORRECTED RELATIVE ELONGATION E_x IN PER CENT
+ = TENSION
- = COMPRESSION
▽: INSTANT OF IMPACT

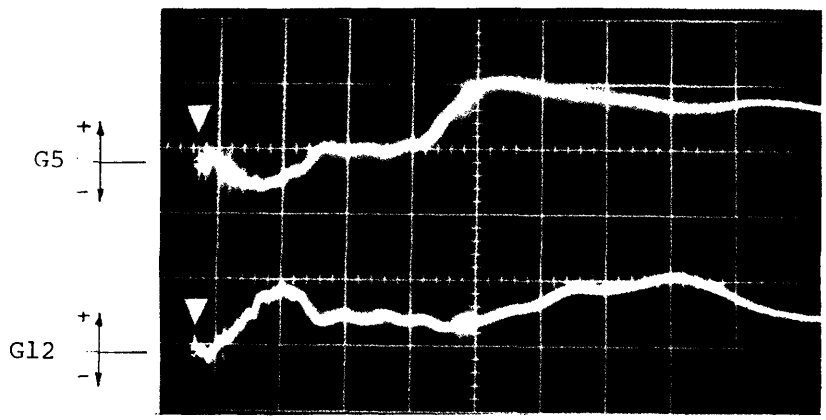

GAGE 5
E_x: 1.5%/DIV
100 μSEC/DIV

GAGE 12
E_x: 1%/DIV
100 μSEC/DIV

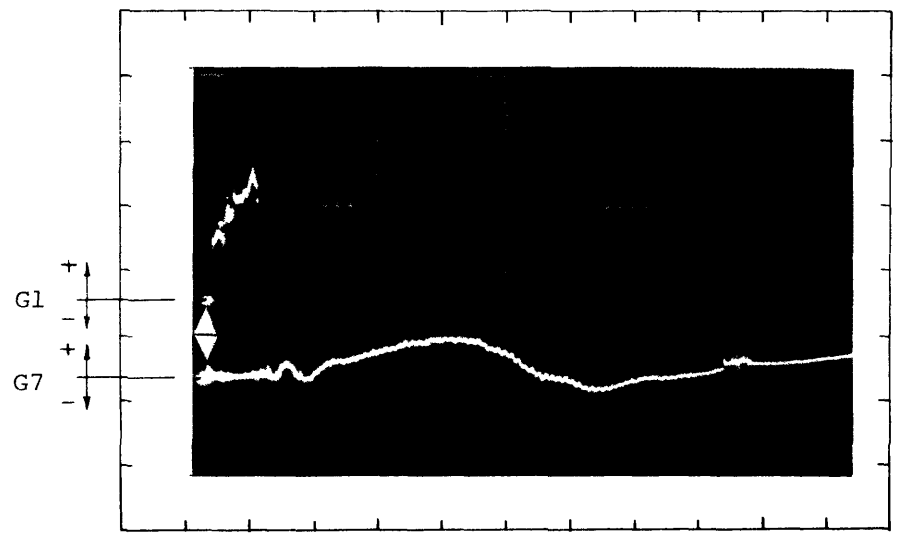

GAGE 1
E_x: 3%/DIV
50 μSEC/DIV

GAGE 7
E_x: 1%/DIV
50 μSEC/DIV

FIG. 12 CONCLUDED (CB-13)

ABSCISSA: TIME
ORDINATE: UNCORRECTED RELATIVE ELONGATION E_x IN PER CENT
+ = TENSION
- = COMPRESSION
∇: INSTANT OF IMPACT

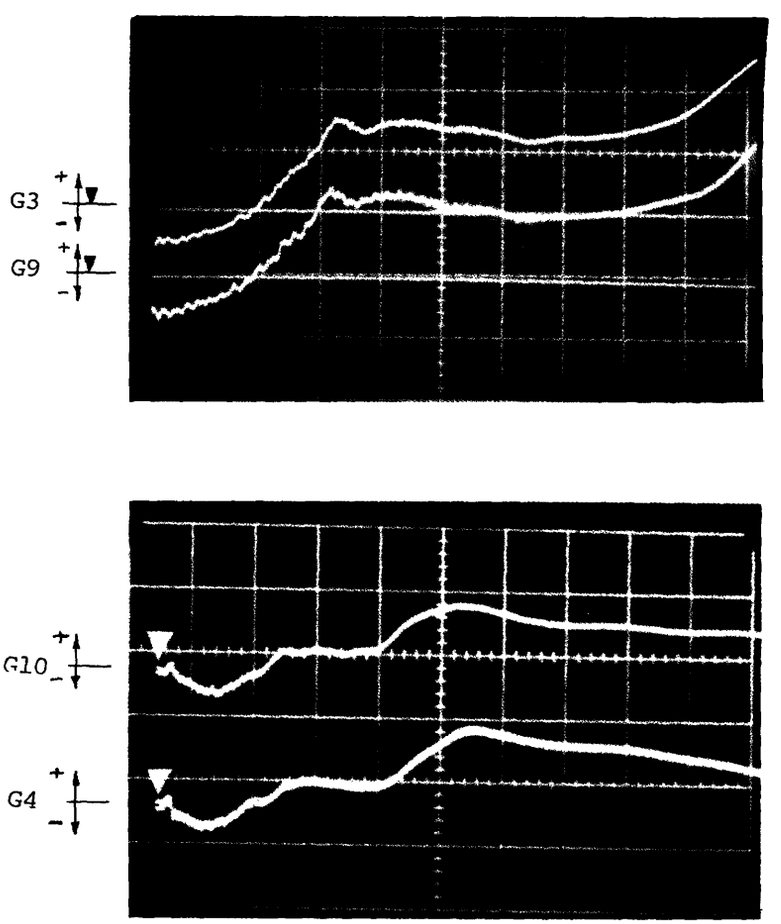

GAGE 3
E_x: 1%/DIV
50 μSEC/DIV

GAGE 9
E_x: 1%/DIV
50 μSEC/DIV

GAGE 10
E_x: 2%/DIV
100 μSEC/DIV

Gage 4
E_x: 2%/DIV
100 μSEC/DIV

FIG. 13 UNCORRECTED TRANSIENT STRAIN RECORDS FOR STEEL-SPHERE IMPACTED 6061-T651 ALUMINUM BEAM MODEL CB-18

ABSCISSA: TIME, 100 μSEC/DIV
ORDINATE: UNCORRECTED RELATIVE ELONGATION E_x IN PER CENT
+ = TENSION
- = COMPRESSION
∇: INSTANT OF IMPACT

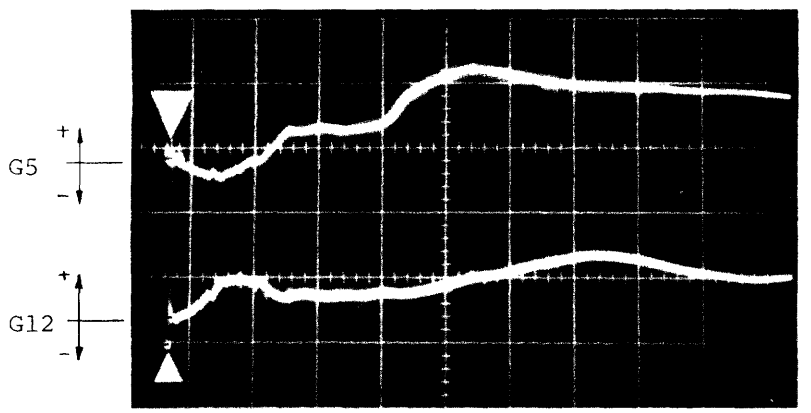

GAGE 5
E_x: 2%/DIV

GAGE 12
E_x: 2%/DIV

FIG. 13 CONCLUDED (CB-18)

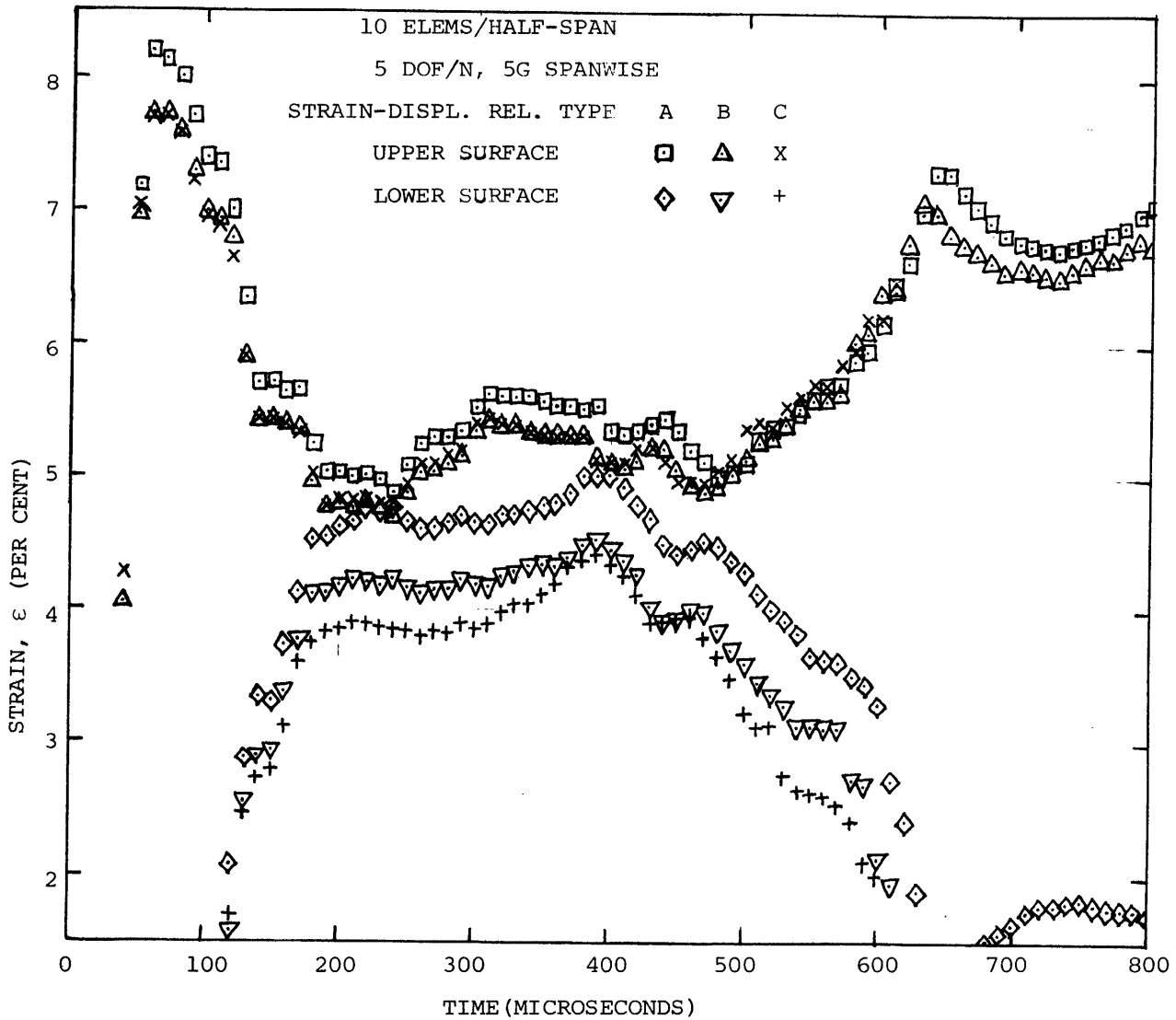

(a) Station x=0

FIG. 14 INFLUENCE OF STRAIN-DISPLACEMENT RELATIONS ON PREDICTED TRANSIENT STRAIN ON IMPULSIVELY-LOADED BEAM CB-1

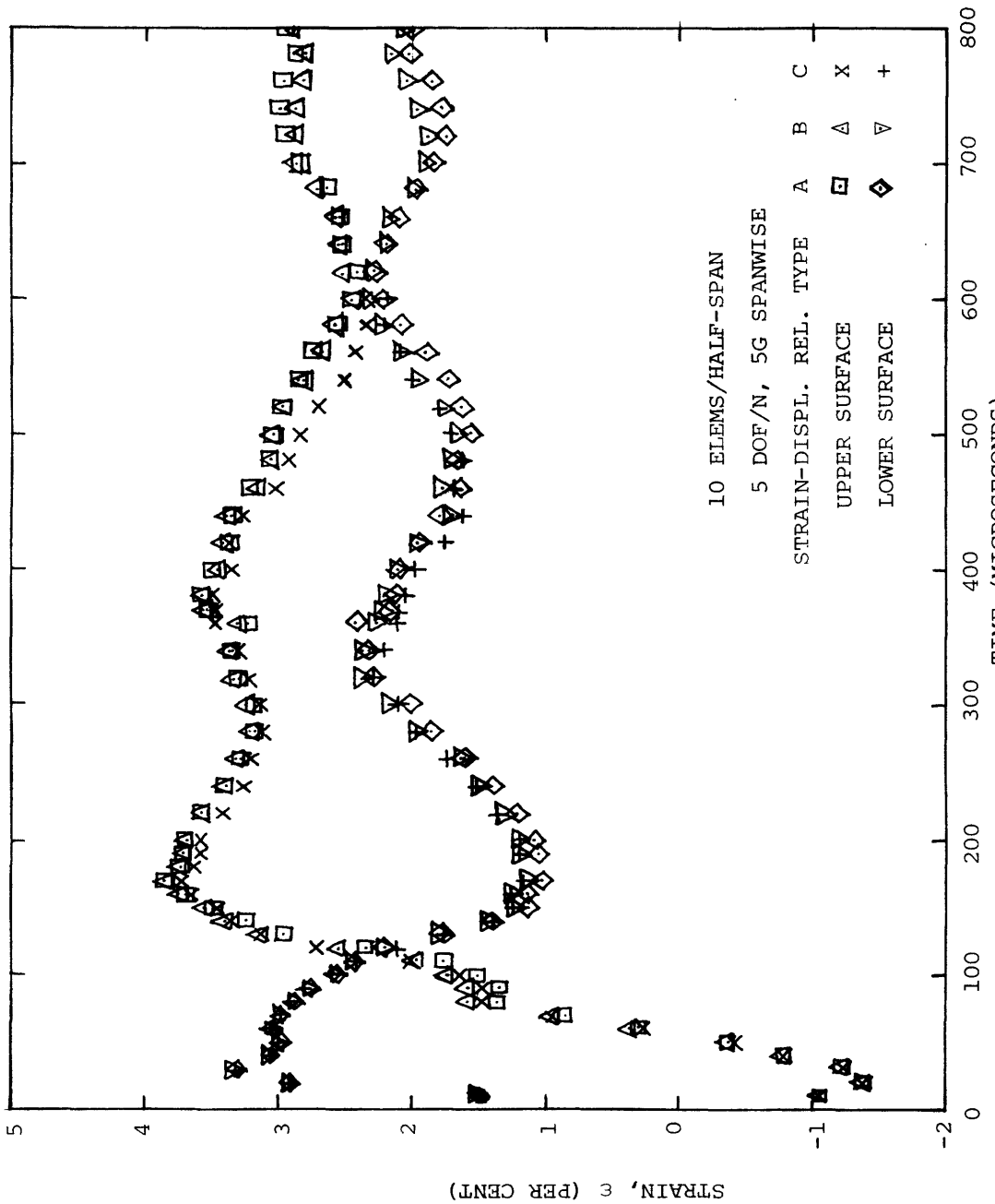

(b) Station x=1.40 in

FIG. 14 CONTINUED (CB-1)

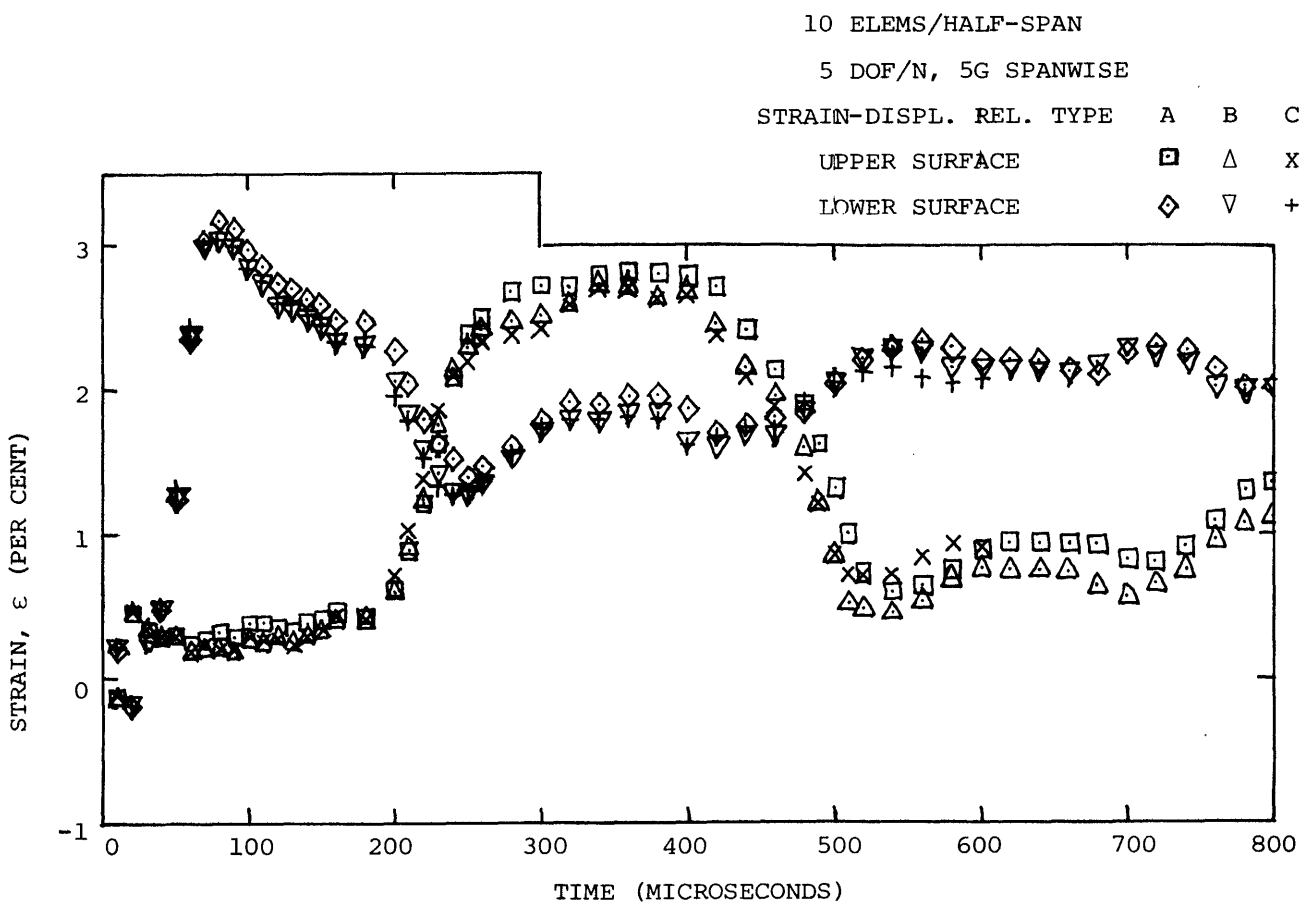

(c) Station x=2.20 in

FIG. 14 CONTINUED (CB-1)

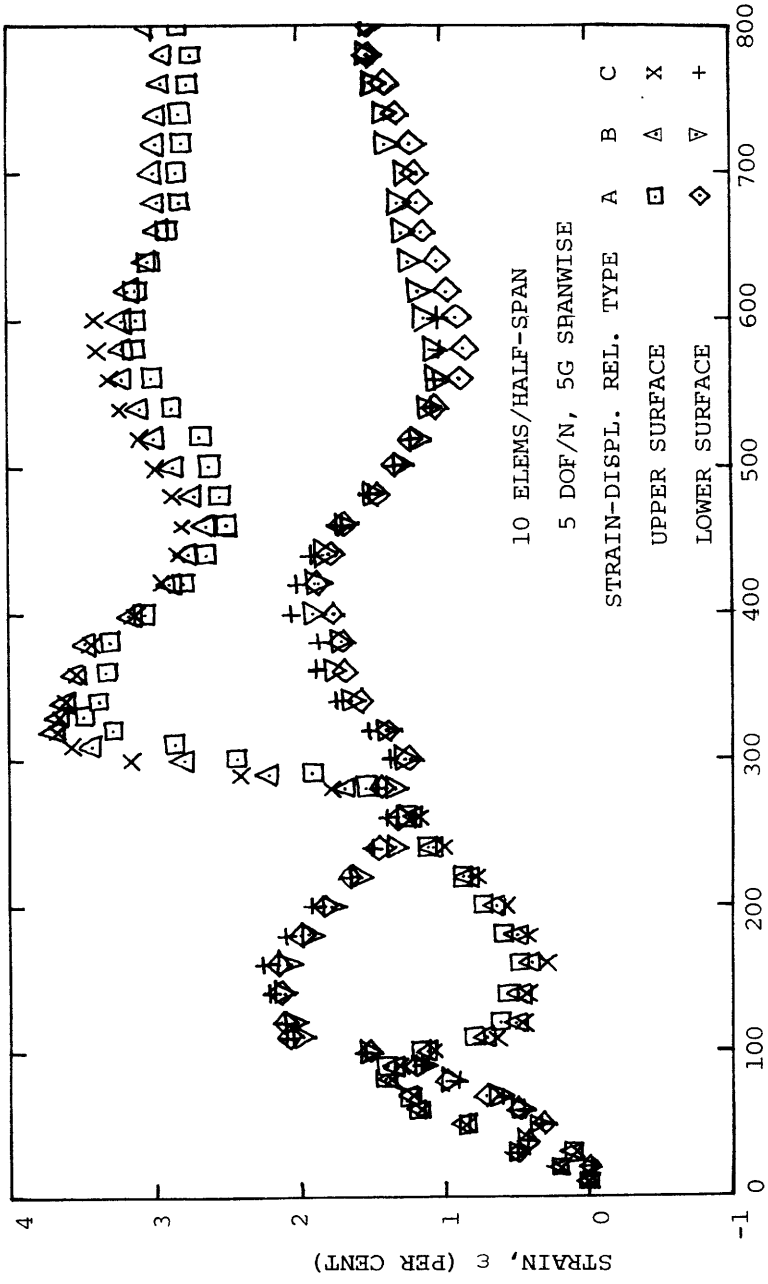

(d) Station x=3.00 in

FIG. 14 CONTINUED (CB-1)

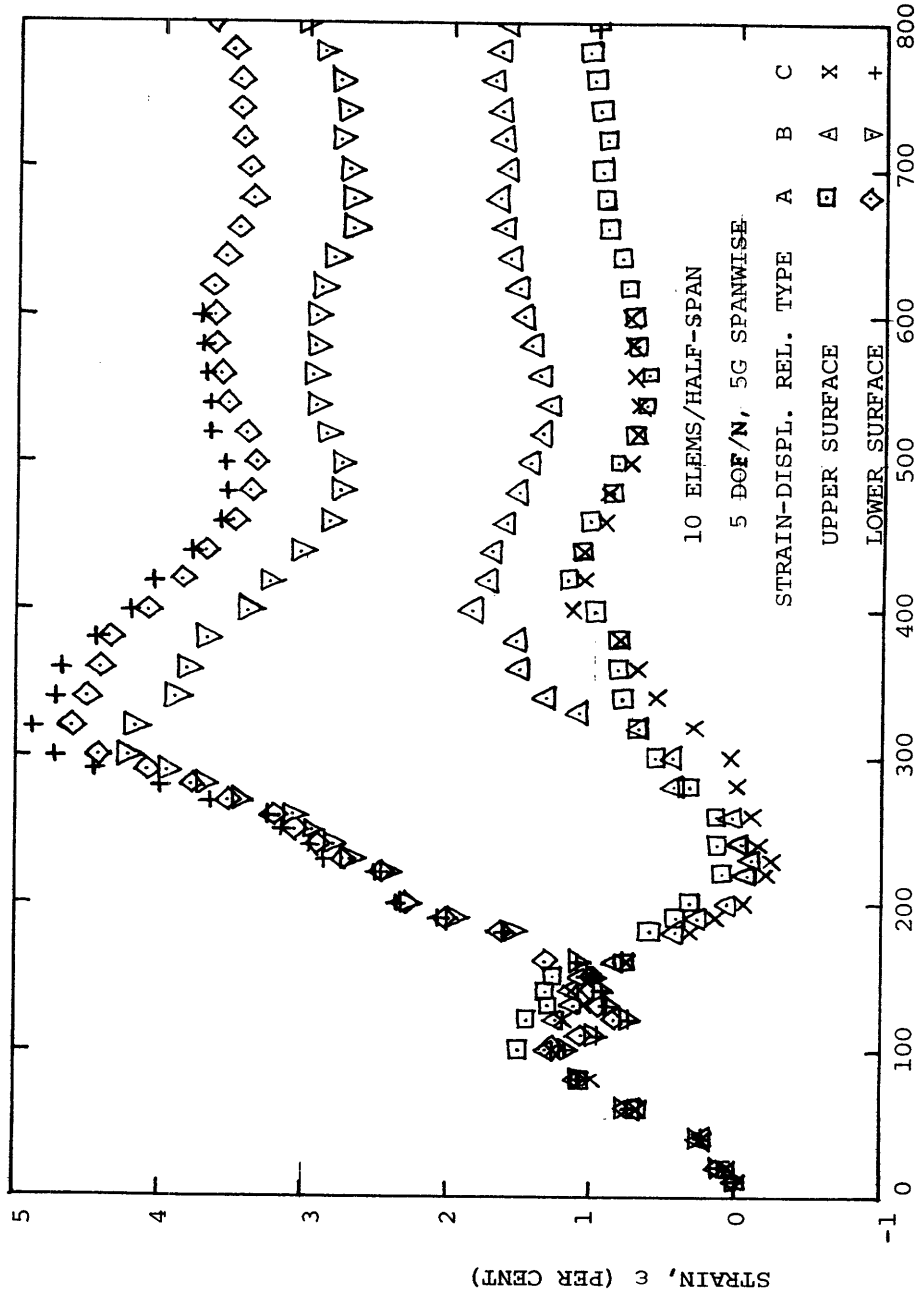

(e) Station x=3.80 in

FIG. 14 CONCLUDED (CB-1)

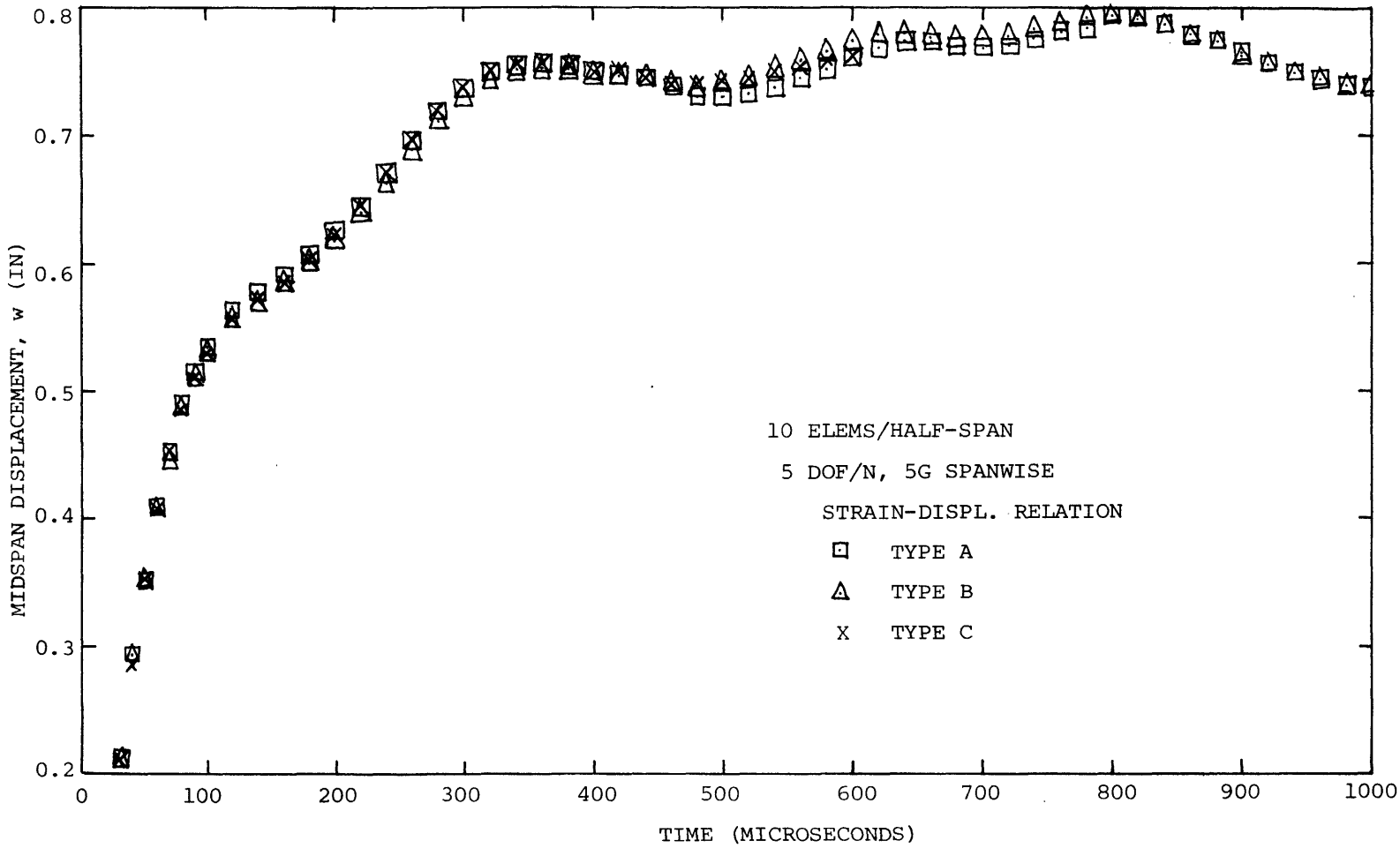

FIG. 15 INFLUENCE OF STRAIN-DISPLACEMENT RELATIONS ON PREDICTED TRANSIENT MIDSPAN DEFLECTION OF IMPULSIVELY-LOADED BEAM CB-1

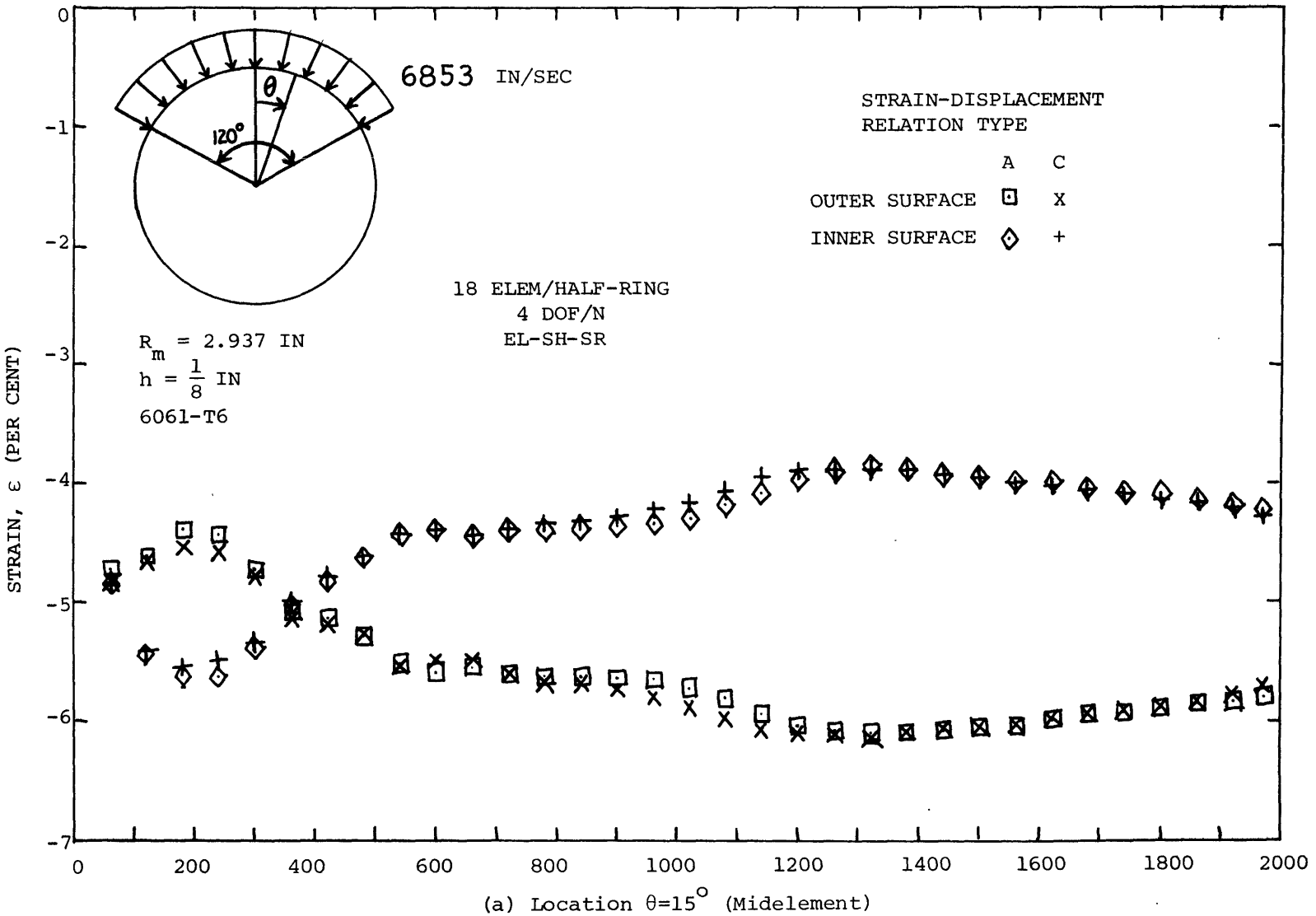

(a) Location $\theta=15^{\circ}$ (Midelement)

FIG. 16 INFLUENCE OF STRAIN-DISPLACEMENT RELATIONS ON PREDICTED TRANSIENT OUTER- AND INNER-SURFACE CIRCUMFERENTIAL STRAIN FOR THE IMPULSIVELY-LOADED FREE CIRCULAR RING

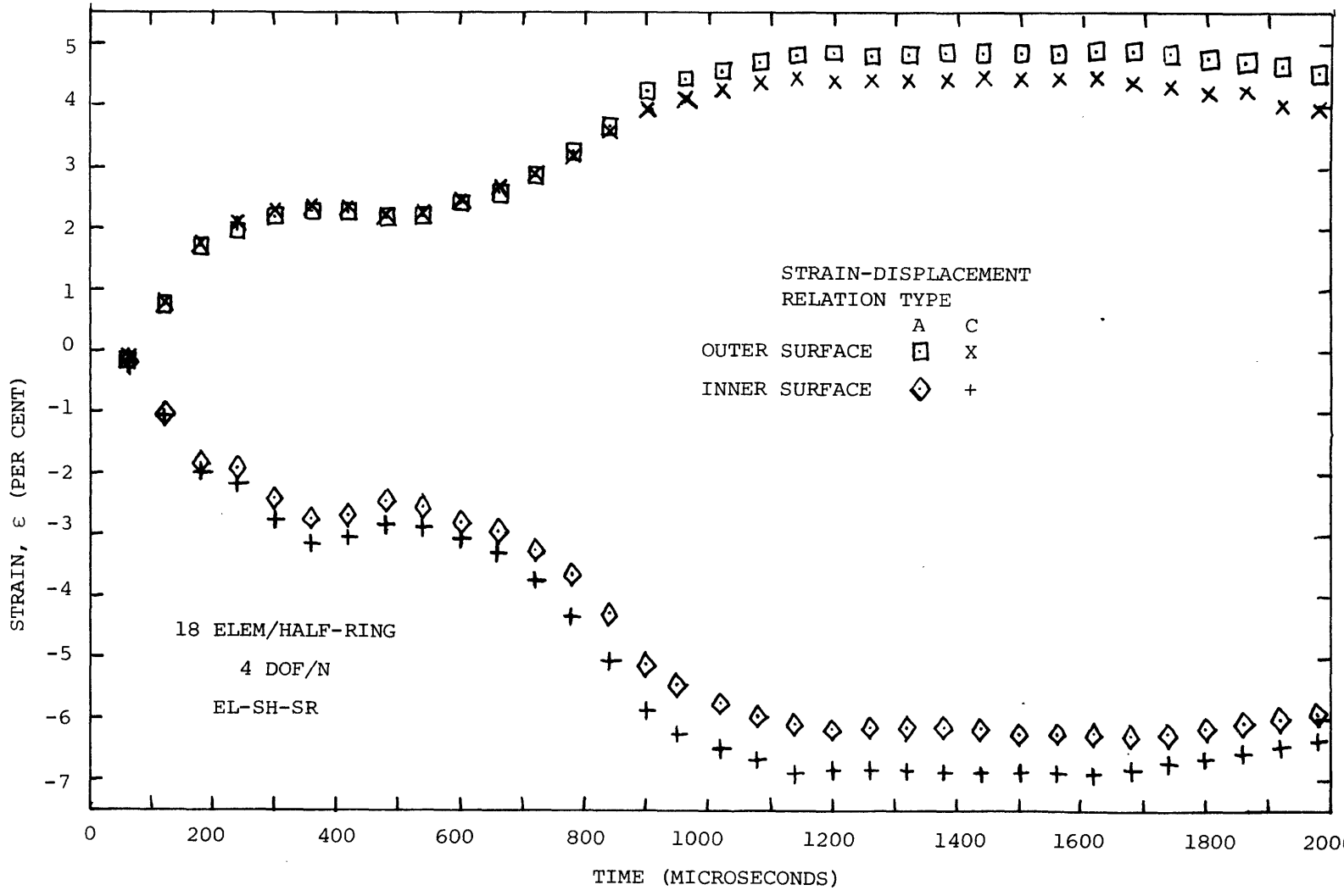

(b) Location $\theta=85^{o}$ (Midelement)

FIG. 16 CONTINUED (FREE RING)

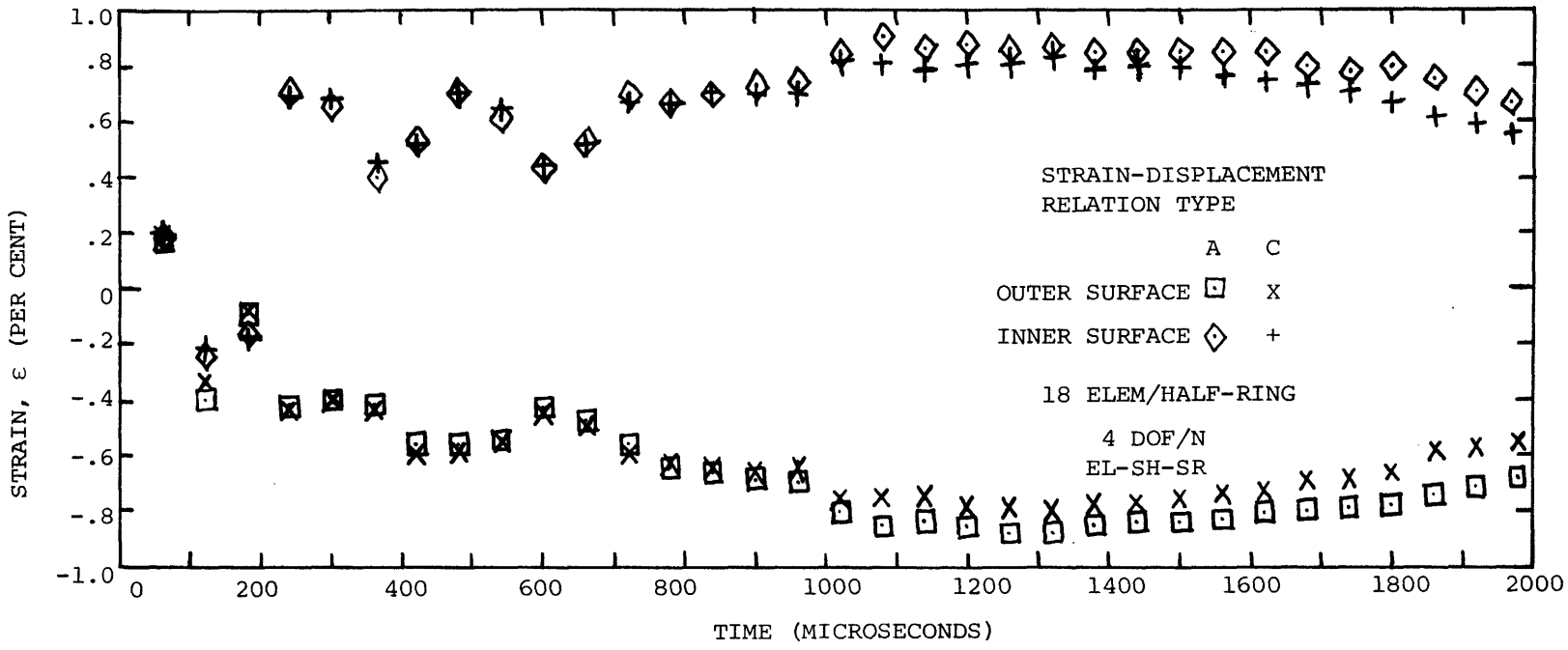

(c) Location $\theta=155^{o}$ (Midelement)

FIG. 16 CONTINUED (FREE RING)

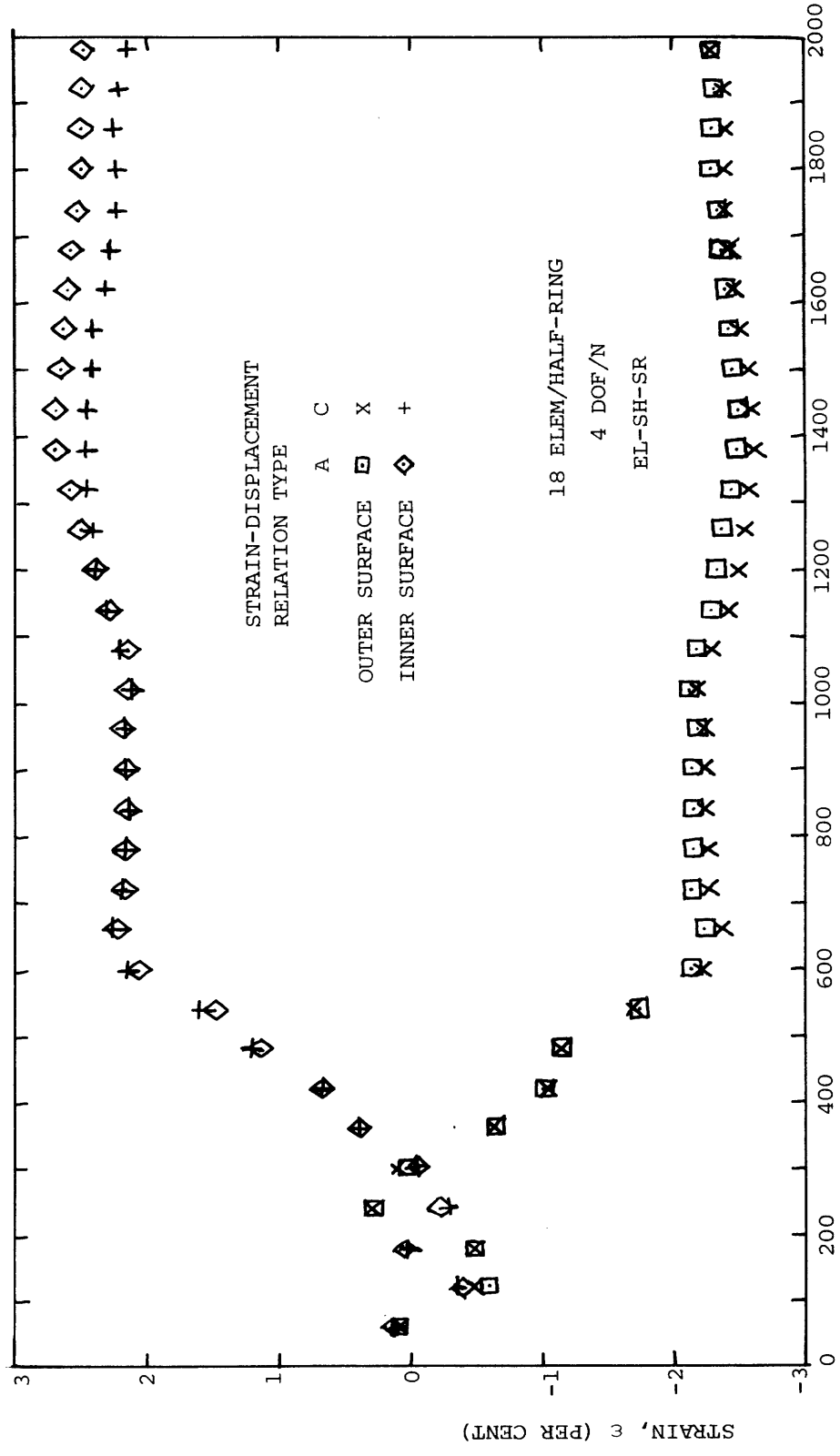

(d) Location $\theta=175^{\circ}$ (Midelement)

FIG. 16 CONCLUDED (FREE RING)

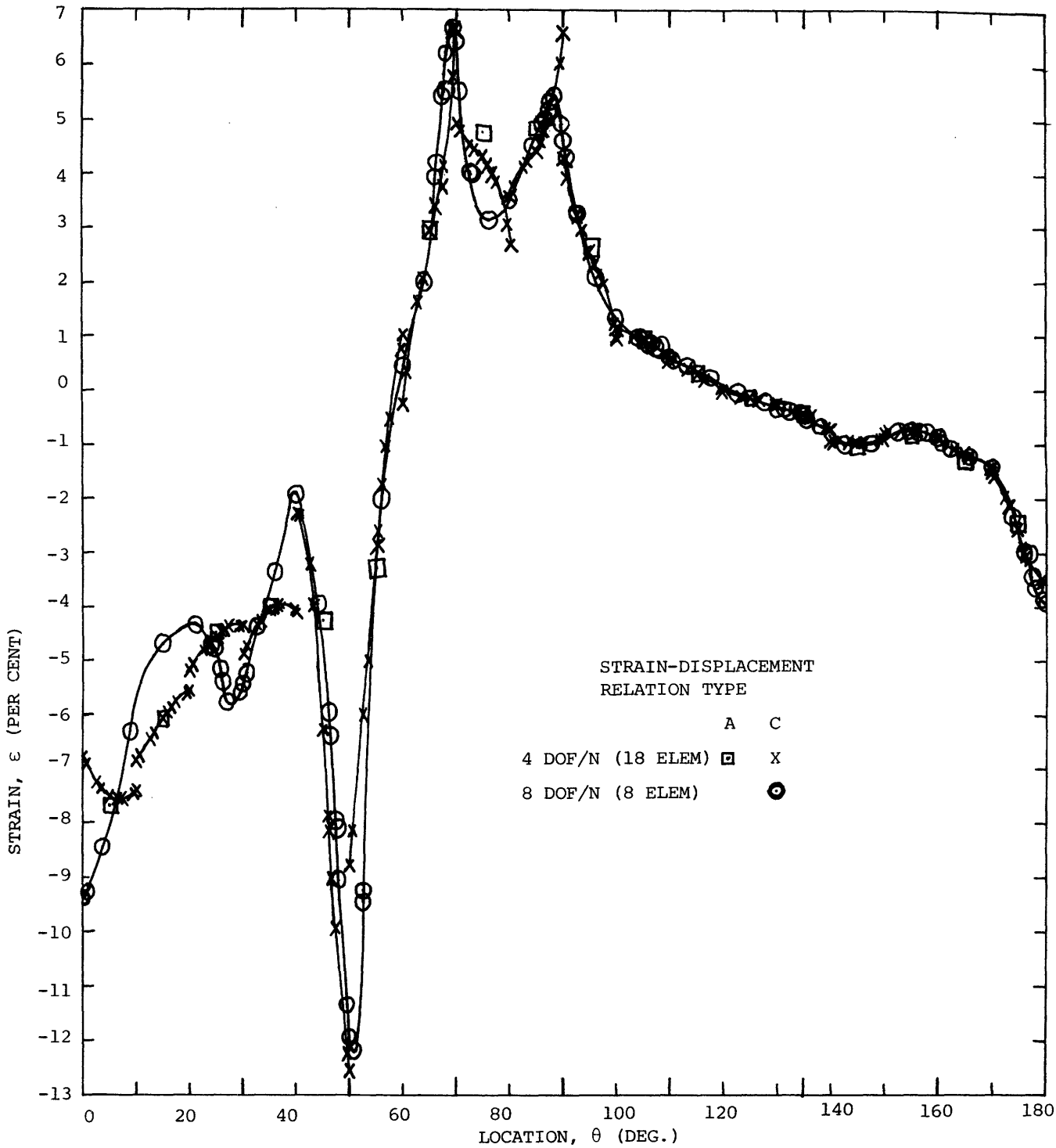

FIG. 17 INFLUENCE OF STRAIN-DISPLACEMENT RELATIONS AND FINITE-ELEMENT TYPE ON THE PREDICTED CIRCUMFERENTIAL DISTRIBUTION OF OUTER-SURFACE STRAIN AT 1500 MICROSECONDS FOR THE IMPULSIVELY-LOADED FREE CIRCULAR RING

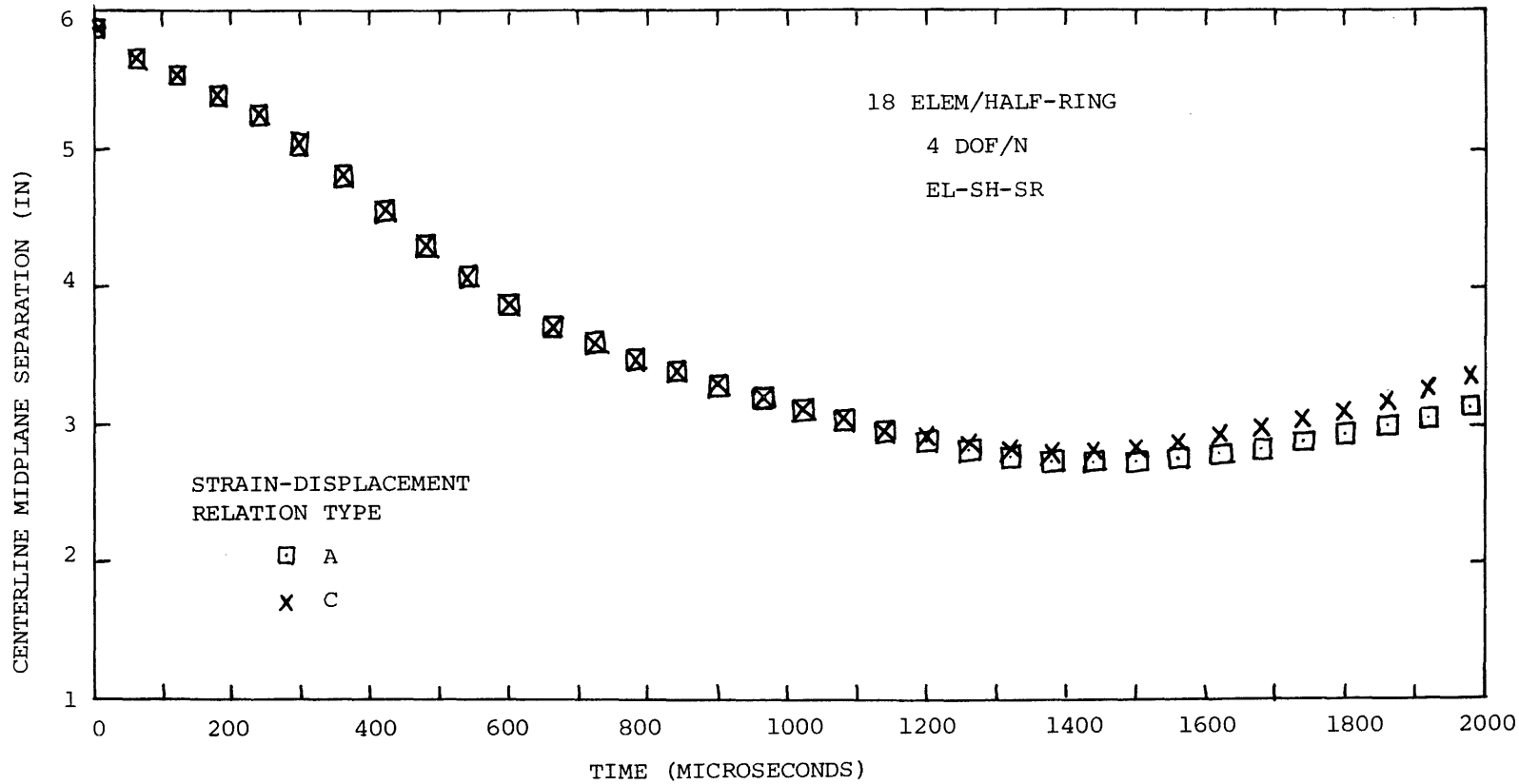

FIG. 18 INFLUENCE OF STRAIN-DISPLACEMENT RELATIONS ON THE PREDICTED TRANSIENT CENTERLINE MIDPLANE SEPARATION FOR THE IMPULSIVELY-LOADED FREE CIRCULAR RING

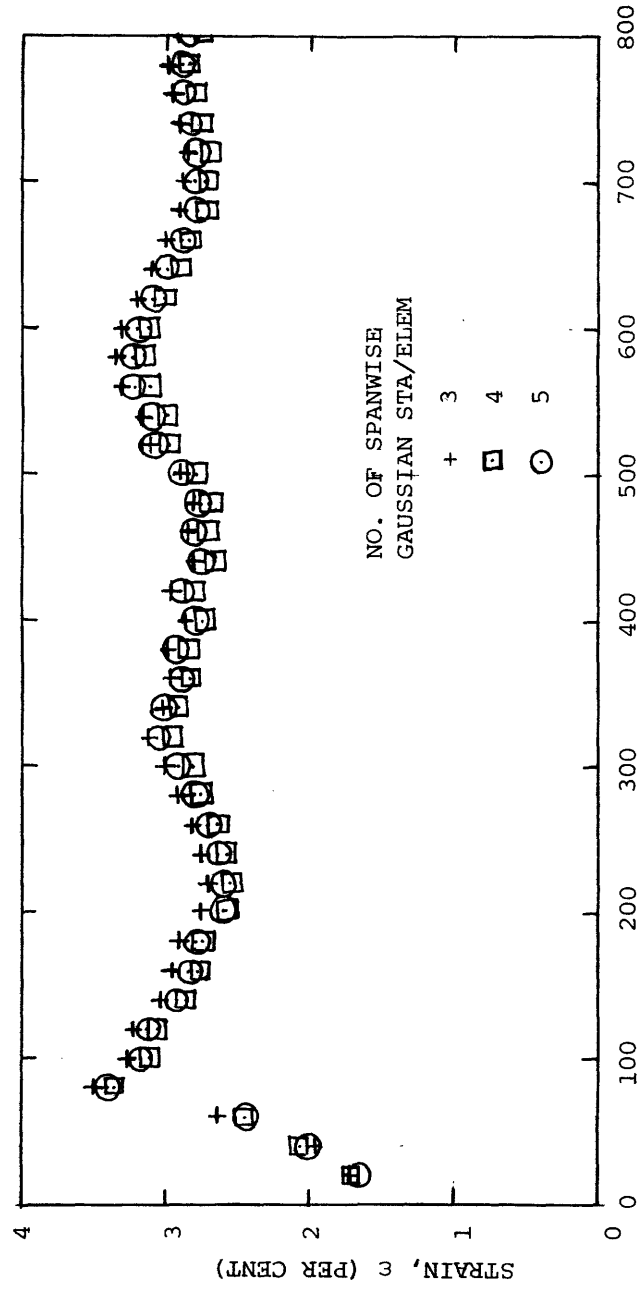

(a) Station x=0.4 in, Upper Surface Nodal-Average Strain

FIG. 19 INFLUENCE OF THE NUMBER OF SPANWISE GAUSSIAN STATIONS ON THE PREDICTED TRANSIENT RESPONSE OF IMPULSIVELY-LOADED BEAM CB-1 (4 DOF/N, 10 ELEM/HALF)

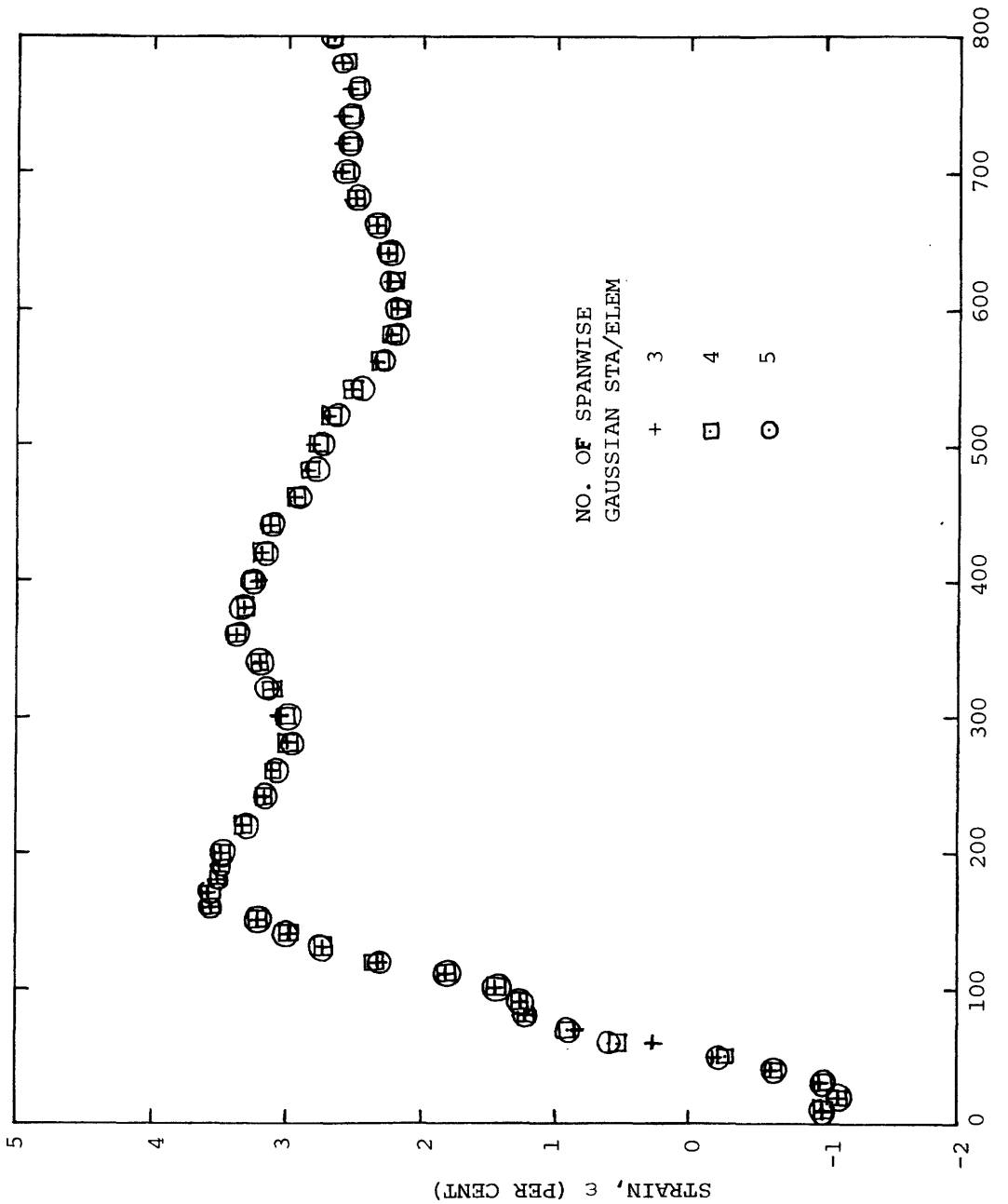

(b) Station x=1.40 in, Upper Surface Midelement Strain

FIG. 19 CONTINUED (CB-1, 4 DOF/N, 10 ELEM/HALF)

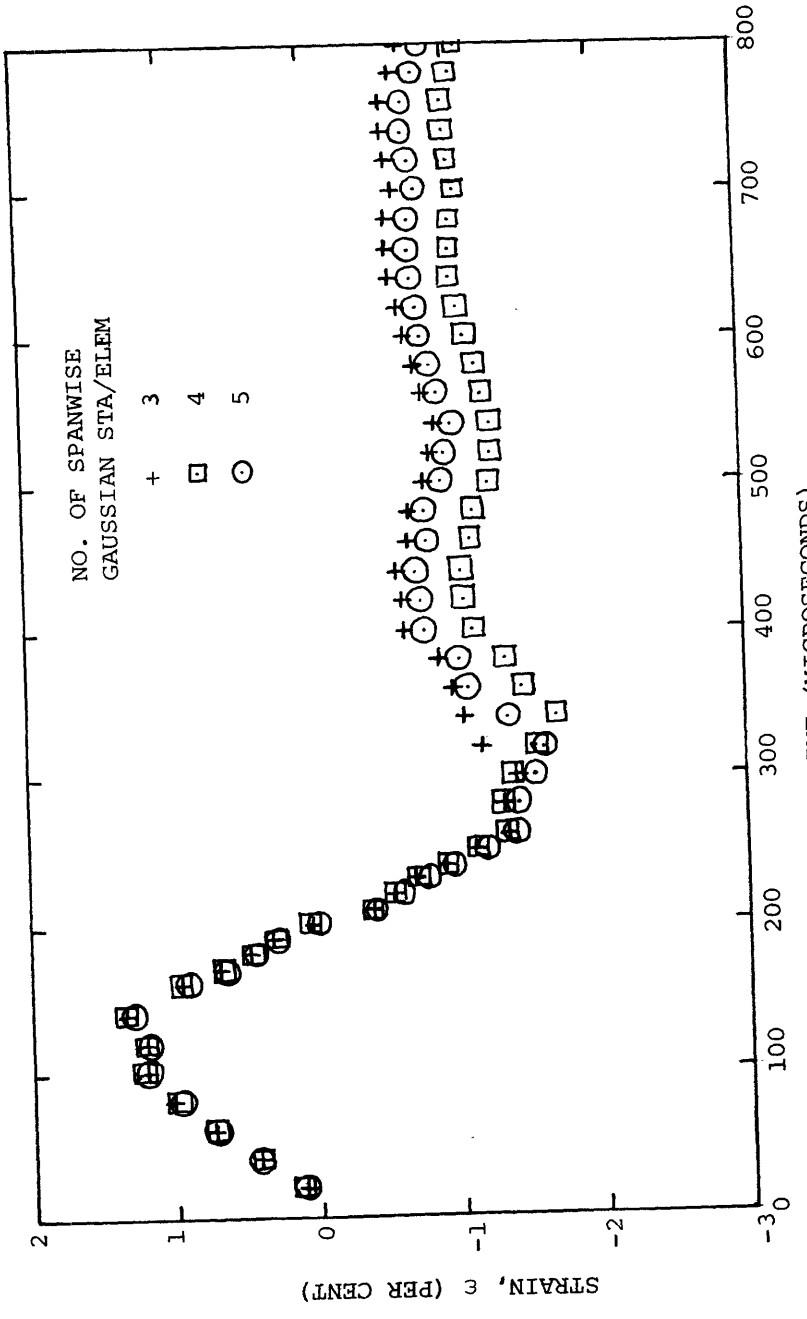

(c) Station x=3.80 in, Upper Surface Midelement Strain

FIG. 19 CONTINUED (CB-1, 4 DOF/N, 10 ELEM/HALF)

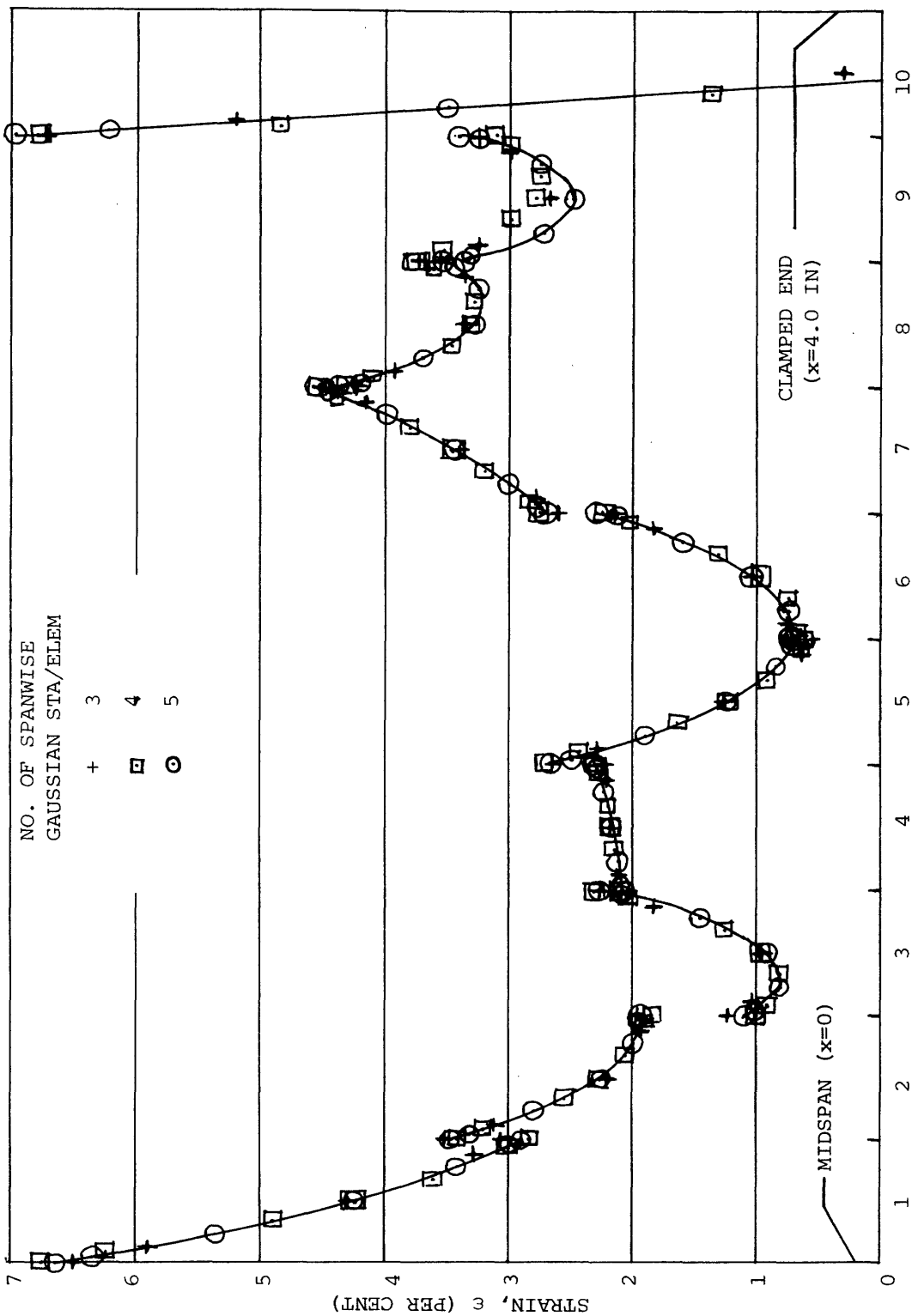

(d) Spanwise Distribution of Upper-Surface Strain at t=600 Microseconds

FIG. 19 CONTINUED (CB-1, 4 DOF/N, 10 ELEM/HALF)

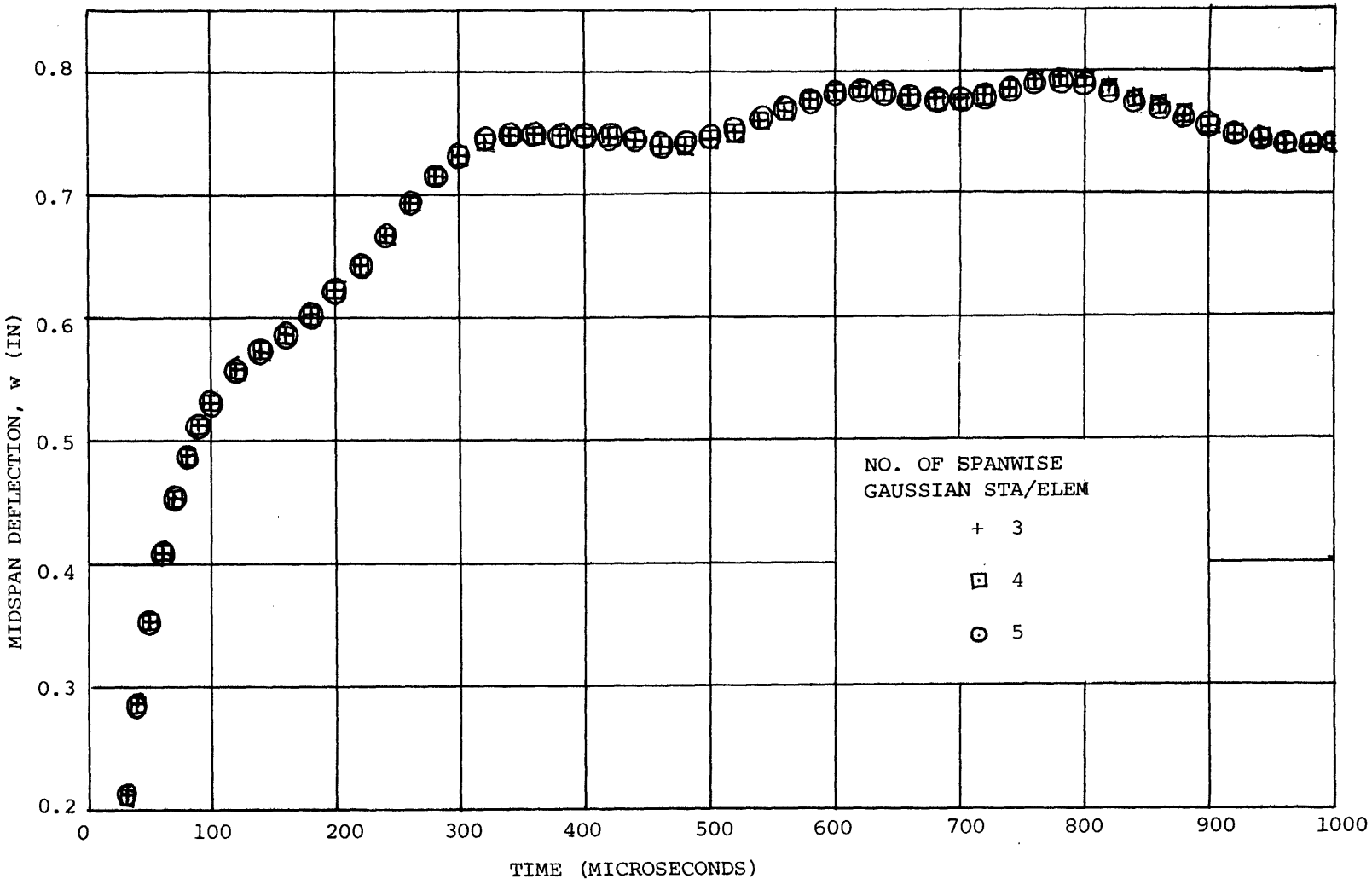

(e) Midspan Deflection

FIG. 19 CONCLUDED (CB-1, 4 DOF/N, 10 ELEM/HALF)

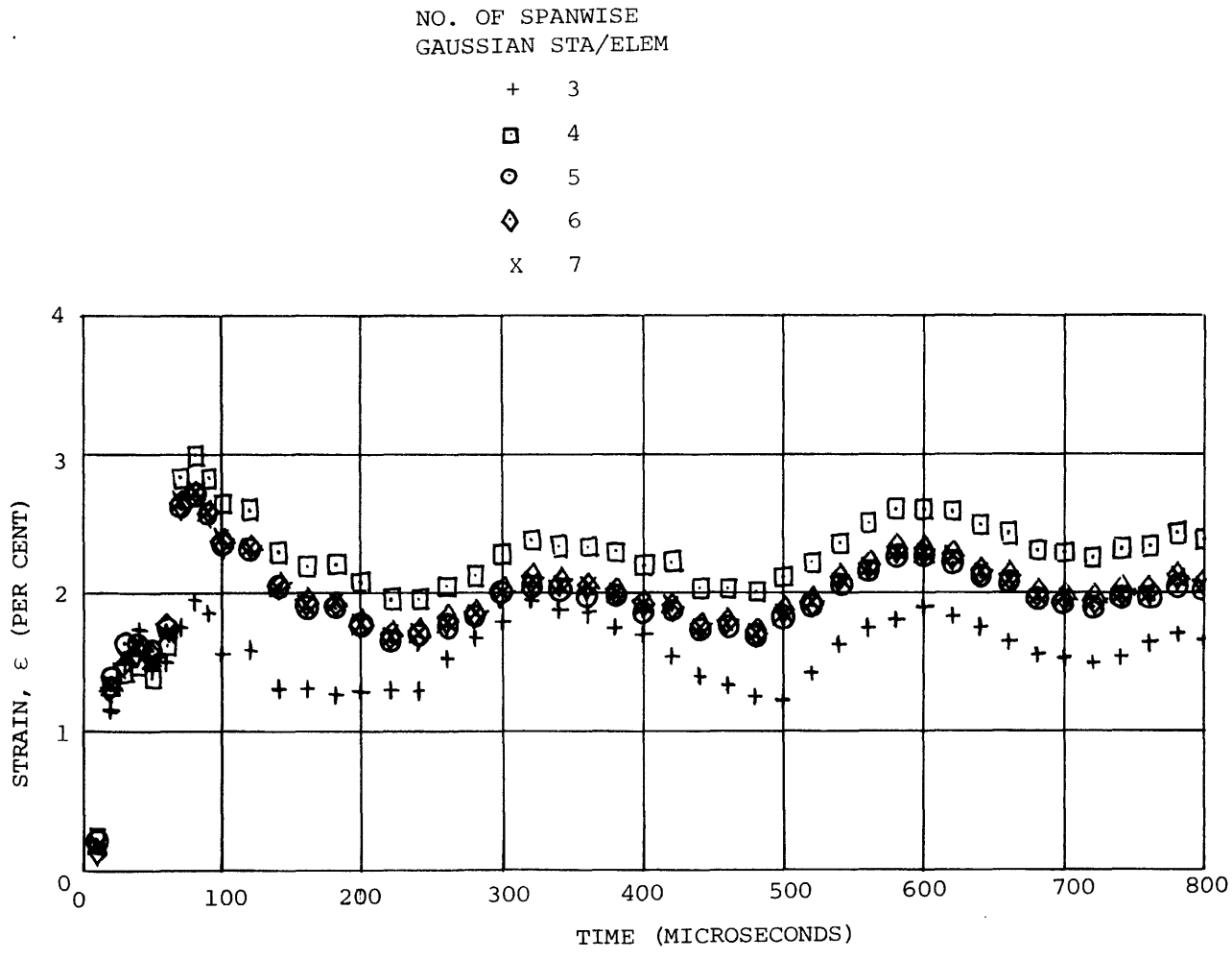

(a) Station x=0.4 in, Upper Surface Nodal Strain

FIG. 20 INFLUENCE OF THE NUMBER OF SPANWISE GAUSSIAN STATIONS ON THE PREDICTED TRANSIENT RESPONSE OF IMPULSIVELY-LOADED BEAM CB-1 (5 DOF/N, 10 ELEM/HALF)

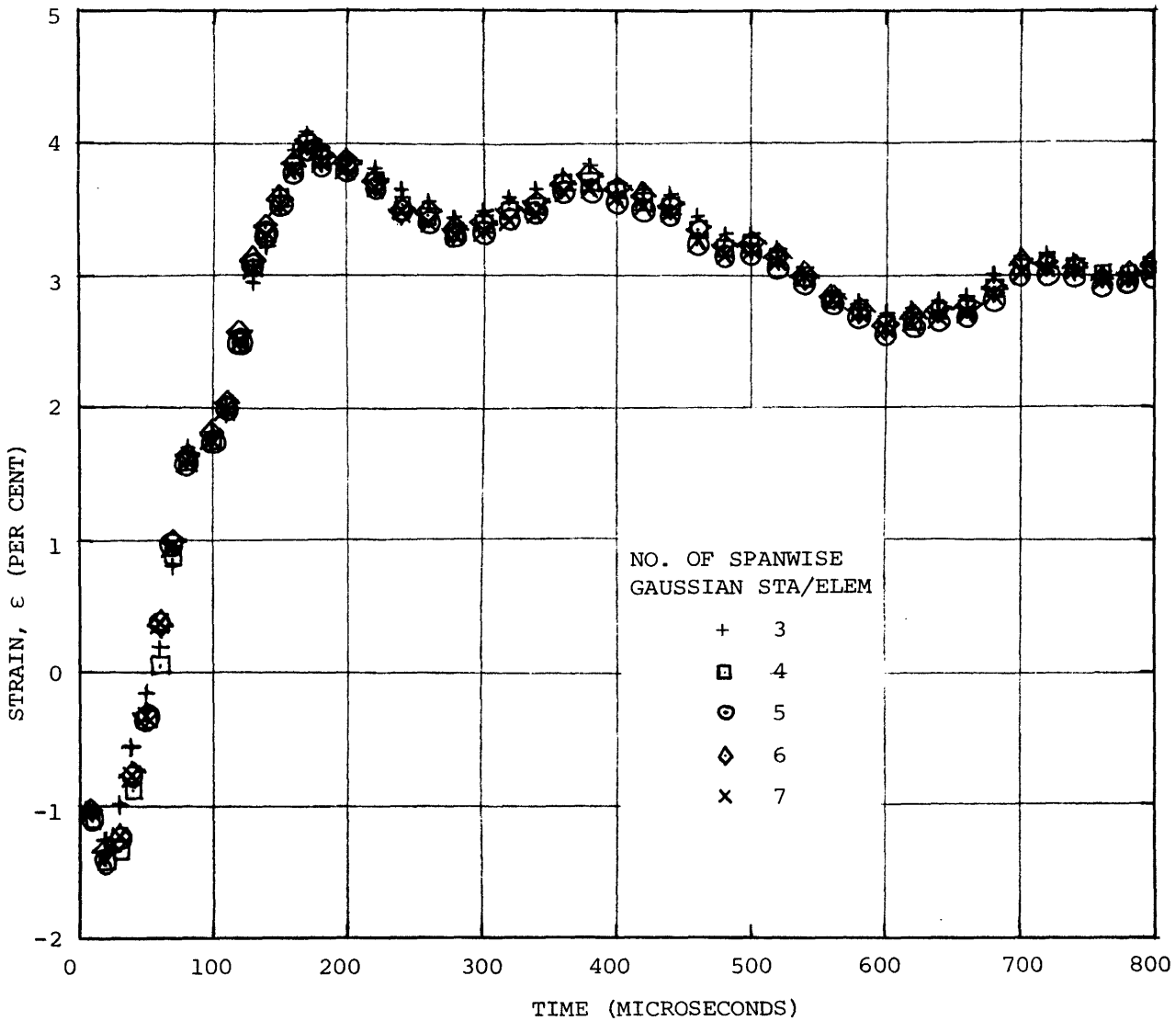

(b) Station x=1.40 in, Upper Surface Midelement Strain

FIG. 20 CONTINUED (CB-1, 5 DOF/N, 10 ELEM/HALF)

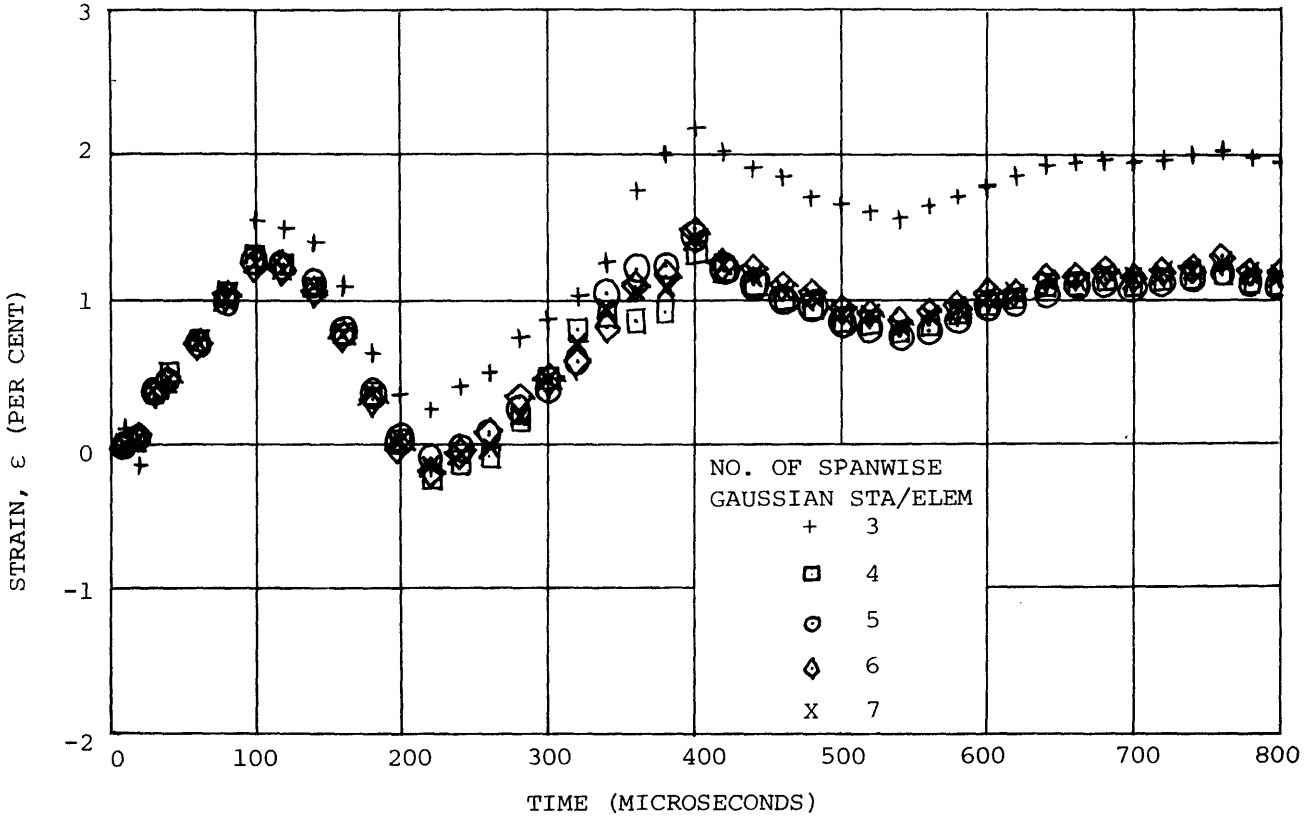

(c) Station x=3.80 in, Upper Surface Midelement Strain

FIG. 20 CONTINUED (CB-1, 5 DOF/N, 10 ELEM/HALF)

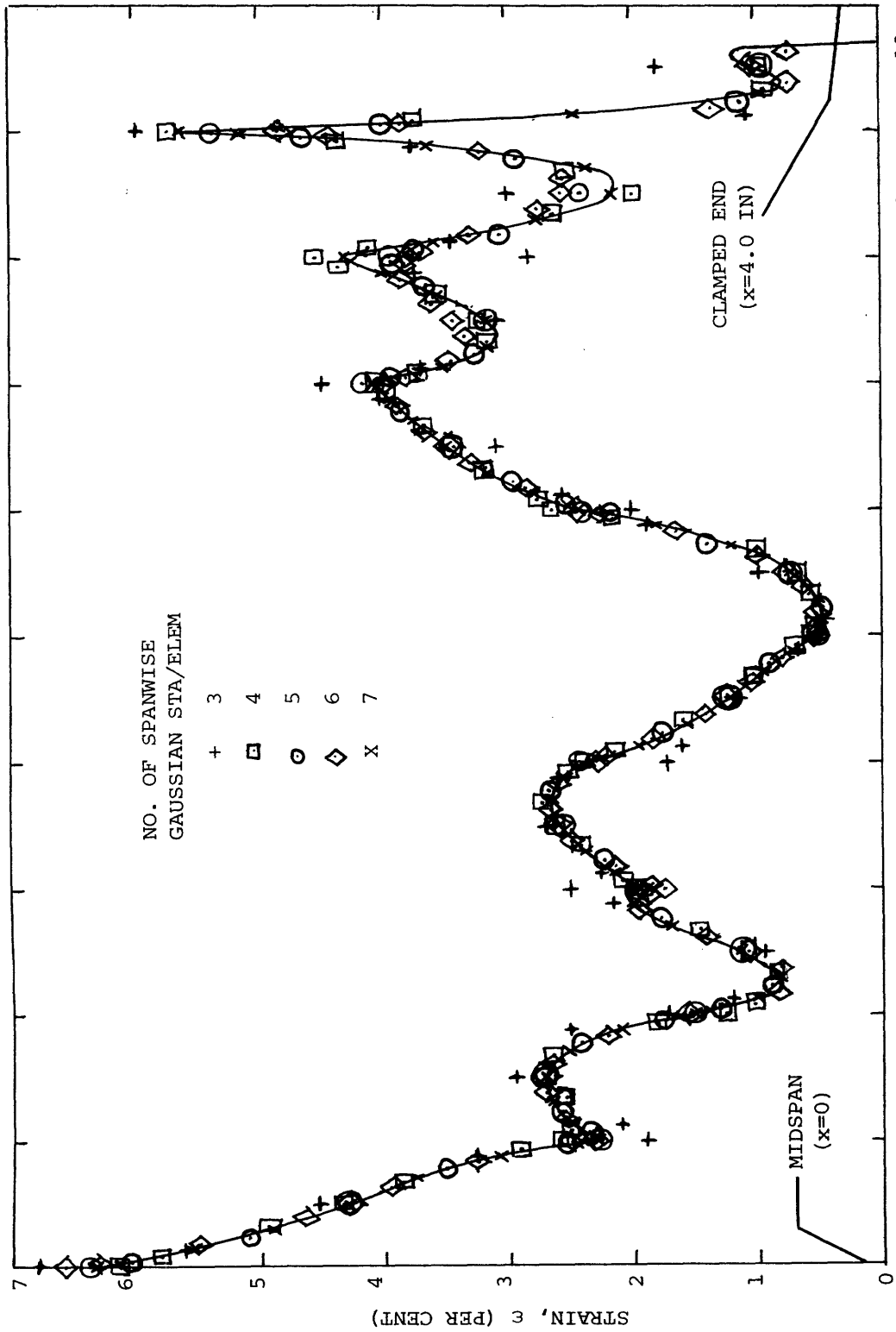

(d) Spanwise Distribution of Upper Surface Strain at t=600 Microseconds

FIG. 20 CONTINUED (CB-1, 5 DOF/N, 10 ELEM/HALF)

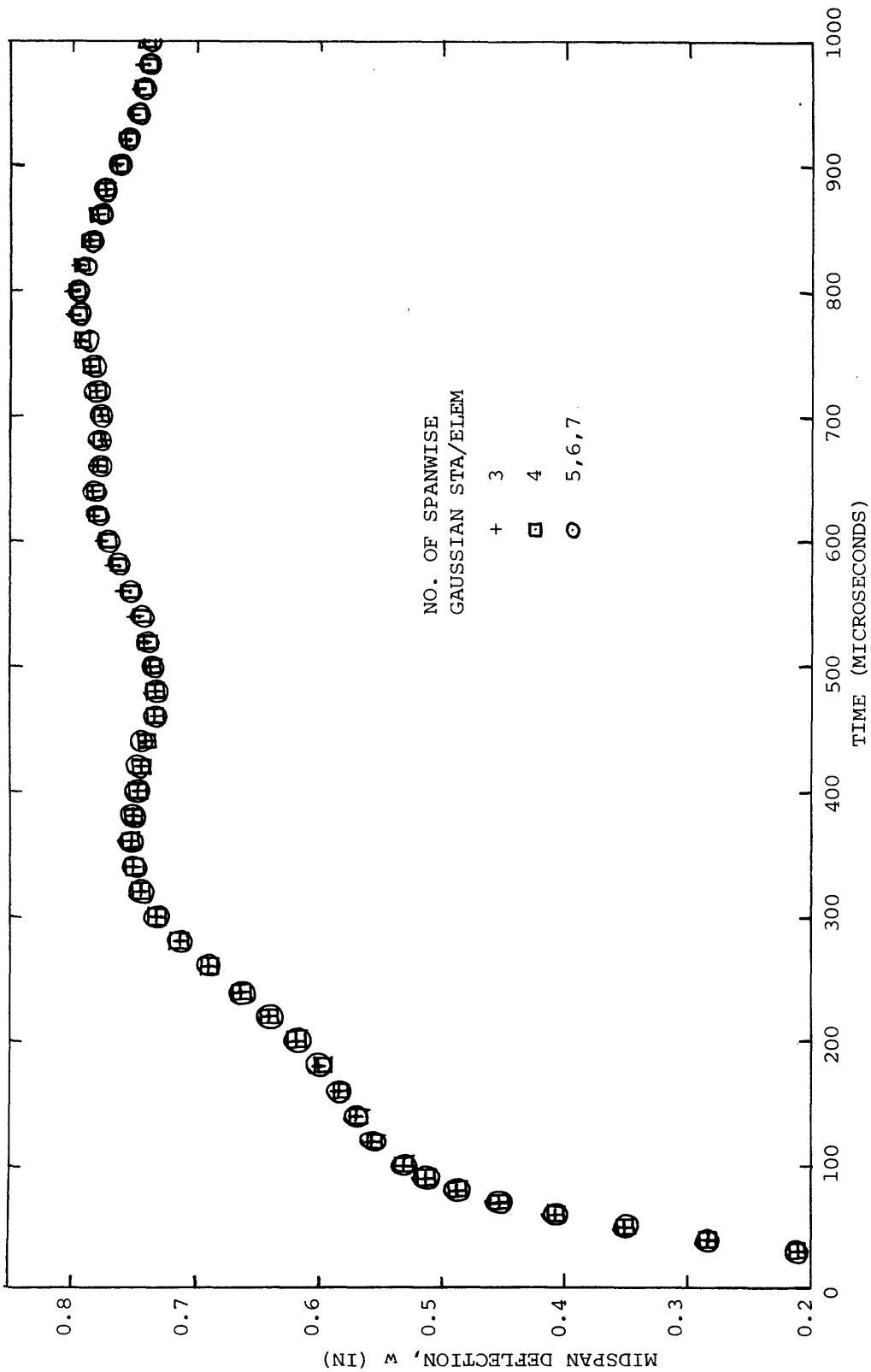

(e) Midspan Deflection

FIG. 20 CONCLUDED (CB-1, 5 DOF/N, 10 ELEM/HALF)

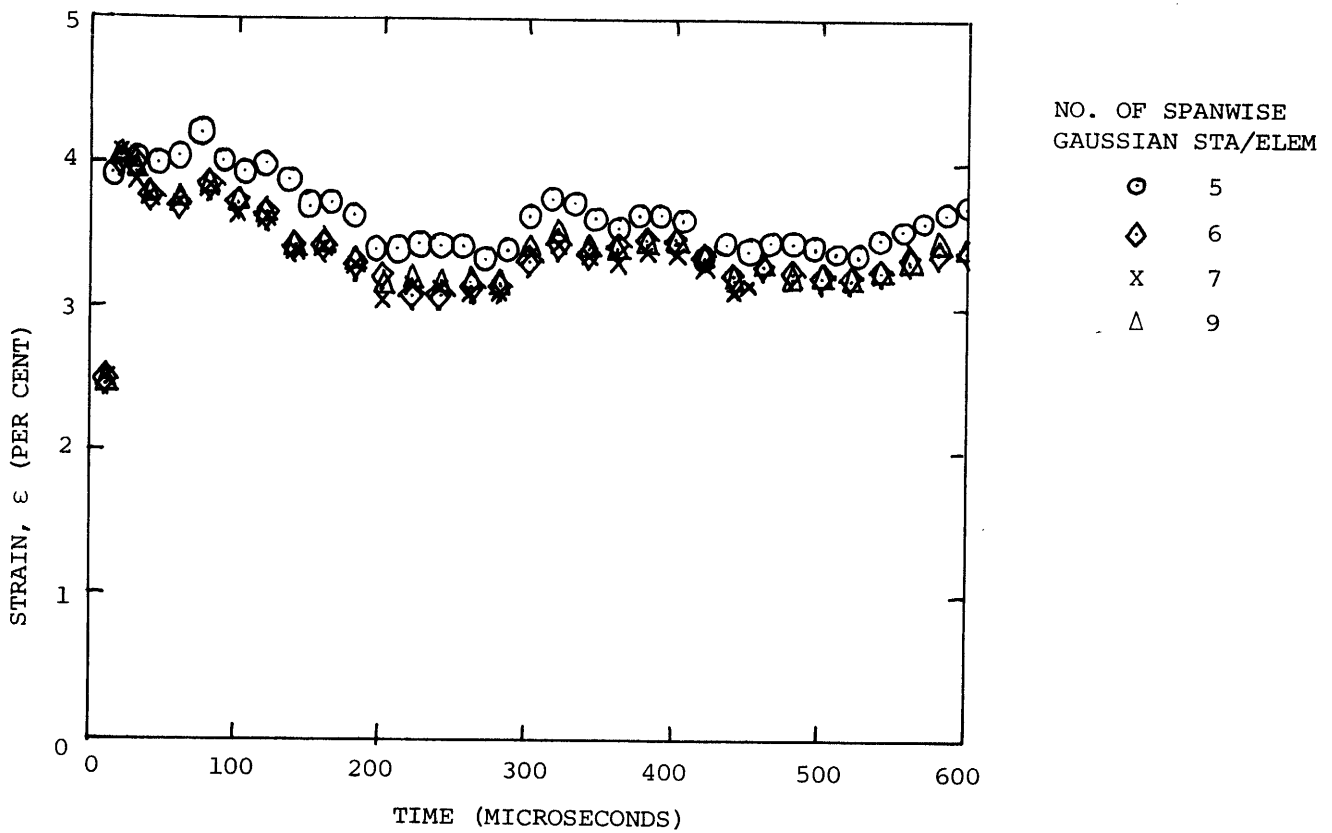

(a) Station x=0.6 in, Upper Surface Nodal Strain

FIG. 21 INFLUENCE OF THE NUMBER OF SPANWISE GAUSSIAN STATIONS ON THE PREDICTED TRANSIENT RESPONSE OF IMPULSIVELY-LOADED BEAM CB-1 (8 DOF/N, 4 ELEM/HALF)

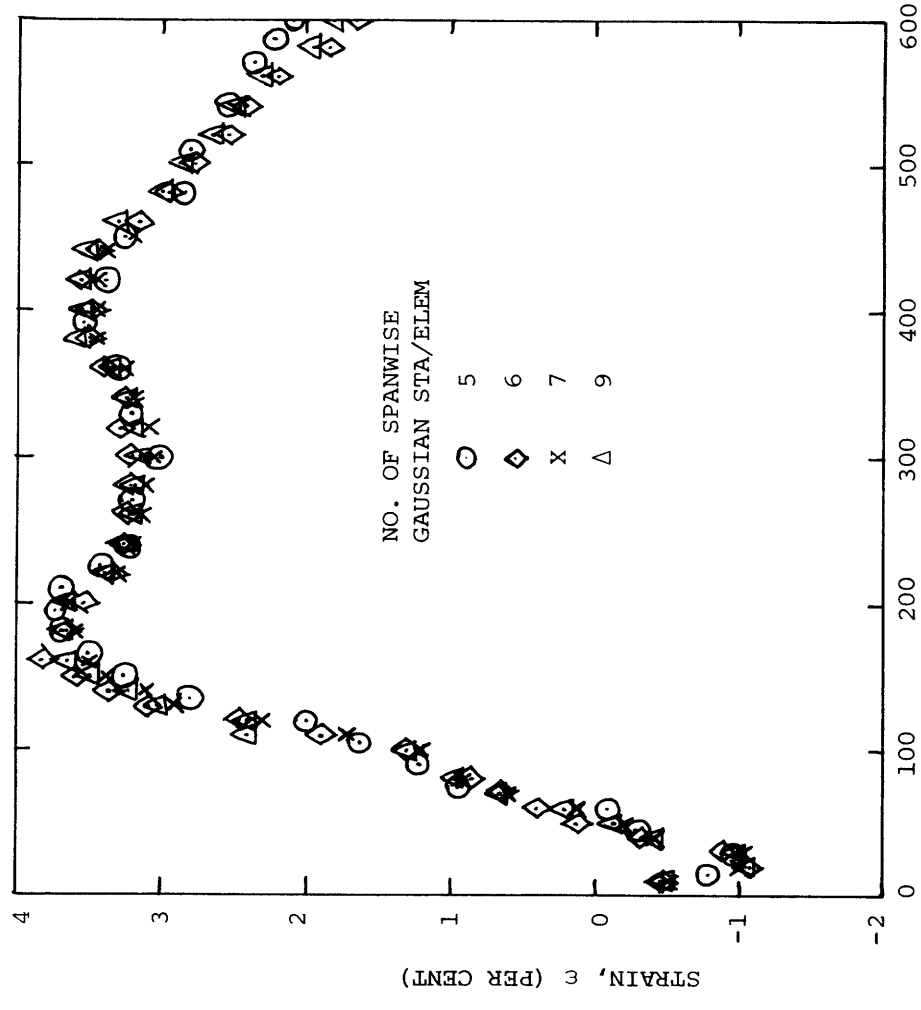

(b) Station x=1.40 in, Upper Surface Strain

FIG. 21 CONTINUED (CB-1, 8 DOF/N, 4 ELEM/HALF)

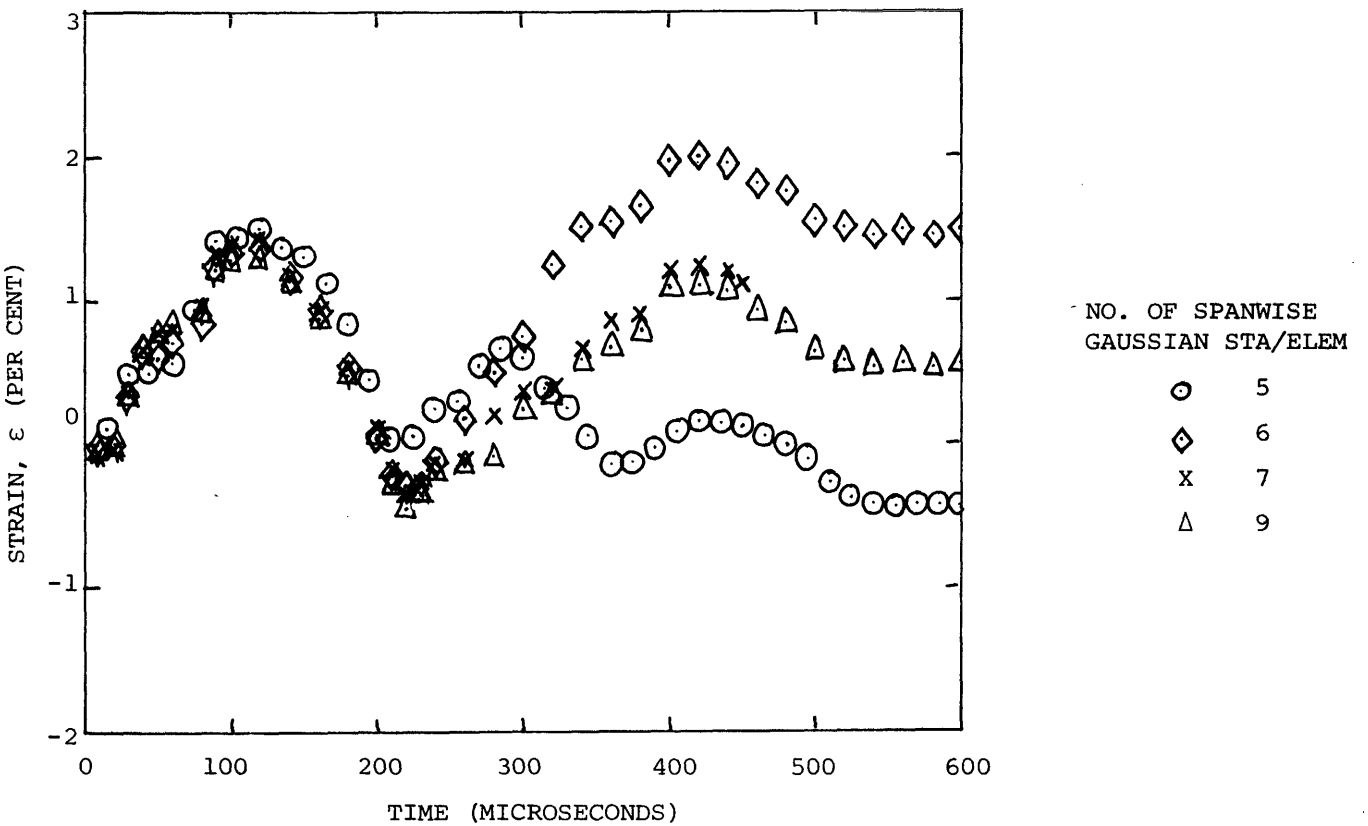

(c) Station x=3.80 in, Upper Surface Strain

FIG. 21 CONTINUED (CB-1, 8 DOF/N, 4 ELEM/HALF)

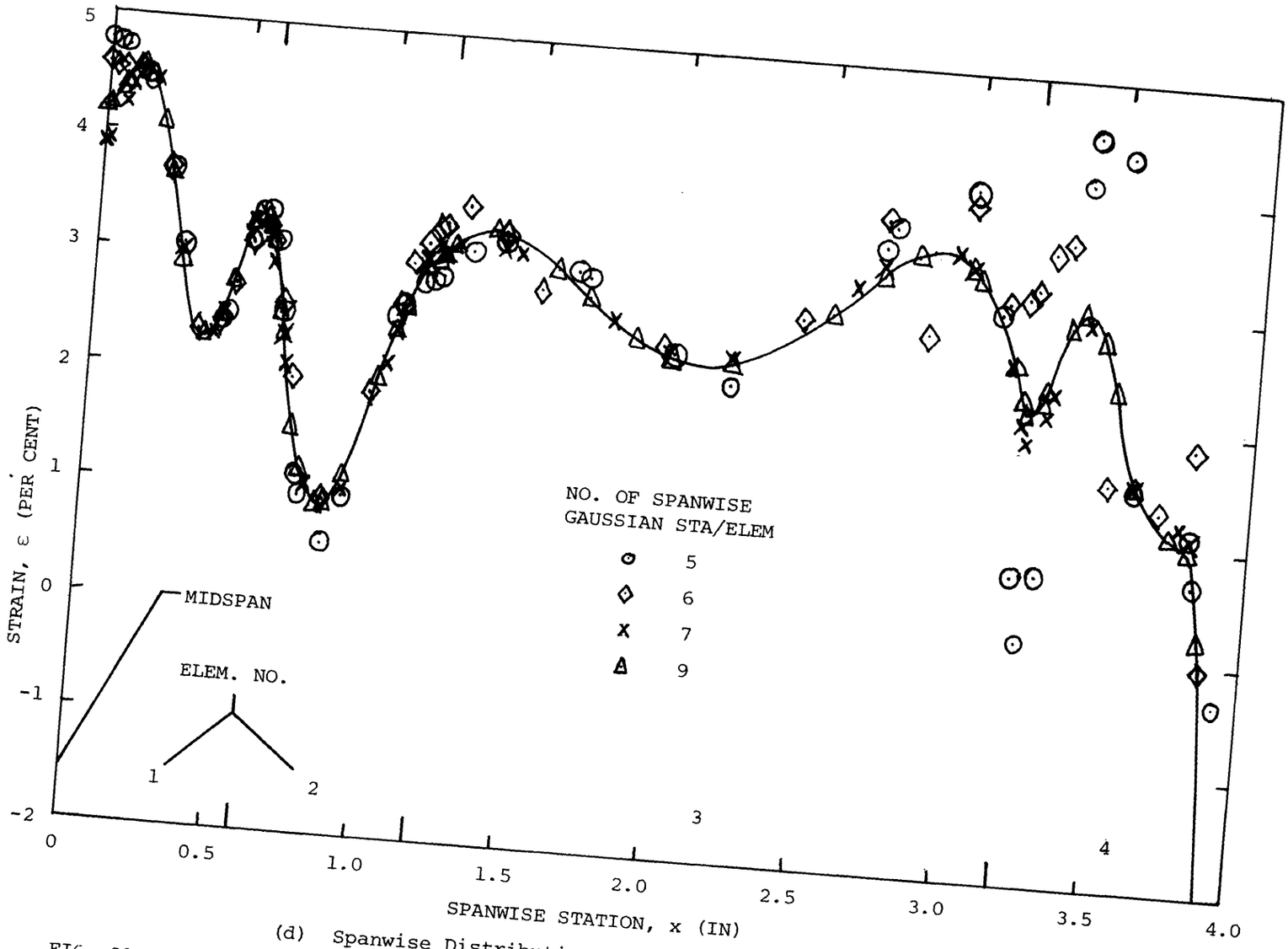

(d) Spanwise Distribution of Upper Surface Strain at t=450 Microseconds

FIG. 21 CONTINUED (CB-1, 8 DOF/IN, 4 ELEM/HALF)

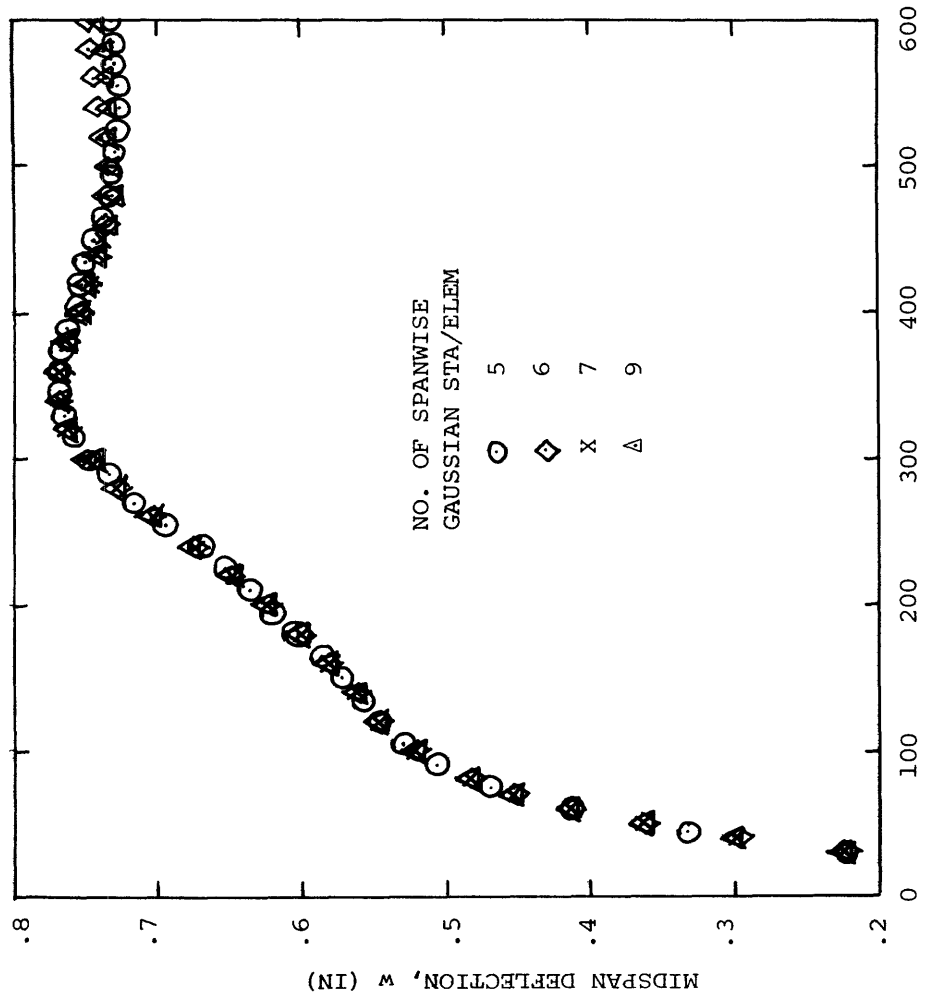

(e) Midspan Deflection

FIG. 21 CONCLUDED (CB-1, 8 DOF/N, 4 ELEM/HALF)

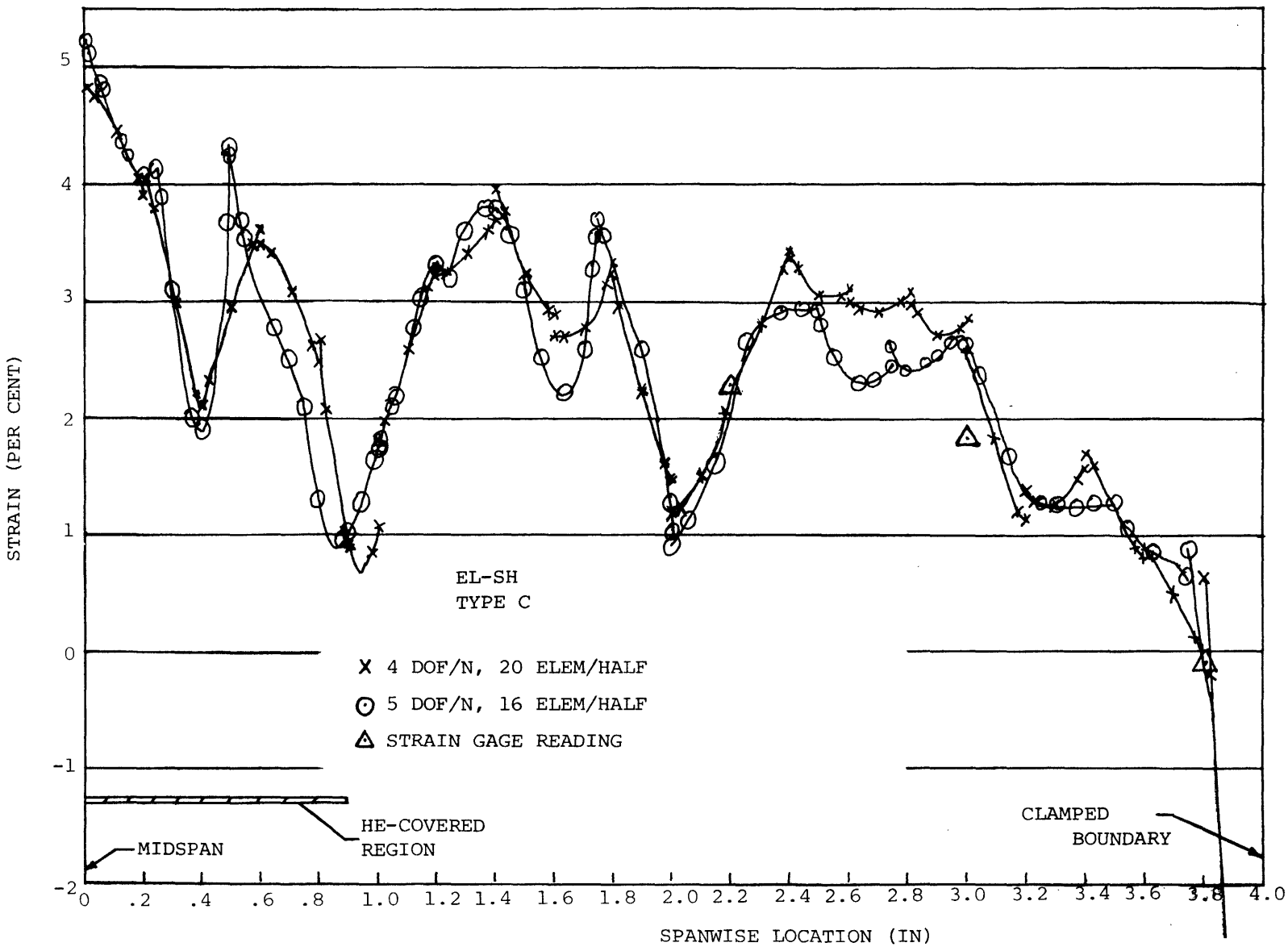

FIG. 22 STRAIN DISTRIBUTION ON NON-LOADED SURFACE OF BEAM CB-1 AT 300 MICROSECONDS FOR 4 DOF/N ELEMENT VS. 5 DOF/N ELEMENT PREDICTIONS

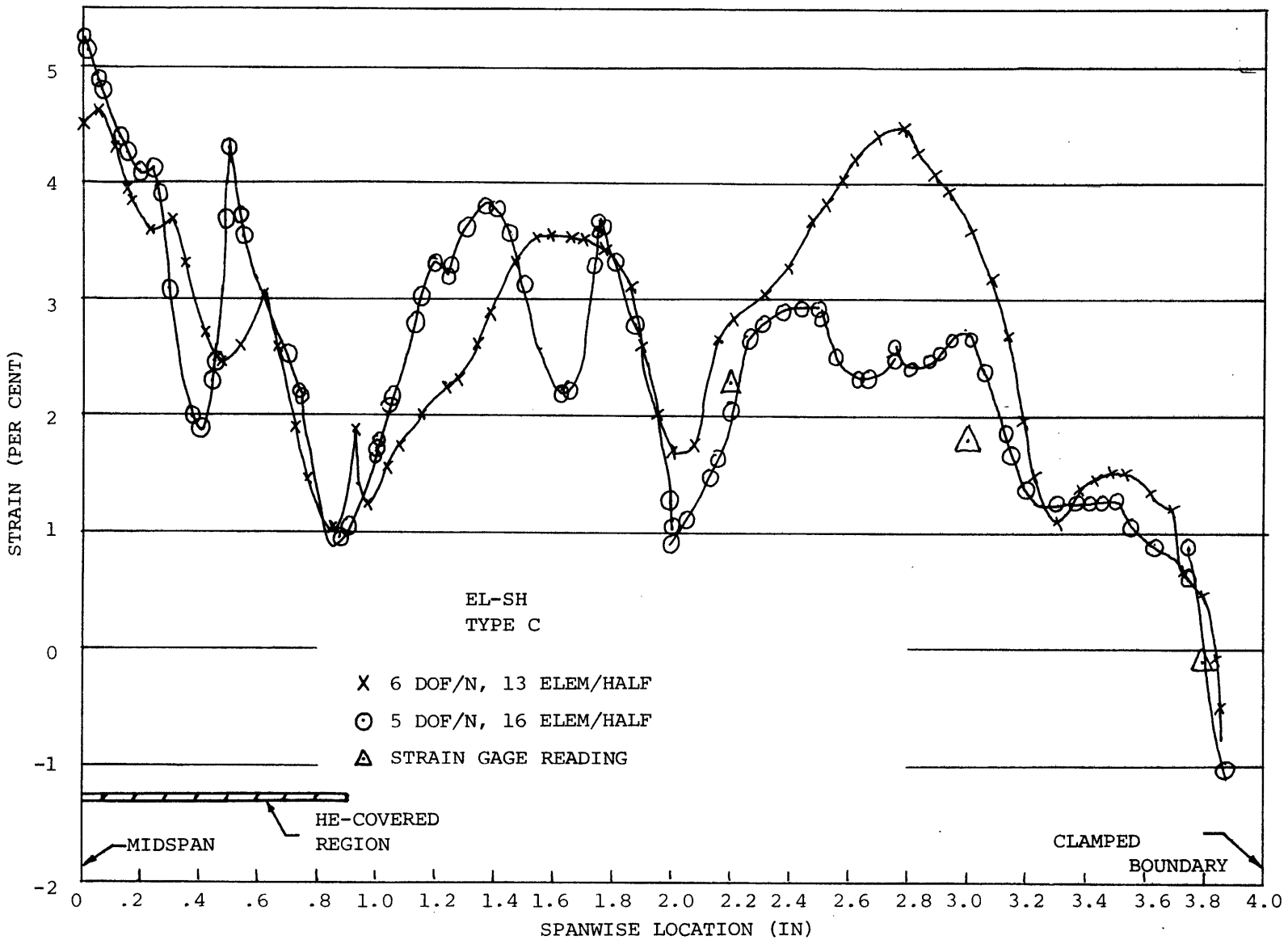

FIG. 23 STRAIN DISTRIBUTION ON NON-LOADED SURFACE OF BEAM CB-1 AT 300 MICROSECONDS FOR 5 DOF/N ELEMENT VS. 6 DOF/N ELEMENT PREDICTIONS

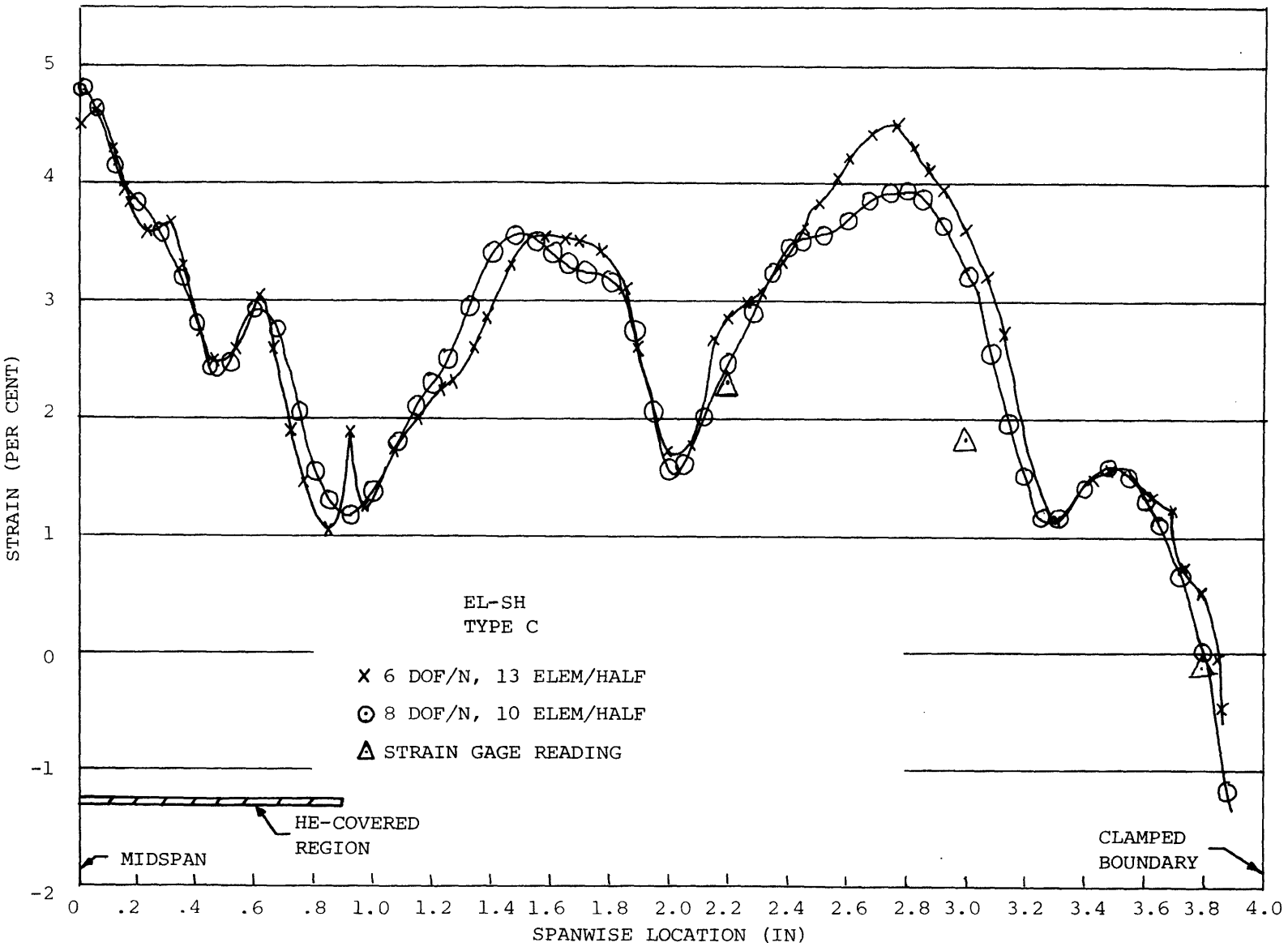

FIG. 24 STRAIN DISTRIBUTION ON NON-LOADED SURFACE OF BEAM CB-1 AT 300 MICROSECONDS FOR 6 DOF/N ELEMENT VS. 8 DOF/N ELEMENT PREDICTIONS

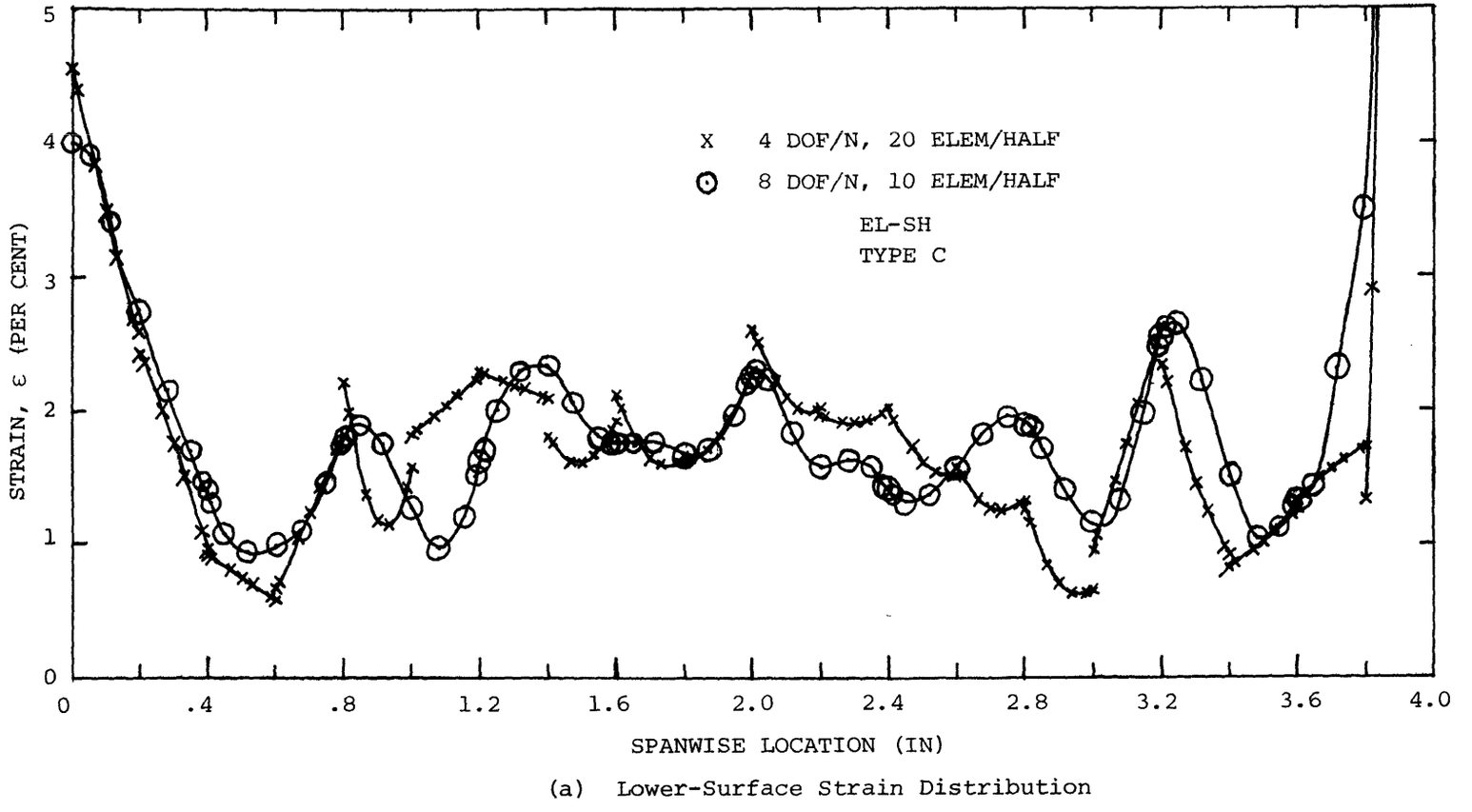

(a) Lower-Surface Strain Distribution

FIG. 25 SPANWISE DISTRIBUTION OF STRAIN ON LOWER AND UPPER SURFACES AT 300 MICROSECONDS FOR 4 DOF/N ELEMENT AND 8 DOF/N ELEMENT PREDICTIONS

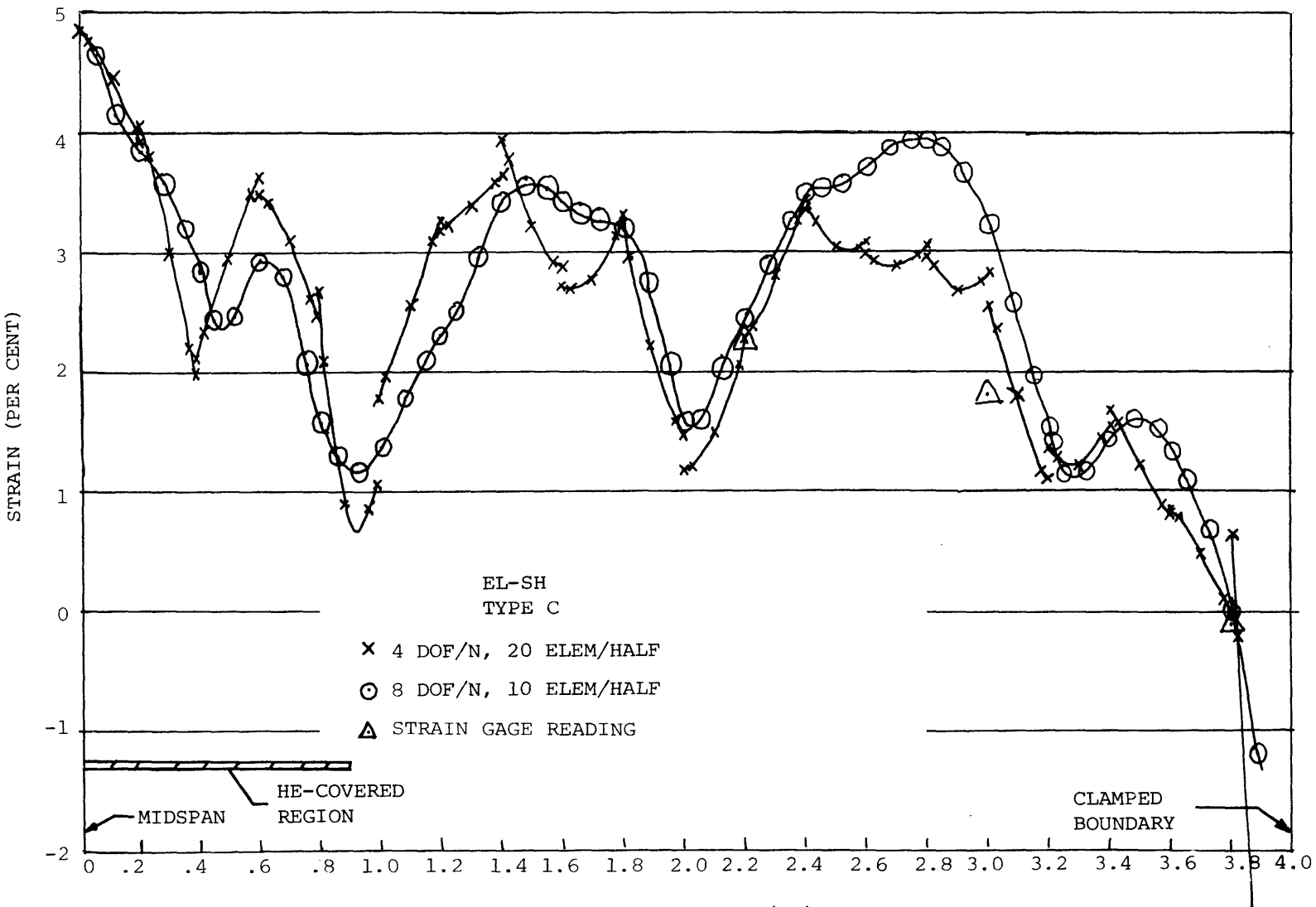

(b) Upper-Surface Strain Distribution

FIG. 25 CONTINUED (CB-1, 4 DOF/N VS. 8 DOF/N)

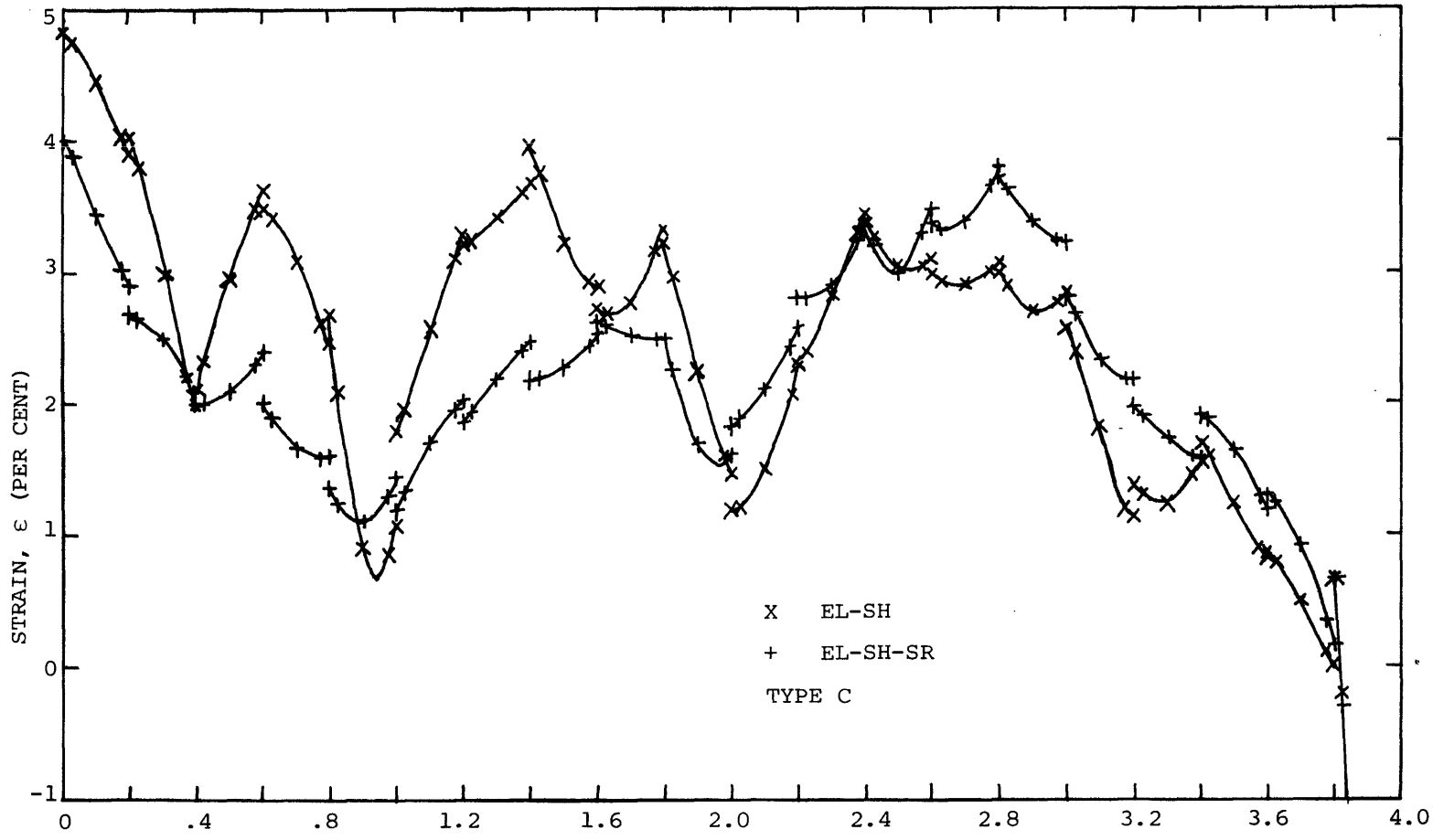

(c) Upper-Surface Strain Distribution, EL-SH vs. EL-SH-SR

FIG. 25 CONTINUED (CB-1, 4 DOF/N, 20 ELEM/HALF)

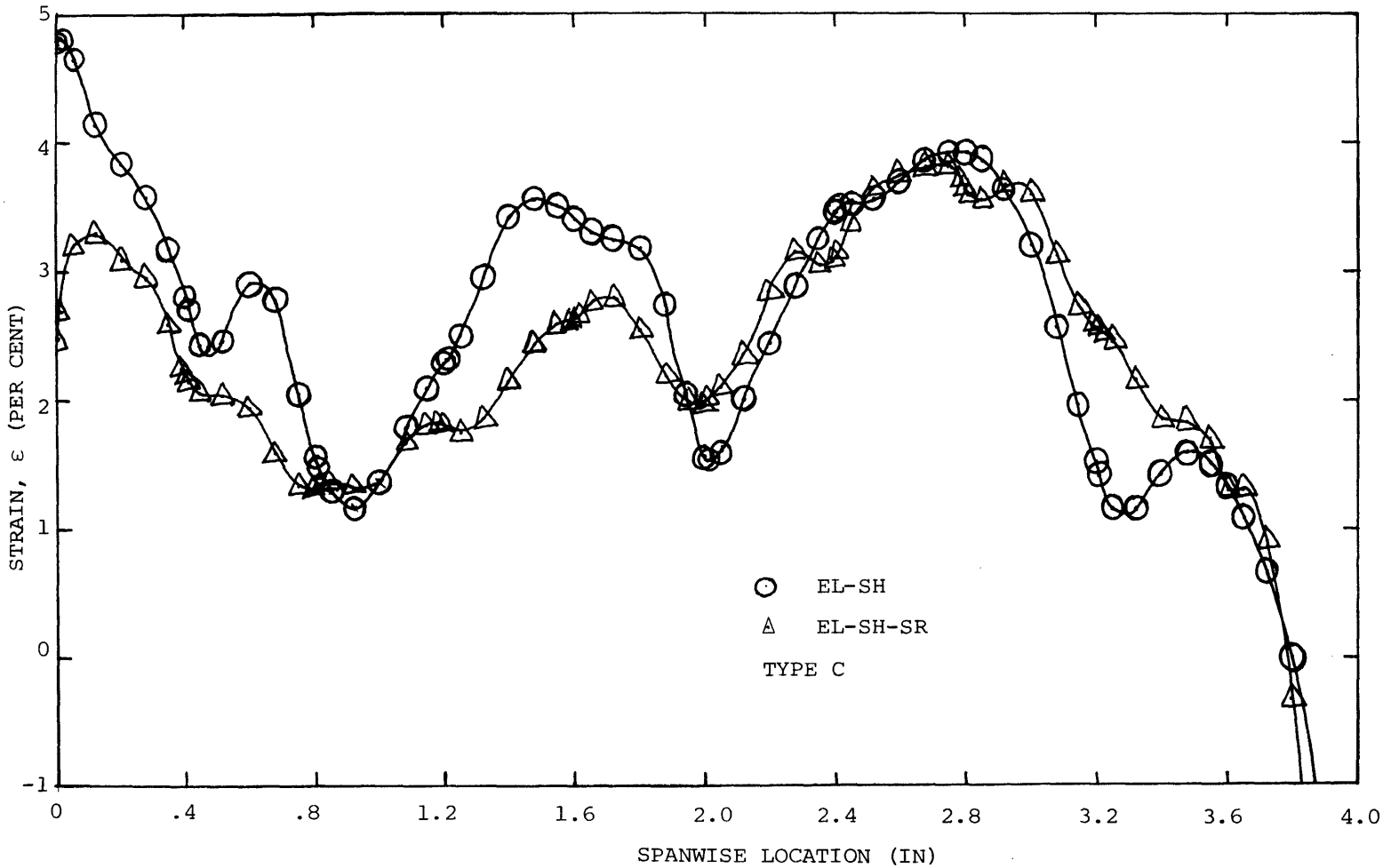

(d) Upper-Surface Strain Distribution, EL-SH vs. EL-SH-SR

FIG. 25 CONCLUDED (CB-1, 8 DOF/N, 10 ELEM/HALF)

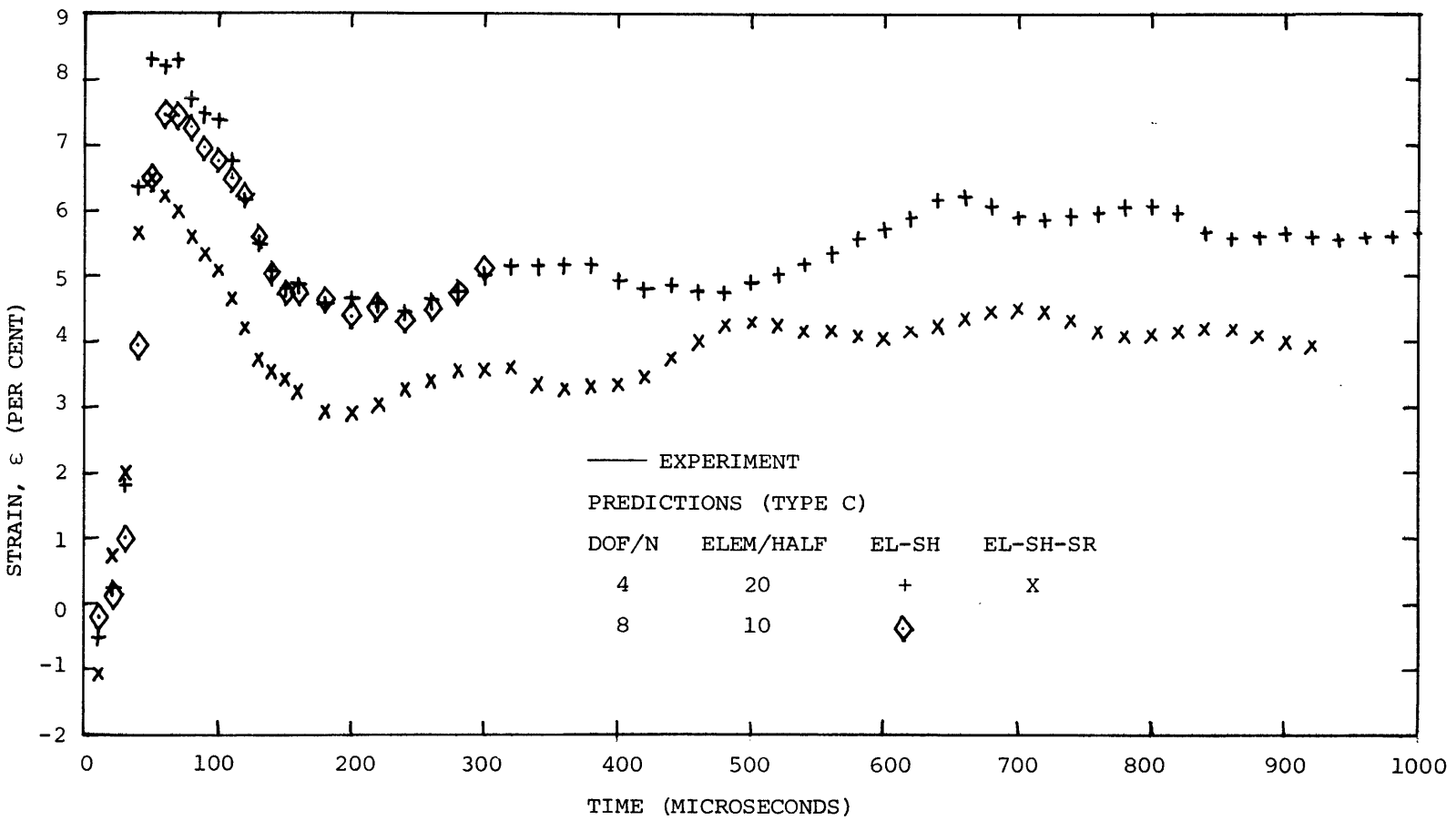

FIG. 26 PREDICTED STRAIN HISTORIES ON THE UPPER SURFACE OF IMPULSIVELY-LOADED BEAM MODEL CB-1 AT STATION x=0 IN

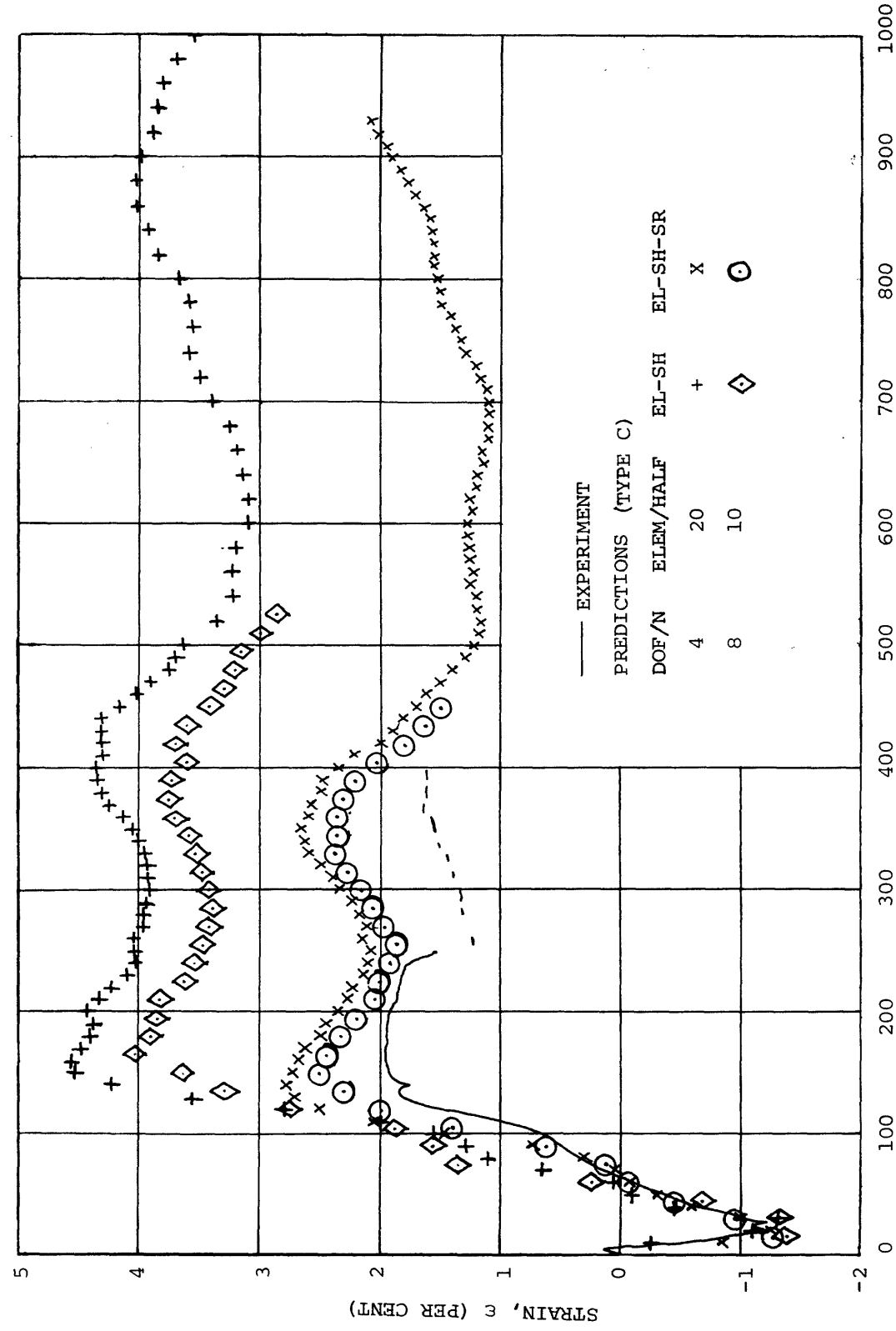

FIG. 27 PREDICTED AND MEASURED STRAIN HISTORIES ON THE UPPER SURFACE OF IMPULSIVELY-LOADED BEAM MODEL CB-1 AT STATION x=1.40 IN

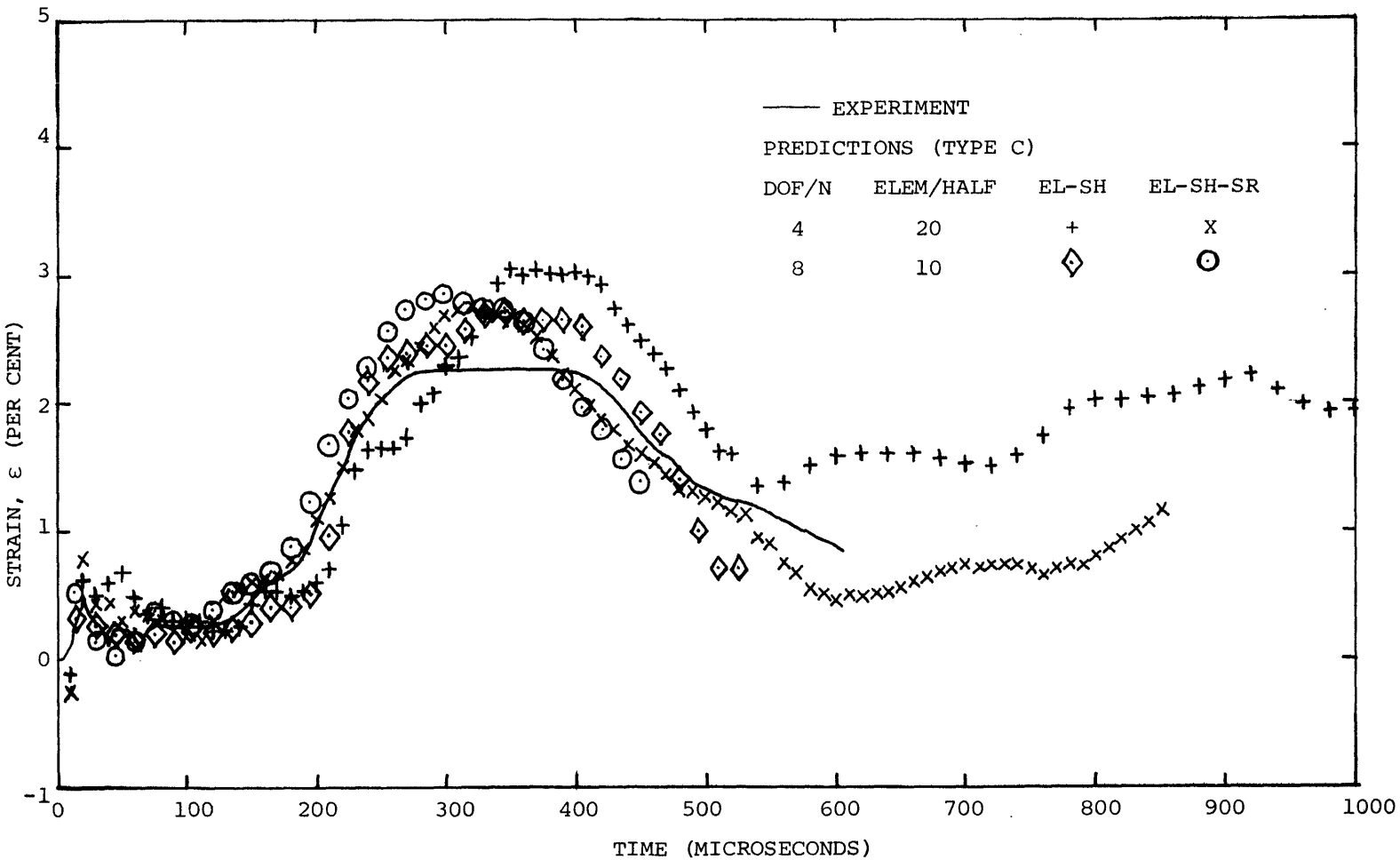

FIG. 28 PREDICTED AND MEASURED STRAIN HISTORIES ON THE UPPER SURFACE OF IMPULSIVELY-LOADED BEAM MODEL CB-1 AT STATION x=2.20 IN

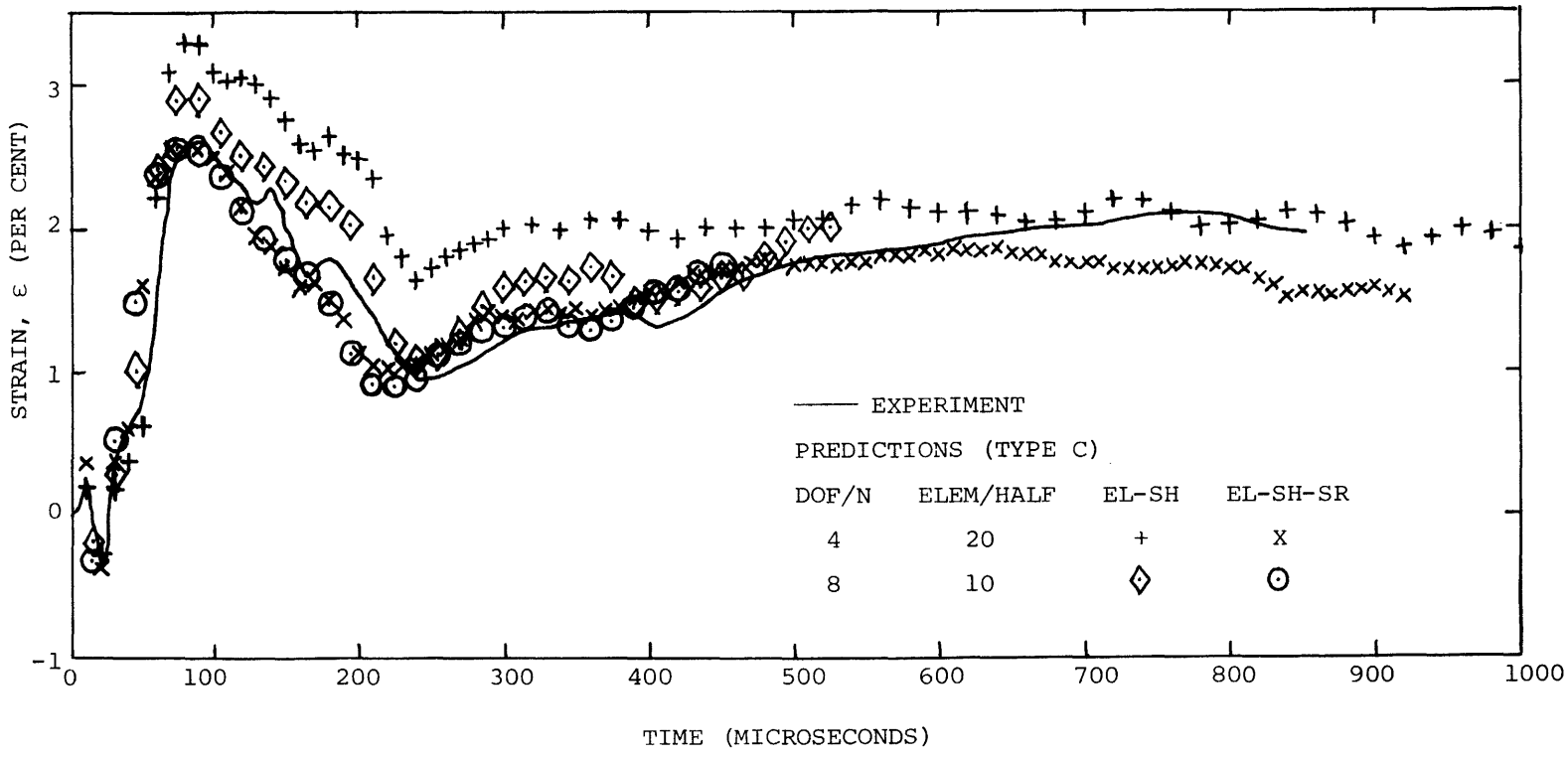

FIG. 29 PREDICTED AND MEASURED STRAIN HISTORIES ON THE LOWER SURFACE OF IMPULSIVELY-LOADED BEAM MODEL CB-1 AT STATION x=2.20 IN

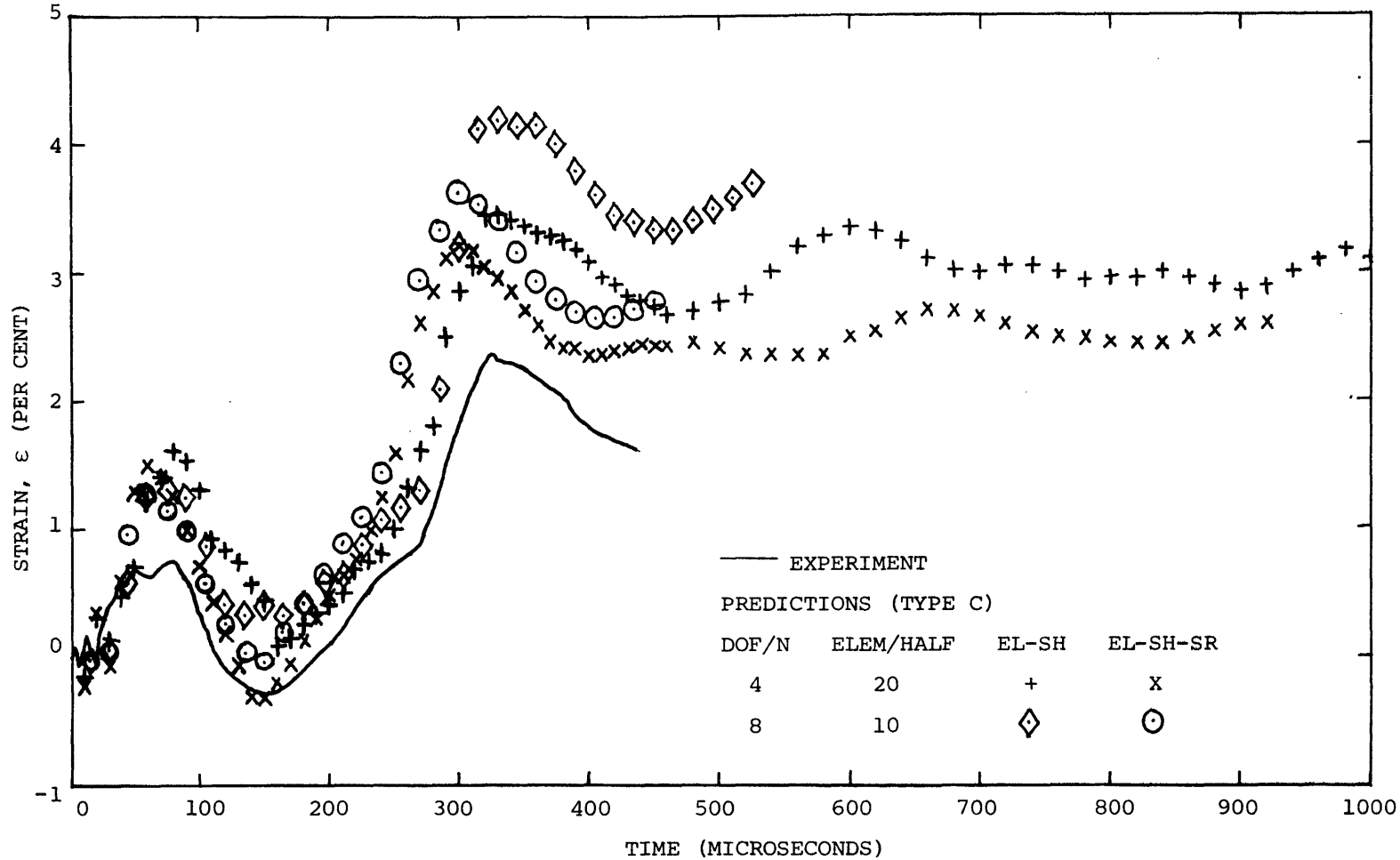

FIG. 30 PREDICTED AND MEASURED STRAIN HISTORIES ON THE UPPER SURFACE OF IMPULSIVELY-LOADED BEAM MODEL CB-1 AT STATION x=3.00 IN

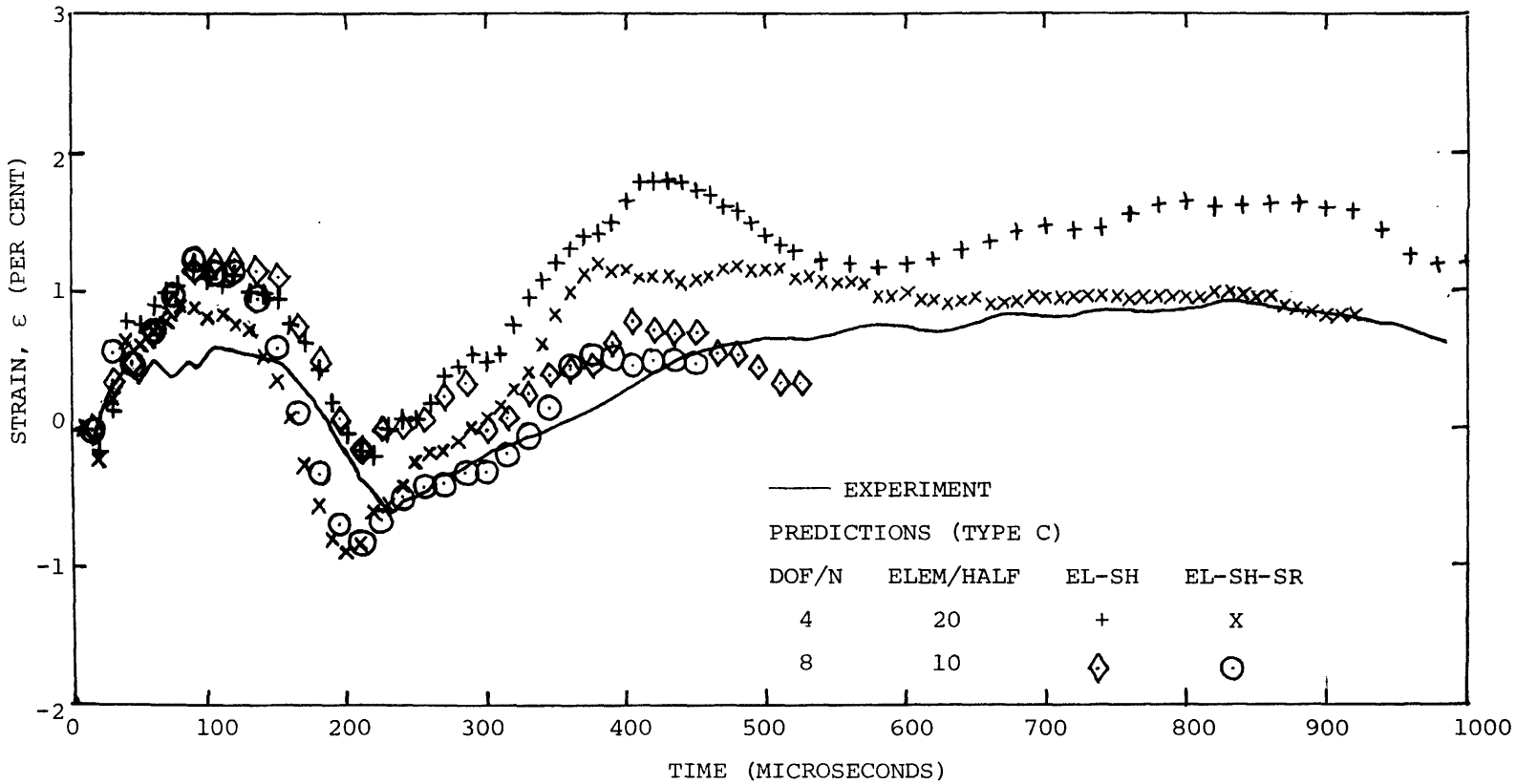

FIG. 31 PREDICTED AND MEASURED STRAIN HISTORIES ON THE UPPER SURFACE OF IMPULSIVELY-LOADED BEAM MODEL CB-1 AT STATION x=3.80 IN

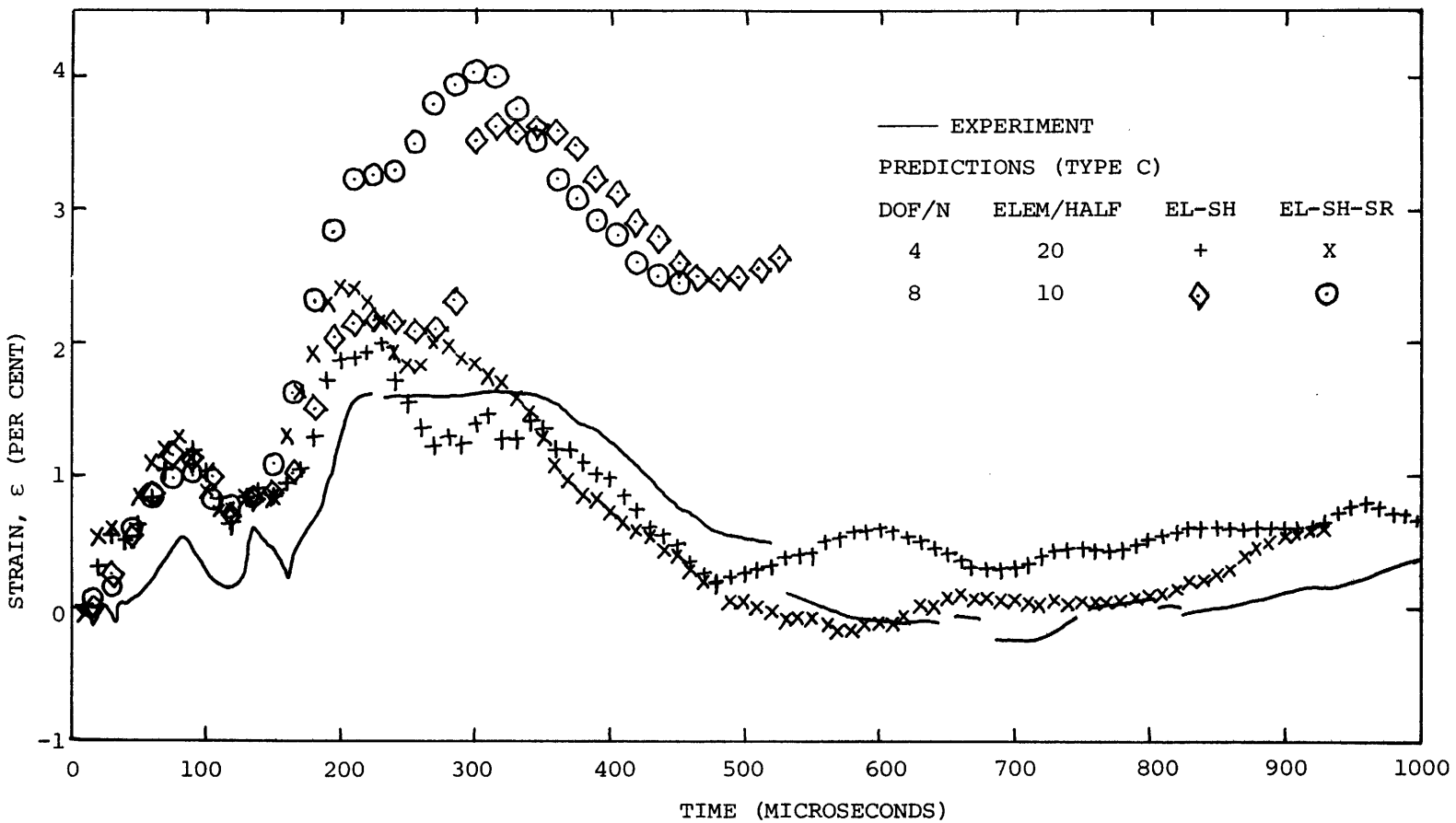

FIG. 32 PREDICTED AND MEASURED STRAIN HISTORIES ON THE LOWER SURFACE OF IMPULSIVELY-LOADED BEAM MODEL CB-1 AT STATION x=3.80 IN

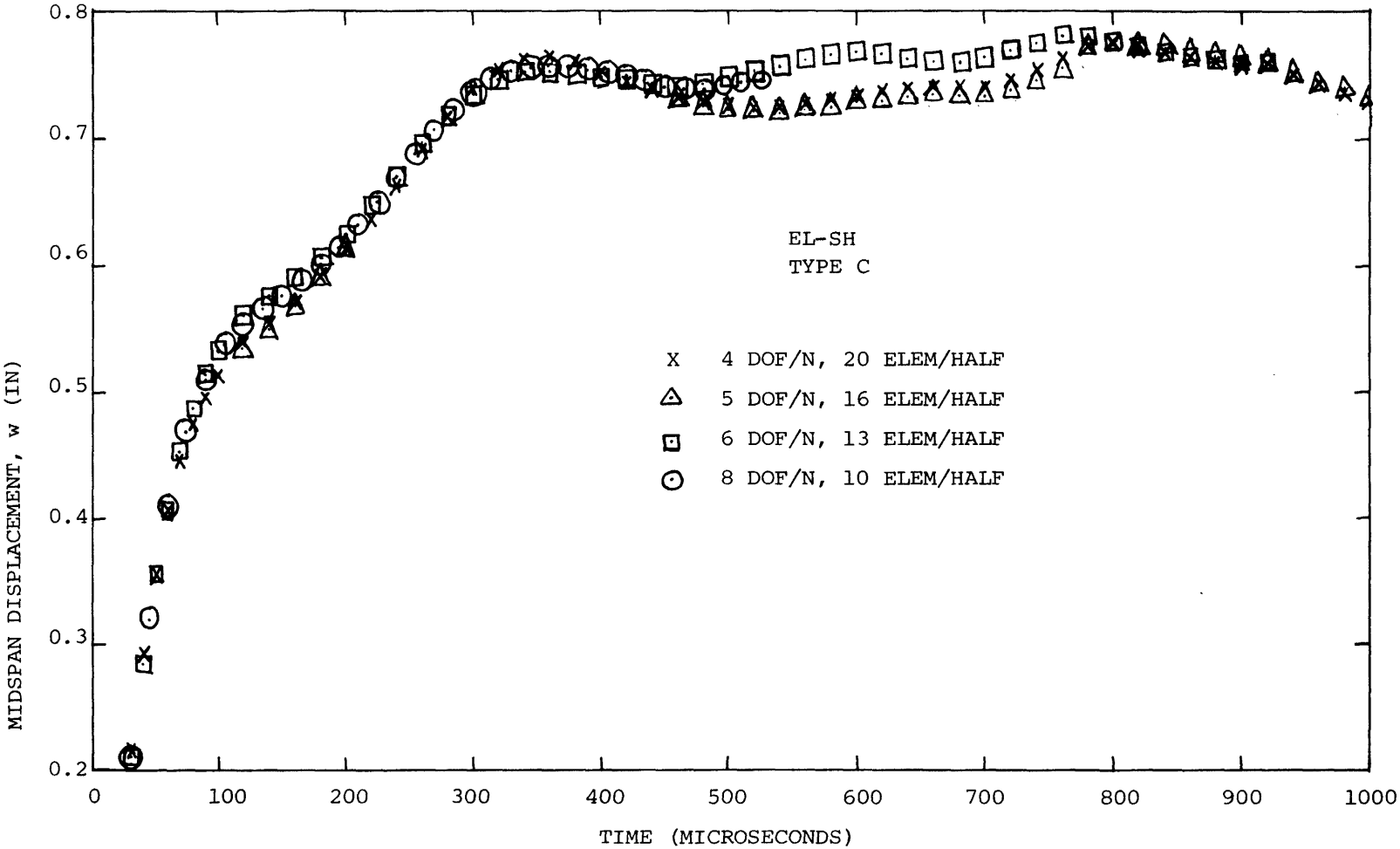

FIG. 33 PREDICTED TRANSIENT MIDSPAN DISPLACEMENT w FOR IMPULSIVELY-LOADED BEAM MODEL CB-1

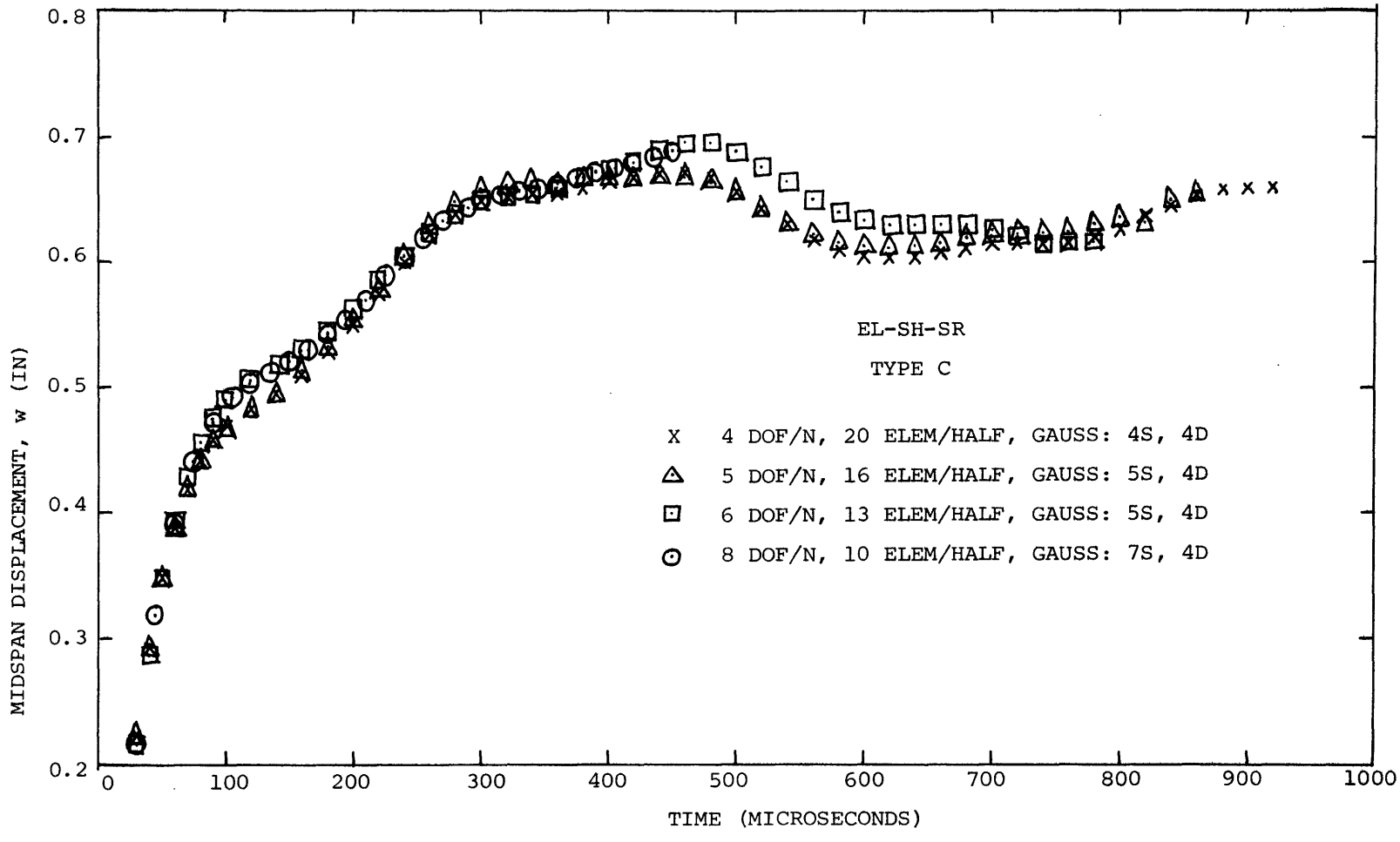

FIG. 34 EL-SH-SR PREDICTED TRANSIENT MIDSPAN DISPLACEMENT w FOR IMPULSIVELY-LOADED BEAM MODEL CB-1

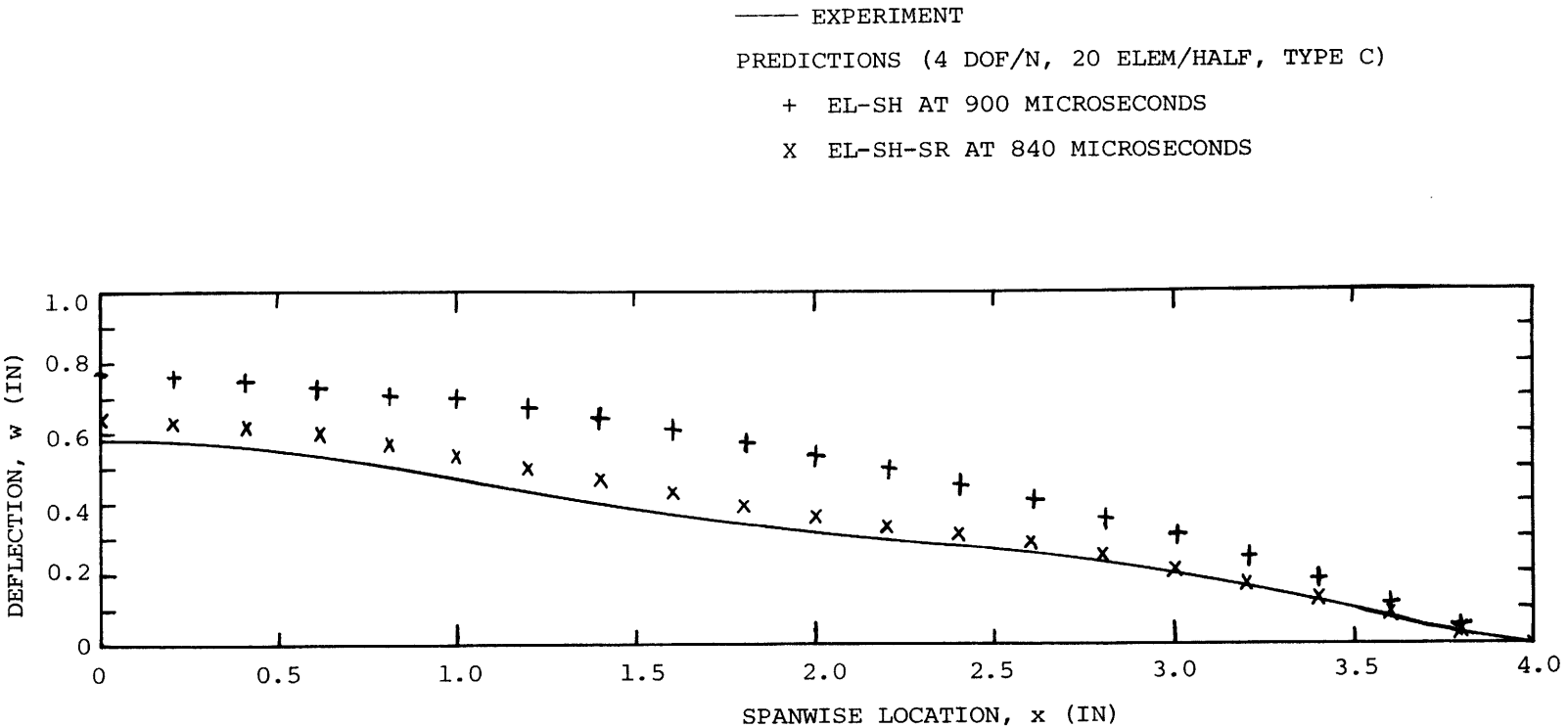

FIG. 35 SPANWISE DISTRIBUTION OF MEASURED AND PREDICTED PERMANENT DEFLECTION FOR IMPULSIVELY-LOADED BEAM CB-1

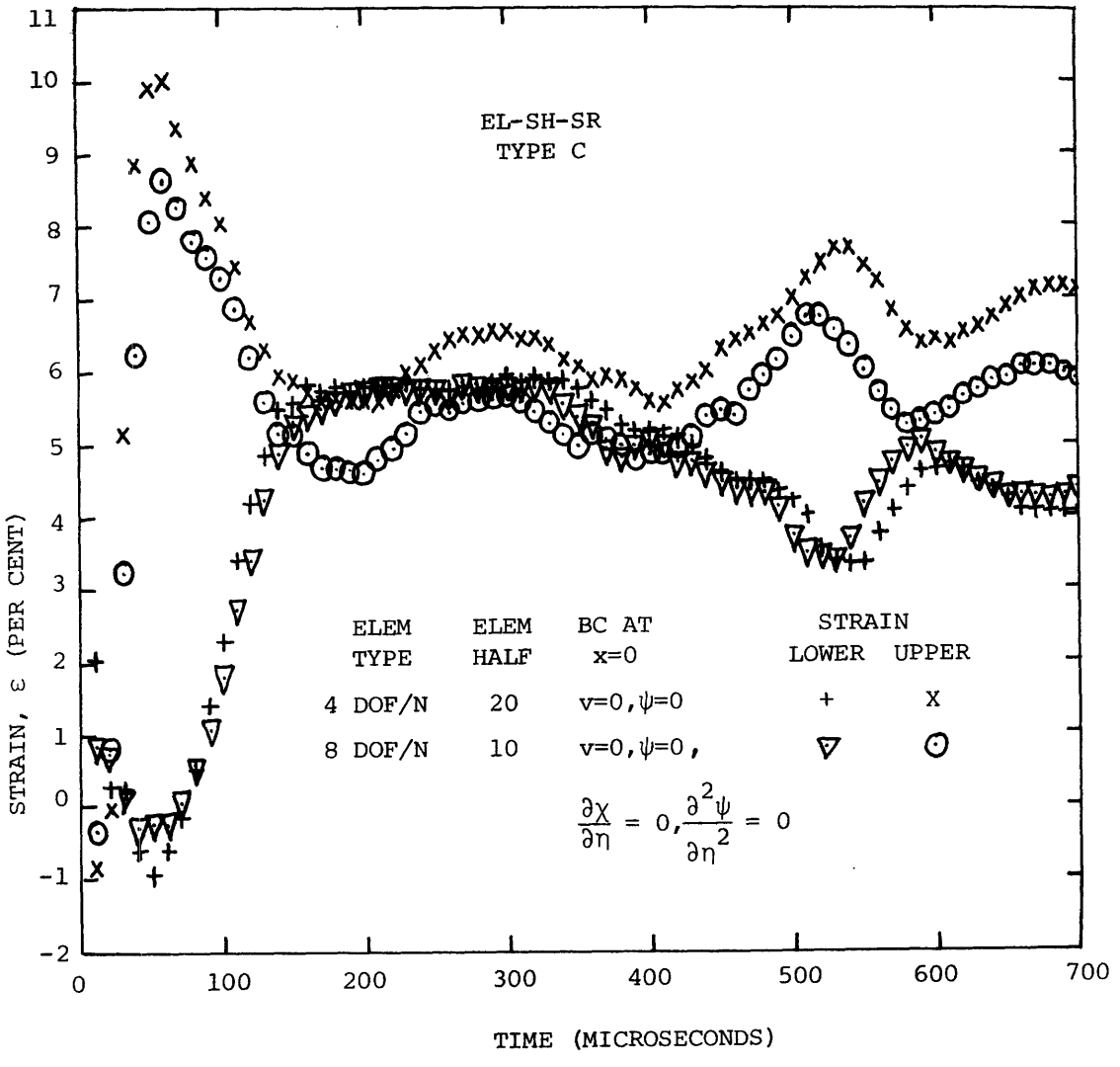

FIG. 36 PREDICTED STRAIN HISTORIES ON THE LOWER AND THE UPPER SURFACE OF IMPULSIVELY-LOADED BEAM CB-4 AT STATION x=0 IN

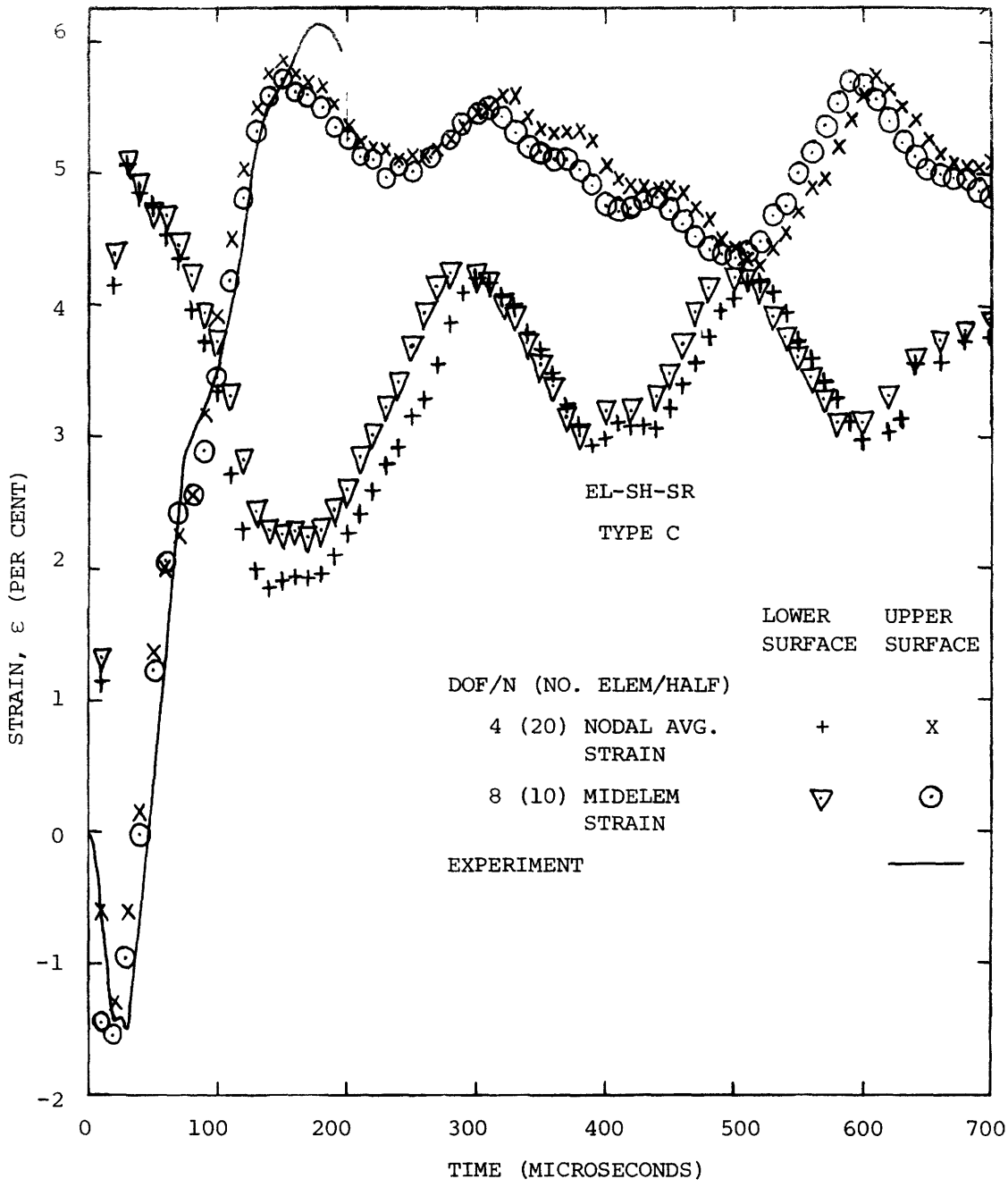

FIG. 37 PREDICTED AND MEASURED STRAIN HISTORIES ON THE LOWER AND THE UPPER SURFACE OF IMPULSIVELY-LOADED BEAM MODEL CB-4 AT STATION x=1.40 IN

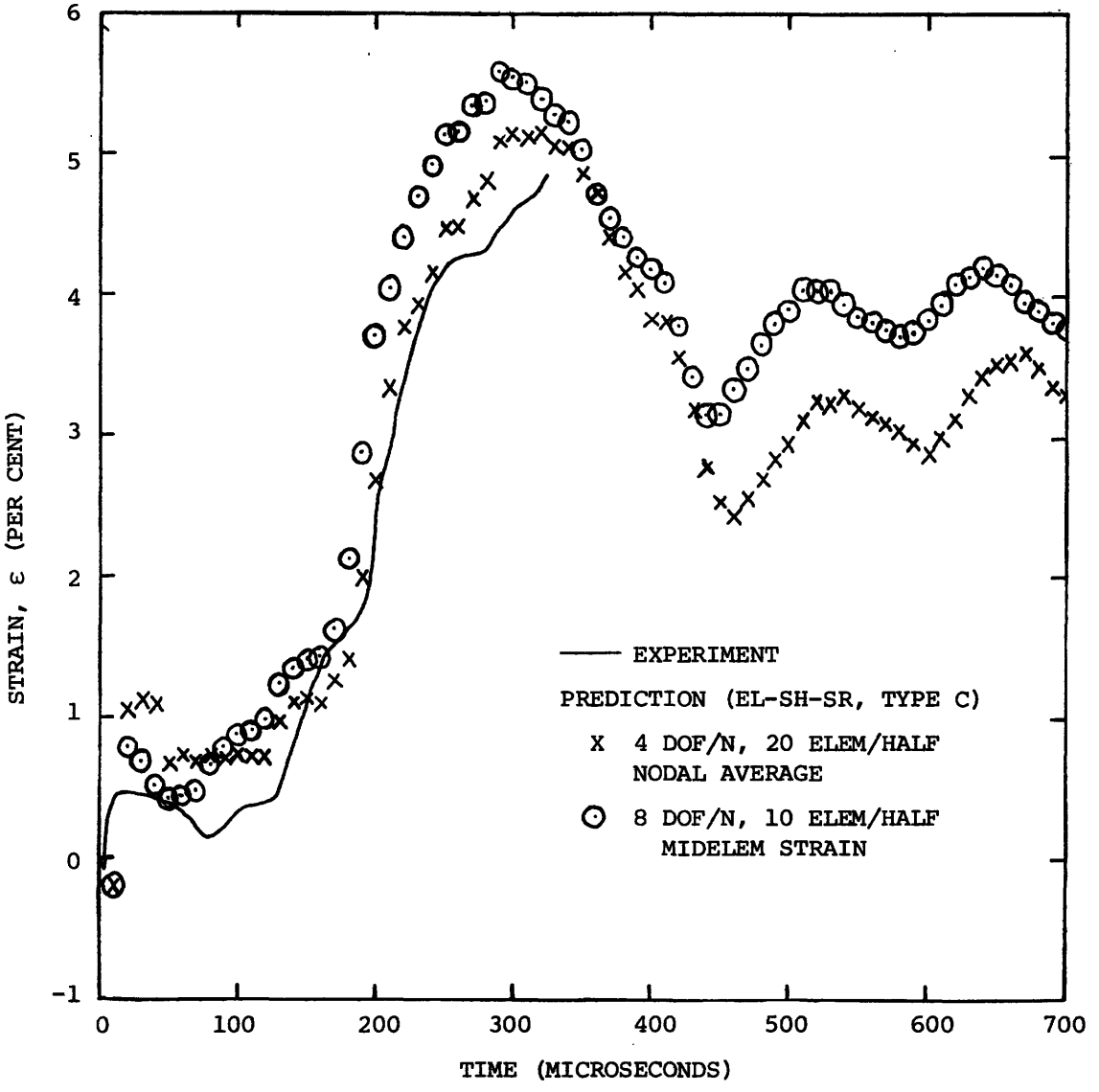

FIG. 38 PREDICTED AND MEASURED STRAIN HISTORIES ON THE UPPER SURFACE OF IMPULSIVELY-LOADED BEAM MODEL CB-4 AT STATION x=2.20 IN

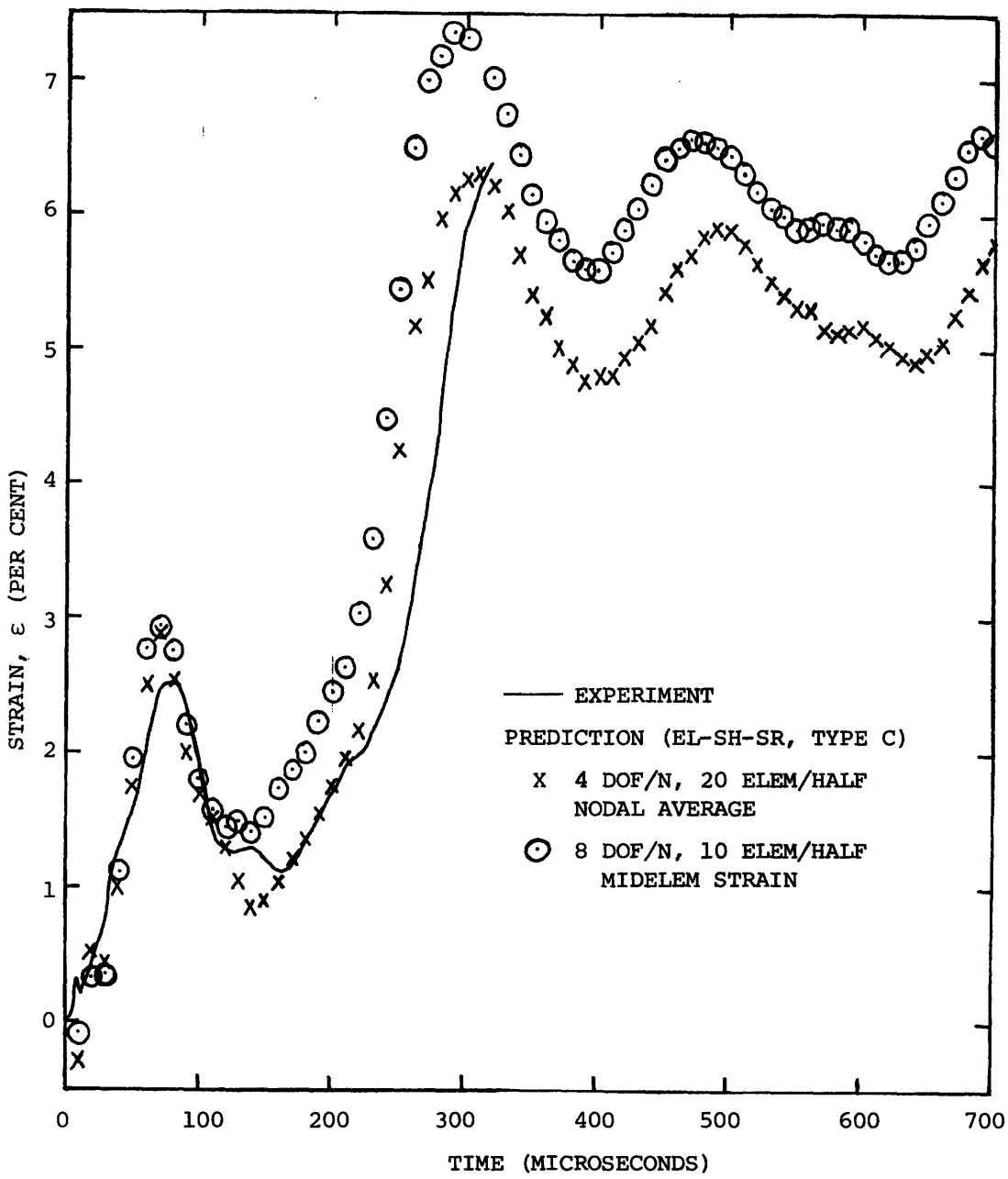

FIG. 39 PREDICTED AND MEASURED STRAIN HISTORIES ON THE UPPER SURFACE OF IMPULSIVELY-LOADED BEAM MODEL CB-4 AT STATION x=3.00 IN

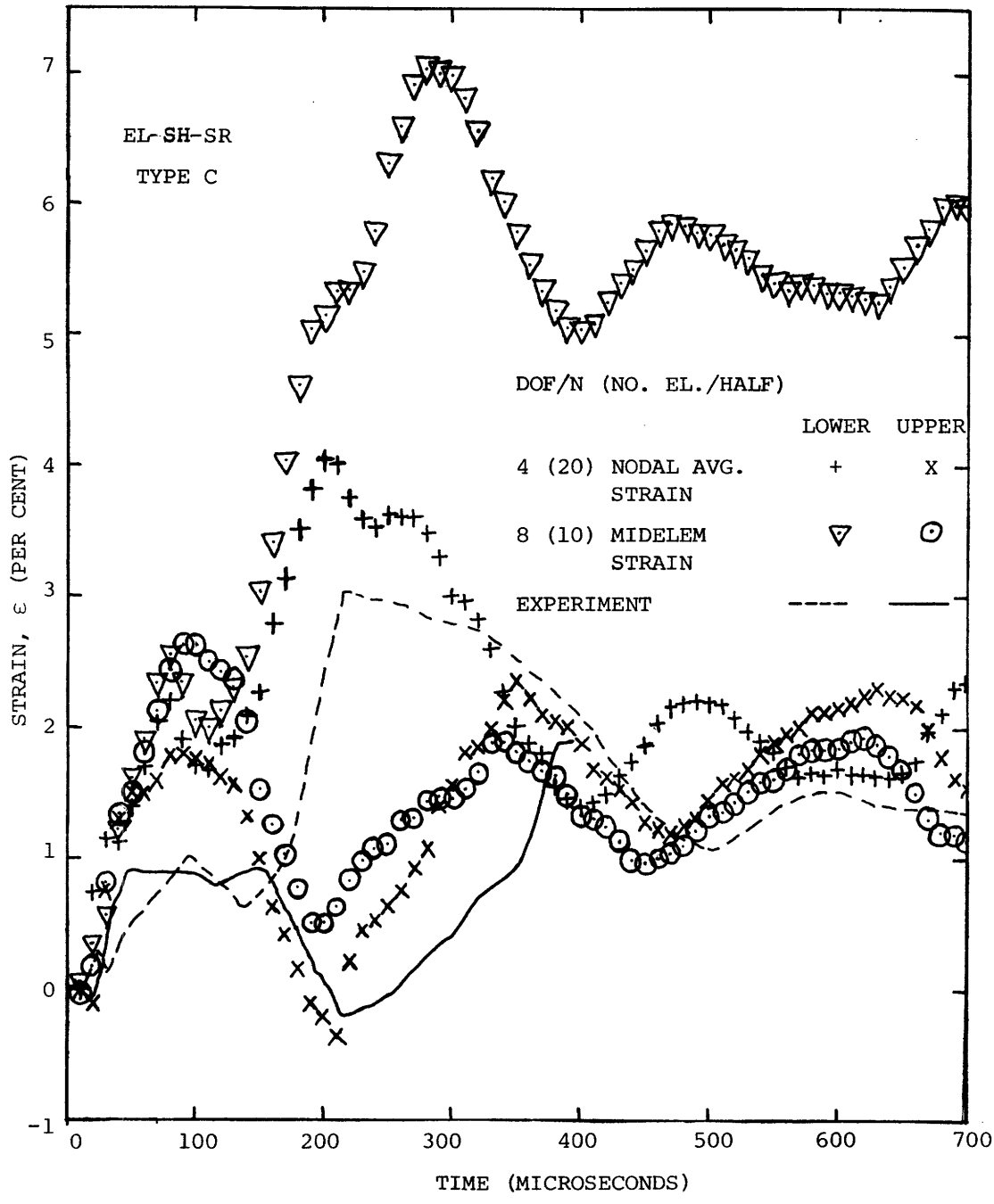

FIG. 40 PREDICTED AND MEASURED STRAIN HISTORIES ON THE LOWER AND THE UPPER SURFACE OF IMPULSIVELY-LOADED BEAM CB-4 AT STATION x=3.80 IN

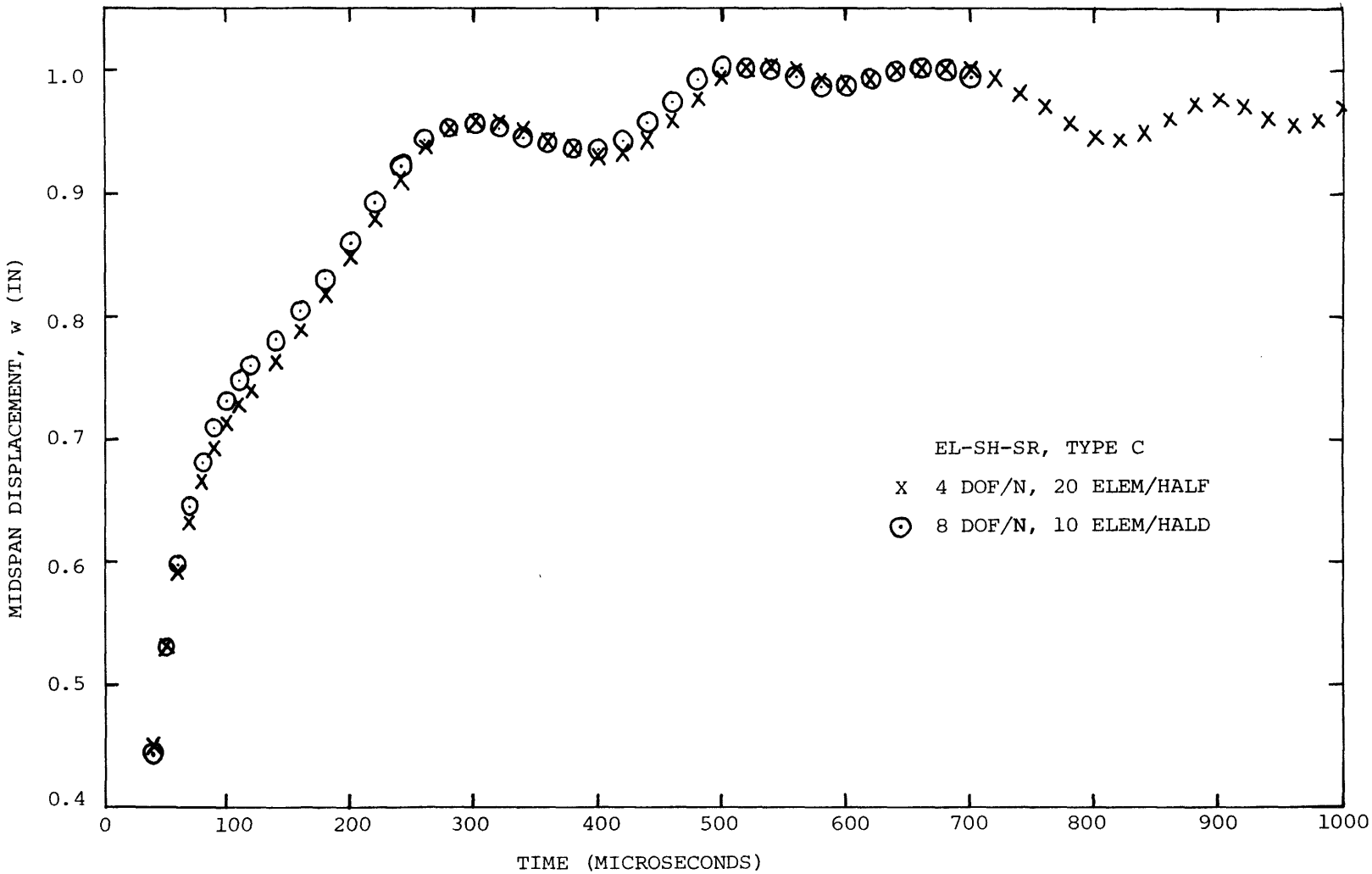

FIG. 41 PREDICTED TRANSIENT MIDSPAN DISPLACEMENT w FOR IMPULSIVELY-LOADED BEAM MODEL CB-4

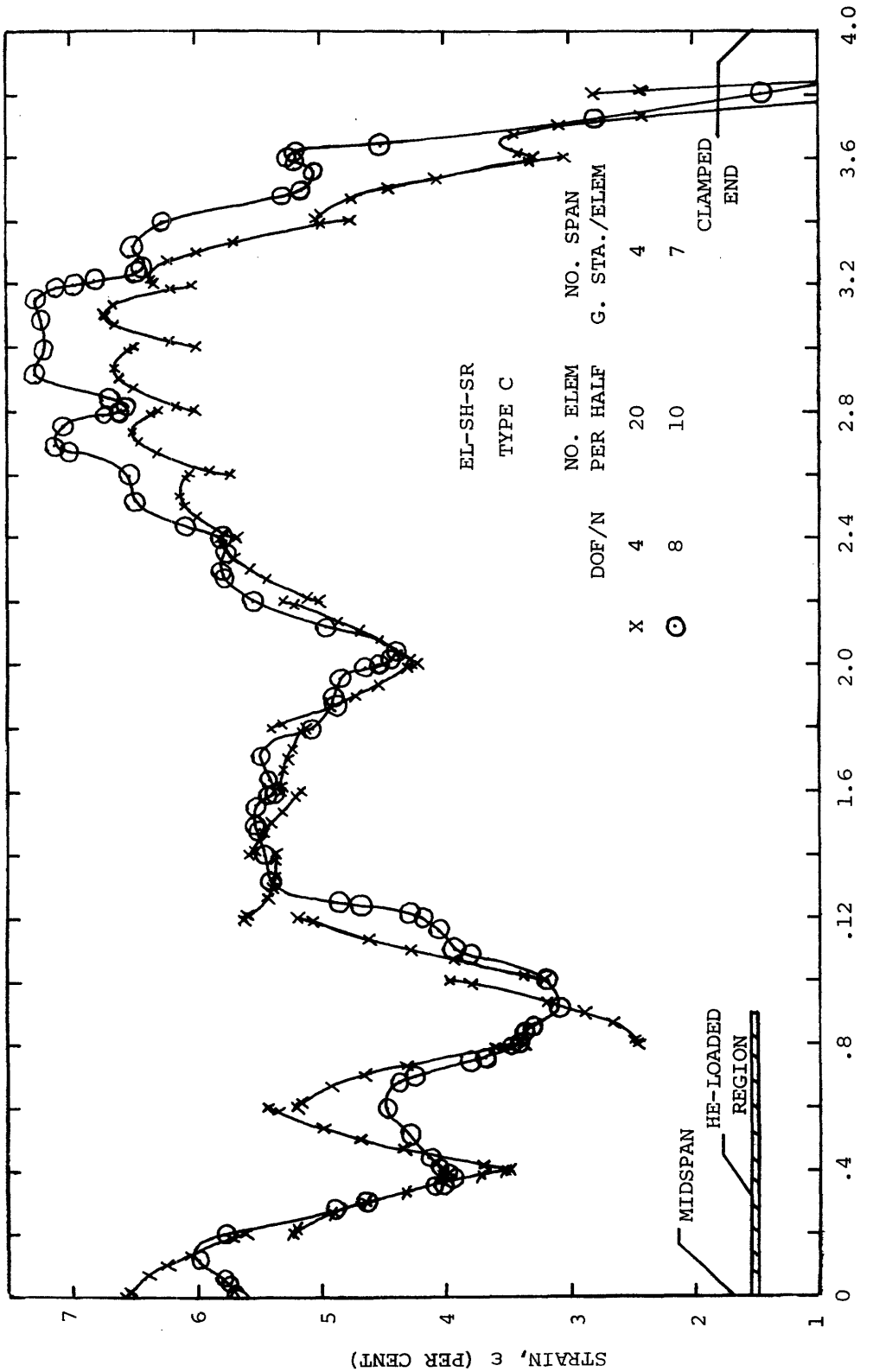

(a) Spanwise Distribution of Upper-Surface Strain at t=300 Microseconds

FIG. 42 SPANWISE DISTRIBUTION OF UPPER-SURFACE STRAIN AND LATERAL DEFLECTION AT GIVEN TIMES FOR IMPULSIVELY-LOADED BEAM CB-4 (4 DOF/N VS. 8 DOF/N ELEMS)

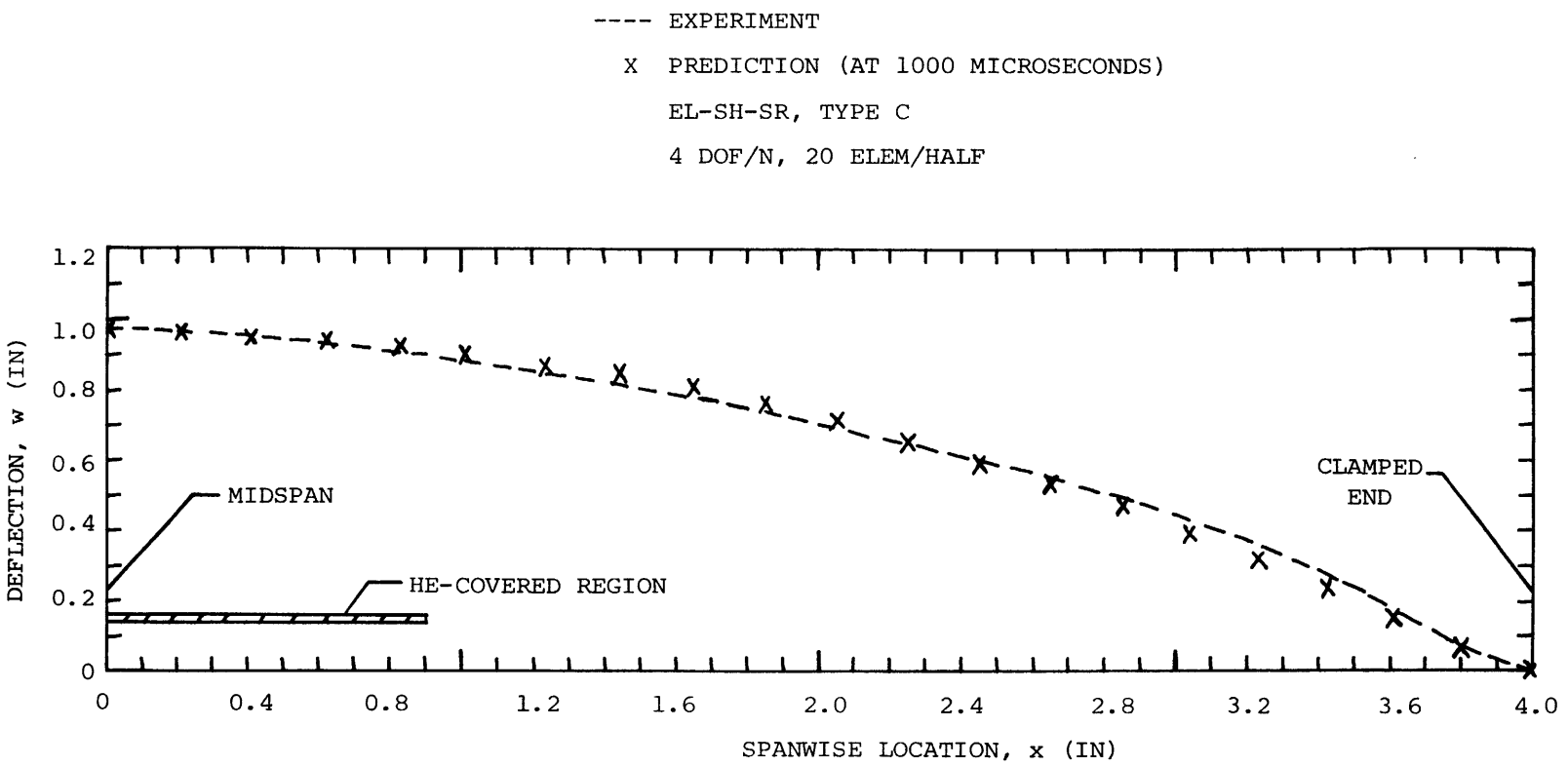

(b) Spanwise Distribution of Measured and Predicted Permanent Deflection

FIG. 42 CONCLUDED (CB-4; EXPERIMENT; 4 DOF/N, 20 ELEM/HALF)

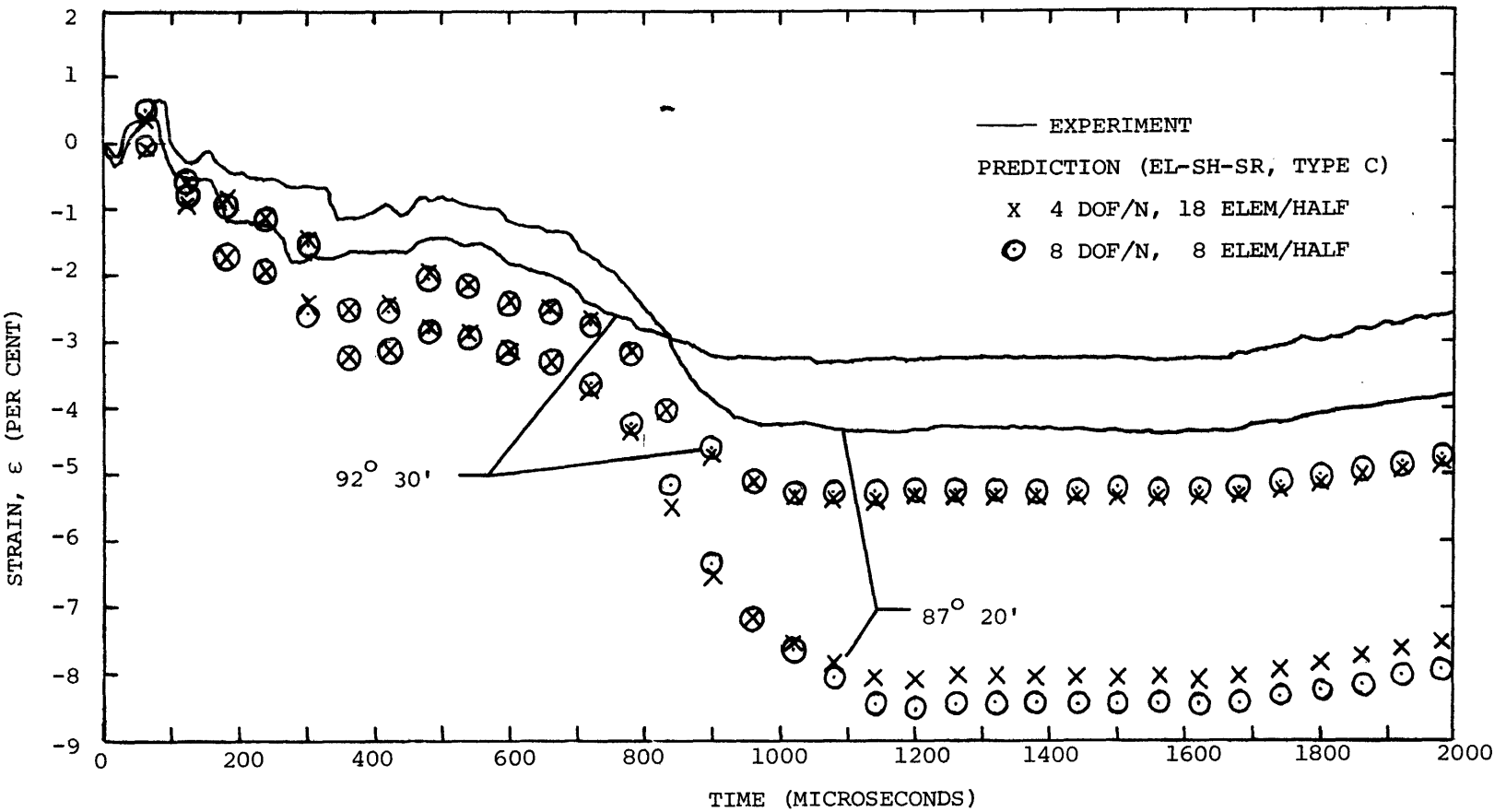

(a) Inside Surface at $\theta=87^{\circ}$ 20' and 92° 30'

FIG. 43 COMPARISONS OF EXPERIMENTAL AND PREDICTED STRAINS ON THE INNER AND THE OUTER SURFACE OF THE IMPULSIVELY-LOADED FREE CIRCULAR RING

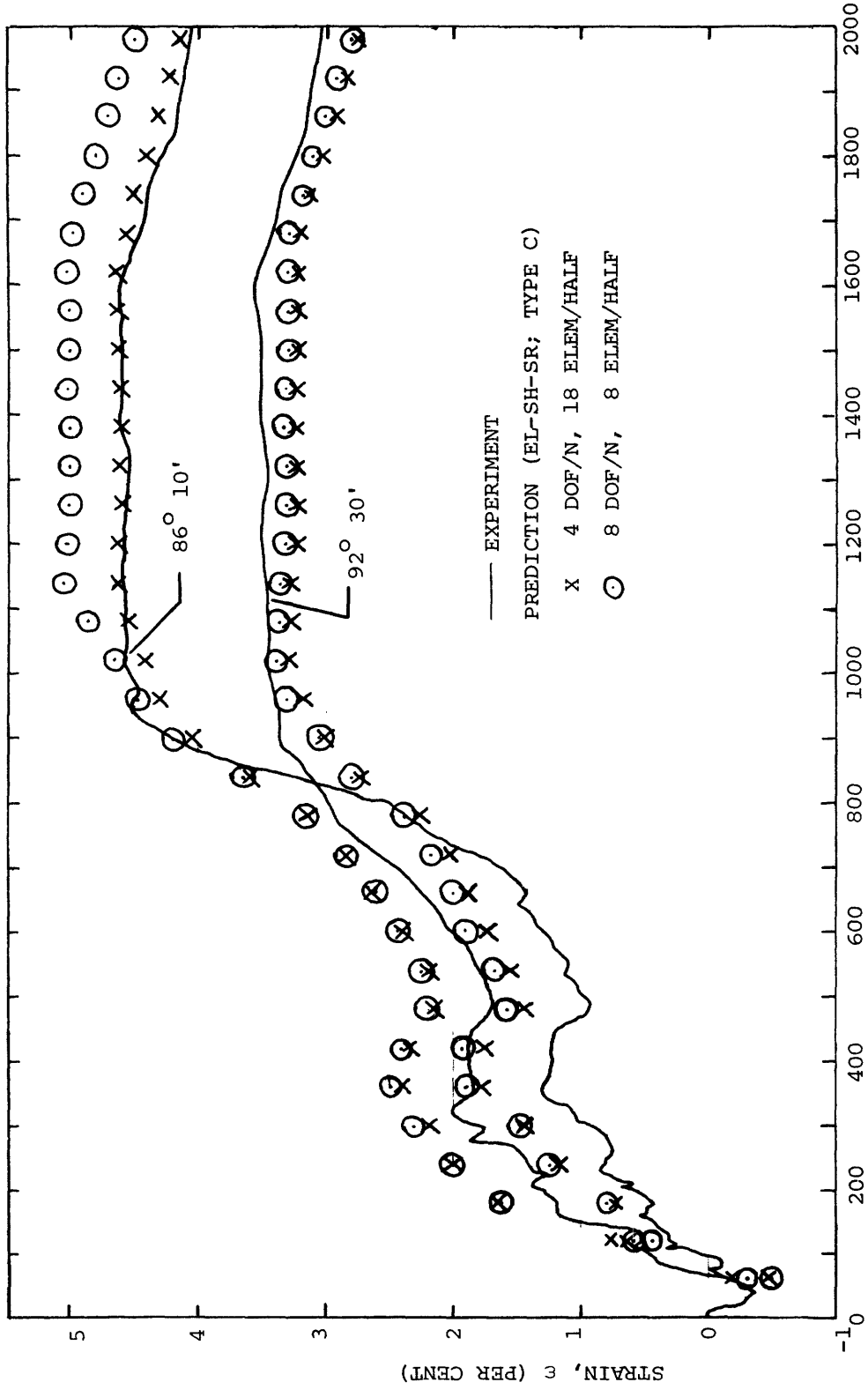

(b) Outside Surface at $\theta=86^{\circ}$ 10' and 92° 30'

FIG. 43 CONTINUED (FREE RING, EXPT., 4 DOF/N, 8 DOF/N)

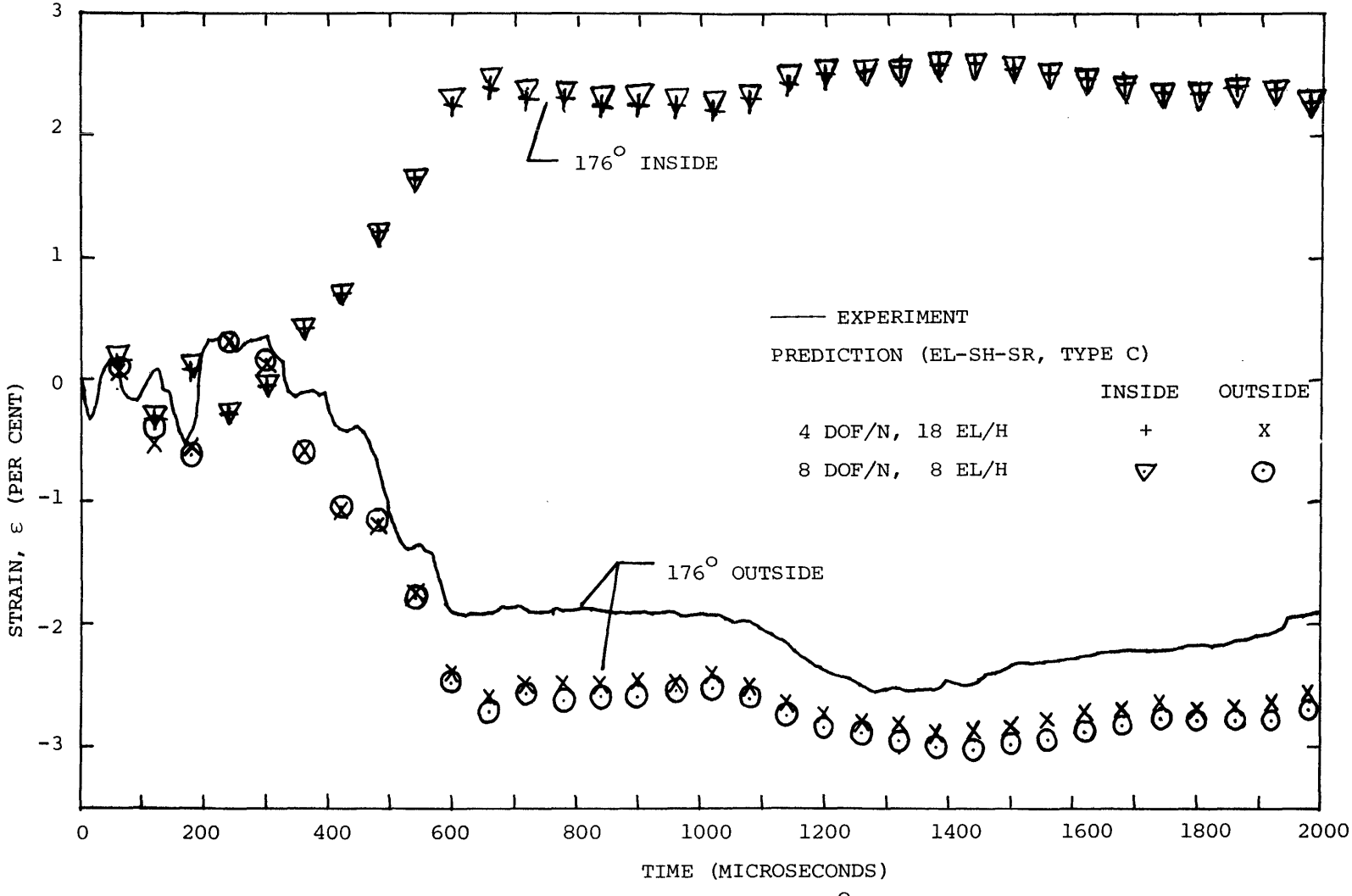

(c) Inside Surface and Outside Surface at $\theta=176^{\circ}$

FIG. 43 CONCLUDED (FREE RING, EXPT., 4 DOF/N, 8 DOF/N)

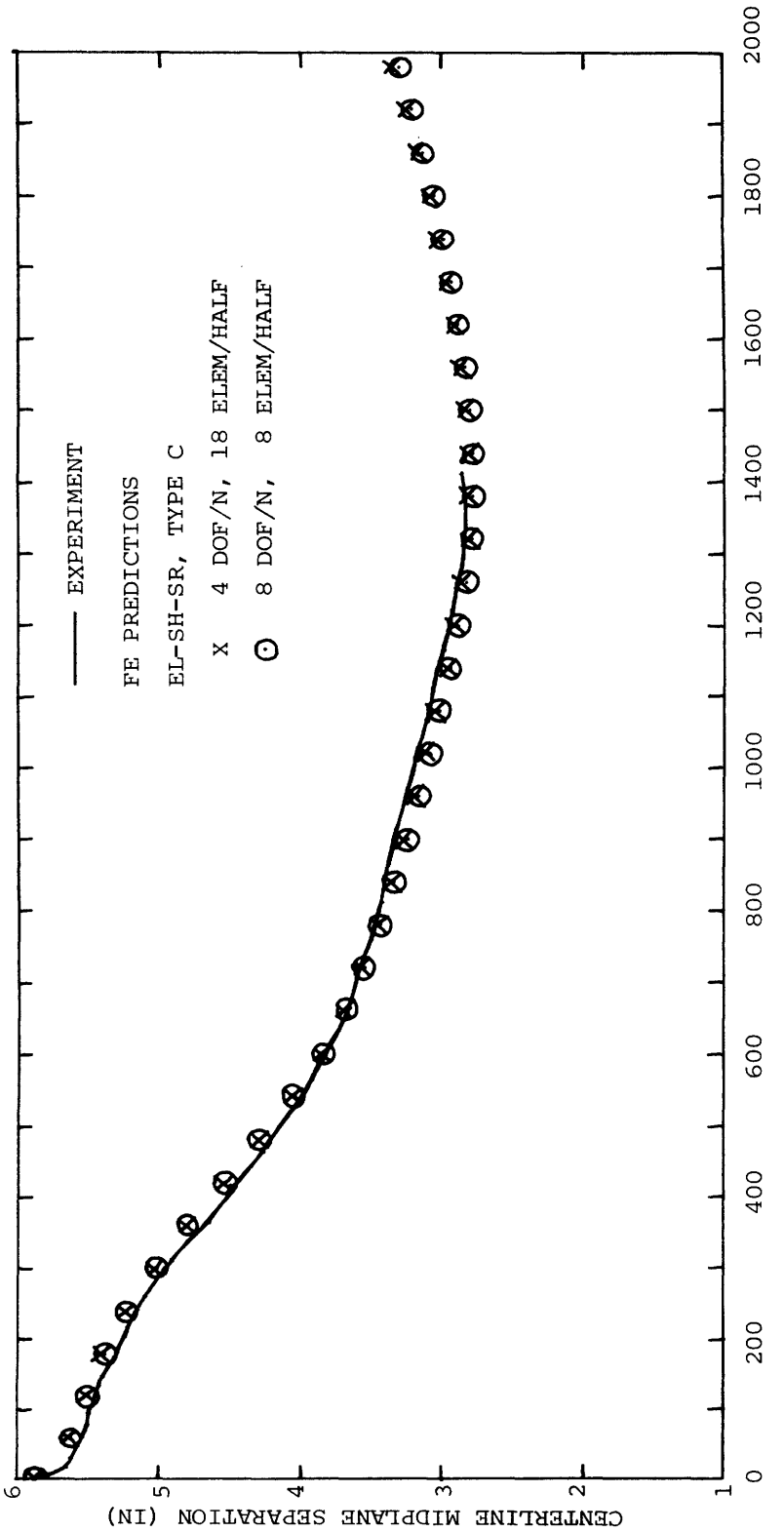

FIG. 44 COMPARISON OF CENTERLINE MIDPLANE SEPARATION PREDICTED BY USING 4 DOF/N AND 8 DOF/N ELEMENTS FOR THE IMPULSIVELY-LOADED FREE CIRCULAR RING

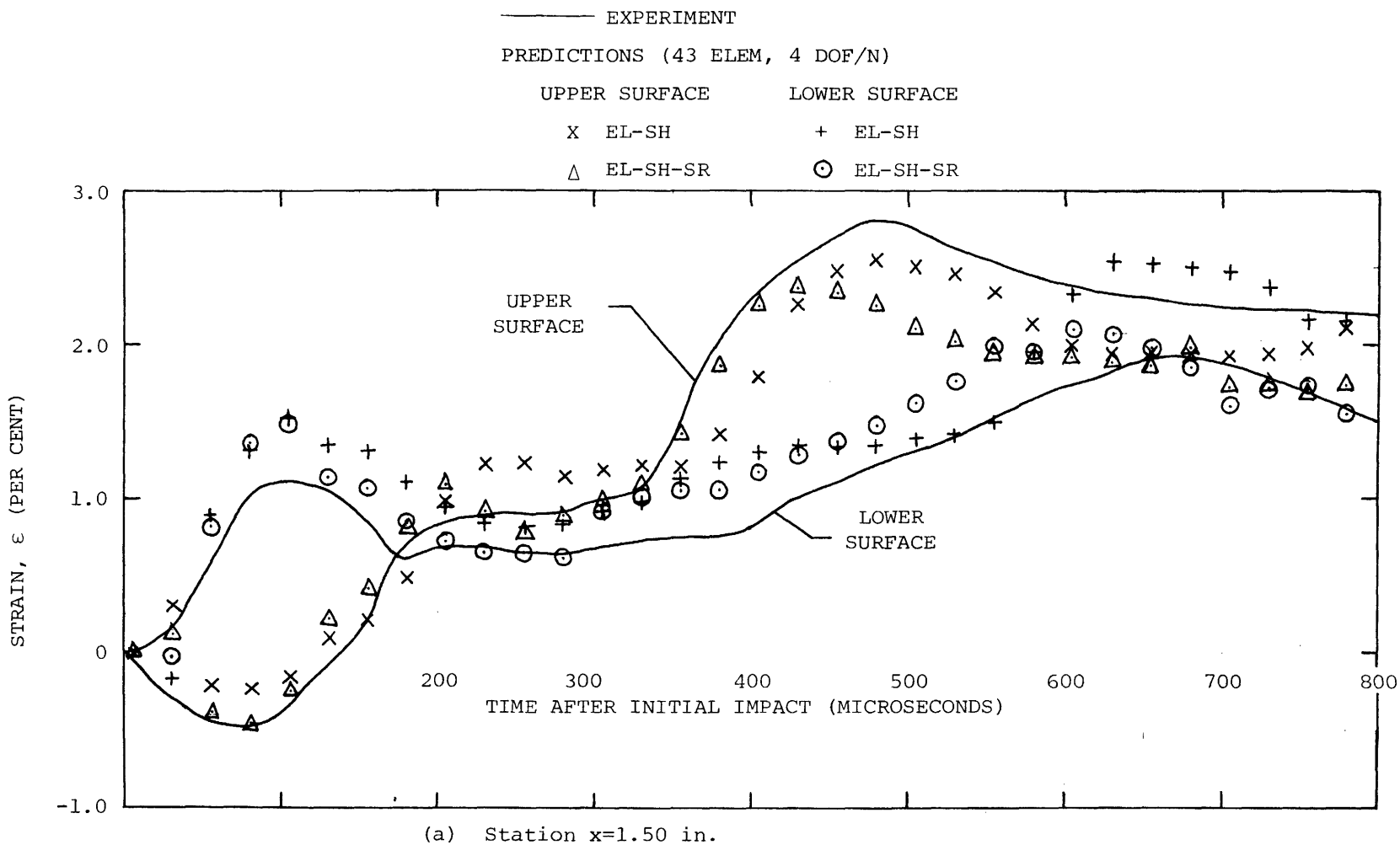

(a) Station x=1.50 in.

FIG. 45 TRANSIENT STRAIN AT VARIOUS SPANWISE STATIONS AND SUPPORT REACTIONS OF STEEL-SPHERE-IMPACTED 6061-T651 ALUMINUM BEAM MODEL CB-18

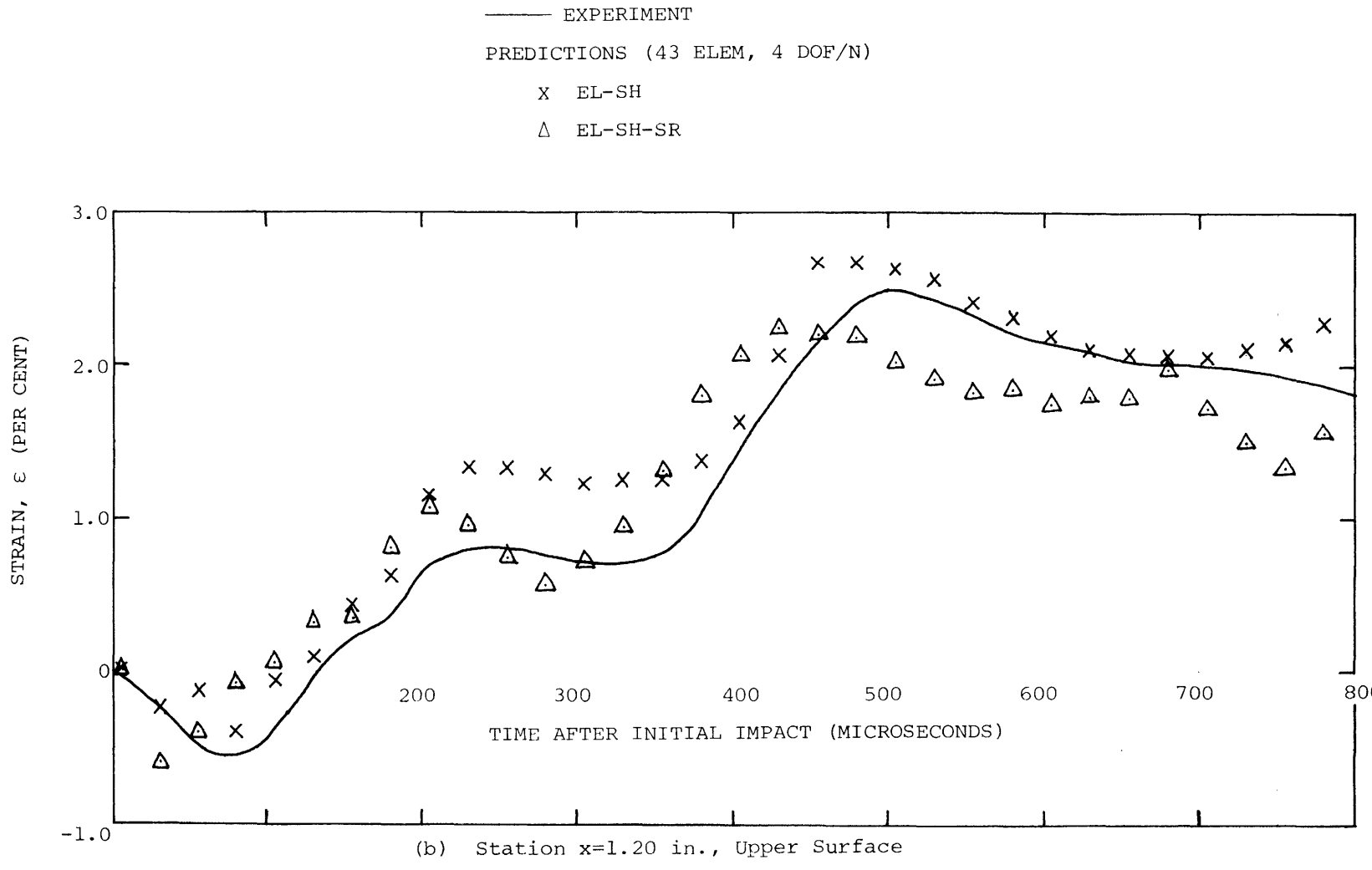

(b) Station x=1.20 in., Upper Surface

FIG. 45 CONTINUED (CB-18)

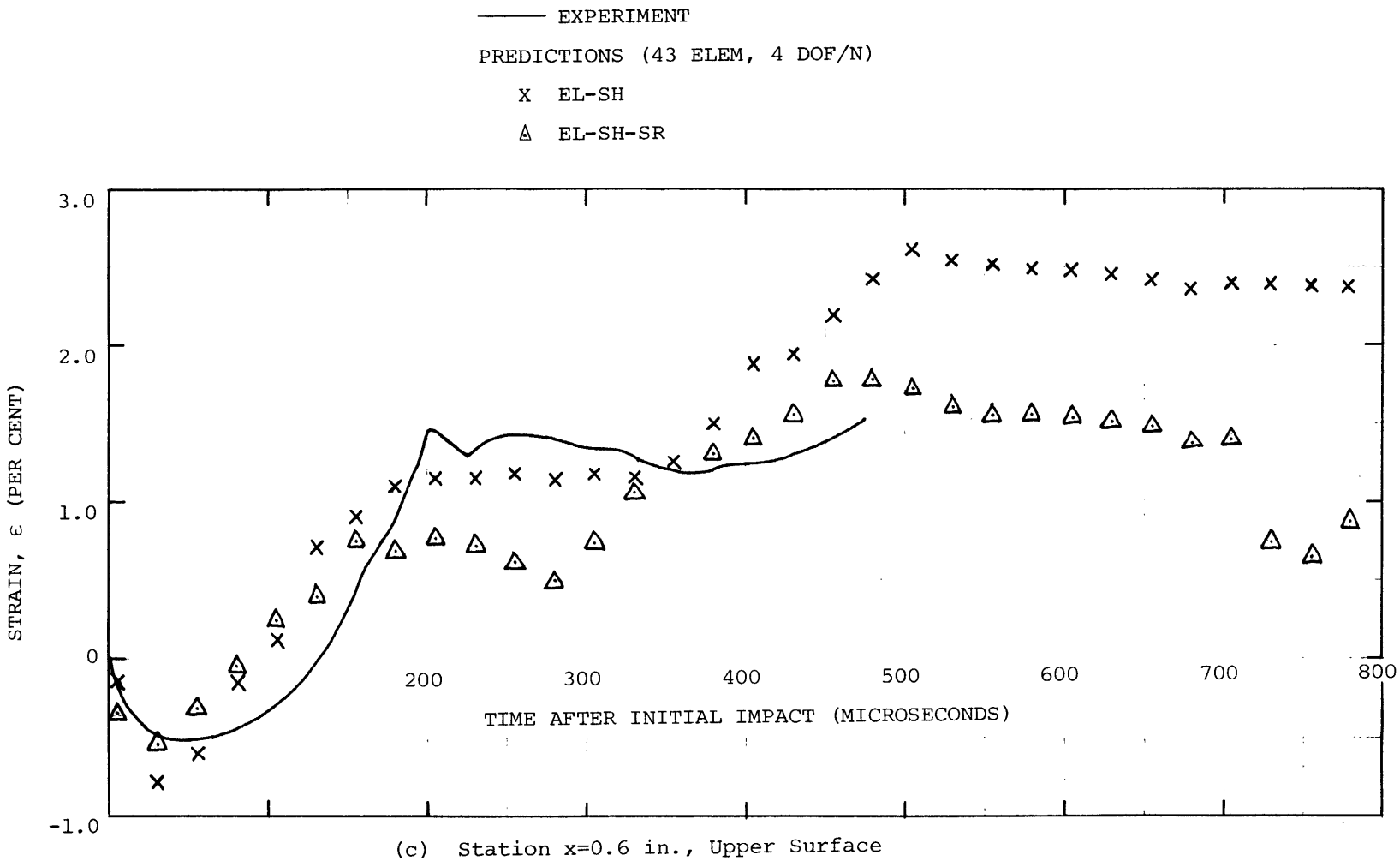

(c) Station x=0.6 in., Upper Surface

FIG. 45 CONTINUED (CB-18)

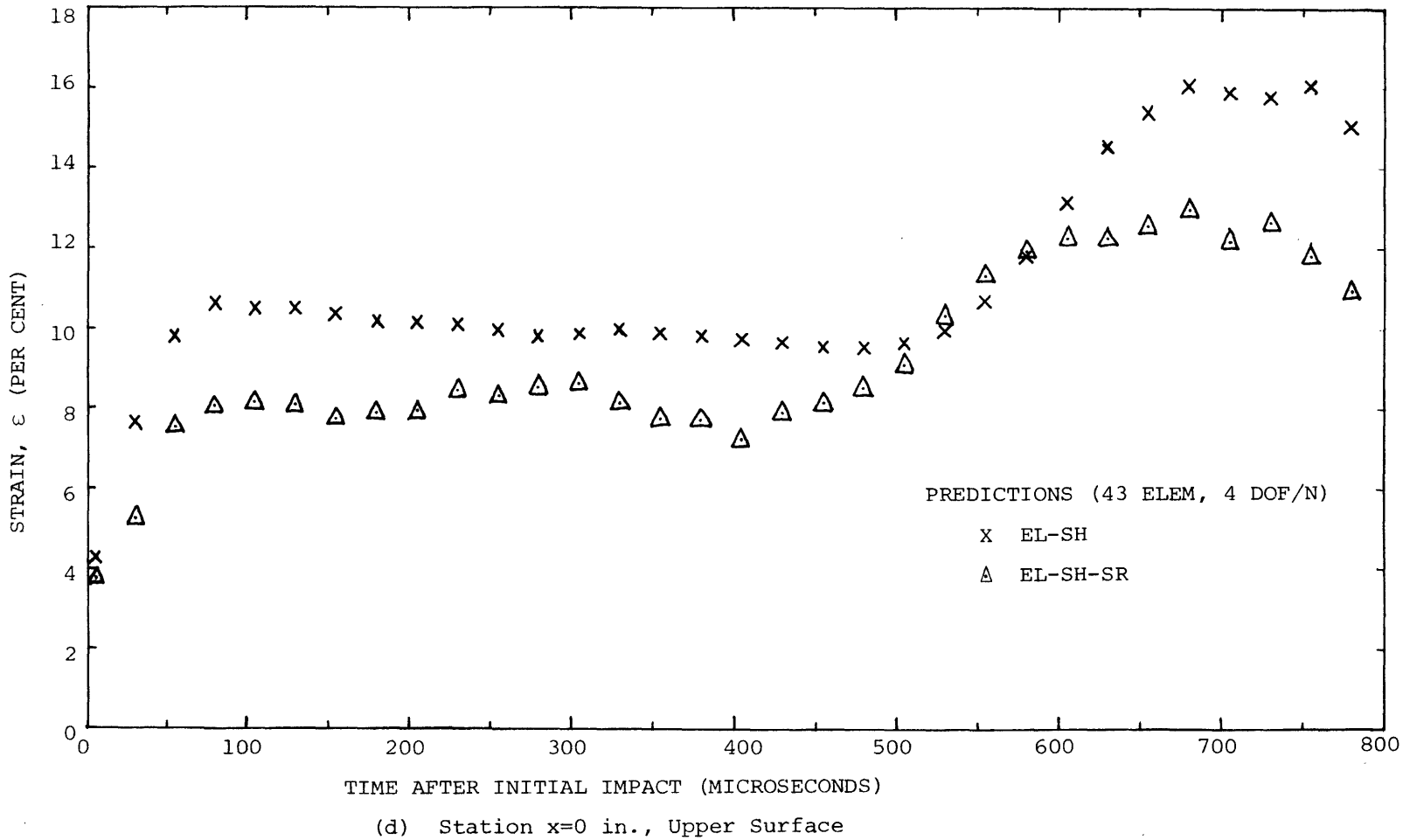

(d) Station x=0 in., Upper Surface

FIG. 45 CONCLUDED (CB-18)

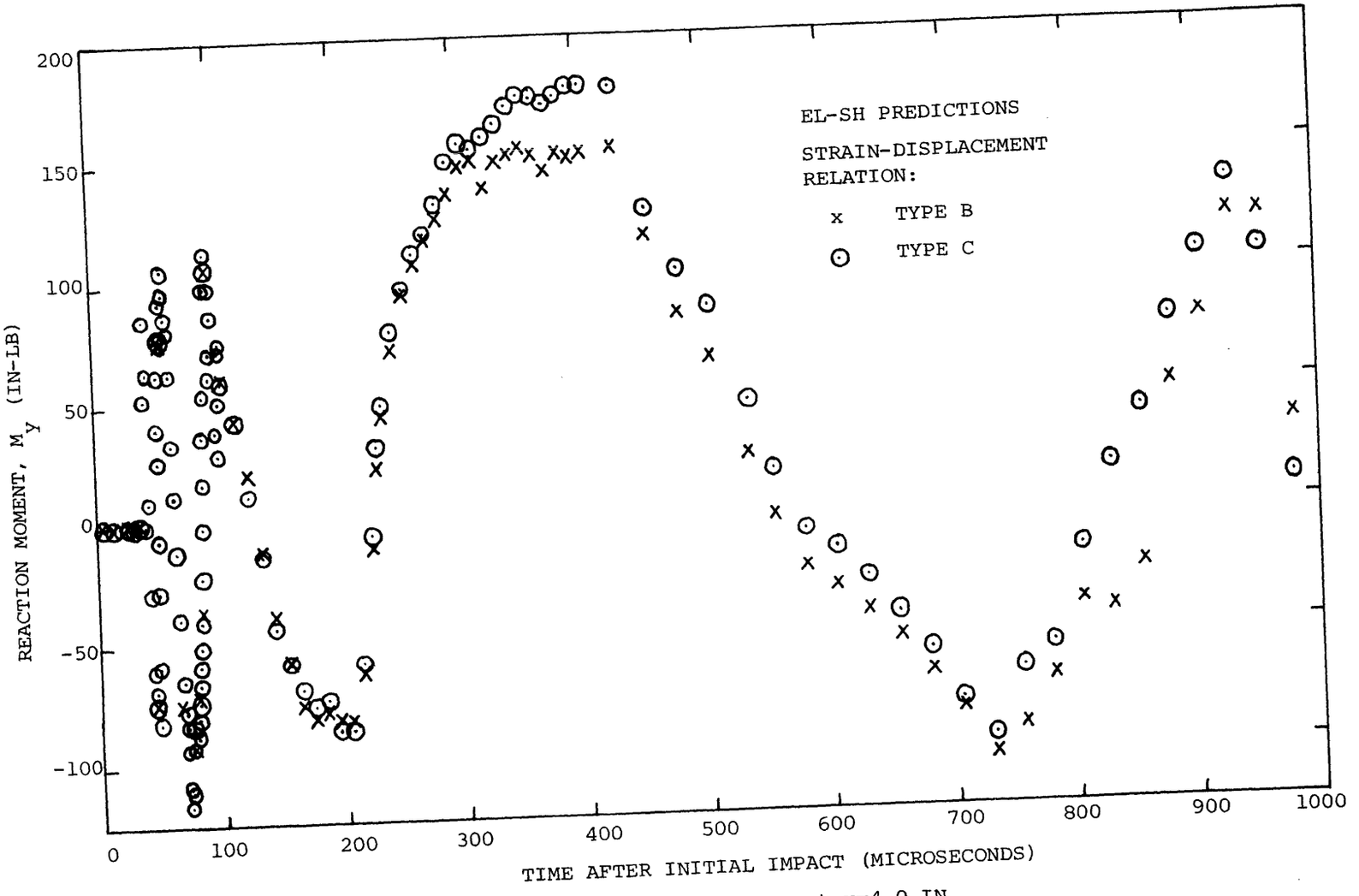

(e) Support Reaction Moment, M_y, at x=4.0 IN

FIG. 45 CONTINUED (CB-18, 43 ELEM, 4 DOF/N, TYPE B VS. TYPE C)

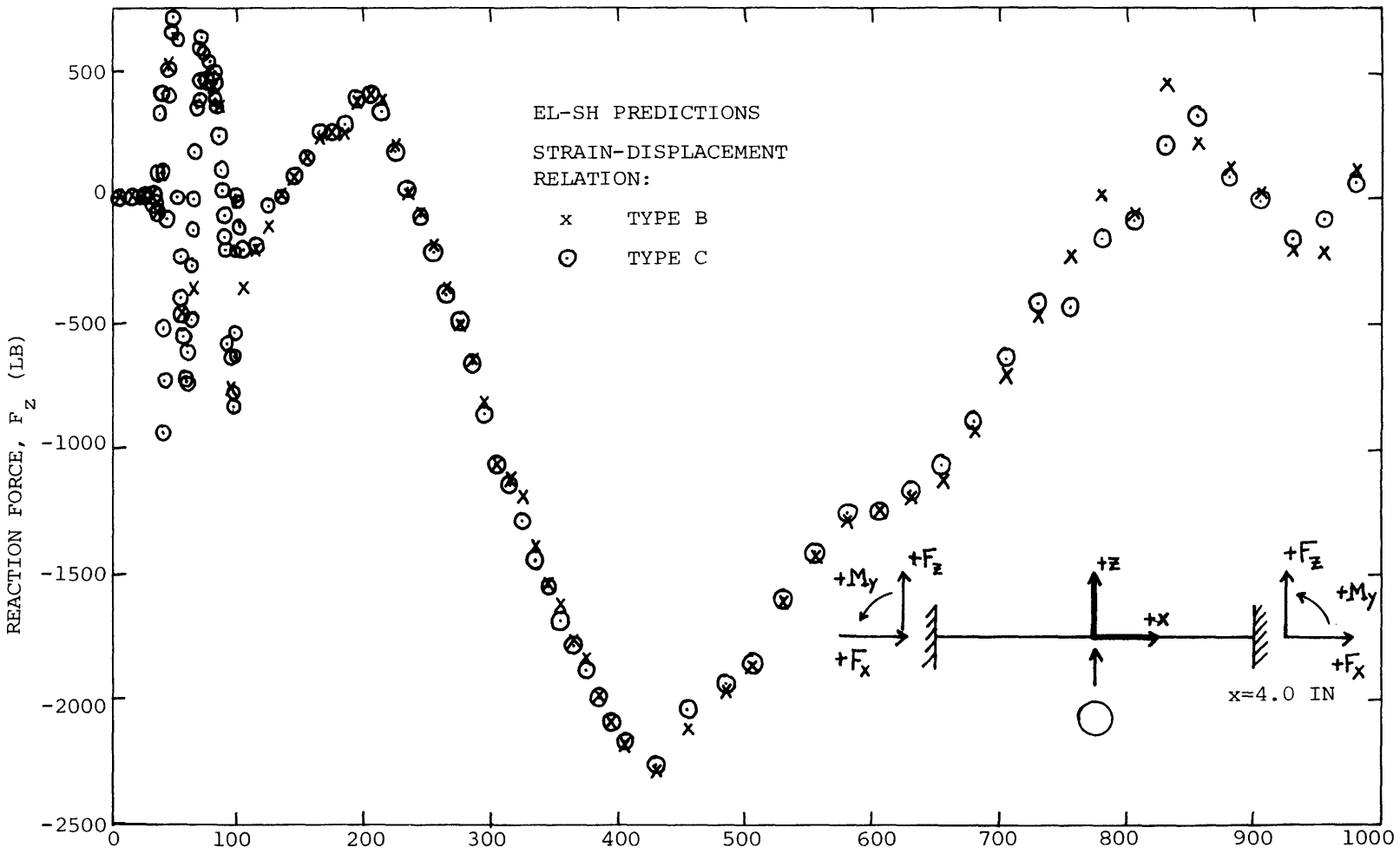

(f) Support Reaction Force, F_z (Normal) at x=4.0 IN

FIG. 45 CONTINUED (CB-18, 43 ELEM, 4 DOF/N, TYPE B VS. TYPE C)

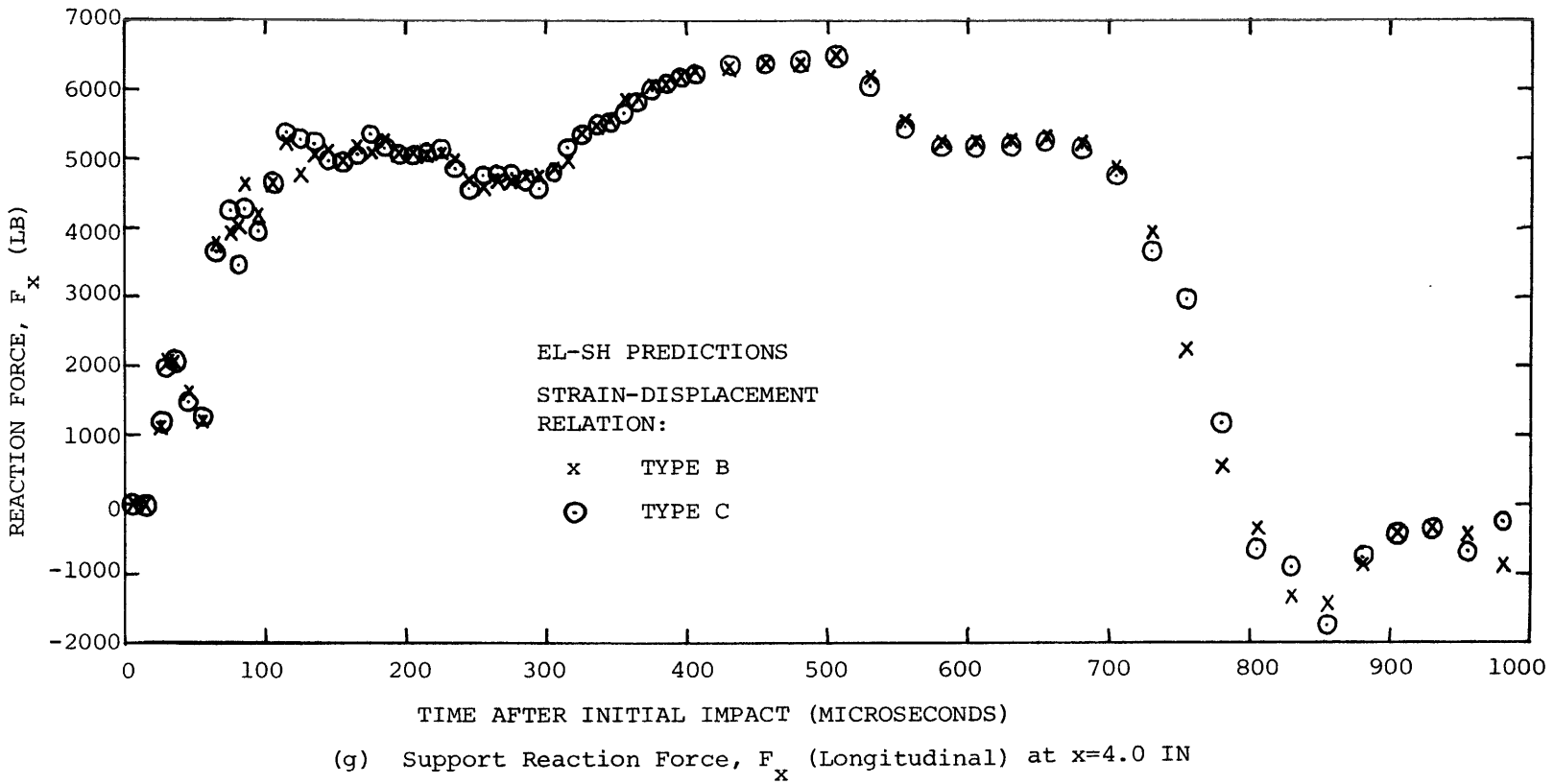

(g) Support Reaction Force, F_x (Longitudinal) at x=4.0 IN

FIG. 45 CONTINUED (CB-18, 43 ELEM, 4 DOF/N, TYPE B VS. TYPE C)

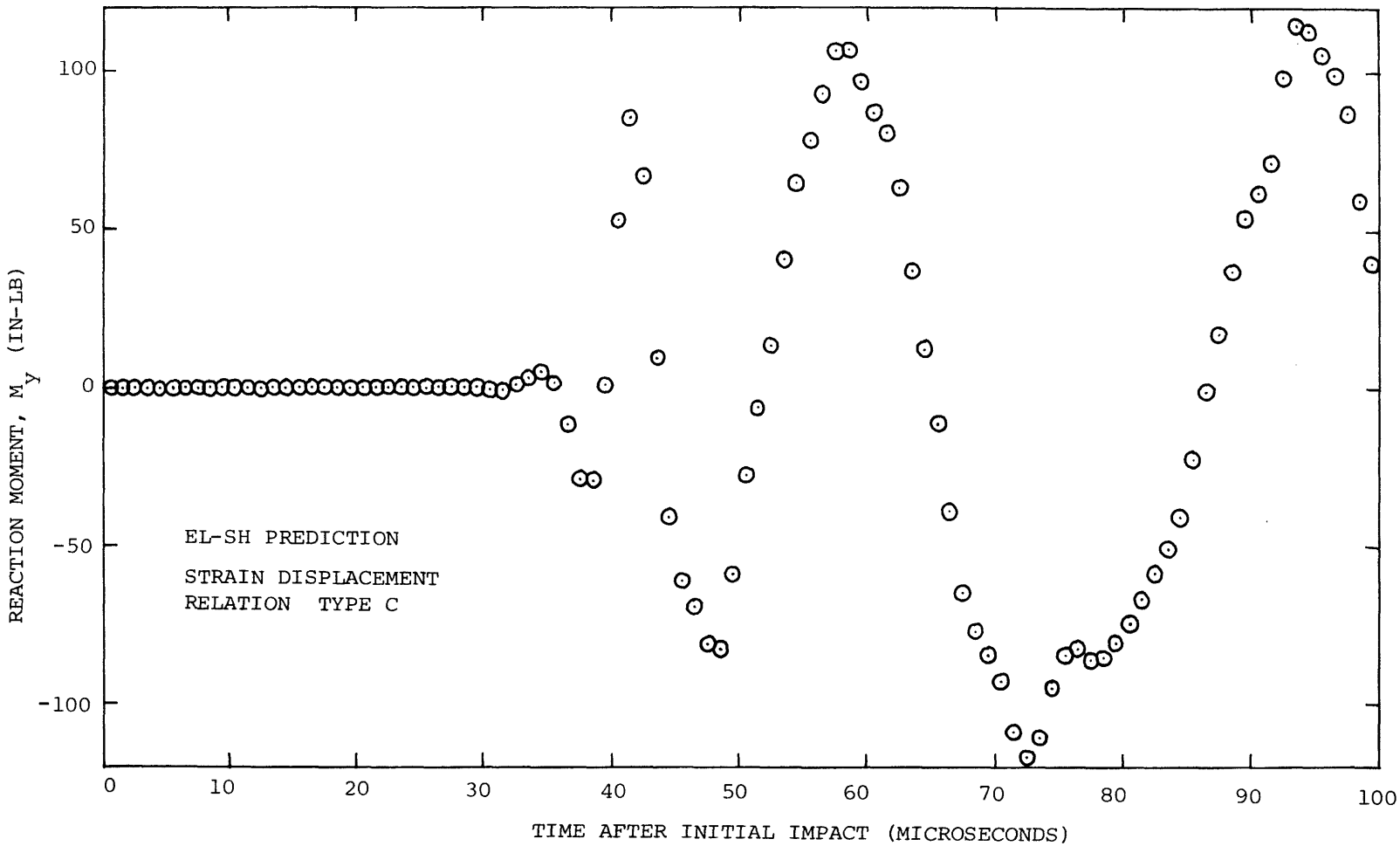

(h) Early Time Support Reaction Moment, M_y at x=4.0 IN

FIG. 45 CONTINUED (CB-18, 43 ELEM, 4 DOF/N)

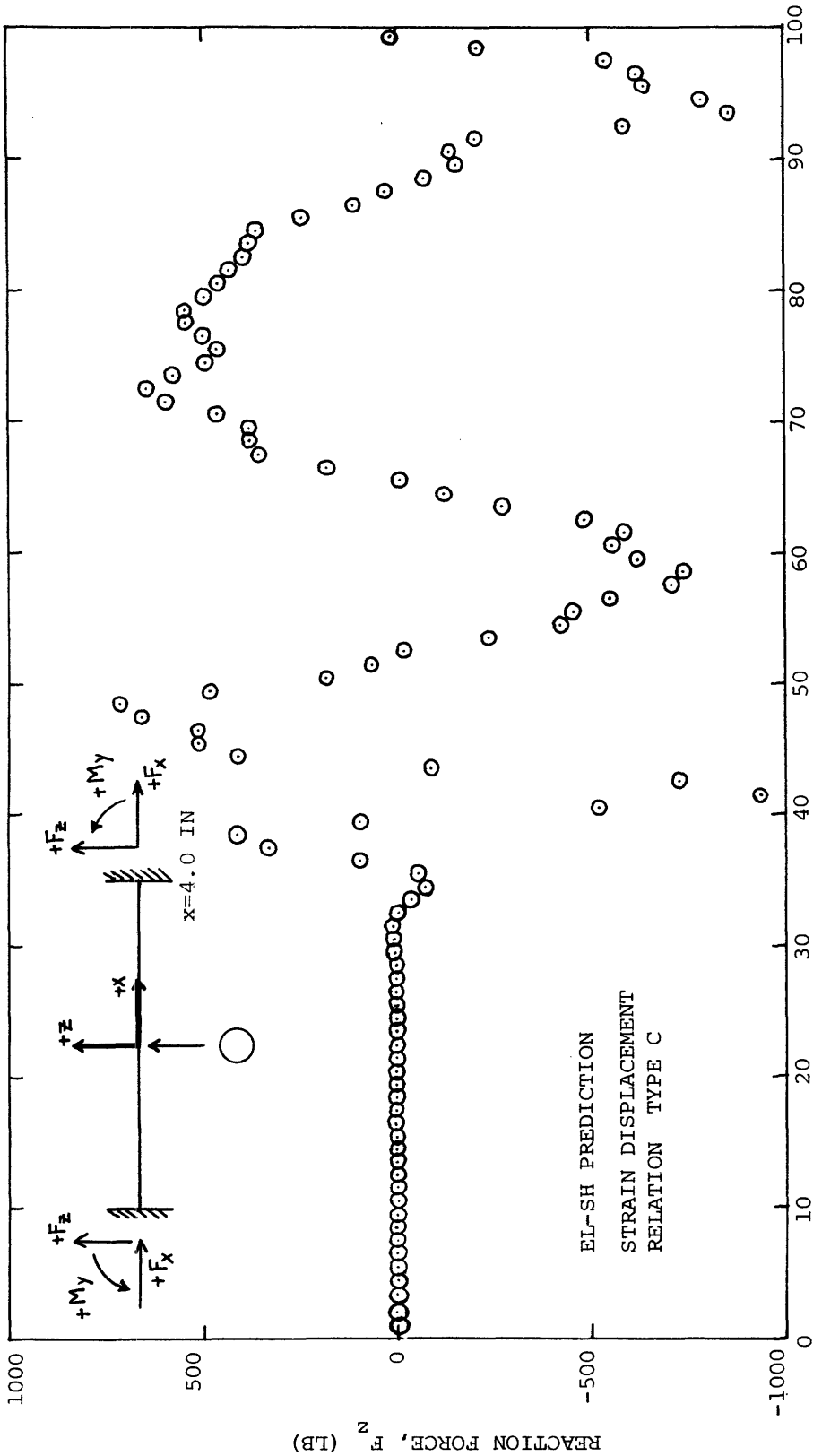

(i) Early Time Support Reaction Force, F_z (Normal) at x=4.0 IN

FIG. 45 CONTINUED (CB-18, 43 ELEM, 4 DOF/N)

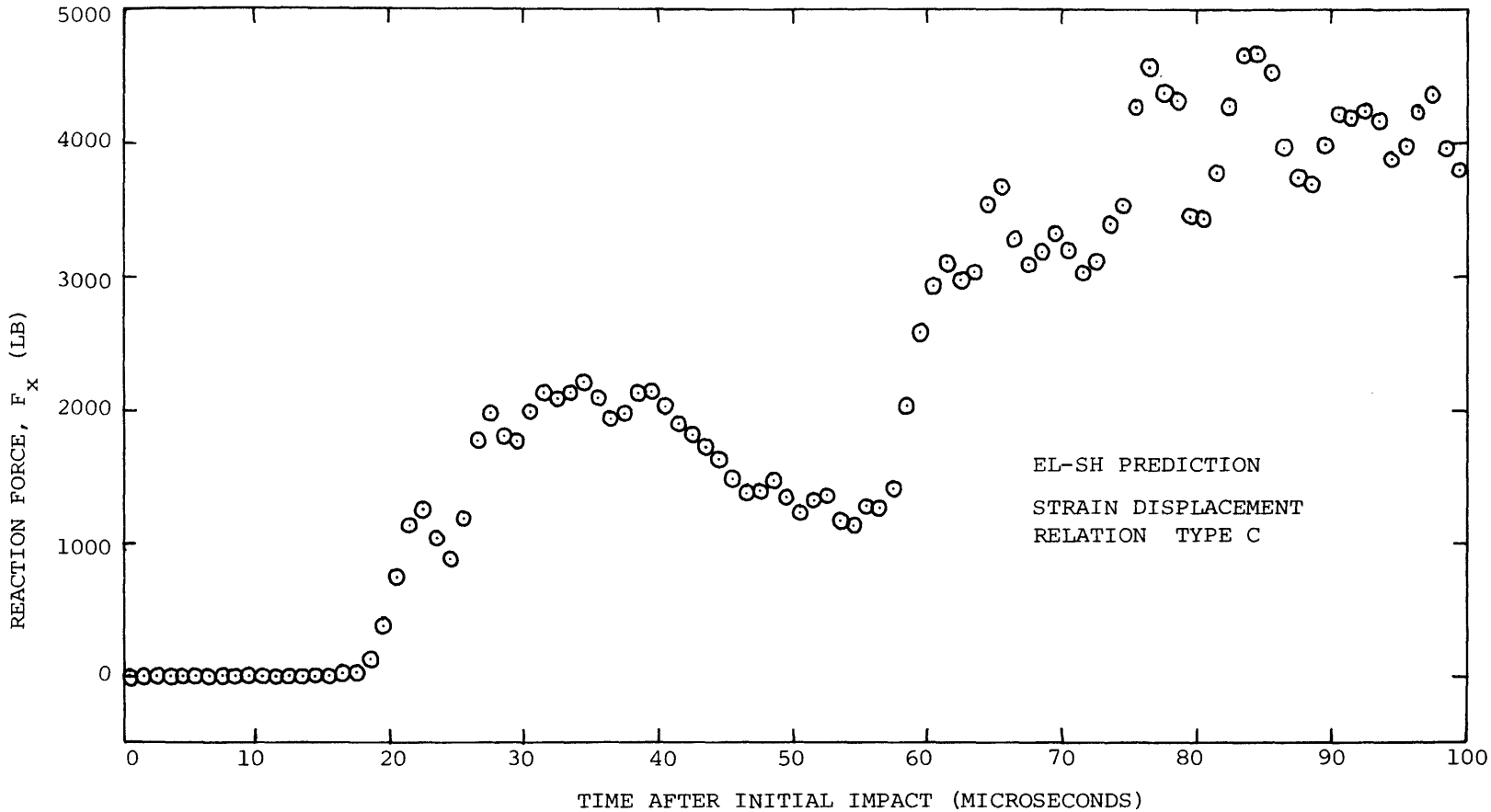

(j) Early Time Support Reaction Force, F_x (Longitudinal) at x=4.0 IN

FIG. 45 CONCLUDED (CB-18, 43 ELEM, 4 DOF/N)

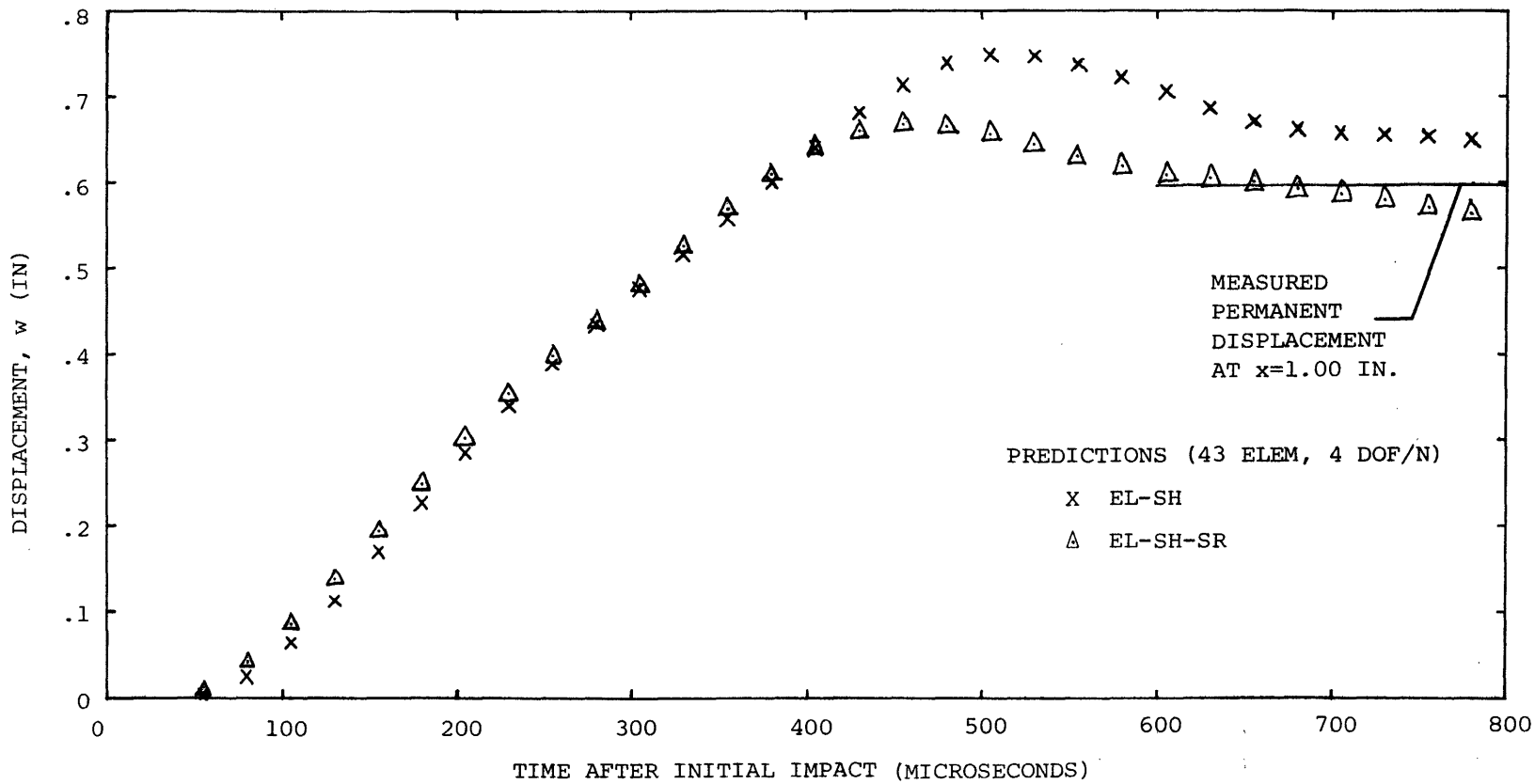

FIG. 46 PREDICTED TRANSIENT AND OBSERVED PERMANENT LATERAL DEFLECTION w AT SPANWISE STATION x=1.0 IN FOR STEEL-SPHERE IMPACTED 6061-T651 ALUMINUM BEAM SPECIMEN CB-18

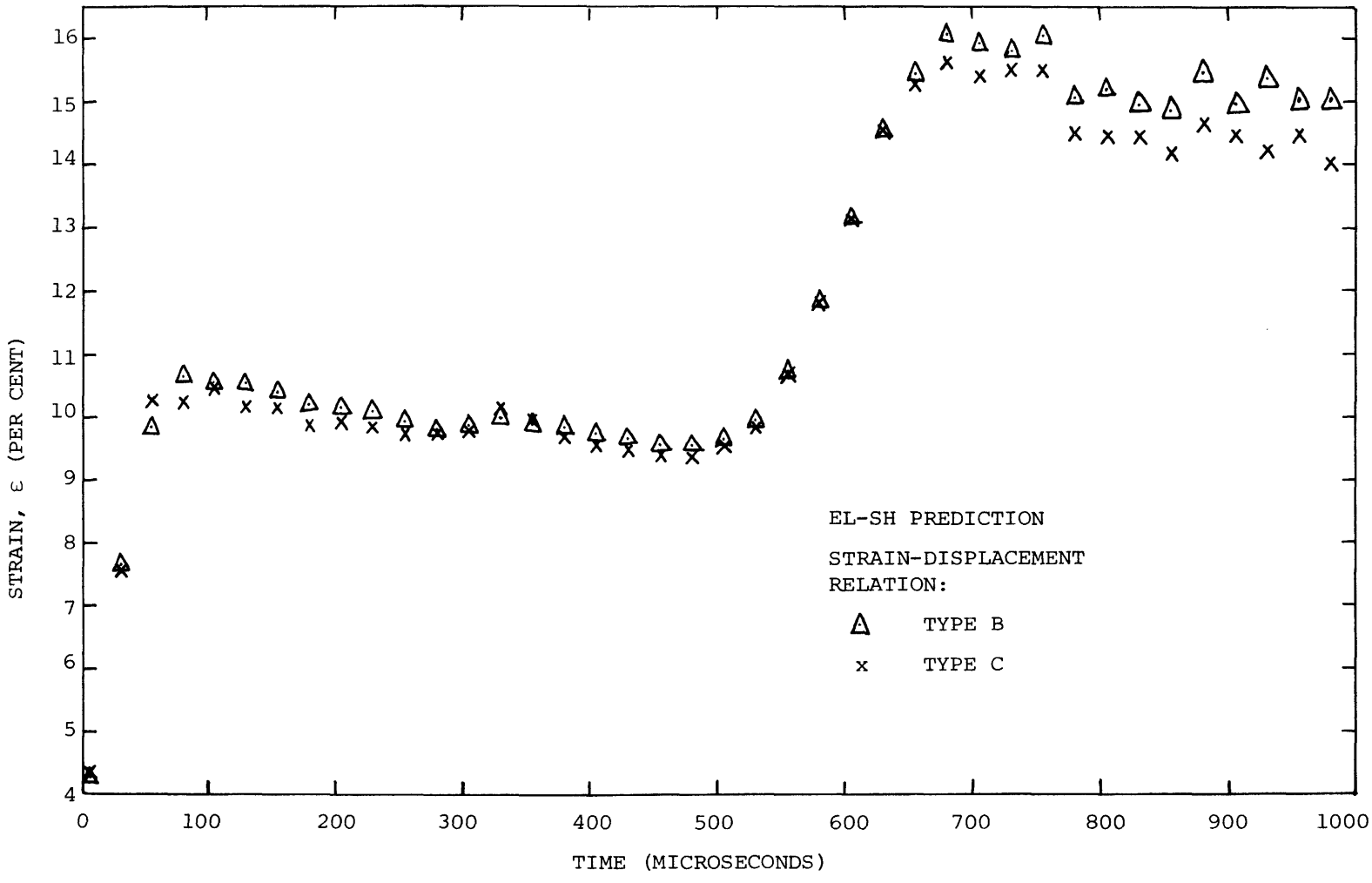

(a) Upper Surface at Midspan (x=0)

FIG. 47 TRANSIENT STRAIN AT VARIOUS SPANWISE STATIONS OF STEEL-SPHERE IMPACTED 6061-T651 ALUMINUM BEAM MODEL CB-18 (43 ELEM, 4 DOF/N, TYPE B VS. TYPE C)

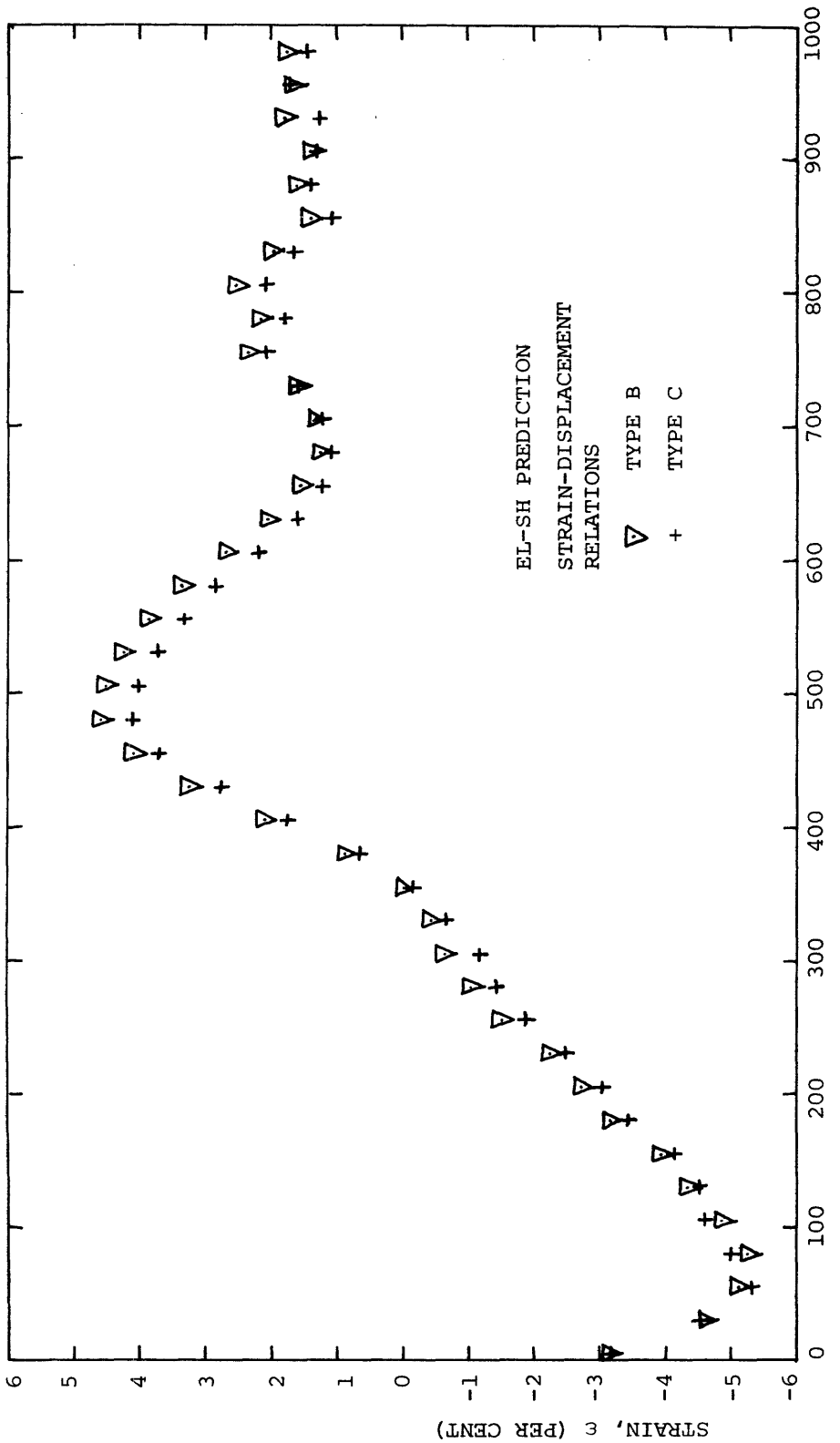

(b) Lower Surface at Midspan (x=0)

FIG. 47 CONTINUED (CB-18, 43 ELEM, 4 DOF/N, TYPE B VS. TYPE C)

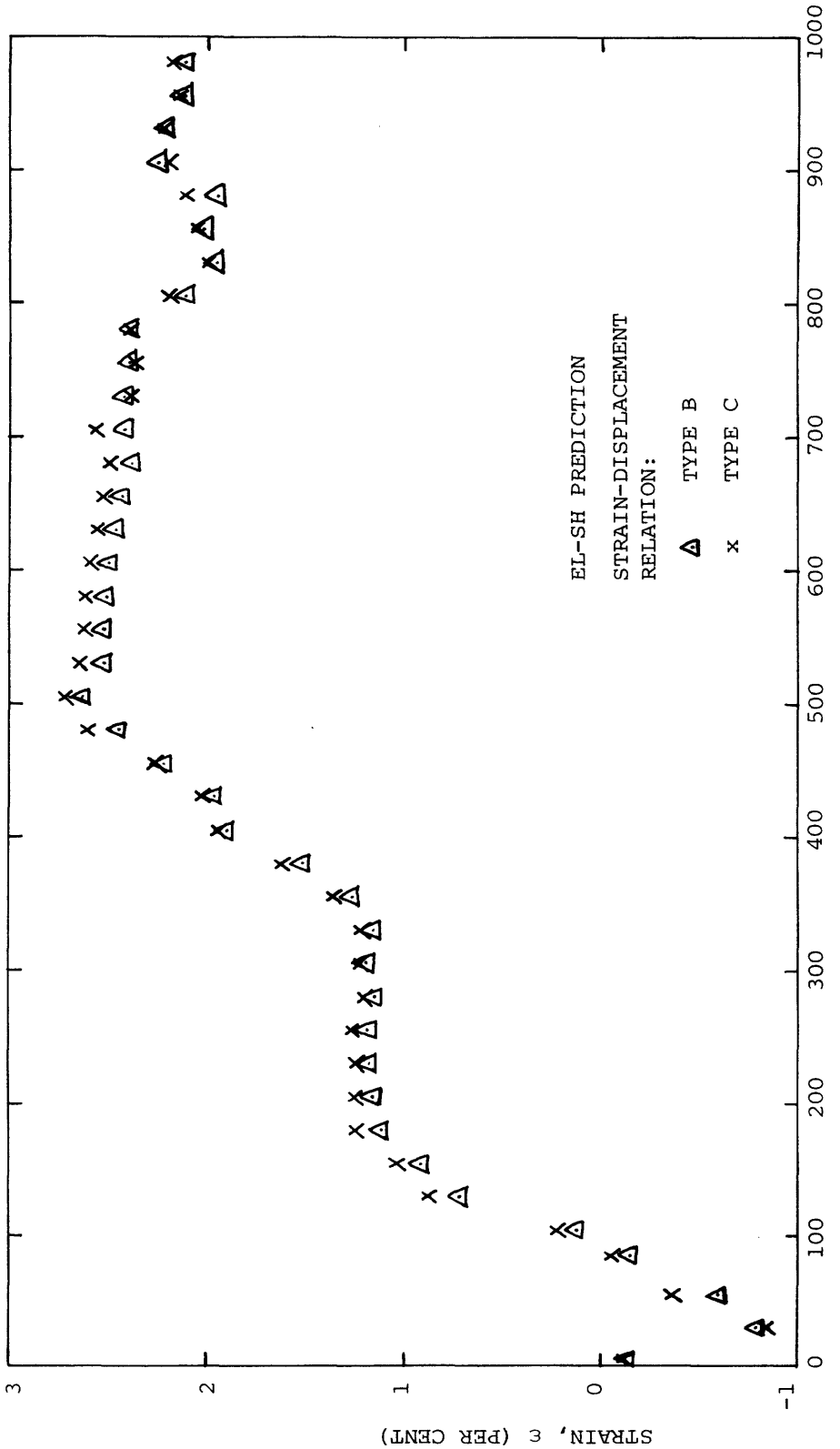

(c) Upper Surface at Station x=0.6 IN

FIG. 47 CONTINUED (CB-18, 43 ELEM, 4 DOF/N, TYPE B VS. TYPE C)

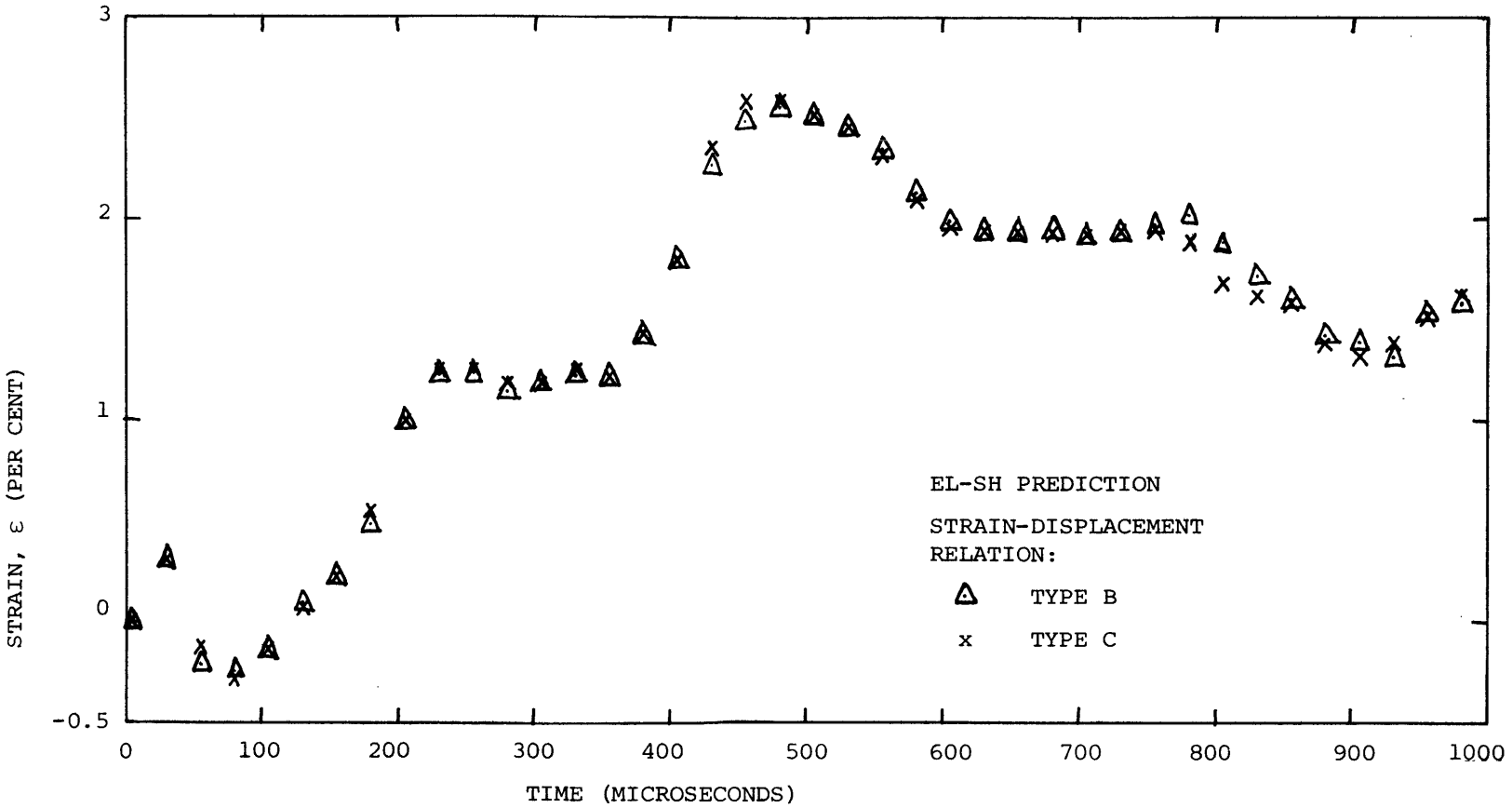

(d) Upper Surface at station x=1.5 IN

FIG. 47 CONTINUED (CB-18, 43 ELEM, 4 DOF/N, TYPE B VS. TYPE C)

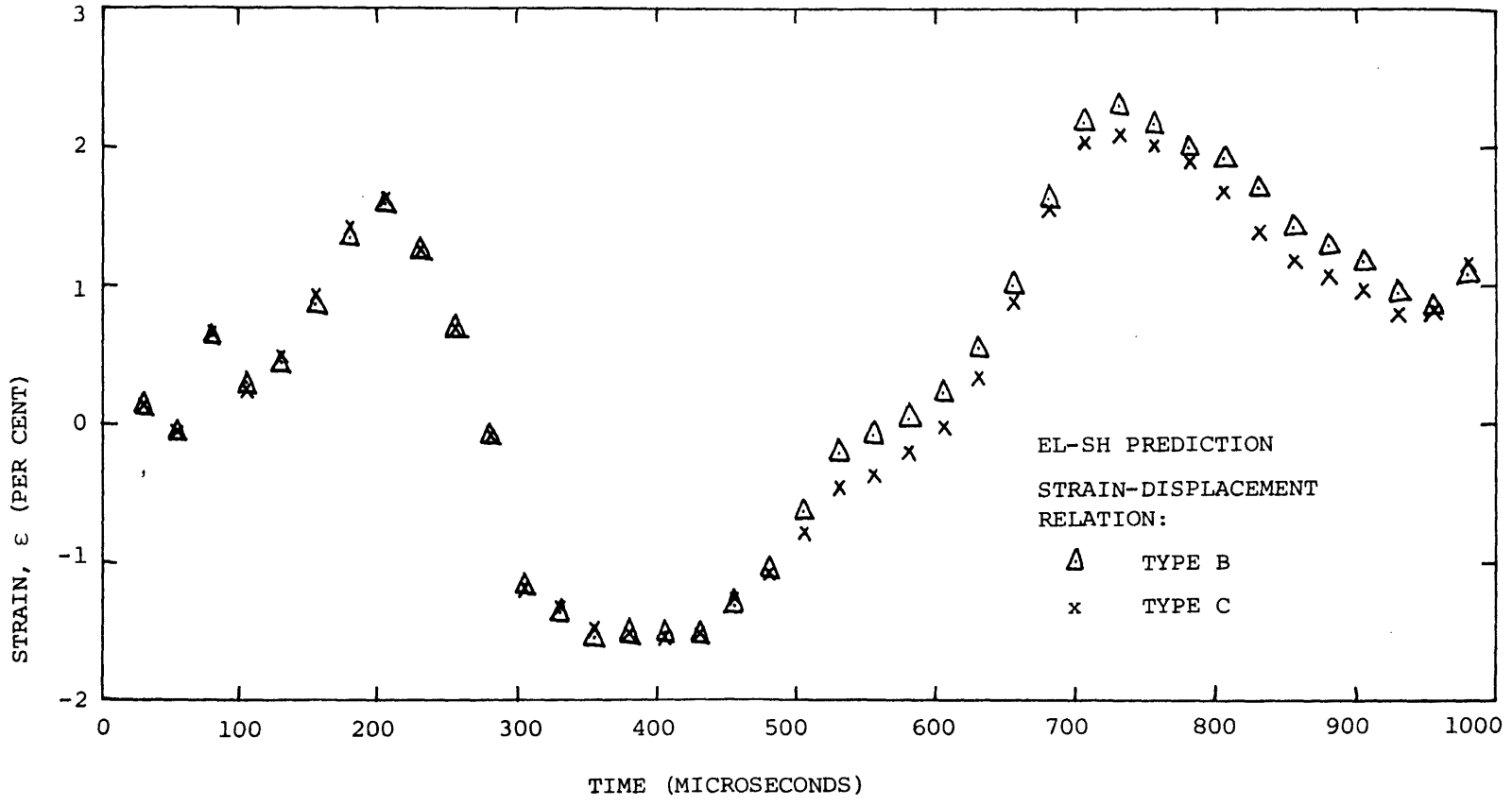

(e) Upper Surface at Station x=3.9 IN

FIG. 47 CONCLUDED (CB-18, 43 ELEM, 4 DOF/N, TYPE B VS. TYPE C)

APPENDIX A

DESCRIPTION OF THE MECHANICAL-SUBLAYER MODEL FOR STRAIN-HARDENING, STRAIN-RATE-SENSITIVE MATERIAL BEHAVIOR

As discussed in Subsection 2.4.2, the yield surface of certain materials will change in case of continued straining beyond the initial yield. The change of the yield surface that characterizes the strain-hardening behavior of the material depends on the loading history. In the present analysis, the strain hardening behavior of the material is accounted for by using the "mechanical sublayer model" (Ref. 54, 55, and 56). In order that the present report be reasonably self-contained, the mechanical sublayer model is described in this appendix.

In the mechanical sublayer model, the uniaxial tension (or compression) test stress-strain curve of the material is first approximated by (n+1) piecewise-linear segments which are defined at coordinates $[(\sigma_k, \varepsilon_k), k = 1, 2, \ldots n]$, as depicted in Fig. A.1a. Next, the material is envisioned as consisting, at any point in the material, of n equally-strained "sublayers" of elastic perfectly-plastic material, with each sublayer having the same elastic modulus E, but an appropriately different yield stress (see Fig. A.1b). For example, the yield stress of the kth sublayer is

$$\sigma_{ok} = E\,\epsilon_k \qquad k = 1, 2, \ldots, n \tag{A.1}$$

Then, the stress value, σ_k, associated with the kth sublayer can be defined uniquely by the strain history and the value of strain and strain-rate present at that point. Taken collectively with an appropriate weighting factor C_k for each sublayer, the stress, σ, at that point corresponding to strain ε may be expressed as

$$\sigma = \sum_{k=1}^{n} C_k\ \sigma_k(\epsilon) \tag{A.2}$$

where the weighting factor C_k for the kth sublayer may readily be confirmed to be

$$C_k = \frac{E_k - E_{k+1}}{E} \tag{A.3}$$

where

$$E_1 \equiv E\,, \quad E_k = \frac{\sigma_k - \sigma_{k-1}}{\epsilon_k - \epsilon_{k-1}} \quad (k=2,3,\ldots,n)\,, \quad E_{n+1} = 0 \tag{A.3a}$$

The elastic perfectly-plastic and linear strain-hardening constitutive relation may be treated as special cases. In the case of elastic perfectly-plastic behavior, there is only one sublayer, and in the case of linear strain-hardening material there are two sublayers and the yield limit of the second sublayer is taken sufficiently high so that the deformation in that sublayer remains elastic.

From the computational point of view, the use of the mechanical sublayer model is very convenient to analyze problems with general loading paths including loading, unloading, reloading, and cyclic loading. Its features include the "kinematic hardening rule" which takes the Bauschinger effect into account (see Fig. A.1c). Also, this mechanical sublayer model may readily accommodate the strain-rate effect. Figure A.2a illustrates schematically the uniaxial stress-strain behavior for a strain-rate dependent, elastic, perfectly-plastic material whose rate dependence is described by Eq. 2.46,

$$\sigma_y = \sigma_o \left(1 + \left| \frac{\dot{\epsilon}}{D} \right|^{\frac{1}{p}} \right) \tag{2.46}$$

while Fig. A.2b depicts the corresponding behavior for a strain-hardening material which is represented by the mechanical sublayer model, each sublayer of which has the same values for the strain-rate constants D and p. For this special type of rate-dependent strain-hardening material, the stress-strain curve at a given strain rate $\dot{\epsilon}$ is simply a constant magnification of the static stress-strain curves along rays emanating from the origin.

One may generalize this uniaxial behavior to the two- or three-dimensional stress case by adopting, for example, the Mises-Hencky yield condition, Eq. 2.44, and flow rule, Eq. 2.45, and applying them to each sublayer of the mechanical sublayer model. The strain-rate dependence may also be generalized by assuming that the $\dot{\epsilon}$ of the one-dimensional case may be replaced by the second invariant of the deviatoric strain-rate tensor as defined by

$$\frac{2}{3}\dot{\epsilon}^2 = \dot{\gamma}^i_j \dot{\gamma}^j_i - \frac{1}{3}\left(\dot{\gamma}^k_k\right)^2 \qquad \text{(A.4)}$$

In terms of the finite increments $\Delta\gamma^i_j$ of strain determined in each timewise calculation step of the present procedure, the "replacement $\dot{\epsilon}$" given by Eq. A.4 becomes:

$$\dot{\epsilon} = \frac{1}{\Delta t}\left[\frac{3}{2}\Delta\gamma^i_j \Delta\gamma^j_i - \frac{1}{2}\left(\Delta\gamma^k_k\right)^2\right]^{\frac{1}{2}} \qquad \text{(A.5)}$$

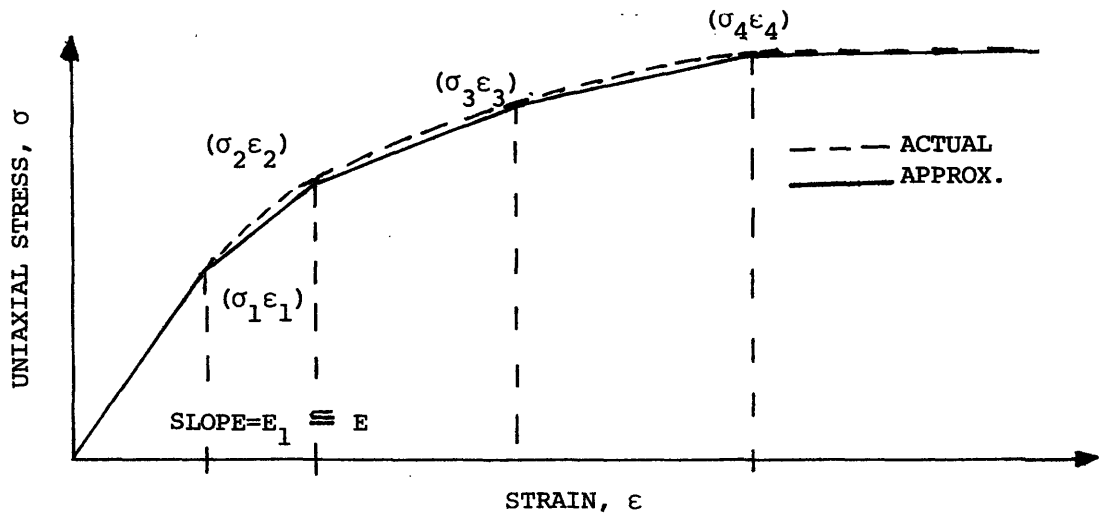

(a) Actual and Approximated Curves

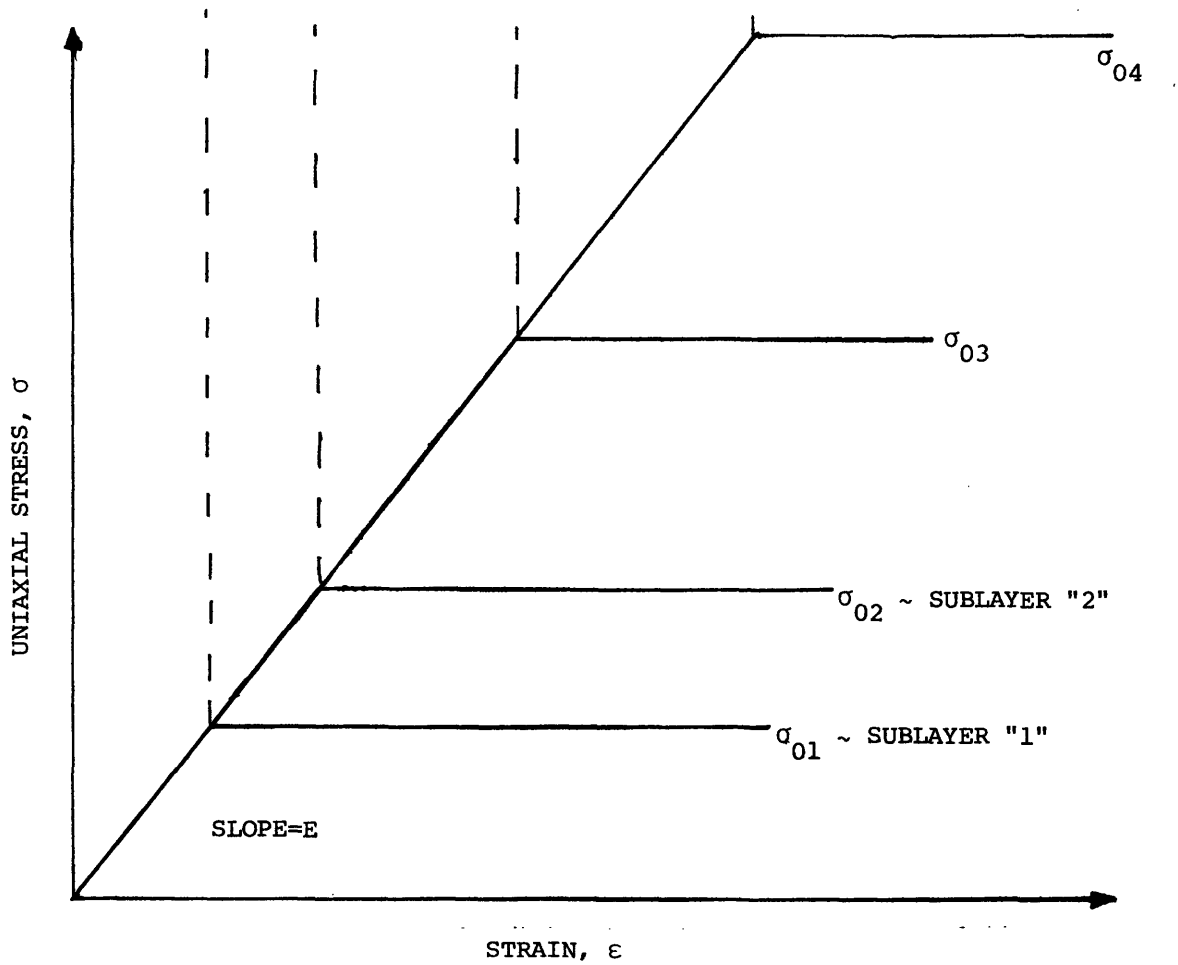

(b) Properties of the Elastic, Perfectly-Plastic Sublayers

FIG. A.1 APPROXIMATION OF A UNIAXIAL STRESS-STRAIN CURVE BY THE MECHANICAL SUBLAYER MODEL

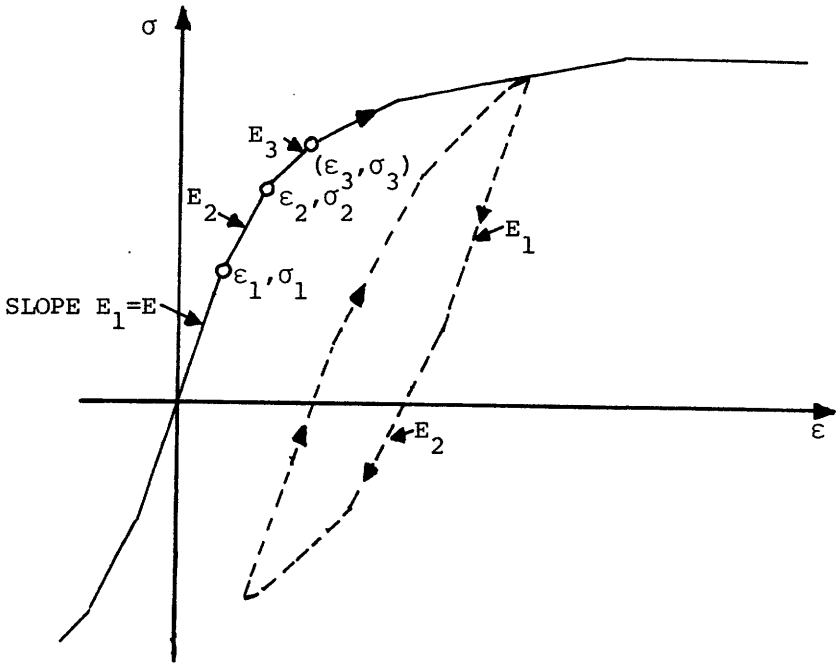

(c) Schematic of Loading, Unloading, and Reloading Paths

FIG. A.1 CONCLUDED

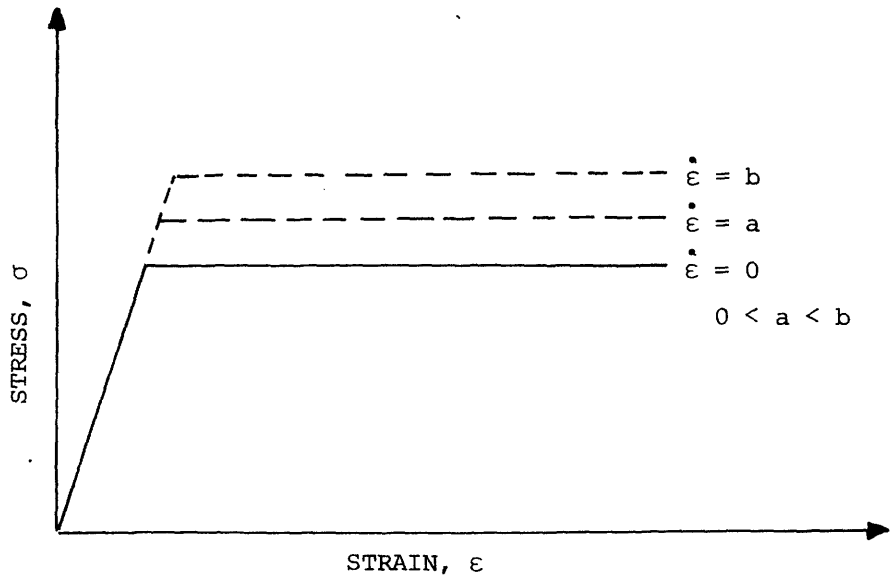

(a) Elastic, Perfectly-Plastic Material

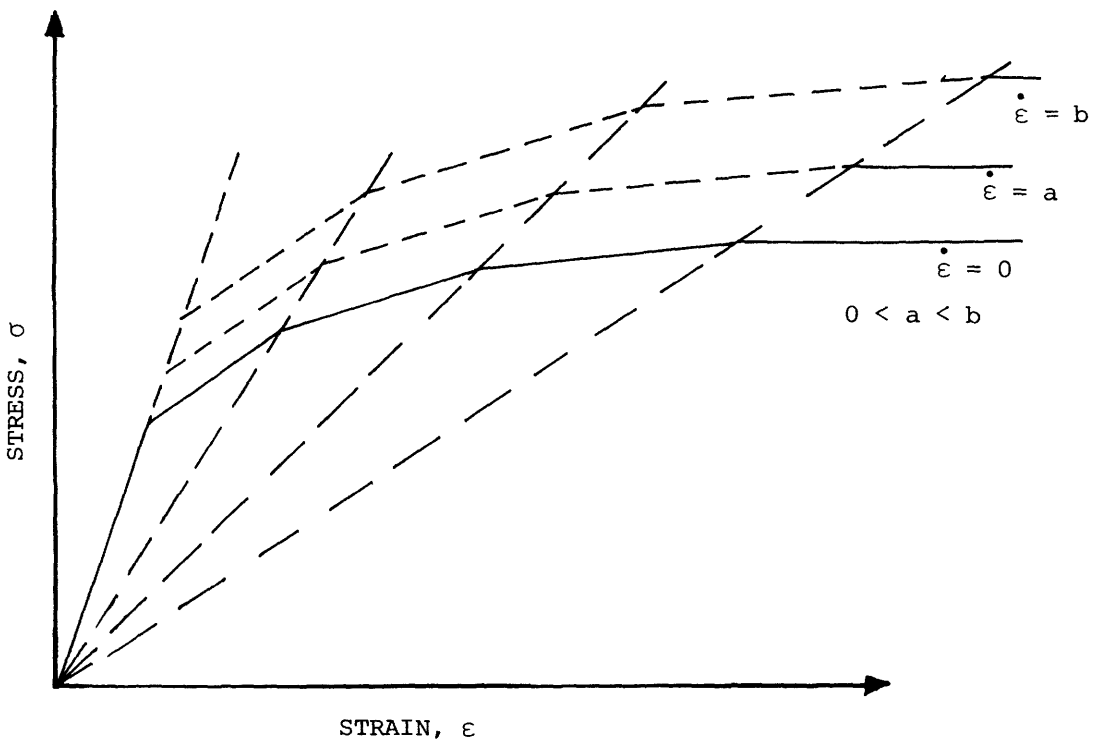

(b) Special Strain Hardening Material

FIG. A.2 SCHEMATIC OF STRAIN-RATE DEPENDENT UNIAXIAL STRESS-STRAIN CURVES

APPENDIX B

DEFINITION OF FINITE ELEMENT MATRICES INDICATED SYMBOLICALLY IN THE TEXT

Included in this appendix are the matrices $[U(\eta)]_{2\times16}$, $[A]_{16\times16}$, $\lfloor D_1 \rfloor_{1\times16}$, $\lfloor D_2 \rfloor_{1\times16}$, $\lfloor D_3 \rfloor_{1\times16}$, and $\lfloor D_4 \rfloor_{1\times16}$ indicated symbolically in Subsection 3.4 for a Bernoulli-Euler curved beam element, in conjunction with the use of the Type C strain-displacement relation as given, for example, by Eq. 3.92. The indicated sizes of these matrices apply to the 8 DOF/N element; for conciseness, the corresponding matrices for the 7, 6, 5, and 4 DOF/N elements are indicated by self-evident "partition-deletion guidelines" in each of the matrices given in the following (see Eqs. 3.92-3.112):

$$\underset{2\times16}{[U(\eta)]} = \left[\begin{array}{cccccccc|cc|cc|cc} \cos\phi & \sin\phi & B_1 & \eta & 0 & 0 & \eta^2 & \eta^3 & 0 & 0 & \eta^4 & \eta^5 & 0 & 0 & \eta^6 & \eta^7 \\ -\sin\phi & \cos\phi & B_2 & 0 & \eta^2 & \eta^3 & 0 & 0 & \eta^4 & \eta^5 & 0 & 0 & \eta^6 & \eta^7 & 0 & 0 \end{array}\right] \tag{B.1}$$

where B_1 and B_2 are given by Eq. 3.64.

$$\underset{1\times16}{\lfloor D_1 \rfloor} \equiv \underset{1\times16}{\lfloor G_\chi \rfloor} \underset{16\times16}{[A]^{-1}}, \quad \chi = \frac{\partial v}{\partial \eta} + \frac{w}{R} = \frac{\partial v}{\partial \eta} - w\frac{\partial \phi}{\partial \eta}$$

$$\underset{1\times16}{\lfloor G_\chi \rfloor} = \left[\begin{array}{cccccccc|cc|cc|cc} 0 & 0 & 0 & 1 & \left(-\eta^2\frac{\partial\phi}{\partial\eta}\right) & \left(-\eta^3\frac{\partial\phi}{\partial\eta}\right) & 2\eta & 3\eta^2 & \left(-\eta^4\frac{\partial\phi}{\partial\eta}\right) & \left(-\eta^5\frac{\partial\phi}{\partial\eta}\right) & & & & & & \\ & & & & & & & & & & 4\eta^3 & 5\eta^4 & \left(-\eta^6\frac{\partial\phi}{\partial\eta}\right) & \left(-\eta^7\frac{\partial\phi}{\partial\eta}\right) & 6\eta^5 & 7\eta^6 \end{array}\right] \tag{B.2}$$

$$\underset{1\times16}{\lfloor D_2 \rfloor} \equiv \underset{1\times16}{\lfloor G_\psi \rfloor} \underset{16\times16}{[A]^{-1}}, \quad \psi = \frac{\partial w}{\partial \eta} - \frac{v}{R} = \frac{\partial w}{\partial \eta} + v\frac{\partial \phi}{\partial \eta}$$

$$\underset{1\times16}{\lfloor G_\psi \rfloor} = \left[\begin{array}{cccccccc|cc|cc|cc} 0 & 0 & 1 & \eta\frac{\partial\phi}{\partial\eta} & 2\eta & 3\eta^2 & \eta^2\frac{\partial\phi}{\partial\eta} & \eta^3\frac{\partial\phi}{\partial\eta} & 4\eta^3 & 5\eta^4 & & & & & & \\ & & & & & & & & & & \eta^4\frac{\partial\phi}{\partial\eta} & \eta^5\frac{\partial\phi}{\partial\eta} & 6\eta^5 & 7\eta^6 & \eta^6\frac{\partial\phi}{\partial\eta} & \eta^7\frac{\partial\phi}{\partial\eta} \end{array}\right] \tag{B.3}$$

$$\underset{1\times16}{[D_3]} \equiv \underset{1\times16}{[G_{-\psi,\eta}]}\,\underset{16\times16}{[A]}^{-1}$$

$$-\frac{\partial\psi}{\partial\eta} = -\frac{\partial^2 w}{\partial\eta^2} + \frac{1}{R}\frac{\partial v}{\partial\eta} + v\frac{\partial}{\partial\eta}\left(\frac{1}{R}\right) = -\frac{\partial^2 w}{\partial\eta^2} - \frac{\partial v}{\partial\eta}\frac{\partial\phi}{\partial\eta} - v\frac{\partial^2\phi}{\partial\eta^2}$$

$$\underset{1\times16}{[G_{-\psi,\eta}]} = \Big[\, 0\ 0\ 0\ -\left(\frac{\partial\phi}{\partial\eta}+\eta\frac{\partial^2\phi}{\partial\eta^2}\right)\ -2\ -6\eta\ -\left(2\frac{\partial\phi}{\partial\eta}+\eta\frac{\partial^2\phi}{\partial\eta^2}\right)\eta$$
$$-\left(3\frac{\partial\phi}{\partial\eta}+\eta\frac{\partial^2\phi}{\partial\eta^2}\right)\eta^2 \;|\; -12\eta^2\ -20\eta^3 \;|\; -\left(4\frac{\partial\phi}{\partial\eta}+\eta\frac{\partial^2\phi}{\partial\eta^2}\right)\eta^3$$
$$-\left(5\frac{\partial\phi}{\partial\eta}+\eta\frac{\partial^2\phi}{\partial\eta^2}\right)\eta^4 \;|\; -30\eta^4\ -42\eta^5 \;|\; -\left(6\frac{\partial\phi}{\partial\eta}+\eta\frac{\partial^2\phi}{\partial\eta^2}\right)\eta^5$$
$$-\left(7\frac{\partial\phi}{\partial\eta}+\eta\frac{\partial^2\phi}{\partial\eta^2}\right)\eta^6\,\Big] \qquad \text{(B.4)}$$

$$\underset{1\times16}{[D_4]} \equiv \underset{1\times16}{[G_{\chi,\eta}]}\,\underset{16\times16}{[A]}^{-1}$$

$$\frac{\partial\chi}{\partial\eta} = \frac{\partial^2 v}{\partial\eta^2} + \frac{1}{R}\frac{\partial w}{\partial\eta} + w\frac{\partial}{\partial\eta}\left(\frac{1}{R}\right) = \frac{\partial^2 v}{\partial\eta^2} - \frac{\partial w}{\partial\eta}\frac{\partial\phi}{\partial\eta} - w\frac{\partial^2\phi}{\partial\eta^2}$$

$$\underset{1\times16}{[G_{\chi,\eta}]} = \Big[\, 0\ 0\ 0\ 0\ -\left(2\frac{\partial\phi}{\partial\eta}+\eta\frac{\partial^2\phi}{\partial\eta^2}\right)\eta\ -\left(3\frac{\partial\phi}{\partial\eta}+\eta\frac{\partial^2\phi}{\partial\eta^2}\right)\eta^2$$
$$2\ \ 6\eta \;|\; -\left(4\frac{\partial\phi}{\partial\eta}+\eta\frac{\partial^2\phi}{\partial\eta^2}\right)\eta^3\ -\left(5\frac{\partial\phi}{\partial\eta}+\eta\frac{\partial^2\phi}{\partial\eta^2}\right)\eta^4 \;|$$
$$12\eta^2\ \ 20\eta^3 \;|\; -\left(6\frac{\partial\phi}{\partial\eta}+\eta\frac{\partial^2\phi}{\partial\eta^2}\right)\eta^5\ -\left(7\frac{\partial\phi}{\partial\eta}+\eta\frac{\partial^2\phi}{\partial\eta^2}\right)\eta^6 \;|$$
$$30\eta^4\ \ 42\eta^5\,\Big] \qquad \text{(B.5)}$$

In the above, it is useful to recall that $\frac{1}{R} = -\frac{\partial\phi}{\partial\eta}$.

$$\underset{16\times16}{[A]} \equiv \Big[\, \underset{16\times8}{A_1} \;\vdots\; \underset{16\times8}{A_2} \,\Big] \qquad \text{(B.6)}$$

where

In order to determine [A] for the 7, 6, 5, and 4 DOF/N elements, delete the following rows and columns from Eq. B.6:

DOF/N	Delete Rows and Columns
7	8,16
6	7,8,15,16
5	6,7,8,14,15,16
4	5,6,7,8,13,14,15,16

Matrix $[A_1]$ is given on page 254 and matrix $[A_2]$ is given on page 255.

$v_i\|_{\eta=0}$	$\cos\phi_i$	$\sin\phi_i$	0	0	0	0	0	0
$w_i\|_{\eta=0}$	$-\sin\phi_i$	$\cos\phi_i$	0	0	0	0	0	0
$\psi_i\|_{\eta=0}$	0	0	1	0	0	0	0	0
$\chi_i\|_{\eta=0}$	0	0	0	1	0	0	0	0
$-\frac{\partial\psi}{\partial\eta}\Big\|_{\eta=0}^{i}$	0	0	0	$-\frac{\partial\phi}{\partial\eta}\Big\|_i$	-2	0	0	0
$\frac{\partial\chi}{\partial\eta}\Big\|_{\eta=0}^{i}$	0	0	0	0	0	0	2	0
$-\frac{\partial^2\psi}{\partial\eta^2}\Big\|_{\eta=0}^{i}$	0	0	0	$-2\frac{\partial^2\phi}{\partial\eta^2}\Big\|_i$	0	-6	$-2\frac{\partial\phi}{\partial\eta}\Big\|_i$	0
$\frac{\partial^2\chi}{\partial\eta^2}\Big\|_{\eta=0}^{i}$	0	0	0	0	$-2\frac{\partial\phi}{\partial\eta}\Big\|_i$	0	0	6
$v_{i+1}\|_{\eta=\eta_i}$	$\cos\phi_{i+1}$	$\sin\phi_{i+1}$	$(Y_{i+1}-Y_i)\sin(\phi_{i+1}+\alpha)$ $-(Z_{i+1}-Z_i)\cos(\phi_{i+1}+\alpha)$	η_i	0	0	η_i^2	η_i^3
$w_{i+1}\|_{\eta=\eta_i}$	$-\sin\phi_{i+1}$	$\cos\phi_{i+1}$	$(Y_{i+1}-Y_i)\cos(\phi_{i+1}+\alpha)$ $+(Z_{i+1}-Z_i)\sin(\phi_{i+1}+\alpha)$	0	η_i^2	η_i^3	0	0
$\psi_{i+1}\|_{\eta=\eta_i}$	0	0	1	$\eta_i\frac{\partial\phi}{\partial\eta}\Big\|_{i+1}$	$2\eta_i$	$3\eta_i^2$	$\eta_i^2\frac{\partial\phi}{\partial\eta}\Big\|_{i+1}$	$\eta_i^3\frac{\partial\phi}{\partial\eta}\Big\|_{i+1}$
$\chi_{i+1}\|_{\eta=\eta_i}$	0	0	0	1	$-\eta_i^2\frac{\partial\phi}{\partial\eta}\Big\|_{i+1}$	$-\eta_i^3\frac{\partial\phi}{\partial\eta}\Big\|_{i+1}$	$2\eta_i$	$3\eta_i^2$
$-\frac{\partial\psi}{\partial\eta}\Big\|_{\eta=\eta_i}^{i+1}$	0	0	0	$-\left(\frac{\partial\phi}{\partial\eta}\Big\|_{i+1}+\eta_i\frac{\partial^2\phi}{\partial\eta^2}\Big\|_{i+1}\right)$	-2	$-6\eta_i$	$-\left(2\frac{\partial\phi}{\partial\eta}\Big\|_{i+1}+\eta_i\frac{\partial^2\phi}{\partial\eta^2}\Big\|_{i+1}\right)\eta_i$	$-\left(3\frac{\partial\phi}{\partial\eta}\Big\|_{i+1}+\eta_i\frac{\partial^2\phi}{\partial\eta^2}\Big\|_{i+1}\right)\eta_i^2$
$\frac{\partial\chi}{\partial\eta}\Big\|_{\eta=\eta_i}^{i+1}$	0	0	0	0	$-\left(2\frac{\partial\phi}{\partial\eta}\Big\|_{i+1}+\eta_i\frac{\partial^2\phi}{\partial\eta^2}\Big\|_{i+1}\right)\eta_i$	$-\left(3\frac{\partial\phi}{\partial\eta}\Big\|_{i+1}+\eta_i\frac{\partial^2\phi}{\partial\eta^2}\Big\|_{i+1}\right)\eta_i^2$	2	$6\eta_i$
$-\frac{\partial^2\psi}{\partial\eta^2}\Big\|_{\eta=\eta_i}^{i+1}$	0	0	0	$-2\frac{\partial^2\phi}{\partial\eta^2}\Big\|_{i+1}$	0	-6	$-2\left(\frac{\partial\phi}{\partial\eta}\Big\|_{i+1}+2\eta_i\frac{\partial^2\phi}{\partial\eta^2}\Big\|_{i+1}\right)$	$-6\left(\frac{\partial\phi}{\partial\eta}\Big\|_{i+1}+\eta_i\frac{\partial^2\phi}{\partial\eta^2}\Big\|_{i+1}\right)\eta_i$
$\frac{\partial^2\chi}{\partial\eta^2}\Big\|_{\eta=\eta_i}^{i+1}$	0	0	0	0	$-2\left(\frac{\partial\phi}{\partial\eta}\Big\|_{i+1}+2\eta_i\frac{\partial^2\phi}{\partial\eta^2}\Big\|_{i+1}\right)$	$-6\left(\frac{\partial\phi}{\partial\eta}\Big\|_{i+1}+\eta_i\frac{\partial^2\phi}{\partial\eta^2}\Big\|_{i+1}\right)\eta_i$	0	6

0	0	0	0	0	0	0	0
0	0	0	0	0	0	0	0
0	0	0	0	0	0	0	0
0	0	0	0	0	0	0	0
0	0	0	0	0	0	0	0
0	0	0	0	0	0	0	0
0	0	0	0	0	0	0	0
0	0	0	0	0	0	0	0
0	0	η_i^4	η_i^5	0	0	η_i^6	η_i^7
η_i^4	η_i^5	0	0	η_i^6	η_i^7	0	0
$4\eta_i^3$	$5\eta_i^4$	$\eta_i^4 \frac{\partial\phi}{\partial\eta}\Big\|_{i+1}$	$\eta_i^5 \frac{\partial\phi}{\partial\eta}\Big\|_{i+1}$	$6\eta_i^5$	$7\eta_i^6$	$\eta_i^6 \frac{\partial\phi}{\partial\eta}\Big\|_{i+1}$	$\eta_i^7 \frac{\partial\phi}{\partial\eta}\Big\|_{i+1}$
$-\eta_i^4 \frac{\partial\phi}{\partial\eta}\Big\|_{i+1}$	$-\eta_i^5 \frac{\partial\phi}{\partial\eta}\Big\|_{i+1}$	$4\eta_i^3$	$5\eta_i^4$	$-\eta_i^6 \frac{\partial\phi}{\partial\eta}\Big\|_{i+1}$	$-\eta_i^7 \frac{\partial\phi}{\partial\eta}\Big\|_{i+1}$	$6\eta_i^5$	$7\eta_i^6$
$-12\eta_i^2$	$-20\eta_i^3$	$-\left(4\frac{\partial\phi}{\partial\eta}\Big\|_{i+1}+\eta_i\frac{\partial^2\phi}{\partial\eta^2}\Big\|_{i+1}\right)\eta_i^3$	$-\left(5\frac{\partial\phi}{\partial\eta}\Big\|_{i+1}+\eta_i\frac{\partial^2\phi}{\partial\eta^2}\Big\|_{i+1}\right)\eta_i^4$	$-30\eta_i^4$	$-42\eta_i^5$	$-\left(6\frac{\partial\phi}{\partial\eta}\Big\|_{i+1}+\eta_i\frac{\partial^2\phi}{\partial\eta^2}\Big\|_{i+1}\right)\eta_i^5$	$-\left(7\frac{\partial\phi}{\partial\eta}\Big\|_{i+1}+\eta_i\frac{\partial^2\phi}{\partial\eta^2}\Big\|_{i+1}\right)\eta_i^6$
$-\left(4\frac{\partial\phi}{\partial\eta}\Big\|_{i+1}+\eta_i\frac{\partial^2\phi}{\partial\eta^2}\Big\|_{i+1}\right)\eta_i^3$	$-\left(5\frac{\partial\phi}{\partial\eta}\Big\|_{i+1}+\eta_i\frac{\partial^2\phi}{\partial\eta^2}\Big\|_{i+1}\right)\eta_i^4$	$12\eta_i^2$	$20\eta_i^3$	$-\left(6\frac{\partial\phi}{\partial\eta}\Big\|_{i+1}+\eta_i\frac{\partial^2\phi}{\partial\eta^2}\Big\|_{i+1}\right)\eta_i^5$	$-\left(7\frac{\partial\phi}{\partial\eta}\Big\|_{i+1}+\eta_i\frac{\partial^2\phi}{\partial\eta^2}\Big\|_{i+1}\right)\eta_i^6$	$30\eta_i^4$	$42\eta_i^5$
$-24\eta_i$	$-60\eta_i^2$	$-4\left(3\frac{\partial\phi}{\partial\eta}\Big\|_{i+1}+2\eta_i\frac{\partial^2\phi}{\partial\eta^2}\Big\|_{i+1}\right)\eta_i^2$	$-10\left(2\frac{\partial\phi}{\partial\eta}\Big\|_{i+1}+\eta_i\frac{\partial^2\phi}{\partial\eta^2}\Big\|_{i+1}\right)\eta_i^3$	$-120\eta_i^3$	$-210\eta_i^4$	$-6\left(5\frac{\partial\phi}{\partial\eta}\Big\|_{i+1}+2\eta_i\frac{\partial^2\phi}{\partial\eta^2}\Big\|_{i+1}\right)\eta_i^4$	$-14\left(3\frac{\partial\phi}{\partial\eta}\Big\|_{i+1}+\eta_i\frac{\partial^2\phi}{\partial\eta^2}\Big\|_{i+1}\right)\eta_i^5$
$-4\left(3\frac{\partial\phi}{\partial\eta}\Big\|_{i+1}+2\eta_i\frac{\partial^2\phi}{\partial\eta^2}\Big\|_{i+1}\right)\eta_i^2$	$-10\left(2\frac{\partial\phi}{\partial\eta}\Big\|_{i+1}+\eta_i\frac{\partial^2\phi}{\partial\eta^2}\Big\|_{i+1}\right)\eta_i^3$	$24\eta_i$	$60\eta_i^2$	$-6\left(5\frac{\partial\phi}{\partial\eta}\Big\|_{i+1}+2\eta_i\frac{\partial^2\phi}{\partial\eta^2}\Big\|_{i+1}\right)\eta_i^4$	$-14\left(3\frac{\partial\phi}{\partial\eta}\Big\|_{i+1}+\eta_i\frac{\partial^2\phi}{\partial\eta^2}\Big\|_{i+1}\right)\eta_i^5$	$120\eta_i^3$	$210\eta_i^4$